

---

Dissertations, Theses, and Masters Projects

Theses, Dissertations, & Master Projects

---

1985

## Stability and transition of the driven magnetohydrodynamic sheet pinch

Russell B. Dahlburg  
*College of William & Mary - Arts & Sciences*

Follow this and additional works at: <https://scholarworks.wm.edu/etd>



Part of the [Plasma and Beam Physics Commons](#)

---

### Recommended Citation

Dahlburg, Russell B., "Stability and transition of the driven magnetohydrodynamic sheet pinch" (1985). *Dissertations, Theses, and Masters Projects*. Paper 1539623755.  
<https://dx.doi.org/doi:10.21220/s2-jgbq-bb62>

This Dissertation is brought to you for free and open access by the Theses, Dissertations, & Master Projects at W&M ScholarWorks. It has been accepted for inclusion in Dissertations, Theses, and Masters Projects by an authorized administrator of W&M ScholarWorks. For more information, please contact [scholarworks@wm.edu](mailto:scholarworks@wm.edu).

## INFORMATION TO USERS

This reproduction was made from a copy of a document sent to us for microfilming. While the most advanced technology has been used to photograph and reproduce this document, the quality of the reproduction is heavily dependent upon the quality of the material submitted.

The following explanation of techniques is provided to help clarify markings or notations which may appear on this reproduction.

1. The sign or "target" for pages apparently lacking from the document photographed is "Missing Page(s)". If it was possible to obtain the missing page(s) or section, they are spliced into the film along with adjacent pages. This may have necessitated cutting through an image and duplicating adjacent pages to assure complete continuity.
2. When an image on the film is obliterated with a round black mark, it is an indication of either blurred copy because of movement during exposure, duplicate copy, or copyrighted materials that should not have been filmed. For blurred pages, a good image of the page can be found in the adjacent frame. If copyrighted materials were deleted, a target note will appear listing the pages in the adjacent frame.
3. When a map, drawing or chart, etc., is part of the material being photographed, a definite method of "sectioning" the material has been followed. It is customary to begin filming at the upper left hand corner of a large sheet and to continue from left to right in equal sections with small overlaps. If necessary, sectioning is continued again beginning below the first row and continuing on until complete.
4. For illustrations that cannot be satisfactorily reproduced by xerographic means, photographic prints can be purchased at additional cost and inserted into your xerographic copy. These prints are available upon request from the Dissertations Customer Services Department.
5. Some pages in any document may have indistinct print. In all cases the best available copy has been filmed.

**University  
Microfilms  
International**

300 N. Zeeb Road  
Ann Arbor, MI 48106



8515336

**Dahlburg, Russell Blackadore**

**STABILITY AND TRANSITION OF THE DRIVEN MAGNETOHYDRODYNAMIC  
SHEET PINCH**

*The College of William and Mary in Virginia*

PH.D. 1985

**University  
Microfilms  
International** 300 N. Zeeb Road, Ann Arbor, MI 48106

**Copyright 1985**

**by**

**Dahlburg, Russell Blackadore**

**All Rights Reserved**



**PLEASE NOTE:**

In all cases this material has been filmed in the best possible way from the available copy. Problems encountered with this document have been identified here with a check mark .

1. Glossy photographs or pages \_\_\_\_\_
2. Colored illustrations, paper or print \_\_\_\_\_
3. Photographs with dark background \_\_\_\_\_
4. Illustrations are poor copy \_\_\_\_\_
5. Pages with black marks, not original copy \_\_\_\_\_
6. Print shows through as there is text on both sides of page \_\_\_\_\_
7. Indistinct, broken or small print on several pages
8. Print exceeds margin requirements \_\_\_\_\_
9. Tightly bound copy with print lost in spine \_\_\_\_\_
10. Computer printout pages with indistinct print \_\_\_\_\_
11. Page(s) \_\_\_\_\_ lacking when material received, and not available from school or author.
12. Page(s) \_\_\_\_\_ seem to be missing in numbering only as text follows.
13. Two pages numbered \_\_\_\_\_. Text follows.
14. Curling and wrinkled pages \_\_\_\_\_
15. Dissertation contains pages with print at a slant, filmed as received \_\_\_\_\_
16. Other \_\_\_\_\_  
\_\_\_\_\_  
\_\_\_\_\_

University  
Microfilms  
International



STABILITY AND TRANSITION  
OF THE  
DRIVEN MAGNETOHYDRODYNAMIC SHEET PINCH

---

A Dissertation

Presented to

The Faculty of the Department of Physics  
The College of William and Mary in Virginia

In Partial Fulfillment  
Of the Requirements for the Degree of  
Doctor of Philosophy

---

by

Russell S. Dahlburg

1985




APPROVAL SHEET

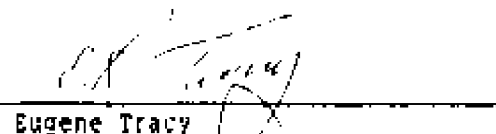
This dissertation is submitted in partial fulfillment of  
the requirements for the degree of

Doctor of Philosophy

  
Russell B. Dahlburg

  
David C. Montgomery

  
George Vahaia

  
Eugene Tracy

  
Henry Krakauer

  
Raymond W. Southworth

© 1985

RUSSELL BLACKADORE DAHLBURG

All Rights Reserved

## TABLE OF CONTENTS

	Page
ACKNOWLEDGEMENTS . . . . .	iv
ABSTRACT . . . . .	v
I. INTRODUCTION . . . . .	2
II. EQUILIBRIUM . . . . .	18
III. LINEAR STABILITY . . . . .	25
IV. NONLINEAR STABILITY . . . . .	35
V. SIMULATION ALGORITHM . . . . .	51
VI. NONLINEAR EVOLUTION OF A PRIMARY DISTURBANCE . . . . .	62
VII. EVOLUTION OF SYSTEM WITH RANDOM INITIAL PERTURBATIONS . . . . .	75
VIII. DISCUSSION . . . . .	86
APPENDIX: PROOF OF IDEAL STABILITY . . . . .	92
REFERENCES . . . . .	97
FIGURES . . . . .	101

#### ACKNOWLEDGEMENTS

The principles which guided this work are due to David Montgomery, whose tireless devotion to the study of magnetohydrodynamic turbulence was for me a constant source of inspiration. I am indebted to Thomas A. Zang, who initiated me into the mysteries of computational fluid dynamics. The numerical analysis performed in this dissertation would have been impossible without his assistance. I am grateful to George Vahala for his help in these investigations at a crucial time in my life. The technical and spiritual assistance provided by my wife, Jill, is gratefully acknowledged. Dartmouth College and the Institute for Computer Applications in Science and Engineering have donated computer time without which this research would not have been possible.

## ABSTRACT

The stability and transition properties of a bounded, current carrying magnetofluid are explored, using the hydrodynamic theory developed for plane shear flows as a guide. A driven magnetohydrodynamic sheet pinch equilibrium is employed. A sixth order, complex eigenvalue equation which governs the normal modes of small oscillations is derived, and solved numerically by the Chebyshev tau method. Eigenfunctions are shown, as well as the curve of neutral stability. The locus of critical Lundquist numbers has the form of a hyperbola. The nonlinear stability of a primary disturbance of the system is considered. For regions in parameter space close to criticality, a nonlinear stability equation of the Landau type is derived. These regions are characterized by low values of the Lundquist numbers, in contrast with the inviscid, highly conducting limit considered by Rutherford (1973). Amplitude phase planes for these disturbances are exhibited. The full set of two dimensional magnetohydrodynamic equations is solved numerically by a semi - implicit, mixed Fourier pseudospectral - finite difference algorithm. Both linear and random perturbations of the system are followed numerically into the nonlinear regime. Current sheets and deflection currents are nonlinear structures found to be significant to the evolution of the system. A secondary instability mechanism, the dynamic rupturing of the current density sheet, is also observed.

**STABILITY AND TRANSITION  
OF THE  
DRIVEN MAGNETOHYDRODYNAMIC SHEET PINCH**

## 1. INTRODUCTION

Stability and transition are two central concepts in fluid mechanics. The study of stability focuses on the effect of perturbations on equilibria. Transition studies focus on the passage from laminar to turbulent states, or in a wider sense, on the passage from linearity to nonlinearity. Such problems have been studied in neutral fluids since the time of Helmholtz and Rayleigh, while the interest of the fusion community might be said to date from the seminal paper of Kruskal and Schwarzschild (1954).

Traditionally, the neutral fluid community has focused its theoretical effort on the study of somewhat idealized problems, e.g., plane shear flows, with the ultimate goal of explaining the complex processes by which laminar flows evolve into turbulent flows. There has resulted a development of very powerful numerical and analytical methods. Many of these flows can be realized quite well in the laboratory, so that experimentation has played a very significant role in advancing the understanding of stability and transition phenomena. The experimental results serve as touchstones in judging the relative merit of theories.

On the other hand, the confined fusion theoretical community generally has attempted to solve more realistic problems in the belief that this would hasten the development of a working fusion reactor. The main interest in fusion research has been to determine and understand the processes that thwart plasma confinement. To this end, the fusion models endeavour to account for a wide range of physical phenomena, e.g., compressibility, toroidal effects, complex magnetic field structures, finite Larmor radius effects, etc. This leads to an obviously considerable complication of the governing differential equations.

These difficulties are compounded by the rather low level of experimental information that is available from the current generation of large magnetic confinement devices. Internal probes cannot be maintained at the high operating temperatures in these devices. External diagnostics, such as coils, provide somewhat indirect information about internal magnetic field structure, electric current density, etc. Numerical simulation has been resorted to in order to answer many of the questions about the stability and transition properties of these devices. The results of the simulations are often the only information that is possessed about the internal workings of these devices, so that the numerical algorithms have in no way been subject to the sort of close comparison that occurs between simulation and experiment in the neutral fluid community.

In this dissertation a magnetohydrodynamic configuration, the driven magnetohydrodynamic sheet pinch, will be investigated by using analytical and numerical methods developed for the study of the stability and transition of plane shear flows. First certain aspects of the hydrodynamic theory will be reviewed, and then the magnetohydrodynamic problem will be introduced. Finally, the motivation and structure of this dissertation will be described.

#### A. Review of Hydrodynamic Theory of Plane Poiseuille flow

The hydrodynamic stability theory of plane shear flows has a long history. We will consider the stability theory developed for plane Poiseuille flow as a representative case. Excellent general treatments of this subject are given by Drazin and Reid (1981) and Herbert (1981). The linear stability theory is well reviewed by Lin (1945), while the nonlinear stability theory is well reviewed by Stuart (1971). Good reviews of the computational work are found in Drazin



and Reid (1981), and Gottleib, Bussaini, and Orszag (1984).

The motion of all incompressible neutral Newtonian fluids is governed by the Navier - Stokes equations, written here in dimensionless form ( cf Batchelor (1967), or Yih (1969) ):

$$\frac{\partial \underline{v}}{\partial t} + \underline{v} \cdot \nabla \underline{v} = -\nabla p + \frac{1}{R} \nabla^2 \underline{v}$$

$$\nabla \cdot \underline{v} = 0$$

where:

$\underline{v}$  = dimensionless fluid velocity = ( u (x,y,z), v(x,y,z), w(x,y,z) )

p = mechanical pressure / mass density

R = Reynolds number = (  $U_c L_c$  ) /  $\nu$

$U_c$  = characteristic velocity

$L_c$  = characteristic length

$\nu$  = kinematic viscosity

We consider steady (  $\frac{\partial}{\partial t} \rightarrow 0$  ), unidirectional (  $\underline{v} = ( u(y), 0, 0 )$  ) flow between rigid, parallel, impenetrable walls at  $y = 1$  and  $y = -1$ . No slip boundary conditions are enforced at the walls,  $u( y = 1 ) = u( y = -1 ) = 0$ . It can be shown that  $p = p( x )$ . For the case  $\frac{dp}{dx} = \text{constant}$ , the normalized velocity profile takes the form  $u( y ) = 1 - y^2$ . This type of flow is termed plane Poiseuille flow.

This flow is laminar, since the fluid slides in planes, i.e., fluid in the plane defined by  $y = y_0$  will always remain in this plane. The flows encount-

ered in nature do not tend to remain organized in this way. Instead a high degree of mixing of the fluid is generally observed. In 1928 Davies and White ( cf. Drazin and Reid (1981) ) experimented with pressure driven flows in rectangular channels with large ratios of width to height which approximated well the geometry required for plane Poiseuille flow. They observed that turbulent flows did exist, and found that the behaviour of the flow was parameterized by the Reynolds number. For Reynolds numbers below approximately 1000, the flow would remain laminar asymptotically, whereas for Reynolds numbers approximately 1000, disturbances of the basic flow pattern would either remain or amplify in time, corresponding to a turbulent state. This transitional value of the Reynolds number, approximately 1000, is called the critical Reynolds number. One of the main tasks faced by the hydrodynamic stability theorists has been to produce this critical value of the Reynolds number as a consequence of a model. If a model predicts some other value of the Reynolds number at criticality, then it is clearly deficient.

The first insight into the stability properties of plane Poiseuille flow was provided by Rayleigh in 1880 during the course of a somewhat more general investigation. Rayleigh considered the growth of infinitesimal disturbances in an inviscid Navier - Stokes fluid using a piecewise linear mean flow profile. This inviscid form of the Navier Stokes equations is often called the Euler equations. At this time viscosity was widely believed to have only a dissipative effect, so that presence of finite dissipation would only serve to retard the growth of the ideally unstable modes. Since the disturbances are infinitesimal, the Euler equations can be linearized about the mean flow profile. Using a normal mode analysis, Rayleigh cast the stability problem in the form of an eigenvalue problem. He arrived at the following necessary condition for the existence of instabilities in inviscid plane shear flows - the mean flow profile

must have an inflection point in it for linearly unstable modes to exist, or equivalently, the mean vorticity must have a maximum in the channel. This result implies that plane Poiseuille flow is ideally stable to infinitesimal perturbations that are normal modes of the system since the mean flow profile is non - inflected within the channel.

Several decades later a linear stability theory for viscous plane shear flows began to be developed ( cf Drazin and Reid (1981) ). Orr in 1907 and Sommerfeld in 1908 independently derived a stability equation that has been named in their honor, viz., the Orr - Sommerfeld equation:

$$(D^2 - \alpha^2)^2 \phi = i \alpha R \left[ \left( U_0 - \frac{\omega}{\alpha} \right) (D^2 - \alpha^2) - (D^2 U_0) \right] \phi$$

$$\phi(y=1) = \phi(y=-1) = 0$$

where:

$\phi(y)$  = perturbed stream function

$U_0(y)$  = mean flow profile

$\alpha$  = real parallel wavenumber

$\omega$  = complex frequency

$R$  = Reynolds number

$$D = \frac{d}{dy}$$

For fixed real alpha and R, this equation defines an eigenvalue problem for the complex eigenfrequency  $\omega$ . The mathematical complexity of this equation defied the powers of mathematical analysis available at the time, and its solution remained an outstanding problem in applied mathematics for almost seventy years.

During the 1920's Prandtl showed that viscosity could have a destabilizing effect by inducing Reynolds stresses which transfer momentum from the mean flow to the disturbance. In 1924 Heisenberg obtained the first solutions of the Orr - Sommerfeld equations by employing a singular perturbation theory. He discovered that linear instabilities did exist in plane Poiseuille flow due to the presence of finite viscosity. Furthermore, he calculated the upper branch of the curve of neutral stability for plane Poiseuille flow, as well as obtaining an estimate for the lower branch ( the curve of neutral stability is defined to be the curve in  $(\alpha, R)$  space which separates the stable region from the unstable region ).

In the 1930's an important result was given by Squire. Squire proved that two dimensional linear instabilities were the most dangerous, so that the minimum critical Reynolds number and parallel wavenumber could be determined through consideration of two dimensional disturbances alone.

The analytic theory reached its zenith in the work of C. C. Lin ( Lin (1955) ). Using refined asymptotic analysis, Lin obtained accurate solutions of the Orr Sommerfeld equation for a variety of plane shear flows. He was able to calculate both branches of the neutral stability curve. His 1955 monograph still remains the authoritative book on the subject.

At about the time that Lin's monograph was in preparation, the discipline of computational fluid dynamics was being born. In 1953 L. B. Thomas published the first numerical solution of the Orr - Sommerfeld equation ( Thomas (1953) ). Thomas used a five point Numerov finite difference scheme with about one hundred points on the half channel. He was able to compute eighteen eigenmodes using approximately three hundred hours of computing time on an IBM selective sequential electronic computer. Thomas calculated a critical Reynolds number of 5780, with a critical alpha of 1.026 for plane Poiseuille flow.

Subsequently, many refinements in the numerical method occurred, of which two have special significance to this work. First, several authors attempted to use spectral methods to solve the Orr - Sommerfeld equation ( cf. Dolph and Lewis (1958), Grosch and Salwen (1968) ). Second, Gary and Helgason (1970) developed an iterative method for reducing the Orr - Sommerfeld equation to a standard eigenvalue problem. The standard eigenvalue problem can easily be solved by the QR algorithm ( Wilkinson (1965) ).

These developments culminated in a 1971 paper by Orszag ( Orszag (1971) ). Using Chebyshev polynomials as basis functions, Orszag combined the Lanczos tau method ( cf. Gottleib and Orszag (1977) ) with the iterative method developed by Gary and Helgason and computed the eigenvalues and critical parameters of the Orr Sommerfeld equation to extremely high accuracy. This high accuracy can be attributed to the excellent convergence properties of the Chebyshev polynomials used for the expansion functions. The accuracy is said to be of infinite order, meaning that the truncation error falls off more rapidly than any power of  $N$ , where  $N$  is the number of Chebyshev polynomials retained in the truncated expansion. Orszag calculated a critical Reynolds number of 5772.22, with a critical alpha of 1.02056 for plane Poiseuille flow.

Parallel to the linear stability theory a nonlinear stability theory for plane shear flows has evolved, motivated primarily by the lack of agreement between the linear theory and the experimental results, as well as by the desire to know what happens to the linearly unstable modes when they achieve finite amplitude and excite the nonlinear terms. These nonlinear stability theories share the common attribute of considering the effect of two dimensional finite amplitude perturbations on the stability of the mean flow profile. The differences in the theories occur in the methods used to simplify the nonlinear prob-

lem to allow for successful analysis, or, more to the point, the decisions concerning which terms to discard and which to keep in the analysis. Such decisions must ultimately have some justification in experience. Many of these theories have focused on the perturbation energy balance ( for instance, Stuart (1958), and Joseph (1976) ), often called the Reynolds - Orr energy equation. This approach focuses on the global properties of the fluid and hence minimizes the importance of localized structures. It has been especially useful for determining the lower bounds of the Reynolds number for the existence of instabilities. An alternative approach has been to employ perturbation methods, and this approach has been somewhat more fruitful than the energy methods with respect to discovering subcritical instabilities. An important early result is due to Meksyn and Stuart (1951). By ignoring the generation of higher harmonics ( the mean field approximation ), they showed that subcritical instabilities could occur in plane Poiseuille flow above Reynolds numbers of about 2900, a value still somewhat above the experimental critical value of about 1900, but lower than that predicted by the linear stability theory. Most of the subsequent development has been directed toward the derivation of Landau type nonlinear instability equations ( cf Landau and Lifshitz (1959) ) using analytical perturbation methods (Stuart (1960), Watson (1960), Reynolds and Potter (1967), Herbert (1983) ). An important numerical result was given by Zahn, Toomre, Speigel, and Gough (1974), who solved a highly truncated form of the Navier Stokes equations to determine the stability boundary of plane Poiseuille flow in the parameter space of parallel wavenumber, Reynolds number, and perturbation amplitude.

The inability of the above analyses to produce the experimental critical Reynolds number for plane Poiseuille flow has motivated the study of the problem by means of numerical simulation. It is hoped that such simulations obviate

the need for simplifying assumptions that might prejudice the results of the analysis. Numerical analysis using spectral methods of computation has had an especially large impact on these problems ( Gottlieb and Orszag (1977) ). Three spectral methods in particular have emerged which vary primarily in the manner in which the continuity of the fluid is enforced ( Gottlieb, Hussaini, and Orszag (1984)). Orszag and Kells (1980) have developed a three level time splitting technique in which the fluid incompressibility is enforced at the intermediate time step. They employ Fourier series in the streamwise and spanwise directions, and a Chebyshev series in the cross - stream direction. Moin and Kim employ a semi - implicit time stepping scheme, and solve the continuity equation directly. They also discretize with Fourier series in the streamwise and spanwise directions, but use either Chebyshev series ( Moin and Kim (1980) ) or stretched finite differences ( Moin and Kim (1982) ) in the cross - stream direction. The Navier - Stokes system is reduced to a block tridiagonal form which can be easily inverted. Kleiser and Schumann (1984) have developed a method similar to that of Moin and Kim, except that they solve the Navier - Stokes system of equations by an iterative technique. The Orszag and Kells code in particular has been applied to the problem of transition to turbulence in plane Poiseuille flow, with extremely successful results. They have found that the restriction of the transition problem to two dimensions is an especially severe one. These authors have found transition behaviour near Reynolds numbers of 1000 due to an interaction between three dimensional infinitesimal perturbations and two dimensional finite amplitude perturbations. Orszag and Patera (1983) have speculated that this is a secondary linear instability mechanism.

## B. Magnetohydrodynamic Pinch Configurations

One of the most important goals of the nuclear fusion effort has been to achieve the magnetic confinement of plasmas in configurations stable enough to allow for heating to thermonuclear temperatures. While the mathematical theory of such equilibria is straightforward ( see, for example, Van Kampen and Felderhof (1967) ), in practice any magnetically confined plasma will be perturbed due to startup conditions, impurities, asymmetries, etc. If these perturbations are amplified in time the plasma - magnetic field system is fundamentally altered. This altered configuration interacts with the externally imposed magnetic fields and electric currents of the confinement device in a manner different than what was intended in the design. In all likelihood plasma confinement will no longer be maintained, confounding the expectation of the designer.

Many of the destructive effects of perturbations are illustrated by the axial pinch configuration. Consider a cylindrical tube of plasma. An axial electric current in this plasma cylinder will generate an azimuthal magnetic field. The interaction of the axial electric current with the azimuthal magnetic field produces a radially inward pressure gradient that confines, or pinches, the plasma ( except at the ends, where particle losses are inevitable -- so let the cylinder be infinite in axial extent ).

The most dangerous perturbations to the system are called the ideal magnetohydrodynamic ( MHD ) instabilities ( cf Bateman (1978) ). The plasma is modelled as a perfectly conducting fluid, with the magnetofluid velocity equal to zero in equilibrium. Small displacements in the magnetofluid surface create changes in the external magnetic field, leading to changes in the magnetic



pressure responsible for confining the magnetofluid. These displacements can amplify, contorting the plasma column, and often leading to a loss of confinement.

These ideal MHD instabilities can be controlled in several ways. Application of an axial magnetic field within the magnetofluid column is one method that has proved to be effective. Bulk motion of the magnetofluid caused by the ideal MHD instability tends to compress these magnetic field lines, producing a restoring force that counteracts the destructive perturbation. Stabilization can also be assisted by applying an axial magnetic field external to the magnetofluid column, as well as by surrounding the column by a highly conducting container made of, e.g., copper.

Unfortunately, the story does not end at this point. The total magnetic field, which is now sheared, is highly susceptible to a variety of resistive instabilities. These instabilities all share the common feature that the magnetic field lines can be torn apart and reconnected to form new magnetic field topologies due to the finite resistivity of the magnetofluid. This flux surface distortion can lead to enhanced transport of momentum and energy, magnetofluid turbulence, and the possible breakdown of the stabilization of the ideal MHD modes. The released magnetic energy from the tearing can also be kinetic energy, resulting in high speed motion of the magnetofluid.

A related pinch configuration which retains many of the effects noted above is the magnetohydrodynamic sheet pinch. This pinch consists of an infinite plane current layer in a single fluid magnetofluid with a DC magnetic field reversing sign at the current layer. Structures of this sort are thought to be of importance in several different physical contexts. Interest first arose in the space physics community, where these structures are believed to account for the acceleration of charged particles to high speeds. An excellent review of this

material is given by Sonnerup (1979). The nuclear fusion community has sustained interest in the MHD sheet pinch because of its analytic tractability, as it can be studied in the Cartesian geometry. This study of this configuration has a somewhat briefer history than that of plane shear flows. The fusion oriented theory is well reviewed by White (1983), and also by Menheimer and Lashmore-Davies (1984).

The interest of the fusion community in the stability properties of the magnetohydrodynamic sheet pinch intensified in 1963, when Furth, Killeen, and Rosenbluth published their influential paper on the linear theory of the tearing mode ( Furth, Killeen and Rosenbluth (1963) ). The term "tearing" refers rather graphically to the tendency of the magnetic field lines to break and re-connect in the resistive magnetofluid. They researched these instabilities in an effort to explain the failures of the ideal single fluid MHD stability theory to accurately predict plasma confinement. These authors examined a plane infinite current layer in a compressible inviscid plasma with a sheared zeroth order magnetic field. Limiting themselves to the case of infinitesimal perturbations, they employed a normal mode analysis to formulate the linear stability problem as an eigenvalue problem, which they solved by the method of matched asymptotic expansions in the high resistive Lundquist number limit. They sought to determine conditions for instability, as well as the scaling of the instability growth rates with various parameters of the system. Subsequently, research in this area has dominated a large portion of the theoretical fusion effort.

Wesson (1966) solved the eigenvalue equations given by Furth, et. al, numerically, using an iterative finite difference method. He relaxed the conditions required for the asymptotic analysis, i.e., he solved the same equations in the inner and outer regions, and found substantial agreement with the analytic results. A related computation has been done by DiBiase and Killeen (1977),

who used an initial value method.

The theories dealing with the temporal evolution of the tearing mode have generally followed the evolution of a single linear mode into the nonlinear regime. A theory treating the nonlinear evolution of the tearing mode was given by Rutherford (1973), who considered an inviscid magnetofluid. Neglecting both the inertial terms and the generation of higher harmonics, he determined that the tearing mode should cease to grow exponentially in time, as is appropriate to the linearly unstable modes, and begin to grow algebraically in time when the second order Lorentz forces become large enough to oppose the perturbed flow. This work was extended by White, Monticello, Rosenbluth, and Maddell (1977), who predicted that these algebraically growing modes should saturate nonlinearly due to distortions of the current profile exterior to the tearing mode. These authors considered a highly conducting inviscid magnetofluid, and assumed that the fundamental disturbance would dominate the nonlinear stability process. A recent analysis of interest is due to Pao, Rosenau, and Guo (1983), who consider a viscous magnetofluid.

Computations that have been performed of the nonlinear evolution of the two dimensional magnetohydrodynamic sheet pinch have exhibited some differences, both in terms of the model and the numerical method employed. Schnack and Killeen (1979 and 1980) employed a conservative finite difference scheme, and used an alternating direction implicit temporal discretization. Using an inviscid, compressible model, they followed the nonlinear evolution of eigenmodes of the linearized problem. They found a period of exponential growth, followed by nonlinear saturation. They were particularly interested in determining the nonlinear effects on the structure of the magnetic field. Matthaeus and Montgomery (1981) employed a Fourier spectral ( Galerkin truncation ) method in space and

used second order Runge - Kutta time stepping. They considered a viscoresistive incompressible magnetofluid in a periodic box with sides  $2\pi$  with two current sheets of opposite sign present. Small random perturbations were imposed initially on both the magnetic and velocity fields, and the system was allowed to evolve without any driving. These authors focused on the nonlinear behaviour of the current density, which emphasizes the high frequency components of the magnetic field. They found that highly localized current structures, which they called filaments, would develop. This localization indicated that many of the high frequency components of the magnetic field were excited, a feature indicative of turbulent behaviour. Decay of the mean is significant during the course of this simulation.

### C. Description of Research

In this thesis the evolution in time of the driven magnetohydrodynamic sheet pinch will be considered using analytical and numerical techniques developed for the study of plane shear flow problems in hydrodynamics. This work represents the development of ideas first proposed by Montgomery (1982 and 1984), viz., that due to the similarity of the MHD equations to the equations of ordinary hydrodynamics, the hydrodynamical methods that have been developed for the study of the stability and transition of plane shear flows could be profitably applied to analogous problems in magnetohydrodynamics. This approach has already proven of value in the study of fully developed, homogeneous, isotropic, two dimensional magnetohydrodynamic turbulence ( Fyfe and Montgomery (1976), Fyfe, Joyce and Montgomery (1977), Fyfe, Montgomery and Joyce (1977), Hossain, et al. (1983), Shebalin, et al. (1983) ). A related analysis for the linear

stability of the nondriven MHD sheet pinch, which exploits this similarity of the governing equations, has been given by Dahiburg, Zang, Montgomery and Bussaini (1983).

In chapter II, the governing equations are given and the magnetohydrodynamic equilibrium to be studied is described. In chapter III the linear stability properties of this system are examined both analytically and numerically. A quiescent MHD analogue of the Orr - Sommerfeld equation is derived which is solved numerically by the Chebyshev tau method. The critical parameters are determined, and the curve of neutral stability is computed. A simple relation between the critical viscous and resistive Lundquist numbers for neutrally stable modes is found. In chapter IV a theory of nonlinear stability is given that relies on certain assumptions about the perturbation energy balance. A Reynolds - Orr energy equation for magnetofluids is formulated. A nonlinear stability equation of the Landau type is derived, and some of the nonlinear stability properties of the system are investigated. The amplitude phase plane for a primary disturbance is given. In chapter V a mixed Fourier pseudospectral finite difference algorithm with a semi-implicit time stepping scheme used for numerical simulation of the full set of two dimensional nonlinear partial differential equations that govern the MHD channel system is given. In chapter VI the nonlinear evolution of a primary disturbance is described. The effect of the nonlinear terms is determined. The deformation of the equilibrium and primary disturbance is described. The generation of higher harmonics is also considered. In chapter VII the evolution of the system with random initial perturbations is described. Several nonlinear structures are seen to evolve, including current sheets and deflection currents. A highly nonlinear structure is seen to develop during the magnetic 0 - point coalescence phase. A secondary

instability mechanism, the dynamic rupturing of the electric current density sheet, is observed and a simple model is given. In the appendix an MHD Rayleigh theorem is proved.

## II. EQUILIBRIUM

The equilibrium that we shall consider consists of an infinite plane layer of electric current, with a DC magnetic field reversing sign at the current layer. The fluid velocity is zero. This configuration is customarily referred to the " magnetohydrodynamic sheet pinch " ( cf Matthaeus and Montgomery (1981) ). This dissertation will focus on a driven version of the magnetohydrodynamic sheet pinch. In this driven version the Ohmic dissipation of the magnetic energy is balanced by an external electric field and variation of the resistivity perpendicular to the mean magnetic field.

The magnetofluid under study is confined between parallel, rigid, impenetrable plates. The plates are regarded as perfect conductors coated with a thin layer of insulating material. No slip boundary conditions are imposed on the viscous magnetofluid at the walls. The normal component of the magnetic field is constrained to equal zero at the walls, but the tangential component of the current is unrestricted. The  $x$  direction is regarded as periodic. All variation in  $z$  is ignored, as is consistent with the presence of a strong, constant, uniform, external DC magnetic field.

The behaviour of the magnetofluid is governed by the two dimensional incompressible MHD equations, written in a dimensionless form:

$$\text{II - 1. } \frac{\partial A}{\partial t} + \underline{v} \cdot \nabla A = \eta(y) \nabla^2 A + E$$

$$\text{II - 2. } \frac{\partial \omega}{\partial t} + \underline{v} \cdot \nabla \omega = \underline{\beta} \cdot \nabla J + \mu \nabla^2 \omega$$

where:

$A$  = magnetic vector potential =  $A(x, y, t)$

$\underline{B} = \nabla \times A \hat{e}_z = (B_x, B_y, 0) = \text{magnetic field} = \underline{B}(x, y, t)$

$J = -\nabla^2 A = \text{electric current density} = J(x, y, t)$

$E$  = constant external electric field

$\eta(y)$  = spatially varying dimensionless magnetic diffusivity

$\underline{v} = \text{flow velocity} = (u, v, 0) = \underline{v}(x, y, t)$

$\underline{\omega} = \nabla \times \underline{v} = (0, 0, \omega) \rightarrow \text{magnetofluid vorticity} = \omega(x, y, t)$

$\mu$  = dimensionless kinematic viscosity

Flow speeds are measured in terms of the Alfvén speed,  $C_A = \frac{|B_c|}{\sqrt{4\pi\rho}}$ .

where  $B_c$  is a characteristic value of the mean field, and  $\rho$  is the mass density of the magnetofluid. The characteristic length is taken to be the half channel width.

We consider an equilibrium with zero mean fluid flow. The motivation behind the choice of specification of the magnetic terms arises from the need to balance the magnetic energy losses due to Ohmic dissipation (Furth et al., (1963), Wesson (1966), Maddell et al. (1976)). Proceeding, we specify that  $u = v = 0$  and  $A = A_0(y, t)$ . This specification reduces II - 1 and II - 2 to:

$$\text{II - 3. } \frac{\partial A_0}{\partial t} = \eta(y) \frac{\partial^2 A_0}{\partial y^2} + E$$

$$\text{II - 4. } B_{0x} \frac{\partial J_0}{\partial x} = 0$$

The temporal variation of  $A_0$  can be eliminated by requiring that:



$$\text{II - 5. } \eta(y) = \eta(y=0) \left( \frac{\partial^2 A_0}{\partial y^2} \Big|_{y=0} \right) \left( \frac{\partial^2 A_0}{\partial y^2} \right)^{-1}$$

$$\text{II - 6. } E = - \eta(y=0) \frac{\partial^2 A_0}{\partial y^2} \Big|_{y=0}$$

The constant electric field maintains the resistive equilibrium, and hence is the magnetohydrodynamic equivalent of the applied pressure in plane shear flows. Clearly  $A_0$  must be restricted to functions that do not possess inflection points in the domain  $y = +1$  to  $y = -1$ , i.e., within the channel.

If we regard  $\mu$  and  $\eta(y=0)$  as characteristic dissipation values, then the governing equations (II - 1 and II - 2) can be written in another dimensionless form:

$$\text{II - 7. } \frac{\partial A}{\partial t} + \underline{v} \cdot \nabla A = \frac{\xi(y)}{S} \nabla^2 A + E$$

$$\text{II - 8. } \frac{\partial \omega}{\partial t} + \underline{v} \cdot \nabla \omega = \underline{B} \cdot \nabla J + \frac{1}{M} \nabla^2 \omega$$

where:

$$S = \frac{1}{\eta(y=0)} \quad = \text{resistive Lundquist number}$$

$$\xi(y) = \left( \frac{d^2 A_0}{dy^2} \Big|_{y=0} \right) \left( \frac{d^2 A_0}{dy^2} \right)^{-1} = \text{dimensionless resistivity}$$

$$M = \frac{1}{\mu} \quad = \text{viscous Lundquist number}$$

where Lundquist numbers are simply Reynolds numbers in which the characteristic velocity is defined to be the Alfvén speed  $C_A$ . The magnetic fields are then measured in terms of the externally supported field  $B_0$ .

It is important to note that the dimensionless resistivity  $\eta(y)$  remains fixed in time, although the mean value of the magnetic vector potential can evolve in time if the system is perturbed. The dimensionless resistivity is defined by the value of the undisturbed equilibrium magnetic vector potential field.

For future purposes we define here a dimensionless conductivity function

$\xi$ , defined as:

$$\text{II - 9} \quad \xi(y) = \frac{1}{\eta(y)}$$

No slip boundary conditions are enforced on the velocity field:

$$u(y=1) = u(y=-1) = 0$$

II - 10

$$v(y=1) = v(y=-1) = 0$$

The normal component of the magnetic field is constrained to equal zero at the walls, or:

$$\text{II - 11} \quad A(y=1) = \text{CONSTANT} ; A(y=-1) = \text{CONSTANT}$$

The current density is unrestrained at the walls, as is implied by the thin

insulating coating ( cf Montgomery (1984) ):

$$\text{II - 12} \quad -\nabla^2 A \Big|_{y=1} ; -\nabla^2 A \Big|_{y=-1} \quad \text{UNRESTRAINED}$$

The mean magnetic vector potential that will be studied in depth in this dissertation is the following:

$$\text{II - 13} \quad A_0(y) = y \tan^{-1} \gamma y - \frac{1}{2\gamma} \ln \left( \frac{1 + \gamma^2 y^2}{1 + \gamma^2} \right) - \tan^{-1} \gamma + \frac{\gamma}{5}$$

with the associated magnetic field:

$$\text{II - 14} \quad B_0(y) = \tan^{-1} \gamma y$$

and current density:

$$\text{II - 15} \quad J_0(y) = -\gamma (1 + \gamma^2 y^2)^{-1}$$

where  $\gamma$  = stretch factor.

This specification of mean fields produces a magnetohydrodynamic sheet pinch configuration. There is an infinite plane layer of electric current centred about  $y = 0$ , at which location the mean magnetic field reverses sign. The mean fluid velocity is zero.

These mean fields are plotted for the case  $\gamma = 8$ ,  $M = S = 100$ , in figures II-1, II-2, and II-3 respectively.

In certain applications it will be more convenient to replace II - 7 and II - 8 by the corresponding magnetic induction equations, equations of motion, and an equation of continuity for the magnetofluid:

$$\text{II - 16. } \frac{\partial B_x}{\partial t} + \underline{v} \cdot \nabla B_x = \underline{B} \cdot \nabla v - \frac{1}{s} \frac{d\xi}{dy} J + \frac{E(y)}{s} \nabla^2 B_x$$

$$\text{II - 17. } \frac{\partial B_y}{\partial t} + \underline{v} \cdot \nabla B_y = \underline{B} \cdot \nabla v + \frac{\xi(y)}{s} \nabla^2 B_y$$

$$\text{II - 18. } \frac{\partial u}{\partial t} + \underline{v} \cdot \nabla u = - \frac{\partial p}{\partial x} - J B_y + \frac{1}{m} \nabla^2 u$$

$$\text{II - 19. } \frac{\partial v}{\partial t} + \underline{v} \cdot \nabla v = - \frac{\partial p}{\partial y} + J B_x + \frac{1}{m} \nabla^2 v$$

$$\text{II - 20. } \frac{\partial u}{\partial x} + \frac{\partial v}{\partial y} = 0$$

where  $p$  is defined to be the mechanical pressure divided by the mass density.

In this formulation the perfectly conducting boundary condition can be expressed as:

$$\text{II - 21. } B_y(y=1) = B_y(y=-1) = 0$$

and the current boundary condition becomes:

$$\text{II - 22. } \hat{n} \times \nabla \times \underline{B} \Big|_{y=1} = \hat{n} \times \nabla \times \underline{B} \Big|_{y=-1} = 0$$

where  $\hat{n}$  is defined to be a unit vector normal to the wall.

For the equilibrium specified ( II - 13 ), II - 18 and II - 19 reduce to:

$$11 - 23 \quad \frac{dp}{dy} = -JB_x$$

i.e., the pressure gradient in the magnetofluid is due entirely to the interaction of the equilibrium current with the equilibrium magnetic field. This pressure gradient tends to force the magnetofluid toward the current sheet from either side - hence the name "magnetohydrodynamic sheet pinch".

As is customary in the study of incompressible fluids, it will often be more convenient to use a stream function representation for the velocity field. The stream function  $\psi$  will be related to the components of the velocity field through the following definitions:

$$11 - 24 \quad U = \frac{\partial \psi}{\partial y}$$

$$11 - 25 \quad V = -\frac{\partial \psi}{\partial x}$$

Of course no physical system will exist in as pristine a state as the equilibrium described in this chapter, especially in an extremely complicated experimental device. There will inevitably be noise or some kind of disturbance present. Our objective in the next few chapters will be to determine how the perturbed system will evolve in time.

### III. LINEAR STABILITY

The obvious way to initiate the study of the effects of perturbing this system is to consider the effects of small disturbances, i.e., to consider the linear stability of the system.

What is meant by stability? Consider a system in equilibrium. We impose small disturbances, e.g., the normal modes of small oscillations for this system, on this equilibrium. If these perturbations decrease as a function of time, we define the system as being stable. If the perturbations amplify or remain constant in time, we define the system as being unstable.

When the geometry, boundary conditions, and initial conditions are fixed, the growth rate of these perturbations, as well as their phase velocity and shape, is completely determined by various parameters which define the problem. For the MHD channel system, these parameters are the size of the perturbation in the direction parallel to the mean magnetic field, and the kinematic viscosity and magnetic diffusivity of the magnetofluid. Small variations in these parameters can produce large variations in the temporal evolution of the magnetofluid.

The linear stability of this system is governed by the quiescent magnetohydrodynamic analogue of the Orr - Sommerfeld equation for the stability of plane shear flows. We present here a simple derivation that takes as its starting point equations II - 7 and II - 8. It must be mentioned that the derivation can be done at much greater length if the starting point is the three dimensional MHD equations. In this more complicated case it is possible to prove a "Squire's theorem" which implies the following - If a three dimensional linear instability can be found at a certain set of Lundquist numbers, then a two dimensional linear instability can always be found at a lower value of the Lundquist numbers. This means that the 2-D disturbances are the most unstable

linearly ( cf. Montgomery (1984) ). We now derive the equations that govern the linear stability of the driven MHD sheet pinch.

We start with the governing equations:

$$\text{III - 1} \quad \frac{\partial \omega}{\partial t} + \frac{\partial \psi}{\partial y} \frac{\partial \omega}{\partial x} - \frac{\partial \psi}{\partial x} \frac{\partial \omega}{\partial y} = \underline{B} \cdot \nabla J + \frac{1}{m} \left( \frac{\partial^2 \omega}{\partial x^2} + \frac{\partial^2 \omega}{\partial y^2} \right)$$

$$\text{III - 2} \quad \frac{\partial A}{\partial t} + \frac{\partial \psi}{\partial y} \frac{\partial A}{\partial x} - \frac{\partial \psi}{\partial x} \frac{\partial A}{\partial y} = \frac{\xi(y)}{s} \left( \frac{\partial^2 A}{\partial x^2} + \frac{\partial^2 A}{\partial y^2} \right) + E$$

Linearize these equations about the equilibrium described in the previous chapter, allowing the resistivity and the electric field to remain fixed in time, i.e.,

$$A(x, y, t) = A_0(y) + A_1(x, y, t) = A_0 + a$$

$$\omega(x, y, t) = \omega_0(y) + \omega_1(x, y, t) = \Omega$$

$$\text{III - 3} \quad \psi(x, y, t) = \psi_0(y) + \psi_1(x, y, t) = \phi$$

$$\underline{B}(x, y, t) = B_0(y) \hat{e}_x + \underline{B}_1(x, y, t) = \underline{B}_0 + \underline{b}$$

$$J(x, y, t) = J_0(y) + J_1(x, y, t) = J_0 + J$$

To first order:

$$\text{III - 4} \quad \frac{\partial \Omega}{\partial t} = B_0 \frac{\partial \phi}{\partial x} + b_y \frac{dJ_0}{dy} + \frac{1}{M} \left( \frac{\partial^2 \Omega}{\partial x^2} + \frac{\partial^2 \Omega}{\partial y^2} \right)$$

$$\text{III - 5} \quad \frac{\partial a}{\partial t} - \frac{\partial \phi}{\partial x} \frac{dA_0}{dy} = \epsilon(y) \left( \frac{\partial^2 a}{\partial x^2} + \frac{\partial^2 a}{\partial y^2} \right)$$

This system of linear partial differential equations can be reduced to a system of linear ordinary differential equations in  $y$  by invoking the periodicity in  $x$  and assuming the existence of a complex frequency  $\omega$ . Let:

$$\text{III - 6} \quad f(x, y, t) \longrightarrow f(y) e^{i\alpha x - i\omega t}$$

Upon making this substitution, III - 4 and III - 5 become respectively:

$$\text{III - 7} \quad -i\omega \Omega = i\alpha B_0 \phi + (DJ_0) b_y + \frac{1}{M} (D^2 - \alpha^2) \Omega$$

$$\text{III - 8} \quad -i\omega a - i\alpha (DA_0) \phi = \frac{\epsilon(y)}{S} (D^2 - \alpha^2) a$$

where:  $D \equiv \frac{d}{dy}$   
Note that:

$$\Omega \equiv -\nabla^2 \phi \longrightarrow -(D^2 - \alpha^2) \phi$$



$$\text{III - 9} \quad b_y = -\frac{\partial a}{\partial x} = -i\kappa a$$

$$j \equiv -\nabla^2 a \rightarrow -(D^2 - \kappa^2)a$$

$$J_0 = -D^2 A_0$$

$$B_0 = DA_0$$

Substituting these quantities into III - 7 and III - 8 and rearranging:

$$(D^2 - \kappa^2)^2 \phi = -i\omega M (D^2 - \kappa^2) \phi$$

$$\text{III - 10} \quad -i\kappa M (DA_0) (D^2 - \kappa^2)a + i\kappa M (D^3 A_0)a$$

$$\text{III - 11} \quad \{D^2 - \kappa^2 + i\omega S \zeta(y)\} a = -i\kappa S \zeta(y) (DA_0) \phi$$

No - slip boundary conditions are enforced on the velocity field:

$$\phi(y=1) = \phi(y=-1) = 0$$

III - 12

$$\left. \frac{d\phi}{dy} \right|_{y=1} = \left. \frac{d\phi}{dy} \right|_{y=-1} = 0$$

The magnetic perturbation is constrained to equal zero at the walls:

$$\text{III - 13} \quad a(y=1) = a(y=-1) = 0$$

These equations represent the quiescent magnetohydrodynamic analogue of

the Orr - Sommerfeld equation for the linear stability of plane shear flows. Furth et. al. have, to some extent, studied the  $M = \infty$ , high  $S$  limit of this system. A related system was studied in greater detail by Dahlburg, et al. (1983), who studied the linear stability of magnetic quasi - equilibria. In that study, the resistivity profile is uncoupled from the mean magnetic vector potential, and there is no external electric field. The linear stability properties of that system and the one studied in this chapter are similar since the resistivity is only significant in the region of the current sheet.

III - 10 and III - 11 are a sixth order, complex set of linear ordinary differential equations. The complicated form of the system makes it analytically intractable. One way to alleviate the difficulty of the analytical problem is to reduce the order of the system of equations by passing to the ideal limit. This is equivalent to examining the limit of infinite  $M$  and  $S$ . In this limit the linear stability equations become:

$$\text{III - 10} \quad 0 = \omega(D^2 - \alpha^2)\phi + \alpha[(DA_0)(D^2 - \alpha^2) - (D^3A_0)]a$$

$$\text{III - 11} \quad \omega = -\alpha(DA_0)\phi$$

In the appendix it is shown that this system is stable to linear perturbations for any choice of equilibrium magnetic field. Hence it can be concluded that any instabilities that occur must be a consequence of finite dissipation.

Equations III - 10 and III - 11 are solved numerically by the Chebyshev tau method as adapted for the Orr-Sommerfeld equation by Orszag (1971). The numeri-

cal method is described in detail in Dahlburg, et al. (1983). We present here a short summary. The various field variables are expanded in Chebyshev series, and the system of equations is truncated by the Lanczos tau method (Gottlieb and Orszag (1977)). Only odd Chebyshev polynomials are needed for the perturbed stream function, while only even Chebyshev polynomials are required for the magnetic eigenfunction. The resulting generalized eigenvalue problem is reduced by the iterative method of Gary and Belgason (1978) to a standard eigenvalue problem. This standard eigenvalue problem is solved by the QR algorithm (Wilkinson (1965)). For cases in which a solution is known, and solutions that are nearby in the parameter space are desired, it is computationally more efficient to replace the step involving the QR algorithm with an iterative method. In these cases inverse Rayleigh - power iteration is employed (Dahlquist, et al. (1974), Ortega and Poole (1981)). This iterative method is especially useful in the computation of the neutral curve.

We find the following results numerically:

1. Linearly unstable modes were not found to exist for mean current density profiles without inflection points in the domain  $y = +1$  to  $y = -1$ . The profiles of this kind that were tested were found to be linearly stable at extremely large values of the Lundquist numbers, on the order of 100,000. In contrast, mean current density profiles with inflection points in the domain  $y = +1$  to  $y = -1$  were found to be linearly unstable at extremely low values of the Lundquist numbers, on the order of 10. Steep current gradients alone were insufficient to provoke linearly unstable modes. No analytical proof of these results has emerged.
2. For those profiles that are linearly unstable, the phase velocities of the unstable modes are always seen equal to zero. This has an important consequence for the eigenfunctions. Let  $p = i(\omega)$ ,  $g = ia$ . Upon substitution,

equations III - 10 and III - 11 become, respectively:

$$(D^2 - \alpha^2)^2 \phi = -\rho M (D^2 - \alpha^2) \phi - \alpha M [(DA_0)(D^2 - \alpha^2) - (D^2 A_0)] g$$

$$\{D^2 - \alpha^2 + \rho S \zeta(y)\} g = \alpha S \zeta(y) (DA_0) \phi$$

Consider cases with  $\rho$  real ( i.e., with  $\omega$  purely imaginary ):

$$(D^2 - \alpha^2)^2 \phi = \omega_i M (D^2 - \alpha^2) \phi - \alpha M [(DA_0)(D^2 - \alpha^2) - (D^2 A_0)] g$$

$$\{D^2 - \alpha^2 - \omega_i S \zeta(y)\} g = \alpha S \zeta(y) (DA_0) \phi$$

By inspection of the above equations it can be seen that the real and imaginary parts of  $\phi$  and  $g$  satisfy the same set of ordinary differential equations. This implies that solutions of these equations are possible in which the imaginary fields are simple multiples of the real fields. The computer code gives the result that, for the linearly unstable modes, the imaginary part of  $a$  and the real part of  $\phi$  are equal to zero. Hence we only consider the real part of  $a$  and the imaginary part of  $\phi$ .

Figure III - 1 shows the unstable magnetic eigenfunction for  $\alpha = 1$ ,

$M = S = 50$ , and  $\gamma = 8$ . Figure III - 2 shows the unstable velocity eigenfunction for the same parameters. Figure III - 3 shows the root mean square  $x$  component of this perturbed magnetic field. Figure III - 4 shows the root mean square  $y$  component of this magnetic field. Figure III - 5 shows the root mean square  $x$  component of this velocity field. Figure III - 6 shows the root mean square  $y$  component of this velocity field.

Figure III - 7 shows the unstable magnetic eigenfunction for  $\alpha = 1$ ,  $M = S = 100$ , and  $\gamma = 0$ . Figure III - 8 shows the unstable velocity eigenfunction for the same parameters. The effect of raising the Lundquist numbers on the eigenfunctions can be seen by comparing these figures with figures III - 1 and III - 2 respectively. The regions of maximum value of the magnetic eigenfunction are seen to move away from  $y = 0$ , while the "hollow" in the centre becomes relatively deeper. The region of maximum velocity eigenfunction are seen to move toward  $y = 0$ , and the gradient of the eigenfunction at the centre increases. The variation of the eigenfunctions with respect to Lundquist number is dealt with more thoroughly by Dahlburg, et al. (1983), for a closely related case.

3. For the non-conducting fluid, only one dissipative mechanism exists. Hence the zone of zero growth rate can be characterized by the curve in  $(\alpha, R)$  space which separates the stable and unstable modes. In contrast, the magnetofluid has two dissipative mechanisms, and thus the zero growth rate zone has the form of a surface in the  $(\alpha, M, S)$  space. A representative "slice" of this neutral surface for the case  $B_0(y) = \arctan(8y)$  is shown in figure III - 9. This "slice", or neutral curve, is taken in the  $(\alpha, M)$  plane with  $S$  held constant at 100. The neutral curve in the  $(\alpha, S)$  space with  $M$  held constant at 100 is geometrically congruent. The form of the neutral curve indicates that stabilization of the modes can always be achieved by decreasing the Lundquist numbers to a sufficiently low enough value. Stabilization is also achieved at both sufficiently high and low enough wavelengths of the disturbance.

On this neutral surface,  $\omega_i = 0$  by definition. Combining this with the previous result (2.) gives :

$$\omega = \omega_r + \omega_i = 0$$

on the neutral surface.

Substituting this result into the linear stability equations ( III - 10 and III - 11 ) gives:

$$(D^2 - \alpha^2)^2 \phi = -i\alpha M (DA_0) (D^2 - \alpha^2) a + i\alpha M (D^3 A_0) a$$

$$(D^2 - \alpha^2) a = -i\alpha S_0^2(y) (DA_0) \phi$$

These equations can be rescaled in terms of one Lundquist number in a variety of different ways. For instance, let  $f = Ma$ . Substituting:

$$(D^2 - \alpha^2)^2 \phi = -i\alpha (DA_0) (D^2 - \alpha^2) f + i\alpha (D^3 A_0) f$$

$$(D^2 - \alpha^2) f = -i\alpha \mathcal{R} S_0^2(y) (DA_0) \phi$$

where  $\mathcal{R} = MS$  is the new Lundquist number. The stability boundary is then determined by this one Lundquist number  $\mathcal{R}$  and the critical  $\alpha$ .

This result implies the existence of a " stability hyperbola " defined by the locus of critical points in the  $M - S$  plane for a unique critical  $\alpha$ . For instance, for  $B_0(y) = \tan^{-1} y$ , it is found numerically that:

$$\mathcal{R}_c = S_c M_c = 1073$$

for  $\alpha_c = 1.4$ . The critical locus is shown in figure III - 10.

This result has recently been confirmed in the course of somewhat different analyses by Horton, Tajima, and Galvao (1983) and by Bondeson and Sobel (1984).

#### IV. NONLINEAR STABILITY

A linearly unstable mode will enlarge itself exponentially in time. At some time during its evolution it will attain a large enough amplitude that the nonlinear terms in the governing equations will no longer be negligible. These nonlinear terms will then act by several processes to alter progressively the system in ways that invalidate the assumptions underlying the linear approximation.

What are these nonlinear processes that occur when the linear disturbance attains finite amplitude? In order to simplify this problem, consider a single eigenmode that varies as  $\exp(ix)$ , often called a primary disturbance. When this disturbance attains finite amplitude, it can interact with itself through the nonlinear terms in the governing equations. This self-interaction will give rise to the first harmonic of the disturbance, often called the secondary disturbance. This new mode can also participate in the exchange of energy with the mean field, so that the energy budget of the system is fundamentally altered by its presence. The primary disturbance will also interact with its own complex conjugate, the result being the deformation of the mean magnetic field. This deformation of the mean field alters the rate of energy transfer between the mean field and the primary disturbance. Hence the growth of the primary disturbance can no longer be characterized by the linear growth rate.

The interaction of the primary disturbance with itself and with its complex conjugate produce the highest order nonlinear effects. By the same sort of processes even higher harmonics of the primary disturbance can be created and the primary disturbance itself can be deformed. The extent of the excitation of higher harmonics is limited only by the level of dissipation present in the system.



It is legitimate to ask what the consequences are of the linear perturbations achieving finite amplitude? The severe nonlinearities present in the governing equations make the analytic exploration of this question difficult. However, by making certain assumptions, some analytic headway can be made.

We can determine the first order nonlinear correction of the mean magnetic vector potential equation due to the finite Lorentz forces. It is assumed that the only significant nonlinear interaction occurs between the mean magnetic vector potential and its primary disturbance. Hence the generation of higher harmonics of the disturbances is considered to be negligible by hypothesis.

First consider the magnetic vector potential equation:

$$IV - 1 \quad \frac{\partial A}{\partial t} + \frac{\partial \psi}{\partial y} \frac{\partial A}{\partial x} - \frac{\partial \psi}{\partial x} \frac{\partial A}{\partial y} = \frac{\xi(y)}{S} \left( \frac{\partial^2 A}{\partial x^2} + \frac{\partial^2 A}{\partial y^2} \right) + E$$

Isolate the linear terms from the nonlinear terms:

$$IV - 2 \quad \frac{\partial A}{\partial t} - \frac{\xi(y)}{S} \left( \frac{\partial^2 A}{\partial x^2} + \frac{\partial^2 A}{\partial y^2} \right) - E = -\frac{\partial \psi}{\partial y} \frac{\partial A}{\partial x} + \frac{\partial \psi}{\partial x} \frac{\partial A}{\partial y}$$

Expand  $A$  and  $\psi$ , allowing for a mean part, the primary disturbance, and its complex conjugate. Let:

$$A(x, y, t) = A_0(y, t) + a(y, t) e^{i\alpha x} + a^*(y, t) e^{-i\alpha x}$$

IV - 3

$$\psi(x, y, t) = \varphi(y, t) e^{i\alpha x} + \varphi^*(y, t) e^{-i\alpha x}$$

Substituting these terms into IV - 2 will give, after averaging over  $x$ :

$$\text{IV - 4} \quad \frac{\partial A_0}{\partial t} - \frac{\xi(y)}{S} \frac{\partial^2 A_0}{\partial y^2} - E = i\alpha \frac{\partial}{\partial y} (a^* \varphi - a \varphi^*)$$

Near the neutral surface, or in the vicinity of a secondary equilibrium, the growth or decay of the perturbation should be negligible, i.e.,  $\frac{\partial A_0}{\partial t} \approx 0$ . This equation will then give an expression for the distortion of the mean current profile.

$$\text{IV - 5} \quad -\frac{d^2 A_0}{dy^2} \equiv J_0(y) = S \zeta(y) E + i\alpha S \zeta(y) \frac{\partial}{\partial y} (a^* \varphi - a \varphi^*)$$

The first term on the right is just the initial unperturbed current profile. The second term represents the distortion of this current profile caused by the action of the perturbation Lorentz forces.

Second, we derive an expression for the perturbation energy balance. It is necessary first to give the magnetic induction equations for the variable resistivity case ( equations II - 16 to II - 20 ). The equation for  $B_x$  is:

$$\text{IV - 6} \quad \frac{\partial B_x}{\partial t} + \underline{v} \cdot \nabla B_x = \underline{B} \cdot \nabla v - \frac{1}{S} \frac{d\xi}{dy} J + \frac{\xi(y)}{S} \left( \frac{\partial^2 B_x}{\partial x^2} + \frac{\partial^2 B_x}{\partial y^2} \right)$$

The  $B_y$  equation is unaltered except for the dissipative term:

$$\text{IV - 7} \quad \frac{\partial B_y}{\partial t} + \underline{v} \cdot \nabla B_y = \underline{B} \cdot \nabla v + \frac{\xi(y)}{S} \left( \frac{\partial^2 B_y}{\partial x^2} + \frac{\partial^2 B_y}{\partial y^2} \right)$$

The equations of motion governing the velocity field are:

$$\text{IV - 8} \quad \frac{\partial u}{\partial t} + \underline{v} \cdot \nabla u = -\frac{\partial p}{\partial x} - J B_y + \frac{1}{M} \left( \frac{\partial^2 u}{\partial x^2} + \frac{\partial^2 u}{\partial y^2} \right)$$

$$\text{IV - 9} \quad \frac{\partial v}{\partial t} + \underline{v} \cdot \nabla v = -\frac{\partial p}{\partial y} + J B_x + \frac{1}{M} \left( \frac{\partial^2 v}{\partial x^2} + \frac{\partial^2 v}{\partial y^2} \right)$$

The continuity of the fluid is assumed.

Linearize IV - 6 through IV - 9 about the equilibrium described in chapter II, allowing for the mean field to have some time dependence. Hence the perturbed magnetic field is here being defined as the difference between the total magnetic field and the mean magnetic field.

$$\text{IV - 10} \quad \frac{\partial b_x}{\partial t} + v \frac{\partial B_0}{\partial y} = B_0 \frac{\partial v}{\partial x} - \frac{1}{S} \frac{dJ}{dy} J + \frac{J(y)}{S} \left( \frac{\partial^2 b_x}{\partial x^2} + \frac{\partial^2 b_x}{\partial y^2} \right)$$

$$\text{IV - 11} \quad \frac{\partial b_y}{\partial t} = B_0 \frac{\partial v}{\partial x} + \frac{J(y)}{S} \left( \frac{\partial^2 b_y}{\partial x^2} + \frac{\partial^2 b_y}{\partial y^2} \right)$$

$$\text{IV - 12} \quad \frac{\partial u}{\partial t} = -\frac{\partial p}{\partial x} - J_0 b_y + \frac{1}{M} \left( \frac{\partial^2 u}{\partial x^2} + \frac{\partial^2 u}{\partial y^2} \right)$$

$$\text{IV - 13} \quad \frac{\partial v}{\partial t} = -\frac{\partial p}{\partial y} + J_0 b_x - J B_0 + \frac{1}{M} \left( \frac{\partial^2 v}{\partial x^2} + \frac{\partial^2 v}{\partial y^2} \right)$$

We now derive an expression for the perturbation energy densities; first the magnetic, then the kinetic, and finally the total perturbation energy density equation.

Multiply IV - 10 by  $b_x$ , IV - 11 by  $b_y$ , and then add the results. After some rearrangement, this gives the following expression for the perturbation magnetic energy density:

$$\frac{1}{2} \frac{\partial}{\partial t} (b_x^2 + b_y^2) = - \frac{dB_0}{dy} v b_x + B_0 \left( \frac{\partial u}{\partial x} b_x + \frac{\partial v}{\partial x} b_y \right)$$

IV - 14

$$+ \frac{\xi(y)}{S} (b_x \nabla^2 b_x + b_y \nabla^2 b_y) - \frac{1}{S} \frac{d\xi}{dy} j b_x$$

Multiply IV - 12 by  $u$ , IV - 13 by  $v$ , and then add the results. After some rearrangement, this gives the following expression for the kinetic energy density:

$$\frac{1}{2} \frac{\partial}{\partial t} (u^2 + v^2) = - \left( u \frac{\partial p}{\partial x} + v \frac{\partial p}{\partial y} \right) - J_0 u b_y$$

IV - 15

$$+ J_0 v b_x + B_0 v j + \frac{1}{M} (u \nabla^2 u + v \nabla^2 v)$$

Adding IV - 14 and IV - 15 gives an expression for the perturbation energy density:

$$\frac{1}{2} \frac{\partial}{\partial t} (u^2 + v^2 + b_x^2 + b_y^2) = -(u \frac{\partial p}{\partial x} + v \frac{\partial p}{\partial y}) - \frac{dB_0}{dy} v b_x$$

IV - 16

$$+ B_0 (b_x \frac{\partial u}{\partial x} + b_y \frac{\partial v}{\partial x}) - J_0 u b_y + J_0 v b_x + B_0 v j$$

$$- \frac{1}{S} \frac{d\xi}{dy} j b_x + \frac{\xi(y)}{S} (b_x \nabla^2 b_x + b_y \nabla^2 b_y)$$

$$+ \frac{1}{M} (u \nabla^2 u + v \nabla^2 v)$$

We simplify IV - 16 by noting that:

$$\nabla^2 b_x = -\frac{\partial j}{\partial y} ; \nabla^2 b_y = \frac{\partial j}{\partial x} ;$$

IV - 17

$$\nabla^2 u = -\frac{\partial \omega}{\partial y} ; \nabla^2 v = \frac{\partial \omega}{\partial x}$$

Substituting this result into IV - 16 gives:

$$\frac{1}{2} \frac{\partial}{\partial t} (b_x^2 + b_y^2 + u^2 + v^2) = -(u \frac{\partial p}{\partial x} + v \frac{\partial p}{\partial y}) - \frac{dB_0}{dy} v b_x$$

$$+ B_0 (b_x \frac{\partial u}{\partial x} + b_y \frac{\partial v}{\partial x}) - J_0 u b_y + J_0 v b_x + B_0 v j$$

IV - 18

$$- \frac{1}{S} \frac{d\xi}{dy} j b_x + \frac{\xi(y)}{S} (b_y \frac{\partial j}{\partial x} - b_x \frac{\partial j}{\partial y})$$

$$+ \frac{1}{M} (v \frac{\partial \omega}{\partial x} - u \frac{\partial \omega}{\partial y})$$

We integrate IV - 18 between the walls at  $y = \pm 1$  and over one period in  $x$  to obtain an expression for the perturbation energy balance. It is assumed that the field variables are periodic in  $x$ . No - slip boundary conditions are im-

posed on the velocity field:

$$u(y=1) = u(y=-1) = 0$$

$$v(y=1) = v(y=-1) = 0$$

The normal component of the perturbed magnetic field is constrained to equal zero at the walls:

$$b_y(y=1) = b_y(y=-1) = 0$$

After some manipulation, we possess the following expression for the perturbation energy balance:

$$\begin{aligned} & \frac{1}{2} \frac{\partial}{\partial t} \int_0^{2\pi} \int_{-1}^1 (u^2 + v^2 + b_x^2 + b_y^2) dx dy = \\ \text{IV - 19} \quad & \int_0^{2\pi} \int_{-1}^1 (u b_y - v b_x) \frac{\partial B_0}{\partial y} dx dy \\ & - \frac{1}{M} \int_0^{2\pi} \int_{-1}^1 \omega^2 dx dy - \frac{1}{S} \int_0^{2\pi} \int_{-1}^1 \xi(y) j^2 dx dy \end{aligned}$$

This integral equation is the driven magnetohydrodynamic equivalent of the Reynolds - Orr energy equation for neutral fluids. The integral term on the left hand side is simply the perturbed energy, magnetic and kinetic. The first term on the right represents the action of the Lorentz forces in moving energy

between the mean and perturbed fields. We will call it the interchange integral. The interchange integral can be either positive or negative. If it is positive, then there is a draining of energy from the mean field to the perturbed fields. If it is negative, then there is a transfer of energy from the perturbed fields to the mean field. The form of the mean magnetic field is seen to be important to the energy interchange. The interchange integral implies that no unstable mode is possible unless the second  $y$  derivative of the mean magnetic field is zero, i.e., the mean electric current density cannot be constant in  $y$ . Obviously if the mean magnetic field is allowed to change with time, then the exchange of energy between the mean and perturbed fields will also change with time. The second integral on the right hand side represents the viscous dissipation of kinetic energy. The third integral on the right hand side represents the Ohmic dissipation of perturbed magnetic energy. The viscous integral and the Ohmic integral are always positive, and both will always serve to decrease the perturbed energy. The only circumstance in which unstable modes will exist is when the interchange integral is positive and greater in magnitude than the sum of the viscous and Ohmic integrals combined.

By employing a method introduced by Stuart (1958) we can obtain some information about the nonlinear stability properties of the primary disturbance. We first rewrite IV - 19 in terms of the stream function  $\psi$  and the magnetic vector potential  $A = A_0 + a$ :

$$\frac{1}{2} \frac{\partial}{\partial t} \int_0^{2\pi} \int_{-1}^1 \left[ \left( \frac{\partial \psi}{\partial y} \right)^2 + \left( \frac{\partial \psi}{\partial x^2} \right)^2 + \left( \frac{\partial a}{\partial y} \right)^2 + \left( \frac{\partial a}{\partial x} \right)^2 \right] dx dy =$$

$$\int_0^{2\pi} \int_{-1}^1 \left[ \frac{\partial \psi}{\partial x} \frac{\partial a}{\partial y} - \frac{\partial \psi}{\partial y} \frac{\partial a}{\partial x} \right] \left( \frac{\partial^2 A_0}{\partial y^2} \right) dx dy$$

IV - 20

$$- \frac{1}{M} \int_0^{2\pi} \int_{-1}^1 \left( \frac{\partial^2 \psi}{\partial x^2} + \frac{\partial^2 \psi}{\partial y^2} \right)^2 dx dy$$

$$- \frac{1}{S} \int_0^{2\pi} \int_{-1}^1 \xi(y) \left( \frac{\partial^2 a}{\partial x^2} + \frac{\partial^2 a}{\partial y^2} \right)^2 dx dy$$

If we assume that only the primary disturbance and its complex conjugate are significant, then:

$$A(x, y, t) = A_0(y, t) + a(y, t) e^{i\alpha x} + a^*(y, t) e^{-i\alpha x}$$

IV - 21

$$\psi(x, y, t) = \phi(y, t) e^{i\alpha x} + \phi^*(y, t) e^{-i\alpha x}$$

We now employ the "shape assumption". We assume that the primary disturbance is equal to the eigenfunction of the linearized problem multiplied by a time amplification factor  $\lambda(t)$ :

$$A(x, y, t) = A_0(y, t) + \lambda(t) \left[ a(y) e^{i\alpha x} + a^*(y) e^{-i\alpha x} \right]$$

IV - 22

$$\psi(x, y, t) = \lambda(t) \left[ \phi(y) e^{i\alpha x} + \phi^*(y) e^{-i\alpha x} \right]$$



where  $a(y)$  and  $\varphi(y)$  are understood to be the eigenfunctions of the linearized problem.

For parameter regions near the neutral curve, or in the vicinity of the a secondary equilibrium, the growth rate of the disturbance will be negligible. Hence the  $\frac{\partial^2 A_0}{\partial y^2}$  term in the Lorentz force integral can be replaced by the equivalent expression IV - 5, which by the shape assumption becomes:

$$\text{IV - 23} \quad \frac{d^2 A_0}{dy^2} = -S\zeta(y)E + 2\alpha S\lambda^2 \zeta(y) \frac{d}{dy}(a_r \varphi_i)$$

We make these substitutions and evaluate the  $x$  integrals. After several pages of algebra, the following expression for the perturbation energy balance is derived:

$$\begin{aligned} & \sum \int_{-1}^1 \left[ \left( \frac{d\varphi_i}{dy} \right)^2 + \alpha^2 \varphi_i^2 + \left( \frac{da_r}{dy} \right)^2 + \alpha^2 a_r^2 \right] dy \Big\} \frac{d\lambda^2}{dt} = \\ & - 2\alpha^2 S \sum \int_{-1}^1 \zeta(y) \left[ \frac{d}{dy}(a_r \varphi_i) \right]^2 dy \Big\} \lambda^4 \\ & + 2\alpha S E \sum \int_{-1}^1 \zeta(y) \frac{d}{dy}(a_r \varphi_i) dy \Big\} \lambda^2 \\ & - \frac{2}{M} \sum \int_{-1}^1 \left[ \left( \frac{d^2 \varphi_i}{dy^2} \right)^2 + 2\alpha^2 \left( \frac{d\varphi_i}{dy} \right)^2 + \alpha^4 \varphi_i^2 \right] dy \Big\} \lambda^2 \\ \text{IV - 24} \quad & - \frac{2}{S} \sum \int_{-1}^1 \left[ \zeta \left( \frac{d^2 a_r}{dy^2} \right)^2 + \zeta \alpha^4 a_r^2 \right. \\ & \left. + \alpha^2 \left[ 2\zeta \left( \frac{da_r}{dy} \right)^2 - \frac{d^2 \zeta}{dy^2} a_r^2 \right] \right] dy \Big\} \lambda^2 \end{aligned}$$

where  $\phi_i$  = imaginary part of the stream function eigenfunction

$a_r$  = real part of the magnetic vector potential eigenfunction

IV - 24 has the form:

$$\text{IV - 25} \quad \gamma_1 \frac{d\lambda^2}{dt} = -2\alpha^2 S \gamma_2 \lambda^4 + 2 \left( \alpha S E \gamma_3 - \frac{\gamma_4}{M} - \frac{\gamma_5}{S} \right) \lambda^2$$

where:

$$\gamma_1 \equiv \int_{-1}^1 \left[ \left( \frac{d\phi_i}{dy} \right)^2 + \alpha^2 \phi_i^2 + \left( \frac{da_r}{dy} \right)^2 + \alpha^2 a_r^2 \right] dy$$

$$\gamma_2 \equiv \int_{-1}^1 \zeta(y) \left[ \frac{d}{dy} (a_r \phi_i) \right]^2 dy$$

$$\gamma_3 \equiv \int_{-1}^1 \zeta(y) \frac{d}{dy} (a_r \phi_i) dy$$

IV - 26

$$\gamma_4 \equiv \int_{-1}^1 \left[ \left( \frac{d^2 \phi_i}{dy^2} \right)^2 + 2\alpha^2 \left( \frac{d\phi_i}{dy} \right)^2 + \alpha^4 \phi_i^2 \right] dy$$

$$\gamma_5 \equiv \int_{-1}^1 \left\{ \xi(y) \left( \frac{d^2 a_r}{dy^2} \right)^2 + \xi(y) \alpha^4 a_r^2 + \alpha^2 \left[ 2\xi \left( \frac{da_r}{dy} \right)^2 - \frac{d^2 \xi}{dy^2} a_r^2 \right] \right\} dy$$

If we define:

$$C_1 \equiv \frac{2}{\gamma_1} \left( \alpha SE \gamma_3 - \frac{\gamma_4}{M} - \frac{\gamma_5}{S} \right) \quad 46$$

$$\text{IV - 27} \quad C_2 \equiv \frac{2\alpha^2 S}{\gamma_1} \quad (\equiv \text{LANDAU CONSTANT})$$

then IV - 25 reduces to:

$$\text{IV - 28} \quad \frac{d\lambda^2}{dt} = C_1 \lambda^2 - C_2 \lambda^4$$

If we define  $\theta = \lambda^2$ , IV - 28 is further simplified:

$$\text{IV - 29} \quad \frac{d\theta}{dt} = C_1 \theta - C_2 \theta^2$$

This equation for the amplitude evolution was first presented by Landau ( cf Landau and Lifshitz (1959) ), and is widely believed to represent the essence of the evolution of nonlinear perturbations on certain systems in the vicinity of the instability threshold ( Herbert (1983) ).

Certain properties of IV - 29 are immediately discernible. For linear disturbances the  $C_2 \theta^2$  term is by definition negligible. This means that the linear growth rate of the energy will be given by  $C_1$ , i.e., by equation IV - 27. If this linear disturbance saturates nonlinearly, then IV - 29 reduces to:

$$\text{IV - 30} \quad 0 = C_1 \theta - C_2 \theta^2$$

and the square of the saturated amplitude is given by:

$$\text{IV - 31} \quad \theta_e = \frac{C_1}{C_2}$$

The expression for the linear growth rate and will be used as a check on the accuracy of the numerical work. This is done by comparing these results with the benchmark results of the eigenvalue code.

Consider the case:

$$\text{IV - 32} \quad B_0(y) = \tan^{-1} \kappa y$$

This implies:

$$\xi(y) = 1 + \kappa^2 y^2$$

IV - 33

$$SE = -\kappa$$

The expression for the linear growth rate ( IV - 27 ) reduces to:

$$\text{IV - 34} \quad - \frac{2}{\gamma_1} \left( \alpha \kappa \gamma_3 + \frac{\gamma_4}{M} + \frac{\gamma_5}{S} \right)$$

The integrals are evaluated accurately by using Simpson's method.

Let the stretch factor  $\kappa = 8$ , and  $\alpha = 1$ . The eigenvalue code gives the the following results for the unstable eigenmode:

CASE # 1 ( M = 5 = 59 ) .  
-----

$$\omega_i = 0.090282$$

IV - 35

CASE # 2 ( M = 6 = 100 )  
-----

$$\omega_i = 0.18223$$

The nonlinear theory gives:

CASE # 1  
-----

$$\omega_i = \frac{c_1}{2} = 0.090278$$

$$c_2 = 1506$$

$$\theta_e = 0.0001374$$

$$\lambda_e = 0.01172$$

IV - 36

CASE # 2  
-----

$$\omega_i = \frac{c_1}{2} = 0.18183$$

$$c_2 = 2186$$

$$\theta_c = 0.0001664$$

$$\lambda_c = 0.01290$$

The amplitude phase plane for CASE # 1 is shown in figure IV - 1, and that for CASE # 2 is shown in figure IV - 2 ( in these plots,  $p$  is defined be the square of the amplitude, i.e.,  $p = \theta$ , and  $p'$  is defined to be the time derivative of  $p$ ). Several features are common to both plots. Near  $p = \theta$  a region of exponential growth is observed. As  $p$  increases in magnitude, the time derivative reaches a maximum and ultimately begins to decay. At the saturation amplitude the growth rate is, by definition, equal to zero. Above the saturation amplitude the growth rate is zero, indicating that a solution with a larger amplitude will decay until it achieves the saturation amplitude. Hence, the point on the curve associated with the saturation amplitude is an attractor in the phase space. By way of comparison, CASE # 2 achieves larger values of  $p'$  than CASE # 1 does, and is predicted to saturate at a larger amplitude.

The distortion of the mean current profile is predicted by equation IV - 23. Figure IV - 3 shows the initial mean current profile for CASE # 1. The perturbed current density for this case is shown in figure IV - 4, and the distorted mean current density profile is shown in figure IV - 5. The analogous results for CASE # 2 are shown in figures IV - 6 through IV - 8. As is consistent with the results of the previous paragraph, the distortion of the mean current density profile is larger at the higher Lundquist numbers.

This analysis implies that the primary disturbance will saturate nonlinearly into a secondary nonturbulent equilibrium, i.e., the nonlinear terms will act to move the system to a 'smooth' final state. This secondary equilibrium can itself be unstable to small perturbations, so that a series of such tran-

sitions is possible. It is necessary, however, to bear in mind that the many simplifying assumptions made in this analysis have caused the neglect of many processes that might have turned out to be of importance, e.g., the generation of higher harmonics, the deformation of the primary disturbance, rapid alterations of the mean magnetic field, etc. Inclusion of any one of these effects could alter the conclusions.

This chapter has illustrated the difficulties involved in mathematical analysis of nonlinear transition problems. It has been necessary to make severe approximations to get any results at all, and apparently the range of validity of the conclusions is extremely limited. In subsequent chapters these results will be compared with the results of numerical simulation.

## V. SIMULATION ALGORITHM

The preceding chapter has made it clear that, if nothing else, it is difficult to obtain much information about the nonlinear behaviour of the driven magnetohydrodynamic sheet pinch by analytical methods. In such cases it is customary to have recourse to the numerical analysis of the problem on a high speed computer. The nonlinear evolution of the driven magnetohydrodynamic sheet pinch is then considered as an initial - boundary value problem. The numerical algorithm that we will employ is based on the Navier - Stokes algorithm developed by Moin and Kim ( Moin and Kim (1980), Moin and Kim (1982) ).

The simulation will trace the nonlinear evolution of the system described in earlier chapters, but the governing equations that are used will be different for numerical reasons. The  $x - y$  plane studied in the previous chapters is now replaced by the  $x - z$  plane, *mutatis mutandis*. The following system of nonlinear, partial differential equations is solved numerically:

$$v - 1 \quad \frac{\partial u}{\partial t} - w \left( \frac{\partial w}{\partial x} - \frac{\partial u}{\partial z} \right) = - \frac{\partial \Pi}{\partial x} - \frac{\partial A}{\partial x} \nabla^2 A + \mu \nabla^2 u$$

$$v - 2 \quad \frac{\partial w}{\partial t} + u \left( \frac{\partial w}{\partial x} - \frac{\partial u}{\partial z} \right) = - \frac{\partial \Pi}{\partial z} - \frac{\partial A}{\partial z} \nabla^2 A + \mu \nabla^2 w$$

$$v - 3 \quad \frac{\partial u}{\partial x} + \frac{\partial w}{\partial z} = 0$$

$$v - 4 \quad \frac{\partial A}{\partial t} + u \frac{\partial A}{\partial x} + w \frac{\partial A}{\partial z} = \eta(z) \nabla^2 A + E$$

where:



$u(x, z, t)$  =  $x$  component of velocity

$w(x, z, t)$  =  $z$  component of velocity

$A(x, z, t)$  = magnetic vector potential

$\Pi(x, z, t) = p + \frac{U^2}{2} + \frac{w^2}{2}$  = pressure head

$\mu = \frac{1}{M}$  = dimensionless viscosity

$\eta(z) = \xi(z)/S$  = dimensionless resistivity

Equations V - 1 through V - 4 relate to the governing equations introduced in chapter II in the following way: equation V - 1 replaces equation II - 18; equation V - 2 replaces equation II - 19; Equation V - 3 replaces equation II - 20; and equation V - 4 replaces equation II - 1.

Equations V - 1 through V - 4 are written in the rotation form in order to semi - conserve total energy pseudospectrally ( Dahlburg and Zang, to be published ). Both equations of motion are used in the numerical algorithm so that the no - slip boundary conditions can be simply imposed at the walls.

The periodic direction (  $x$  ) is naturally discretized by the Fourier pseudospectral method ( Gottlieb and Orszag (1977) ). In the spirit of the pseudospectral method, computations are performed in the space of greatest convenience. For instance, configuration space derivatives are evaluated without phase error in Fourier space, with simple multiplications and additions being the only operations required. Nonlinear terms are more easily evaluated in configuration space.

The perpendicular direction (  $z$  ) is discretized with second - order finite differences on a stretched mesh. The finite difference formulae are found by

taking derivatives of the three - point second order Lagrange interpolating polynomial - the resulting expression being used for the numerical derivative at the central point.

The second order Lagrange interpolating polynomial to the function  $f(z)$  is:

$$P(z) = \frac{(z - z_i)(z - z_{i+1})}{(z_{i-1} - z_i)(z_{i-1} - z_{i+1})} f(z_{i-1})$$

v - 5

$$+ \frac{(z - z_{i-1})(z - z_{i+1})}{(z_i - z_{i-1})(z_i - z_{i+1})} f(z_i) + \frac{(z - z_{i-1})(z - z_i)}{(z_{i+1} - z_{i-1})(z_{i+1} - z_i)} f(z_{i+1})$$

Differentiating once and evaluating at the central point  $z_i$  gives:

$$\left. \frac{dP}{dz} \right|_{z=z_i} = \frac{z_i - z_{i+1}}{(z_{i-1} - z_i)(z_{i-1} - z_{i+1})} f(z_{i-1})$$

v - 6

$$+ \frac{2z_i - (z_{i-1} + z_{i+1})}{(z_i - z_{i-1})(z_i - z_{i+1})} f(z_i) + \frac{(z_i - z_{i-1})}{(z_{i+1} - z_{i-1})(z_{i+1} - z_i)} f(z_{i+1})$$

This expression is used for evaluating the first derivative of  $f(z)$  at  $z = z_i$ .

Differentiating the Lagrange interpolating polynomial twice and evaluating the resulting expression at  $z = z_i$  gives:

$$\left. \frac{d^2 P}{dz^2} \right|_{z=z_i} = \frac{2f(z_{i-1})}{(z_{i-1} - z_i)(z_{i-1} - z_{i+1})}$$

v - 7

$$+ \frac{2f(z_i)}{(z_i - z_{i-1})(z_i - z_{i+1})} + \frac{2f(z_{i+1})}{(z_{i+1} - z_{i-1})(z_{i+1} - z_i)}$$

This expression is used to evaluate the second derivative of  $f(z)$  at  $z = z_i$ . Note that  $z$  derivative operators can be computed initially and then stored. The pressure head is evaluated on a staggered grid. The standard mesh points are located halfway between the staggered grid points to give second order accuracy on the  $z$  derivatives of the pressure head.

The mesh prescription depends on the physical problem under consideration. For this problem fine scale structures are expected to develop at the walls and near the centre of the channel. To increase the resolution in these regions, the mesh should contain many grid points near the walls and the channel centre. The staggered mesh  $\zeta_k$  is prescribed first:

$$\zeta_k = -\cos \left[ \frac{(k - \frac{1}{2})\pi}{k_{\max}} \right] \left| \cos \left[ \frac{(k - \frac{1}{2})\pi}{k_{\max}} \right] \right|$$

v - 8

$$k = 1, 2, 3, \dots, k_{\max}$$

The standard mesh  $\bar{z}_k$  is given by:

$$v - 9 \quad z_k = \frac{1}{2} (z_{k-1} + z_k) \quad ; \quad k = 2, 3, 4, \dots, k_{max}$$

$$z_1 = -1.0 \quad ; \quad z_{k_{max}+1} = 1.0$$

A semi - implicit method is used to discretize the system in time. All nonlinear terms and the parallel diffusion terms are advanced in time by the second order Adams - Bashforth method. The perpendicular diffusion terms are discretized by the Crank - Nicolson method. This method is used because of its excellent stability properties for diffusion problems on meshes with small grid spacing. This method, however, is sometimes known to produce erroneous oscillations ( Dahlquist, Bjorck, and Anderson (1974) ). In this magnetohydrodynamic code, as well as in its hydrodynamic counterpart, for small fluid velocities the pressure head is seen to oscillate when it is advanced in time by the Crank - Nicolson method. This objectionable feature is removed if the pressure head is temporally discretized by the backward Euler method ( T.A. Zang, private communication ). Note also that this discretization decreases the amount of computational work required for each time step.

To illustrate better the algorithm, isolate the terms that are discretized explicitly in time, let:

$$H_i \equiv w \left( \frac{\partial w}{\partial x} - \frac{\partial v}{\partial z} \right) - \frac{\partial A}{\partial x} \nabla^2 A + \mu \frac{\partial^2 v}{\partial x^2}$$

$$H_3 \equiv -U \left( \frac{\partial W}{\partial X} - \frac{\partial U}{\partial Z} \right) - \frac{\partial A}{\partial Z} \nabla^2 A + \mu \frac{\partial^2 W}{\partial X^2}$$

v - 10

$$H_4 \equiv -U \frac{\partial A}{\partial X} - W \frac{\partial A}{\partial Z} + \eta(z) \frac{\partial^2 A}{\partial X^2} + E$$

Substituting into v - 1 to v - 4 gives:

$$v - 11 \quad \frac{\partial U}{\partial t} = H_1 - \frac{\partial \Pi}{\partial X} + \mu \frac{\partial^2 U}{\partial Z^2}$$

$$v - 12 \quad \frac{\partial W}{\partial t} = H_3 - \frac{\partial \Pi}{\partial Z} + \mu \frac{\partial^2 W}{\partial Z^2}$$

$$v - 13 \quad \frac{\partial U}{\partial X} + \frac{\partial W}{\partial Z} = 0$$

$$v - 14 \quad \frac{\partial A}{\partial t} = H_4 + \eta(z) \frac{\partial^2 A}{\partial Z^2}$$

Discretizing this system in time:

$$U^{n+1} = U^n - \Delta t \left( \frac{\partial \Pi}{\partial X} \right)^{n+1} + \frac{\Delta t}{2} \left[ 3H_1^n - H_1^{n+1} \right]$$

$$v - 15 \quad + \frac{\mu \Delta t}{2} \left[ \left( \frac{\partial^2 U}{\partial Z^2} \right)^{n+1} + \left( \frac{\partial^2 U}{\partial Z^2} \right)^n \right]$$

$$W^{n+1} = W^n - \Delta t \left( \frac{\partial \Pi}{\partial z} \right)^{n+1} + \frac{\Delta t}{2} \left[ 3H_3^n - H_3^{n-1} \right]^{57}$$

$$v - 16 \quad + \frac{\mu \Delta t}{2} \left[ \left( \frac{\partial^2 W}{\partial z^2} \right)^{n+1} + \left( \frac{\partial^2 W}{\partial z^2} \right)^n \right]$$

$$v - 17 \quad \left( \frac{\partial U}{\partial x} \right)^{n+1} + \left( \frac{\partial W}{\partial z} \right)^{n+1} = 0$$

$$A^{n+1} = A^n + \frac{\Delta t}{2} \left[ 3H_4^n - H_4^{n-1} \right]$$

$$v - 18 \quad + \frac{\eta(z) \Delta t}{2} \left[ \left( \frac{\partial^2 A}{\partial z^2} \right)^{n+1} + \left( \frac{\partial^2 A}{\partial z^2} \right)^n \right]$$

where the superscript  $n$  indexes the time step.

This system of partial differential equations is Fourier transformed in the  $x$  direction, resulting in a set of ordinary differential equations in  $z$  for each value of  $k_x$ .

$$v - 19 \quad U^{n+1} + ik_x \Delta t \Pi^{n+1} - \frac{\mu \Delta t}{2} \left( \frac{\partial^2 U}{\partial z^2} \right)^{n+1} = Q_1$$

$$v - 20 \quad W^{n+1} + \Delta t \left( \frac{\partial \Pi}{\partial z} \right)^{n+1} - \frac{\mu \Delta t}{2} \left( \frac{\partial^2 W}{\partial z^2} \right)^{n+1} = Q_3$$

$$v - 21 \quad ik_x U^{n+1} + \left( \frac{\partial W}{\partial z} \right)^{n+1} = 0$$

$$v - 22 \quad A^{n+1} - \frac{\eta(z) \Delta t}{2} \left( \frac{\partial^2 A}{\partial z^2} \right)^{n+1} = Q_4$$

where the functions  $Q$  represent terms involving the pressure head, velocity fields, magnetic fields, and electric fields at time steps  $n$  and  $n - 1$ . The fields are now to be regarded as one dimensional Fourier transformed quantities.

When this system of equations is discretized in  $z$ , the continuity equation being evaluated on the staggered mesh, an algebraic system of equations for the Fourier transformed field variables results. This algebraic system is block-tridiagonal and can be solved by standard elimination methods. The system of equations is most efficiently solved when the system of equations is ordered and scaled to establish diagonal dominance and so avoid the need for pivoting. This ordering and scaling is an extremely crucial consideration in the design of the vectorized version of this algorithm.

Periodic boundary conditions in  $x$  on all fields are built into the algorithm. No-slip boundary conditions are imposed on the velocity field at  $z = +1$  and  $z = -1$ .

$$u(z = 1) = u(z = -1) = 0$$

$$w(z = 1) = w(z = -1) = 0$$

The normal component of the magnetic field is constrained to equal zero at the walls, i.e.,

$$A(z = 1) = A(z = -1) = \text{CONSTANT}$$

Boundary conditions on the pressure are unnecessary ( Moin and Kim (1989) ).

Two different forms of initialization are possible. The code can be initialized with eigenmodes from the codes developed for the linear problem, or it can be initialized with random noise perturbations.

When the initial perturbations are taken from the eigenvalue code, the initial fields take the form:

$$\begin{aligned}
 A(x, z, t=0) &= A_0(z) + \epsilon a_r \cos \alpha x \\
 v - 23 \quad u(x, z, t=0) &= \epsilon \frac{d\phi_i}{dz} \sin \alpha x \\
 w(x, z, t=0) &= -\epsilon \alpha \phi_i(z) \cos \alpha x
 \end{aligned}$$

where:

$a_r$  = real part of the magnetic eigenfunction

$\phi_i$  = imaginary part of the velocity eigenfunction

$\epsilon \ll 1$

The code can also be initialized with random noise perturbations. Some care must be taken in doing this to ensure that the noise fulfills the boundary conditions as well as the constraints mandated by the solenoidality of the fields.

For the perturbed magnetic field a mixed exponential - trigonometric expansion suffices. The arguments of the trigonometric functions in  $z$  are chosen so as to set the perturbed vector potential and current equal to zero at the walls. The initial magnetic vector potential is given by:



$$A(x, z, t=0) = A_0(z) + \epsilon \sum_{n,m} \left[ (A_{mn} \cos mx + B_{mn} \sin mx) \cos \frac{n\pi z}{2} + (C_{mn} \cos mx + D_{mn} \sin mx) \sin \frac{(n+1)\pi z}{2} \right]$$

v - 24 WHERE:

$$m = 1, 2, 3, \dots, m_{\max}; \quad n = 1, 3, 5, \dots, n_{\max}$$

$$\epsilon \ll 1$$

$A_{mn}, B_{mn}, C_{mn}, D_{mn} \equiv$  RANDOM REAL NUMBERS WITH ZERO MEAN AND UNIT VARIANCE

The perturbed stream function is expanded in a complex exponential series in  $x$ , and in Chandrasekhar - Reid polynomials in  $z$ . The perturbed velocity field components are found by taking the appropriate partial derivatives of the perturbed stream function. The initial stream function is given by:

$$\psi(x, z, t=0) = \epsilon \sum_{n,m} \left[ (Q_{mn} \cos mx + R_{mn} \sin mx) \left( \frac{\cosh \lambda_n z}{\cosh \lambda_n} - \frac{\cos \lambda_n z}{\cos \lambda_n} \right) + \right.$$

$$\left. (S_{mn} \cos mx + T_{mn} \sin mx) \left( \frac{\sinh \mu_n z}{\sinh \mu_n} - \frac{\sin \mu_n z}{\sin \mu_n} \right) \right]$$

WHERE:

$$m = 1, 2, 3, \dots, m_{\max}; \quad n = 1, 2, 3, \dots, n_{\max}$$

$$\epsilon \ll 1$$

$Q_{mn}, R_{mn}, S_{mn}, T_{mn} \equiv$  RANDOM REAL NUMBERS WITH ZERO MEAN AND UNIT VARIANCE

$$\lambda_n \equiv \text{POSITIVE ROOTS OF } (\tanh \lambda + \tan \lambda = 0)$$

$$\mu_n \equiv \text{POSITIVE ROOTS OF } (\coth \mu - \cot \mu = 0)$$

Several versions of this code exist, both in scalar and vector form. The most optimized version is on the CDC CYBER 205 supercomputer at the Institute for Computational Studies at Colorado State University. The numerical simulations reported in this thesis were performed with this version of the code. This version of the code has been vectorized to the fullest extent possible. The code takes approximately 0.25 seconds per time step at a spatial resolution of 64 Fourier modes by 129 finite difference points. The bulk of the computational time is spent in solving the block-tridiagonal equations, even though this section of the code has been vectorized over the  $x$  wavenumbers to improve the speed (Jang, private communication). The data generated during the runs was processed on the CRAY computers at the National Magnetic Fusion Energy Computer Center at the Lawrence Livermore National Laboratory.

## VI. NONLINEAR EVOLUTION OF A PRIMARY DISTURBANCE

In this chapter the evolution of a small primary disturbance into the nonlinear regime will be simulated numerically. The most obvious candidate for the small primary disturbance is the linearly unstable eigenmode of the system with  $\alpha$  equal to one. In this chapter we will determine by numerical simulation what happens to this mode when the nonlinear terms in the equations governing the system begin to get excited.

In chapter IV the significant nonlinear processes for the case of a system dominated by a single unstable primary mode and its higher harmonics were given. Those nonlinear processes are reviewed here. When the primary disturbance achieves finite amplitude it will interact with itself and generate the first harmonic of the disturbance. The finite amplitude perturbation will also interact with its complex conjugate and so distort the mean profile. By the same sort of process, still higher harmonics of the disturbance are generated by the interaction of the secondary harmonic with itself, the interaction of the tertiary harmonic with itself, etc. The finite amplitude perturbation can itself be distorted by the interaction of the secondary harmonic with its complex conjugate, and so forth. The analysis given in chapter IV ignored the generation of higher harmonics and the distortion of the primary disturbance in order to decrease the difficulty of the nonlinear stability problem. Numerical simulation will allow us to determine how valid the assumptions of chapter IV were with respect to the importance of the various nonlinear processes on the evolution of the primary disturbance.

Several diagnostics are employed to characterize the time evolution of the system. Contour plots are used to display within the computational box four

significant scalar fields; the magnetic vector potential  $A(x, z, t)$ , the velocity stream function  $\psi(x, z, t)$ , the electric current density  $j(x, z, t)$ , and the vorticity of the magnetofluid  $\omega(x, z, t)$ . In the two dimensional case, lines of constant magnetic vector potential are equivalent to magnetic field lines (since  $\mathbf{B} = \nabla A \times \mathbf{e}_z$ ). The components of the velocity field are related to the stream function  $\psi$  in the following way:

$$v = -\frac{\partial \psi}{\partial z} \quad ; \quad \omega = \frac{\partial \psi}{\partial x}$$

The electric current density and the vorticity are superior diagnostics for determining the presence of nonlinearity and / or turbulence in the system, since these fields emphasize the high frequency parts of the magnetic and velocity spectra, respectively. The electric current density plots also reveal the regions of high Ohmic dissipation. Where the electric current density is large, the Ohmic dissipation will be significant. In the same way, the vorticity plots reveal the regions of high viscous dissipation.

The time evolution of several global quantities also provides useful information about the state of the system. Of obvious significance are the energies in the various fields, which provide a global measure of the degree of excitation of these fields:

$$\text{kinetic energy} \quad e_v \quad : \quad \frac{1}{2} \int_0^{2\pi} \int_{-1}^1 (v^2 + \omega^2) dx dz$$

$$\text{magnetic energy } E_B : \frac{1}{2} \int_0^{2\pi} \int_{-1}^1 (B_x^2 + B_z^2) dx dz$$

$$\text{perturbed magnetic energy } e_B : \frac{1}{2} \int_0^{2\pi} \int_{-1}^1 [(B_x - B_0)^2 + B_z^2] dx dz$$

$$\text{total energy} : E_B + e_v$$

$$\text{one dimensional modal magnetic energy} : \frac{1}{2} \int_{-1}^1 |\underline{B}(k_x, z)|^2 dz$$

$$\text{one dimensional modal kinetic energy} : \frac{1}{2} \int_{-1}^1 |\underline{v}(k_x, z)|^2 dz$$

The computed configuration space energies are volume averaged to allow for comparison with the one dimensional (1 - D) modal energies.

Growth rates for the perturbations can be computed from the perturbed energies.

$$\begin{array}{l} \text{kinetic energy} \\ \text{growth rate} \end{array} : \frac{1}{e_v} \frac{de_v}{dt}$$

$$\begin{array}{l} \text{perturbed magnetic energy} \\ \text{growth rate} \end{array} : \frac{1}{e_b} \frac{de_b}{dt}$$

These growth rates are not computed at each time step, but rather after several time steps, typically fifty or one hundred. This is done because the evaluation of the global quantities is a computationally expensive step involving output, and hence the number of such evaluations must be kept to a minimum.

Also followed are several of the ideal invariants of two dimensional magnetohydrodynamics ( Pyfe and Montgomery (1976) ):

$$\text{cross helicity} : \frac{1}{2} \int_0^{2\pi} \int_{-1}^1 \underline{v} \cdot \underline{B} \, dx \, dz$$

$$\begin{array}{l} \text{mean square} \\ \text{vector potential} \end{array} : \frac{1}{2} \int_0^{2\pi} \int_{-1}^1 A^2 \, dx \, dz$$

The activation of the small scale structures in the system is reflected in

the field enstrophies, which provide a global measure of the amount of dissipative activity present in the system ( Matthaeus and Montgomery (1988) ).

$$\text{enstrophy} : \int_0^{2\pi} \int_{-1}^1 \omega^2 dx dz$$

$$\text{magnetic enstrophy} : \int_0^{2\pi} \int_{-1}^1 j^2 dx dz$$

It would have been more appropriate for the analysis of the driven magnetohydrodynamic sheet pinch to weight the magnetic enstrophy with the dimensionless resistivity function, but this was not done.

Several methods are used to monitor the accuracy of the run, some more valuable than others. We describe these methods here, as well as several general accuracy checks for the code.

An obvious question about the code is this - can the code reproduce the equilibrium solution when it is initially unperturbed? The answer is yes, to within six digits for several thousand time steps. However, care must be taken in defining the resistivity profile to use numerical derivatives of the mean magnetic vector potential rather than analytical derivatives. This is quite similar to the manner in which the external pressure gradient must be computed for the case of plane Poiseuille flow.

A good check on the accuracy of the code is to see how well it can reproduce the linear growth rate when it is initially perturbed with the appropriate

magnetic and velocity eigenfunctions. In this code the growth rates of the perturbed velocity field and the perturbed magnetic field are monitored, so that either or both of these can be compared with the linear growth rate predicted by the eigenvalue code. The growth rate computed by the eigenvalue code is regarded as the benchmark growth rate. This is one way to ensure that the finite difference grid is accurately resolving the internal boundary layer.

The energy in the  $l/4$  modal energy is monitored to check for aliasing errors ( cf Gottlieb and Orszag (1977) ), where  $l$  is defined to be the number of Fourier modes in the  $x$  direction. When this mode interacts with itself the result is aliased back to the mean, due to the use of the discrete fast Fourier transform. The aliasing error is expected to become significant if the energy in the  $l/4$  modal energies exceeds order  $10^{-8}$  of the energy in the mean, although this ratio is not universally agreed upon.

The Kolmogoroff dissipation wavenumber, as defined by Shebalin, et al. (1983), is monitored. This number, determined on the basis of dimensional analysis, approximately determines the spatial scales at which dissipation is occurring in a turbulent fluid. Shebalin et. al. define the dissipation wavenumber to be

$$k_D = \left[ \eta^{-3} \left| \frac{dE_\theta}{dt} \right|_\eta + \nu^{-3} \left| \frac{dE_v}{dt} \right|_\nu \right]^{1/4}$$

where:

$$\left| \frac{dE_\theta}{dt} \right|_\eta = \text{Ohmic dissipation rate}$$

$$\left| \frac{dE_v}{dt} \right|_\nu = \text{viscous dissipation rate}$$



For the variable resistivity case considered here, the value of resistivity at  $z$  equal to zero is used since this will give the most pessimistic value. This diagnostic is expected to be of significance when the system has a high degree of nonlinear excitation present, for only then will the system have a dissipation range.

To ensure the stability of the explicit temporal discretization, two Courant numbers are monitored throughout the run, although more such numbers could be given ( e.g. a dissipation number ). the standard Courant number for fluid mechanical problems is monitored at every grid point ( cf Roache (1972), Moir and Kim (1982) ):

$$C(t) = \max \left\{ \Delta t \left[ \left| \frac{U}{\Delta x} \right| + \left| \frac{W}{\Delta z} \right| \right] \right\} < \frac{1}{\pi}$$

An magnetohydrodynamic Courant number is given by Frisch, Pouquet, Sulem and Meneguzzi (1983):

$$C_{MHD} = \frac{\Delta t}{h} \sup ( |v + \underline{B}|, |v - \underline{B}| ) < 1$$

$h$  = local mesh spacing

This number is of limited utility, since it is intended for the Elsasser formulation of the MHD equations. It has, despite this, served as a useful leading indicator of numerical instabilities.

Next, details will be given regarding a run following the evolution of an unstable eigenfunction into the nonlinear regime. The code is initialized with the equilibrium magnetic field  $B_0(z) = \arctan(8z)$ . The Courant numbers are

specified to be  $M = S = 100$ . The unstable eigenmode for this equilibrium with  $\alpha = 1$ ,  $M = S = 100$  is used as the perturbation. Hence this corresponds to CASE # 2 of chapter IV. The code is run with 32 Fourier modes in  $x$  and 129 finite difference points on a stretched mesh in  $z$ .  $\Delta t = 0.392699 \times 10^{-2}$  initially and is adjusted as required by the Courant numbers to ensure numerical stability. The value chosen for epsilon in equations V - 23 is 0.001.

The initial value of the mean magnetic energy is 0.756019. The initial value of the perturbed magnetic energy is  $0.1980 \times 10^{-4}$ , or 0.00262% of the mean magnetic energy. The value of the kinetic energy is  $0.2330 \times 10^{-4}$ , or 0.00308% of the mean magnetic energy. The perturbed energies are entirely in the  $k_x = 1$  magnetic and velocity modes. The initial values of the perturbation energies are chosen to be small enough to be in the linear regime, yet not too far away from the nonlinear regime as to require a prohibitive amount of computational time to attain finite amplitude.

Figure VI - 1 shows the initial mean magnetic profile. The initial primary magnetic disturbance is shown in figure IV - 2. Figure VI - 3 is a contour plot of the initial magnetic vector potential. The initial perturbation is barely barely distinguishable. The initial velocity stream function is shown in figure VI - 4. Four large eddies are apparent. Figure VI - 5 shows the initial electric current density. The initial perturbation can be detected as a slight bowing of the lines of constant current density. Figure VI - 6 shows the initial vorticity.

The time evolution of the various global quantities that characterize the run is exhibited in figures VI - 7a through VI - 7e.

The growth rate for the linear modes computed by the eigenvalue code is  $\omega_i = 0.18223$ . After 50 time steps the nonlinear code returns the result that

the perturbed magnetic energy growth rate is 0.18296, which differs from the eigenvalue by 0.4086%. At the same time the kinetic energy growth rate is 0.18176, which differs from the eigenvalue by 0.2579%. Closer results would be possible by sampling the energy more frequently, but this process is time consuming for the computation.

A result for longer times is revealing. Using the growth rate from the eigenvalue code we can predict what the perturbed energies should be at some future time if they are growing according to the linear theory. At  $t = 3.926$  the perturbed magnetic energy should equal  $0.8280 \times 10^{-4}$ , and the kinetic energy should equal  $0.9745 \times 10^{-4}$ . The nonlinear code returns  $0.8235 \times 10^{-4}$  for the perturbed magnetic energy, and  $0.9599 \times 10^{-4}$  for the kinetic energy. The magnetic prediction is off by 0.5555%, while the velocity prediction is off by 1.498%. This implies that, in this particular run, the velocity field responds first to the nonlinearities in the governing equations. In fact, by this time some excitation is evident in the higher harmonics of the 1D modal energies (although this is perhaps not evident on the plots, Figures VI - 7d and VI - 7e).

The primary disturbance ceases growth at approximately  $t = 16.5$ , with decay in the primary velocity field preceding decay in the primary magnetic field. At  $t = 15.70796$ , the mean magnetic energy equals 0.73309, or 96.97% of its initial value. This indicates that the mean magnetic field is being deformed in such a way as to favor energy transfer to the perturbation, rather than vice versa. At this time the magnetic energy in the primary disturbance equals  $0.15294 \times 10^{-2}$ , or 0.21% of the mean magnetic energy. The kinetic energy in the primary disturbance is equal to  $0.1178 \times 10^{-2}$ , or 0.16% of the mean magnetic energy.

It must be noted that by this time,  $t = 15.70796$ , the generation of higher harmonics of the primary disturbance has become significant. This is especially true of the primary disturbance of the magnetic field. At this time the per-

turbed magnetic energy is equal to  $0.2661 \times 10^{-2}$ , of which 57.5% is in the primary disturbance, 27.5% is in the secondary disturbance, and 9.0% is in the tertiary disturbance. The generation of higher harmonics is somewhat less pronounced in the velocity field. At this time the kinetic energy is equal to  $0.1435 \times 10^{-2}$ , of which 82.1% resides in the primary disturbance, 15.8% in the secondary disturbance, and 1.92% in the tertiary disturbance. These energy ratios imply that the harmonics of the primary disturbance are entering into the dynamics of the system in a significant manner, and hence their generation cannot be ignored in any model of the nonlinear evolution of the primary disturbance.

Several plots which exhibit various quantities at  $t=15.70796$  are helpful. Figure VI - 8 shows the mean magnetic profile. The deformation of the mean profile appears to be simply a small decline from its initial value. The primary magnetic disturbance is shown in figure VI - 9. While the hollow in the centre of the disturbance appears to be relatively deeper, the shape assumption seems to be fairly well justified. The secondary magnetic disturbance is shown in figure VI - 10. In general form it is similar to the primary magnetic disturbance, except that some curvature of the disturbance is evident in the exterior regions. The tertiary magnetic disturbance is shown in figure VI - 11. Although it is perhaps not evident, there is a slight hollow in the centre of this disturbance.

Figure VI - 12 is a contour plot of the magnetic vector potential at  $t = 15.70796$ . A small closed magnetic field structure, commonly referred to as a magnetic 0 - point, is evident at the centre of the contour plot ( cf Matthaeus and Montgomery (1981) ). The magnetic field structure at  $( x = 0, z = 0 )$  or at  $( x = 2\pi, z = 0 )$  is commonly referred to as a magnetic X - point. Figure VI - 13 shows the velocity stream function at this time. It

can be seen that the nonlinear terms in the governing equations have had the effect of concentrating the regions of high velocity in the vicinity of the closed magnetic field structure. Figure VI - 14 shows the electric current density at this time, revealing that the current density has developed a "peaked" structure within the closed magnetic field structure. A well developed current sheet is evident. Figure VI - 15 shows the vorticity of the magnetofluid at this time. Some wall effects are evident. Certain of these structures will be discussed in greater detail in the next chapter, although in a different context.

The mean current profile at  $t = 15.70796$  is shown in figure VI - 16. This plot should be compared with the theoretically predicted mean current profile in figure IV - 8. The mean current profile has decayed at the centre, as was predicted, but the magnitude of the distortion is far less than was predicted.

After achieving these maximum values, the primary disturbance is seen to decay while the secondary disturbance ascends in value. After some time the bulk of the perturbed energy resides in the secondary disturbance, which takes on an approximately constant value.

The secondary disturbance dominates the system until the end of the run. Only very gradual changes are observed in the global quantities after approximately  $t = 40$ , with the exception of the mean magnetic energy. It appears that the rate at which energy is being removed from the mean magnetic field is approximately equal to the rate at which it is being dissipated, since very little change is observed in the magnitude of the perturbed energies. At  $t = 70.688$ , the mean magnetic energy is equal to 6.2970, a 16.7% decrease from its initial value. This large distortion indicates the significance of the nonlinear interactions in the systems evolution. At this time most of the energy resides in the secondary disturbance. The perturbed magnetic energy is equal to

$0.5231 \times 10^{-2}$ , of which 82.7%, or  $0.4325 \times 10^{-2}$  is in the secondary magnetic mode. The kinetic energy is equal to  $0.1276 \times 10^{-2}$  of which 94.1%, or  $0.1201 \times 10^{-2}$  is in the secondary velocity mode. The perturbed magnetic energy is 0.83% of the mean magnetic energy, while the kinetic energy is 0.20% of the mean magnetic energy. These percentages are roughly constant over the last half of the run.

The lack of change in the system in the later stages of the run is well illustrated by comparison of contour plots taken at two widely separated times. For  $t = 54.980$ , contour plots of scalar fields are shown in figures VI - 17 through VI - 20. The corresponding fields at  $t = 70.688$  are shown in figures VI - 21 through VI - 24. Some minor decay of the perturbed fields has occurred, but the field configuration has remained relatively constant.

It is apparent that the nonlinear stability theory outlined in chapter IV must be modified to account for the generation of higher harmonics, although the best way to do this is uncertain. Obviously in this run the generation of higher harmonics has been significant, and is perhaps responsible for the failure of the primary disturbance to saturate nonlinearly. However, the second half of this run indicates that a state resembling nonlinear saturation can be achieved by the secondary disturbance.

Inspection of the energy versus time plots shows that the mean magnetic energy is apparently asymptoting toward a value around 62.0, while the perturbed energies are seen to be decaying at an extremely low rate. This appears to be consistent with two interpretations. First, the change in the perturbed energies is so slight over thousands of time steps that it could be argued that the secondary mode has indeed saturated nonlinearly, whereas the primary disturbance had failed to do so. In this case a double magnetic 0 - point structure with large fluid flows will constitute the saturated state of the system. Second, it

could be argued that the system is asymptotically stable in the sense of Liapunov. The perturbation in the secondary is apparently decaying very slowly with time, while the mean is evidently asymptoting toward some constant value. An extrapolation of this to very long times would indicate the difference between the mean and the perturbation is tending toward zero as time tends toward infinity. More computing is required to resolve this issue.

## VII. EVOLUTION OF SYSTEM WITH RANDOM INITIAL PERTURBATIONS

In this chapter the nonlinear evolution of the randomly perturbed system is described. By randomly perturbed is meant the following, many magnetic and velocity modes are excited initially. This differs from the case considered previously in that it is possible, from the outset, that the interactions among many modes are dynamically significant. Furthermore, many of the symmetries that were present in the previous case are here broken, implying that the system will evolve in a less constrained manner. This latter situation more closely models the noisy interior of a magnetically confined fusion plasma. Numerical simulation is especially well suited for problems of this kind, where it is difficult to determine the appropriate simplifying assumptions necessary for successful analysis. Our goal is to follow numerically the evolution of the magnetohydrodynamic sheet pinch into the nonlinear regime and to identify the structures that develop.

In the run described here small random perturbations are imposed on the magnetofluid system with the initial equilibrium field given by  $B(z) = \arctan(\theta z)$ . Hence, the initial mean current profile has a peak value of  $\theta$  at  $z = 0$  ( see figures II - 1 through II - 3 ). The exact formulation of the perturbations is given in equations V - 24 and V - 25. For the perturbed magnetic vector potential expansion,  $m_{MAX} = 16$ ,  $n_{MAX} = 7$ . For the velocity field expansion,  $m_{MAX} = n_{MAX} = 8$ . The random number coefficients are generated by the IMSL subroutine GGNML. The value chosen for  $\epsilon$  is 0.002. We specify  $M = S = 400$ . The time step initially equals 0.0019635, and is adjusted as required by the Courant numbers to ensure numerical stability.

The initial size of the perturbed fields relative to the mean magnetic



field can be determined globally by a consideration of the various volume averaged energies at  $t = 0$ ; the mean magnetic energy equals  $0.75601947$ , the perturbed magnetic energy equals  $0.21026 \times 10^{-3}$ , and the kinetic energy equals  $0.22079 \times 10^{-3}$ . Using these energy values, initially the perturbed magnetic energy is  $0.0278\%$  of the mean magnetic energy, while the kinetic energy is initially  $0.0292\%$  of the mean magnetic energy.

Figures VII - 1a through VII - 1d are contour plots of, respectively, the initial magnetic vector potential, the initial velocity stream function, the initial electric current density, and the initial magnetofluid vorticity. The random nature of the initial perturbations is evident.

The various global quantities which characterize the evolution of the system are shown in figures VII - 2a through VII - 2e.

The first stage in the time evolution of the system is a period of relatively unsystematic magnetohydrodynamic activity. A net loss of perturbed energy occurs, which is perhaps due to the decaying of the damped modes. The mean magnetic energy remains unchanged.

Around  $t = 15$  growth of the perturbations in both the magnetic and velocity fields is evident. A comparison of the perturbed energy plots ( figure VII - 2a ) with the 1D modal energy plots ( figures VII - 2d through VII - 2e ) reveals that most of the growth of the perturbed energy is contained in the lower  $k_x$  modes. This behaviour agrees somewhat with the expectations formed from the linear theory. For the parameters chosen, several of the eigenmodes with integral values of  $\alpha$  (  $= k_x$  ) are linearly unstable ( as can be inferred by comparison of figures II - 9 and II - 10). The  $k_x = 1$  perturbation is the most unstable linear mode, with a growth rate of  $0.19$ .

Note, however, that some decay in the mean magnetic energy is apparent after approximately  $t = 14.7$ , implying that by this time the nonlinear effects

have become significant. Hence the linear theory, which assumes the stationarity of the mean, will no longer serve as an adequate description of the behaviour of the system. The size at which the perturbations attain finite amplitude can be inferred from the 1D modal energy ratios at, say,  $t = 14.72622$ . At this time the mean magnetic energy equals 0.755202, so it has lost 0.0168% of its initial value. The perturbed magnetic energy is  $0.31026 \times 10^{-3}$ , or 0.041% of the mean magnetic energy. The kinetic energy is  $0.87740 \times 10^{-4}$ , or 0.012% of the mean magnetic energy. Note that the ratio of perturbed energy to mean energy is at this time actually less than it was initially, which seems somewhat paradoxical. This seeming paradox is explained by the observation that this diagnostic, the ratio of perturbed energy to mean magnetic energy, obscures the fact that at this time the perturbed energy is now somewhat more concentrated in fewer modes, a matter which is now addressed.

The 1D modal energy plots show that the early phases of growth are dominated by the  $k_x = 2$  magnetic and velocity modes. At  $t = 19.635$ , the perturbed magnetic energy is equal to  $0.16971 \times 10^{-2}$ . 63.14% of this energy is in the  $k_x = 2$  magnetic mode, with 33.19% of the remainder residing in the  $k_x = 1$  mode. The kinetic energy is equal to  $0.3771 \times 10^{-3}$ , of which 77.94% is in the  $k_x = 2$  velocity mode. The dominance of this mode is clearly seen in the contour plot of the magnetic vector potential at this time, figure VII - 3a. This multiple magnetic island structure persists for thousands of timesteps. In this respect these results differ from the non-driven simulation reported by Matthaeus and Montgomery (1981), who report seeing only single island structures emerge from random noise initial conditions. It can be conjectured that the evolution of the mean magnetic field is in some way responsible for this discrepancy. Matthaeus et. al. report a 19% loss of mean magnetic energy during

their run. By contrast, the mean magnetic energy in this driven run is 0.7514096 at  $t = 19.635$ , or 99.39% of its initial value.

At  $t = 19.635$  the individual magnetic X - points do possess the characteristic form described by Matthaeus et. al. Spikes, or filaments of the electric current density form at the magnetic X - points, indicating that a large amount of Ohmic dissipation is occurring at these locations ( figure VII - 3c ). The peak value of the current density is approximately equal to 14.3, which represents a 28.75% increase over the initial mean value. The electric current density within the magnetic islands is relatively flat and forceless, with a value of approximately 5.5, or a 31.25% decrease from the initial mean value. High speed expulsion of the magnetofluid from the vicinity of the magnetic X - point parallel to the mean magnetic field is evident ( figure VII - 3b ). This acceleration of the magnetofluid implies that some of the magnetic energy released at the magnetic X - point is being transformed into kinetic energy, rather than being dissipated Ohmically. The magnetofluid vorticity is seen to form quadrupole like structures about each magnetic X - point, as reported by Matthaeus (1982).

Subsequently, the time evolution of the system is dominated by processes of a radically different kind which further increase the level of nonlinearity. Given the presence of multiple magnetic O - points, they will interact with each other in such a way as to merge, or coalesce ( Finn and Kaw (1977), Matthaeus and Montgomery (1977) ). It is during this phase of island coalescence that the system becomes most nonlinear. This is evidenced by the rapid increase in the enstrophy at this time, indicating an enhanced excitation of the small scales. Apparently, the asymmetries present in the system at this time predispose the magnetic islands to move towards each other in one direction rather than the other. The magnetic O - points are seen to coalesce fairly rapidly ( within

about two thousand time steps ). One of the X point structures establishes itself as dominant, while the other, subordinate, X point becomes the site of the island coalescence ( figures VII - 4a and VII - 4c ). The current density at the dominant magnetic X - point increases in time while the current density at the subordinate magnetic X - point decreases until, as seen in figure VII - 4c, no filamentary structure is evident at the coalescence site. Note also that as the magnetic islands approach each other the electric current density within each of them increases in magnitude and begins to form a peaked structure. The eddies associated with the dominant X point are also seen to enlarge themselves until they fill the computational box.

The magnetic O - point coalescence phase corresponds to a rise in the perturbed energies which takes the system well into the nonlinear state. The perturbed energies achieve their largest values for the run during this stage. The maximum kinetic energy is approximately equal to  $0.31 \times 10^{-2}$ , and the time it is achieved leads by approximately two time units the peak in the perturbed magnetic energy, which is approximately equal to 0.9102. The total perturbed energy is thus approximately 1.67% of the mean energy at its peak.

The peak in the  $k_x = 1$  1D modal energy plot at approximately  $t = 39$  is associated with the end of the magnetic O - point coalescence phase. Subsequently the system enters a relatively quiescent phase characterized by the transfer of energy in the  $k_x = 1$  magnetic mode to the higher  $x$  harmonics of the disturbance. This increase in magnetic nonlinearity finds its configuration space analogue in the evolution of the dominant electric current density filament into a sheet - like structure, the sheet being roughly parallel to the mean magnetic field ( figure VII - 5c ). The nonlinearity of this structure is evident from the 1D modal magnetic energy plots at  $t = 39.2699$ . 59.4% of the perturbed

magnetic energy resides in the  $k_x = 1$  mode, 25.9% in the  $k_x = 2$  mode, 9.8% in the  $k_x = 3$  mode, with the remaining 4.9% being distributed in the higher magnetic modes.

Apparently the magnetofluid is expelled from the weak magnetic field corners of the X point in such a way as to raise the local current density there (note, however, that the peak value of the current density within the sheet decreases as the sheet evolves). As the current sheet develops, the magnetofluid jets are seen to be localized at the extremities of the electric current density sheet, implying that this is where the energy being released by the magnetic reconnection is being most effectively converted into kinetic energy (figure VII - 5b). This motion of the magnetofluid jets away from the magnetic X point has the consequence that the vorticity quadrupoles now have the appearance of being centred about the magnetic island.

The role which the resistivity profile plays in the formation of the electric current density sheet is unclear. The nature of magnetic reconnection regions is, in general, a somewhat controversial subject, and several competing models exist. The formation of electric current density sheets in the magnetic reconnection zone of uniform resistivity plasmas has been advocated for some time by Syrovatskii (1971) and coworkers in solar physics. Kadomtsev (1975) has argued that electric current density sheets will appear in the magnetic reconnection zones in tokamak plasmas. Electric current density sheets have also been observed in numerical simulations of uniform resistivity magnetofluids by Brushlinskii, et. al. (1980), and more recently by Biskamp (1984). The seeming insignificance of the resistivity profile to the formation of electric current density sheets at the site of magnetic reconnection in these instances suggests that the magnetic field and flow structure are of more importance in the formation of the current sheet.

Associated with the formation and expansion of the current sheet is the contraction of the remaining magnetic 0 - point in the direction parallel to the mean magnetic field. This contraction is accompanied by the formation of a positive electric current density " spike " of large magnitude within the magnetic 0 point. At  $t = 39.2699$  the peak current value within the magnetic 0 - point is approximately 7.25, compared with a peak value of approximately 8.37 within the electric current density sheet. This contraction of the magnetic 0 - point is probably due to the " squeezing " effect caused by the magnetofluid jets on either side of the magnetic 0 - point, and hence must be deemed an artifact of the periodicity of the system. In a nonperiodic system the magnetic 0 - point would be convected away from the magnetic X - point. The Lorentz forces within this structure at the magnetic 0 - point are directed approximately radially outward, indicating that this structure impedes the attempts of the magnetofluid to enter into it. Similar structures have also recently been seen in numerical simulations relevant to solar physics, where the current density " spike " at the magnetic 0 - point is called a deflection current ( Forbes, private communication ).

As is evident from figure VII - 6c, the current density sheet is not a stable structure. By  $t = 51.05186$  the current sheet has ruptured into two distinct filaments. This instability is of a fundamentally different kind than those seen earlier ( Syrovatskii (1979) ). The earlier instabilities were those appropriate to the infinite plane current layer described in chapter II. In contrast, the current sheet is a nonlinear structure of finite extent. Furthermore, the infinite plane current layer is a static configuration, whereas the current sheet is essentially dynamic. From its inception, large amounts of magnetofluid flow into and out of the current sheet. By contributing to the growth

of the current sheet, the flow can be considered to be a cause of the instability rather than a consequence.

The hallmark of this instability is the breakup of the electric current density sheet into two distinct filaments. The physical processes responsible for this rupturing are not well understood, but a possible scenario is the following. Magnetic field lines are dragged into the current sheet region by the motion of the magnetofluid. The magnetic field lines tear and reconnect within this region, with the excess energy being dissipated Ohmically or transformed into kinetic energy. The latter process results in magnetofluid being expelled from the weak magnetic field corner of the X point at high velocity, where it raises the local current density, probably by the stretching of magnetic field lines. The entrainment of ambient magnetofluid is greatest in the vicinity of the magnetofluid jets. As the current sheet expands these regions of maximum magnetofluid entrainment are increasingly separated spatially from each other, implying that the rate at which magnetic field lines are being convected into the current sheet begins to vary along the direction of its expansion. When the electric current density sheet attains some critical value of length in the direction parallel to the mean magnetic field, the rate of magnetic flux reconnection within the sheet does vary, and electric current density proto-filaments appear at the extremities where the magnetofluid jetting is occurring. These proto-filaments exert a greater attractive force on the magnetofluid than the other sections of the current sheet do, so more magnetofluid is pulled into the proto-filament region, further enhancing the current density there. Likewise, the amount of magnetofluid flowing into the central region of the current sheet declines, lessening the rate at which magnetic flux is swept into this region, and the current density there decreases.

As is compatible with the presence of two magnetic X - points, a second magnetic O - point is seen at  $t = 54.97885$  ( figure VII - 7a ) between the two current density filaments. The eddy structure becomes somewhat confused, apparently attempting to set up the the flow pattern seen at  $t = 19.63495$  ( figure VII - 3b ).

These two magnetic O - points quickly respond to each others presence and rush to coalesce, suggesting that the entire process described in this chapter might be cyclical in nature. As was mentioned previously, the magnetic O - point coalescence phase was seen to be the most nonlinear phase of the system's time evolution. The system becomes so nonlinear that by  $t = 58$  the aliasing error from the pseudospectral part of the calculation is significant enough to require halting the calculation. Figures VII - 8a through VII - 8d are contour plots exhibiting the scalar fields at the ultimate time of the run,  $t = 58.906$ . Certain physical features evident in these contour plots will be discussed in greater detail later.

The nonlinear evolution of the driven magnetohydrodynamic sheet pinch with random initial perturbations is seen to display several different stages which are characterized by different physical processes. The perturbed system apparently attempts to nonlinearly relax to the lower energy state containing the electric current density sheet, but is foiled in its attempt to equilibrate by the secondary instabilities of the sheet. A repetition of these processes seems likely.

In an attempt to obtain more information about the long term state of the driven magnetohydrodynamic sheet pinch, as well as to resolve better certain highly nonlinear phenomena, a subsequent run was performed in all respects the same as the one just reported except that both of the Lundquist numbers were



decreased to 200 to augment the numerical resolution. The various global quantities which characterize the run are shown in figures VII - 9a through VII - 9e. The early behaviour of this system is seen to be qualitatively similar to the Lundquist number equal to 400 run. We will describe a highly nonlinear structure which develops, and then briefly characterize the long - term behaviour of the system.

Contour plots at  $t = 54.9788$  show that the magnetic 0 - points are in a phase of coalescence ( figure VII - 10a ). The subordinate electric current density filament is still visible, as is evidence of the peaking of the electric current density within each of the coalescing magnetic 0 - points ( figure VII - 10c ). Vestiges of the subordinate eddies are also visible ( figures VII - 10b and VII - 10d ).

As the coalescence of the magnetic 0 - points proceeds, an unusual and short lived structure is seen to develop at the coalescence site. This structure is well formed at  $t = 58.986$ . Figure VII - 11a shows the two magnetic 0 - points in an advanced state of coalescence. At this time, a negative current filament of large magnitude forms at the coalescence site ( figure VII - 11c ). This negative current filament is situated on a stagnation point and hence must be due to an induced electric field. This highly localized current density structure is evidence of the excitation of many frequencies of the magnetic field. The high state of excitation of the energy containing modes is clearly visible in the one dimensional modal energy plots ( figures VII - 9d and VII - 9e ). The Lorentz forces in this structure are directed in such a way as to expel the magnetofluid toward the walls ( figure VII - 11b ). The highly nonlinear character of this magnetofluid motion is evident from the contour plots of the vorticity at this time ( figure VII - 11d ), where much small scale structure is evident in the vicinity of the coalescence site. Note that this is

the same highly nonlinear structure that appeared in the Lundquist number equal to 400 run and precipitated the breakdown of numerical resolution.

Subsequently several more cycles of behaviour similar to those described earlier are seen to occur, although the perturbed energies achieve lesser values at their maxima. It appears that the mean magnetic energy approaches a constant value as time proceeds. At  $t = 161.008$ , the ultimate time of this run, the mean magnetic energy equals  $0.571894$ , or approximately 75% of its initial value of  $0.756019$ . Contour plots of this ultimate state are shown in figures VII - 12a through VII - 12d, exhibiting behaviour similar to that seen earlier.

## VIII. DISCUSSION

In this thesis the stability and transition properties of a bounded, current carrying magnetofluid have been examined, using the theory developed for plane shear flows as a guide. This approach has proven useful in discovering new relationships and structures. The main results are summarized here and suggestions for extensions of this work are given.

The equilibrium considered was a driven magnetohydrodynamic sheet pinch. The mean flow velocity equals zero. A constant electric field and a spatially varying resistivity profile were utilized to balance the Ohmic dissipation of the mean field magnetic energy. Mean magnetic vector potential profiles with inflection points in the domain were excluded from consideration.

When the magnetohydrodynamic sheet pinch is not driven by an external electric field, the decay of the mean magnetic field is from the outset a significant factor in the evolution of the perturbed system. This is especially true at the low values of the resistive Lundquist number that are currently accessible computationally. The electric field hinders this dissipation of the mean profile in the perturbed system, and thus permits other physical processes to dominate the evolution of the system. Driving the system also generates complex behaviour for many Alfvén transit times, indicating that the electric field enters into the dynamics by keeping the system externally excited.

The mean magnetic profile that was chosen was one appropriate to the driven magnetohydrodynamic sheet pinch. It was, however, somewhat arbitrary in that any one of an infinitude of such solutions of the mean field equations could have been chosen. The reasons for the choice of mean magnetic profile ( $B(y) = \arctan(\delta y)$ ) used were partly physical and partly

numerical. This type of profile was chosen because it is linearly unstable, with the perturbations requiring only a moderate amount of computational time before nonlinearities become significant. The mean field profile can be well resolved numerically. However, a more rational approach is needed to determine appropriate magnetic equilibria. In contrast, the equilibria used in plane shear flow problems emerge as unique solutions to the steady state, unidirectional Navier Stokes equations. An infinitude of mean field solutions are possible for the driven magnetohydrodynamic sheet pinch, and some criterion is needed to determine which solution is the most likely on physical grounds.

The linear stability of the system was investigated by a normal mode analysis. A sixth order system of complex ordinary differential equations which governs the normal modes of the system was derived. An algorithm based on the Chebyshev tau method was developed to solve these equations numerically. Linearly unstable modes were only found for mean current profiles with inflection points in the channel. For inflected current profiles, linearly unstable modes were found for rather low values of the Lundquist numbers. The neutral stability curve was calculated and shown. The form of the neutral stability curve indicates that stabilization can be achieved either by increasing the Lundquist numbers, or by increasing or decreasing the parallel wavenumber. The locus of critical Lundquist numbers was shown to take the form of a hyperbola.

Certain nontrivial details of the linear analysis remain to be done. The locus of critical Lundquist numbers is by definition the locus of points in the  $M - S$  space upon which the growth rate of the linear perturbations equals zero. It would be informative to determine the the form of the loci for non-zero values of the growth rate. Unfortunately, on these other loci  $\alpha$  might not be constant as it is on the critical locus, and this will greatly complicate

the task of determining the curves. A related, but simpler, task would be to determine the curves of constant growth rate in a reduced space, e.g., the  $(\alpha, M)$  space. Finally, with minor modifications to the existing code it would be possible to examine the three dimensional linearly unstable modes. These modes vary with a second wavenumber,  $\beta$ , which determines the wavelength of the perturbation in the direction perpendicular to the mean magnetic field.

The nonlinear stability of a primary disturbance of the system was investigated by an energy method. A Reynolds Orr energy equation was derived for the driven magnetohydrodynamic sheet pinch. For regions in the vicinity of criticality, the nonlinear stability properties are represented by a stability equation of the Landau type ( cf Landau and Lifshitz (1959) ). The derivation of this equation relied on certain assumptions about the nonlinear behaviour, viz., that the primary disturbance retained the form of the eigenfunction upon achieving finite amplitude, and that the generation of higher harmonics of the primary disturbance was negligible. The nonlinear behaviour of a primary disturbance predicted by this model is represented in the amplitude phase plane plots.

The results of the numerical simulation imply that more of the nonlinear effects must be added to the nonlinear stability model, in particular the generation of the secondary and tertiary harmonics of the primary disturbance. This would likely result in the addition of extra terms to the Landau nonlinear stability equation, as well as some variation in the Landau constant. It is possible that the energy method might have to be abandoned for being relatively insensitive to local phenomena, and that a theory based on analytical perturbation methods might be superior.

For mean current profiles with inflection points in the domain, linearly unstable modes were found for low values of the Lundquist numbers. For these cases the question of whether or not subcritical instabilities exist appears to be uninteresting. For mean current profiles without inflection points, no linearly unstable modes were found. These profiles might, however, be unstable to perturbations of finite amplitude. This could be determined most readily by a nonlinear stability analysis.

A computer code based on the large - eddy simulation algorithm of Moin and Kim ( Moin and Kim (1980), Moin and Kim (1982) ) was developed in order to solve the full set of two - dimensional incompressible MHD equations. The algorithm is mixed Fourier pseudospectral - finite difference, and uses a semi - implicit temporal discretization. The pressure head is evaluated on a staggered grid. A highly vectorized form of this code has been developed for use on the CDC CYBER 205 supercomputer. An obvious improvement to this algorithm would be to make make the code fully spectral, which would provide greater spatial resolution for the same array sizes. This could be accomplished by replacing the finite difference discretization in the perpendicular direction with a discretization based on Chebyshev polynomials. This would be especially beneficial if the code were upgraded to include all three spatial dimensions, when optimization of the algorithm would be paramount.

The nonlinear evolution of a primary disturbance in the parameter regime near the stability boundary was observed. The primary disturbance chosen was the unstable eigenmode of the system with parallel wavenumber equal to unity. The generation of higher harmonics and deformation of the mean magnetic profile were seen to be significant. Deformation of the primary disturbance was slight. A quasi - steady state structure with multiple magnetic islands was seen to form and persist for thousands of time steps.

The nonlinear evolution of the randomly perturbed system exhibited several interesting structures. Electric current density sheets and deflection currents were observed. A complex structure was seen during the coalescence of magnetic 0 points, characterized by a negative current "spike" and the expulsion of the magnetofluid toward the walls. This phase of the system's evolution corresponding to the coalescence of magnetic 0 points is the time of the most nonlinear behaviour. A secondary instability mechanism, the dynamic rupturing of the electric current density sheet (cf Syrovatskii (1979)) was observed. This secondary instability mechanism is apparently responsible for the cyclic behaviour of the system.

The numerical simulations have revealed that the nonlinear evolution of the driven magnetohydrodynamic sheet pinch is extremely complex. More simulations are required to determine how the nonlinear evolution scales with respect to the various parameters which define the system. Of especial interest is raising the Lundquist numbers as far as is computationally possible to allow for the excitation of many spatial scales. This would assist in the understanding of the turbulent phenomena encountered during the nonlinear evolution. It would also be of interest to study the nonlinear evolution of finite amplitude perturbations on both linearly stable and unstable profiles. A recent effort in this direction is due to Matthaeus and Lamkin (1985).

The limiting of the numerical simulation to two spatial dimensions is perhaps the severest restriction that has been made. By neglecting the third spatial dimension, many degrees of freedom have been removed, and the nonlinear evolution of the system has hence been somewhat constricted. It has only come

to light recently in the study of plane shear flows how severe the penalty can be for neglecting the third spatial dimension ( cf. Orszag and Kells (1984) ). The similarity of the incompressible MHD equations to the Navier Stokes equations implies that, by analogy, the true nonlinear behaviour of the driven magnetohydrodynamic sheet pinch will only be revealed when all three spatial dimensions are included in the computation.



APPENDIX. PROOF OF IDEAL STABILITY ( MAGNETOHYDRODYNAMIC RAYLEIGH THEOREM )

In this appendix the linear stability properties of the driven magneto-hydrodynamic sheet pinch are examined in the limit of zero viscosity and resistivity.

The governing equations are:

$$A - 1 \quad (D^2 - \alpha^2)^2 \phi = -i\omega M (D^2 - \alpha^2) \phi - i\alpha M (DA_0) (D^2 - \alpha^2) a + i\alpha M (D^3 A_0) a$$

$$A - 2 \quad \{ D^2 - \alpha^2 + i\omega S \zeta(y) \} a = -i\alpha S \zeta(y) (DA_0) \phi$$

where  $D = \frac{d}{dy}$ .

To simplify the following proof, we will make some substitutions. Let:

$$B \equiv DA_0$$

$$b \equiv -i\alpha a$$

$$A - 3 \quad V \equiv -i\alpha \phi$$

$$\alpha C \equiv \omega$$

Substitute the variables defined in A - 3 into A - 1 and A - 2:

$$(D^2 - \kappa^2)^2 v = -i\kappa M c (D^2 - \kappa^2) v - i\kappa M B (D^2 - \kappa^2) b \\ + i\kappa M (D^2 B) b$$

A1 - 4

$$A1 - 5 \quad \{ D^2 - \kappa^2 + i\kappa S \zeta(y) c \} b = -i\kappa S \zeta(y) B v$$

In the ideal limit,  $B \rightarrow \infty$  and  $M \rightarrow \infty$ . In this limit, A - 4 and A - 5 become, respectively:

$$A - 6 \quad 0 = -c (D^2 - \kappa^2) v - B (D^2 - \kappa^2) b + (D^2 B) b$$

$$A - 7 \quad c b = -B v$$

Use A - 7 to substitute for b in A - 6, which becomes:

$$\begin{aligned}
 0 &= c^2(D^2 - \alpha^2)v - B(D^2 - \alpha^2)(Bv) + (D^2B)(Bv) \\
 &= (c^2 - B^2)D^2v - \alpha^2(c^2 - B^2)v \\
 &\quad - 2B(DB)(v)
 \end{aligned}$$

A - 8

$$= \frac{d}{dy} \left[ (c^2 - B^2) \frac{dv}{dy} \right] - \alpha^2(c^2 - B^2)v$$

Multiply A - 8 by  $v^*$ .

$$A - 9 \quad v^* \frac{d}{dy} \left[ (c^2 - B^2) \frac{dv}{dy} \right] - \alpha^2(c^2 - B^2) |v|^2 = 0$$

Integrate A - 9 between the walls, utilizing the free-slip boundary condition;  $v(y = 1) = v(y = -1) = 0$ .

$$0 = \int_{-1}^1 v^* \frac{d}{dy} \left[ (c^2 - B^2) \frac{dv}{dy} \right] dy - \alpha^2 \int_{-1}^1 (c^2 - B^2) |v|^2 dy$$

$$A - 10 \quad = - \int_{-1}^1 (c^2 - B^2) \left| \frac{dv}{dy} \right|^2 dy - \alpha^2 \int_{-1}^1 (c^2 - B^2) |v|^2 dy$$

$$= - \int_{-1}^1 (C^2 - B^2) \left( \left| \frac{dv}{dy} \right|^2 + \alpha^2 |v|^2 \right) dy$$

Separate A - 11 into its real and imaginary parts.

REAL PART:

$$A - 11 \quad \int_{-1}^1 (C_r^2 - C_i^2 - B^2) \left( \left| \frac{dv}{dy} \right|^2 + \alpha^2 |v|^2 \right) dy = 0$$

IMAGINARY PART:

$$A - 12 \quad C_r C_i \int_{-1}^1 \left( \left| \frac{dv}{dy} \right|^2 + \alpha^2 |v|^2 \right) dy = 0$$

For A - 12 to hold, one of the following must be true:

$$v(y) = 0 \quad ;$$

$$A - 13 \quad C_r = 0 \quad ;$$

$$C_i = 0$$

We restrict ourselves to cases with non-trivial eigenfunctions, which eliminates the first possibility ( $v = 0$ ). An examination of the A - 11 shows that the equality cannot be met if  $C_r = 0$ , which implies that:

$$A - 14 \quad C_i = 0$$

i.e., the system is stable for all equilibrium magnetic profiles in the ideal limit.

Note also that the A - 11 determines a bound on the disturbance phase velocities in the ideal limit:

$$C_r^2 \in \left[ \min B^2, \max B^2 \right]$$

## REFERENCES

- Batchelor, G.K., "An Introduction to Fluid Mechanics", Cambridge University Press, Cambridge ( UK ) (1967).
- Bateman, G., "MHD Instabilities", The MIT Press, Cambridge (1978).
- Biskamp, D., Phys. Lett., vol. 105A, 124 (1984).
- Bondeson, A., and Sobel, J.R., Phys. Fluids, vol. 27, 2026 (1984).
- Brushlinskii, K.V., Zaborov, A.M., and Syrovatskii, S.I., Sov. J. Plasma Phys., vol. 6, 165 (1980).
- Dahlburg, R.B., Zang, T.A., Montgomery, D., and Hussaini, M.Y., Proc. Nat. Acad. Sci. U.S.A., vol. 80, 5790 (1983).
- Dahlquist, G., Björck, A., and Anderson, N., "Numerical Methods", Prentice - Hall, Inc., Englewood Cliffs NJ (1974).
- Dibiase, J.A. and Killeen, J., J Comp. Phys., vol. 24, 158 (1977).
- Dolph, C.L. and Lewis, D.C., Quart. Appl. Math., vol. 16, 97 (1958).
- Drazin, P.G., and Reid, W.B., "Hydrodynamic Stability", Cambridge University Press, New York, 1961.
- Finn, J.M., and Kaw, P.K., Phys. Fluids, vol. 20, 72 (1977).
- Frisch, U., Pouquet, A., Sulem, P. -L., and Meneguzzi, M., Journal de Mecanique Theorique et Appliquee, Numero Special, 191 (1983).
- Furth, B., Killeen, J., and Rosenbluth, M.N., Phys. Fluids, vol. 6, 459 (1963).
- Fyfe, D., and Montgomery, D., J. Plasma Phys., vol. 16, 101 (1982).
- Fyfe, D., Joyce, G., and Montgomery, D., J. Plasma Phys., vol. 17, 317 (1977).
- Fyfe, D., Montgomery, D., and Joyce, G., J. Plasma Phys., vol. 17, 369 (1977).
- Gary, J., and Helgason, R., J. Comp. Phys., vol. 5, 169 (1979).
- Gottlieb, D., and Orszag, S., "Numerical Analysis of Spectral Methods: Theory

- and Applications ", NSF - CBMS monograph no. 26, SIAM, Philadelphia (1977).
- Gottlieb, D., Bussaini, M.Y., and Orszag, S.A., in " Spectral Methods for Partial Differential Equations ", eds. Voight, R.G., Gottlieb, D., and Bussaini, M.Y., SIAM, Philadelphia, 1984.
- Grosch, C.E. and Salwen, B., J. Fluid Mech., vol. 34, 177 (1968).
- Herbert, T., " Stability of Plane Poiseuille Flow -- Theory and Experiment ", Virginia Polytechnic and State University report VPI - E - 81 - 35, 1981, to be published in Fluid Dynamics Transactions.
- Herbert, T., J. Fluid Mech., vol. 126, 167 (1983).
- Horton, W., Tajima, T., and Galvao, R., " Quasilinear Evolution of Tearing Modes During Magnetic Reconnection ", Institute for Fusion Studies report IFSR # 115, October 1983.
- Hossain, M., Matthaeus, W.H., and Montgomery, D., J. Plasma Phys., vol. 30, 479 (1983).
- Joseph, D.D., " Stability of Fluid Motions ", Springer Tracts in Natural Philosophy, Vols. 27 and 28, Springer Verlag, Berlin (1976).
- Kadomtsev, B.B., Sov. J. Plasma Phys., vol. 1, 369 (1975).
- Kleiser, L., and Schumann, U., in " Spectral Methods for Partial Differential Equations ", eds. Voight, R.G., Gottlieb, D., and Bussaini, M.Y., SIAM, Philadelphia, 1984.
- Kruskal, M., and Schwarzschild, M., Proc. Roy. Soc. A, vol. 233, 348 (1954).
- Landau, L.D., and Lifshitz, E.M., " Fluid Mechanics ", Pergamon Press, London (1959).
- Lin, C.C., Quart. Appl. Math., vol. 3, 117 (1945).
- Lin, C.C., " The Theory of Hydrodynamic Stability ", Cambridge University Press, Cambridge ( U.K. ) (1955).
- Manheimer, W.M., and Lashmore - Davies, C., " MHD Instabilities in Simple Plasma

- Configuration ", Naval Research Laboratory, Washington DC (1984).
- Matthaeus, W.B., and Montgomery, D., Ann. Rev. N. Y. Acad. Sci., vol. 357, 203 (1980).
- Matthaeus, W.B., and Montgomery, D.C., J. Plasma Phys., vol. 25, 11 (1981).
- Matthaeus, W.B., Geophys. Res. Lett., vol. 9, 660 (1982).
- Matthaeus, W.B., and Lamkin, S.L., Phys. Fluids, vol. 28, 303 (1985).
- Meksyn, D., and Stuart, J.T., Proc. Roy. Soc. A, vol. 208, 517 (1951).
- Moin, P., and Kim, J., J. Comp. Phys., vol. 35, 381 (1980).
- Moin, P., and Kim, J., J. Fluid Mech., vol. 118, 341 (1982).
- Montgomery, D., Physica Scripta T2 / 2, 506 (1982).
- Montgomery, D., in " Spectral Methods for Partial Differential Equations ", eds. Voight, R.G., Gottlieb, D., and Hussaini, M.Y., SIAM, Philadelphia (1984).
- Orszag, S.A., J. Fluid Mech., vol. 50, 689 (1971).
- Orszag, S.A., and Kells, L.C., J. Fluid Mech., vol. 96, 161 (1980).
- Orszag, S.A. and Patera, A.T., J. Fluid Mech., vol. 128, 347 (1983).
- Ortega, J.M., and Poole, W.G., " An Introduction to Numerical Methods for Differential Equations ", Pitman Publishing Inc., Marshfield MA (1981).
- Pao, Y.P., Rosenau, P., and Guo, S.G., Comm. Pure Appl. Math, vol. 36, 615 (1983).
- Roache, P.J., " Computational Fluid Dynamics ", Hermosa Publishers, Albuquerque (1972).
- Rutherford, P.B., Phys. Fluids, vol. 16, 1903 (1973).
- Reynolds, W.C., and Potter, M.C., J. Fluid Mech, vol. 27, 465 (1967).
- Schnack, D., and Killeen, J., Nucl. Fusion, vol. 19, 877 (1979).
- Schnack, D., and Killeen, J., J. Comp. Phys., vol. 25, 110 (1980).
- Shebalin, J.V., Matthaeus, W.B., and Montgomery, D., J. Plasma Phys., vol. 29,



- 525 (1983).
- Sonnerup, B.U.O., *Solar System Plasma Physics*, vol. 3, 45 (1979).
- Stuart, J.T., *J. Fluid Mech.*, vol. 4, 1 (1958).
- Stuart, J.T., *J. Fluid Mech.*, vol. 9, 353 (1969).
- Stuart, J.T., *Ann. Rev. Fluid Mech.*, vol. 3, 347 (1971).
- Syrovatskii, S.I., *Sov. Phys. JETP*, vol. 33, 933 (1971).
- Syrovatskii, S.I., *Izv. Akad. Nauk SSSR, Ser. Fiz.*, vol. 43, 695 (1979).
- Thomas, L.B., *Phys. Rev.*, vol. 91, 789 (1953).
- Van Kampen, N.G., and Felderhof, B.U., "Theoretical Methods in Plasma Physics". John Wiley and Sons, Inc., New York (1967).
- Waddell, B.V., Rosenbluth, M.N., Monticello, D.A., and White, R.B., *Nucl. Fusion*, vol. 16, 528 (1976).
- Watson, J., *J. Fluid Mech.*, vol. 9, 371 (1969).
- Wesson, J., *Nucl. Fusion*, vol. 6, 139 (1966).
- White, R.B., Monticello, D.A., Rosenbluth, M.N., and Waddell, B.V., *Phys. Fluids*, vol. 20, 869 (1977).
- White, R.B., in "Handbook of Plasma Physics, vol. 1", eds. Galeev, A.N., and Sudan, R.N., North Holland Publishing Company, (1983).
- Wilkinson, J.H., "The Algebraic Eigenvalue Problem", Clarendon Press, Oxford (1965).
- Yih, C.S., "Fluid Mechanics; A Concise Introduction to the Theory", McGraw - Hill, New York (1969).
- Zahn, J.P., Toomre, J., Spiegel, E.A., and Gough, J., *J. Fluid Mech.*, vol. 64, 319 (1974).

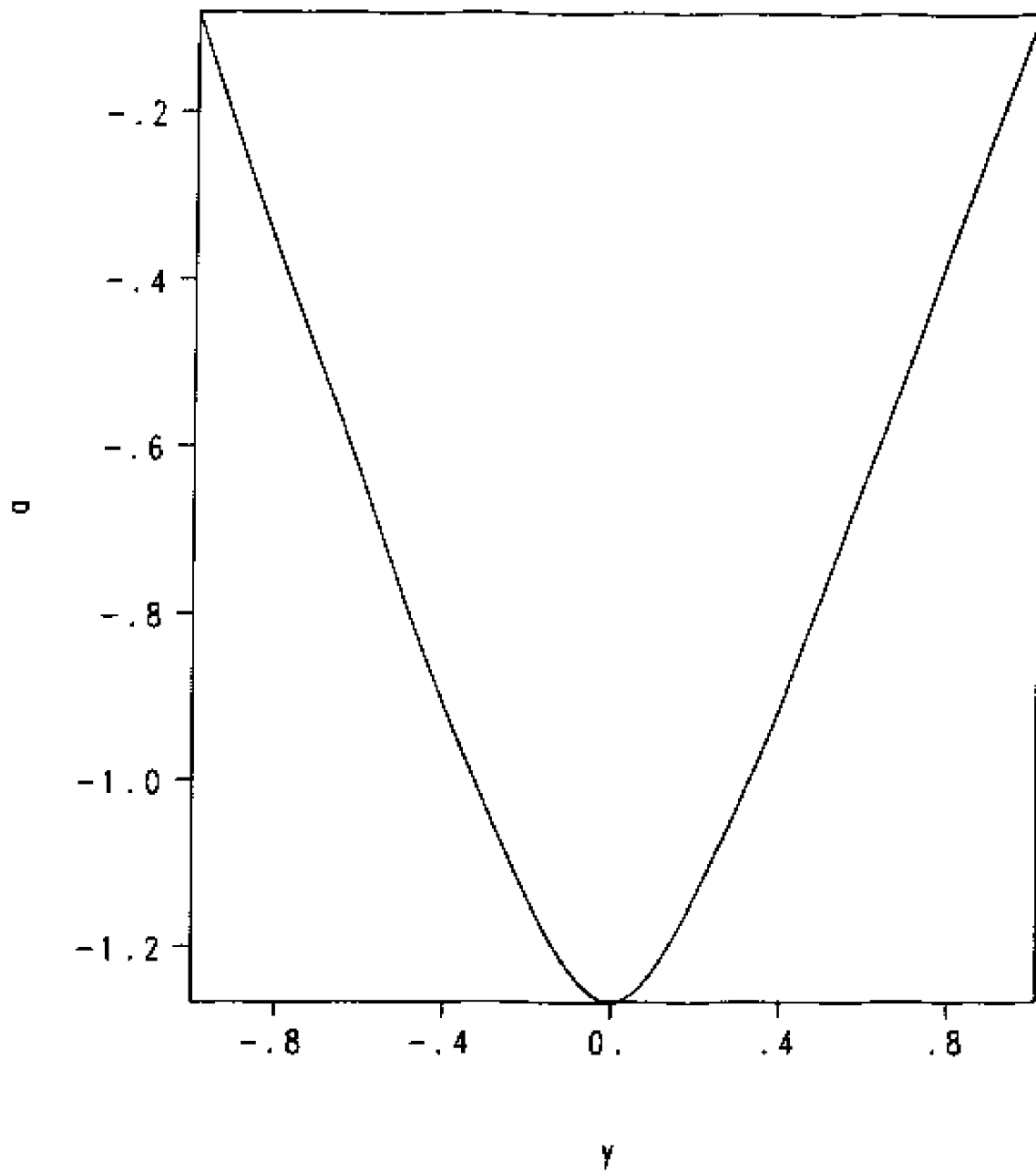


Figure II - 1. Equilibrium magnetic vector potential:  $S = 100$ ,  $\gamma = 0$ .

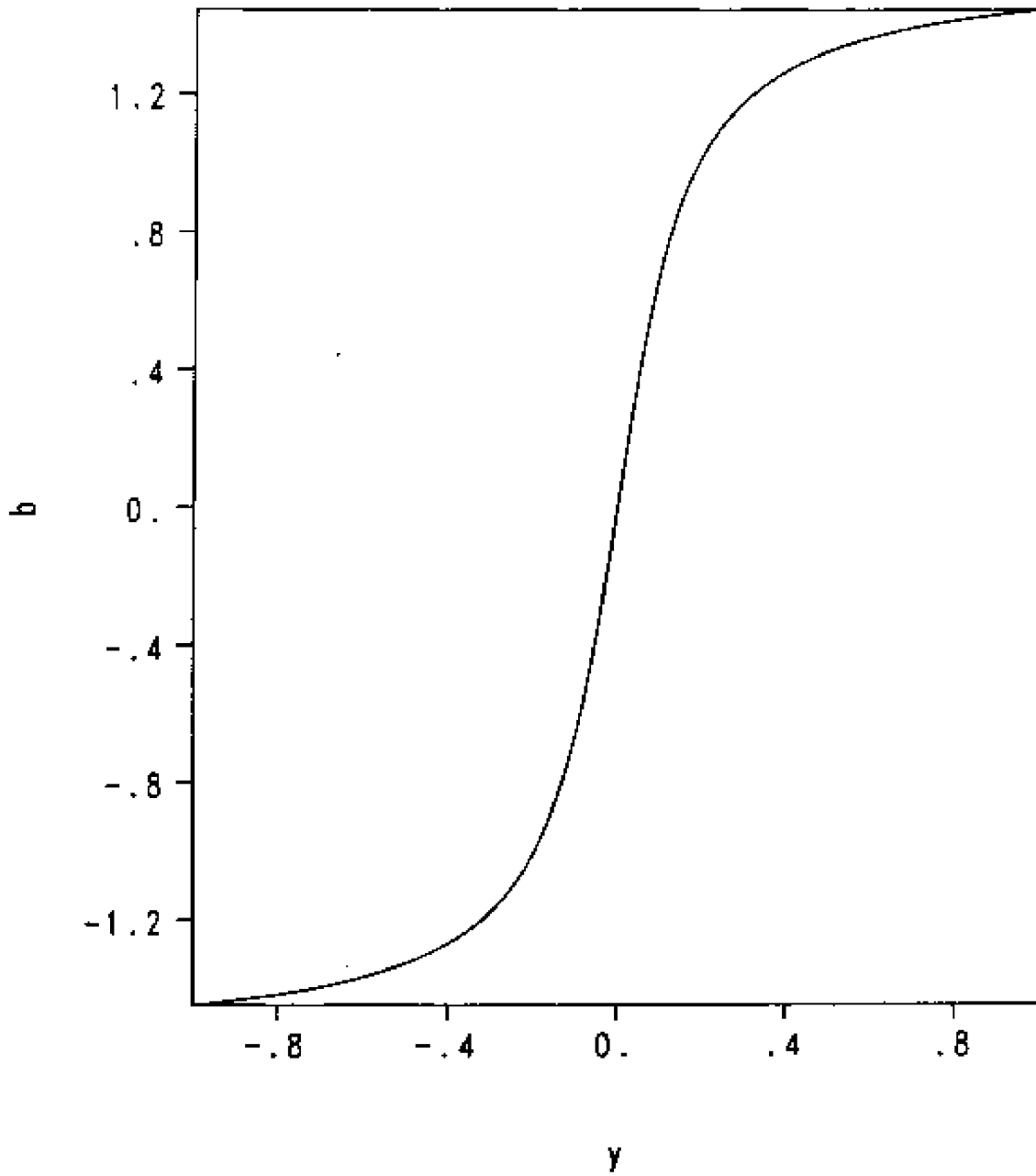


Figure 11 - 2. Equilibrium magnetic field:  $S = 100$ ,  $\gamma = 3$ .

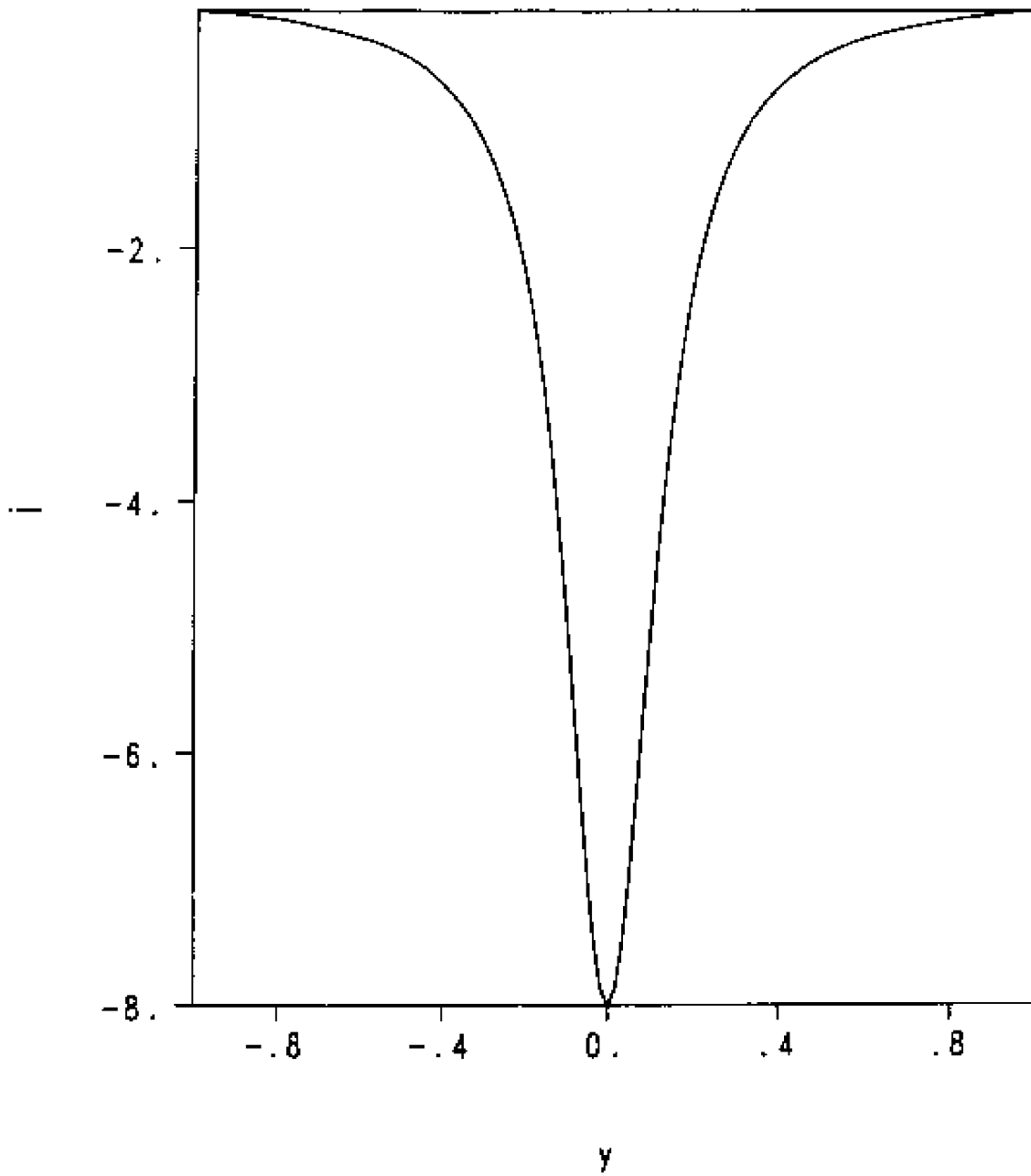


Figure II - 3. Equilibrium electric current density,  $S = 100$ ,  $\gamma = 3$ .

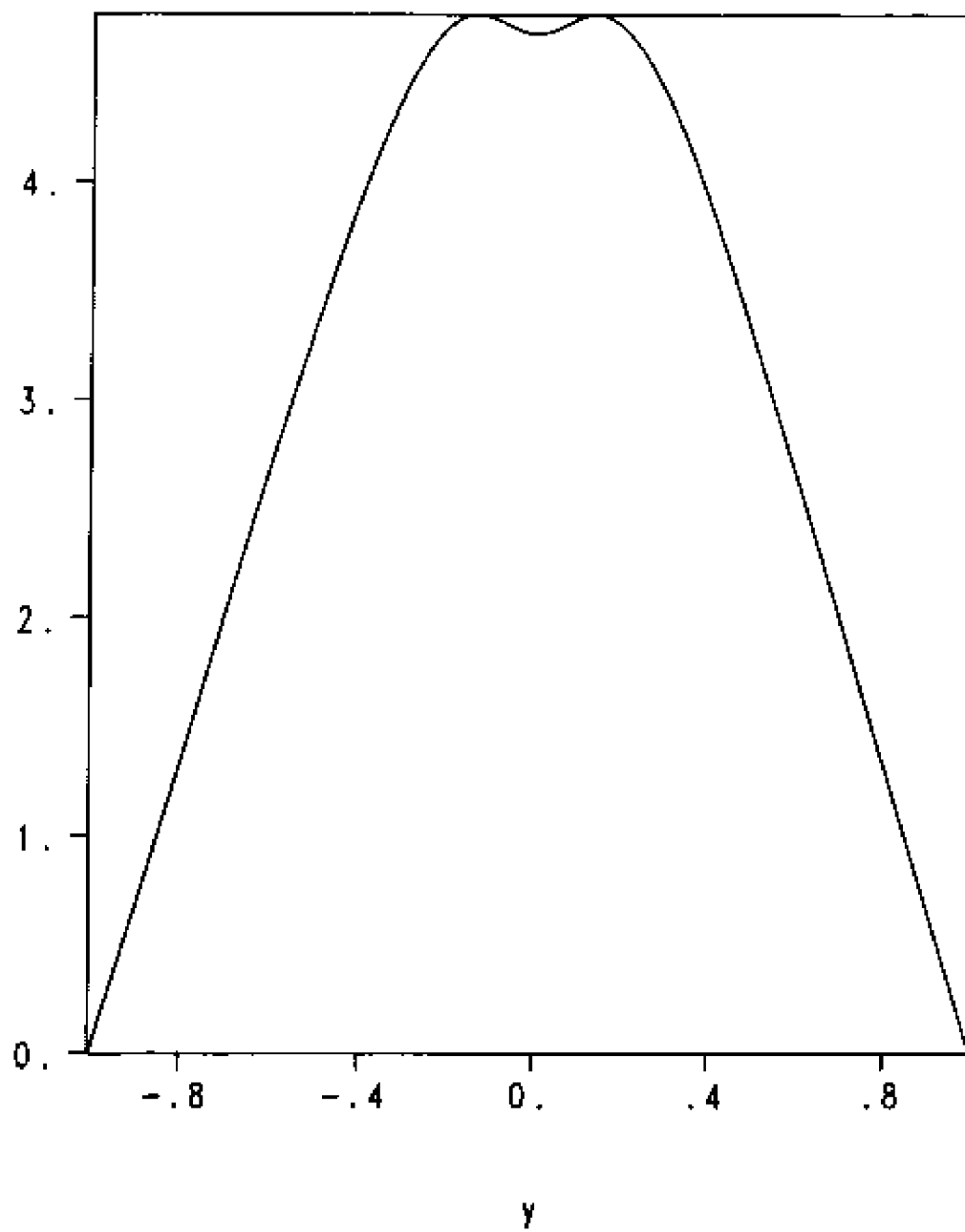


Figure III - 1. Magnetic eigenfunction:  $B_0(y) = \arctan(\theta y)$ ,  $\alpha = 1$ .

$$M = S = 50.$$

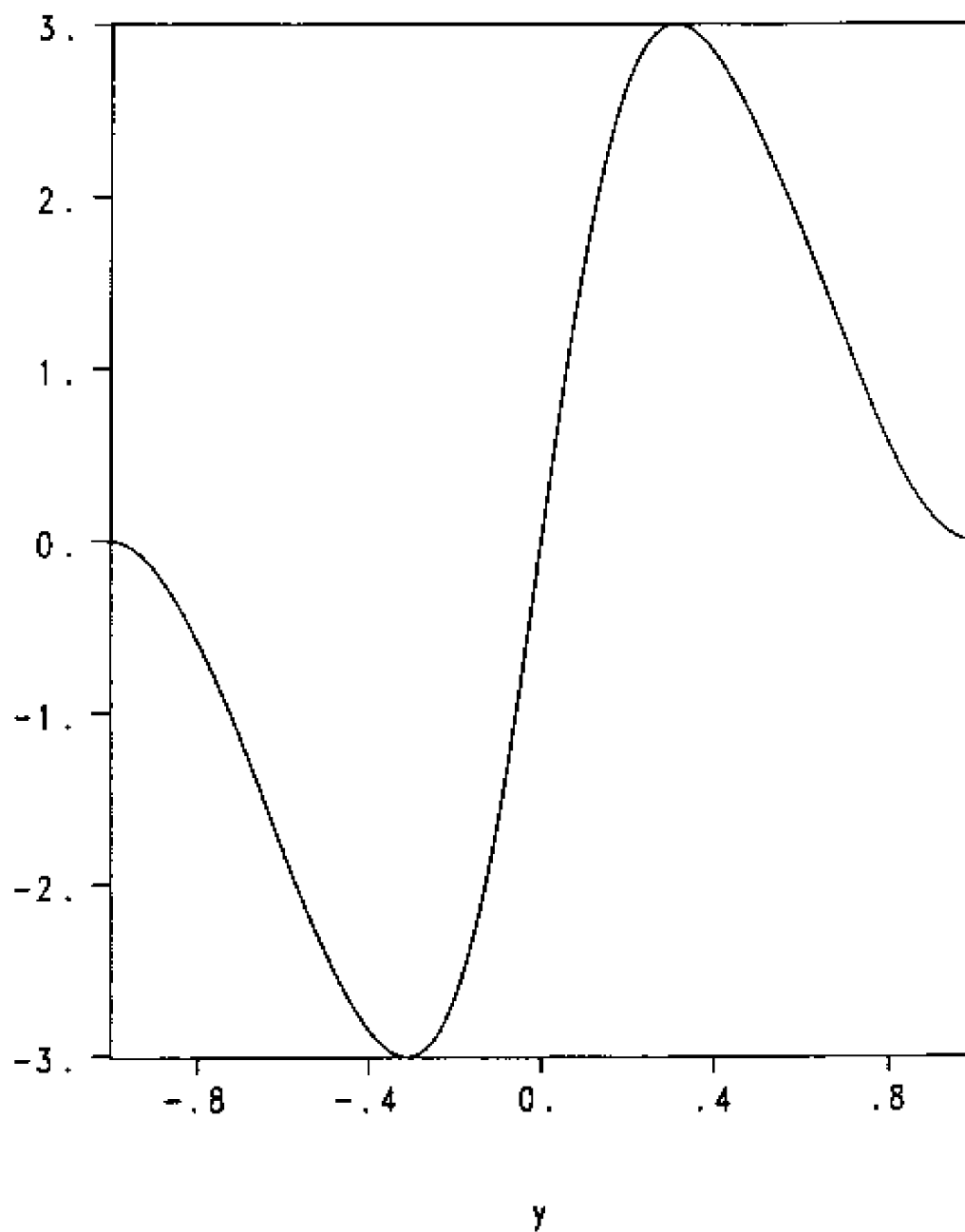


Figure III - 2. Velocity eigenfunction:  $B_0(y) = \arctan(8y)$ ,  $\alpha = 1$ .  
 $\mathfrak{M} = \mathfrak{S} = 50$ .

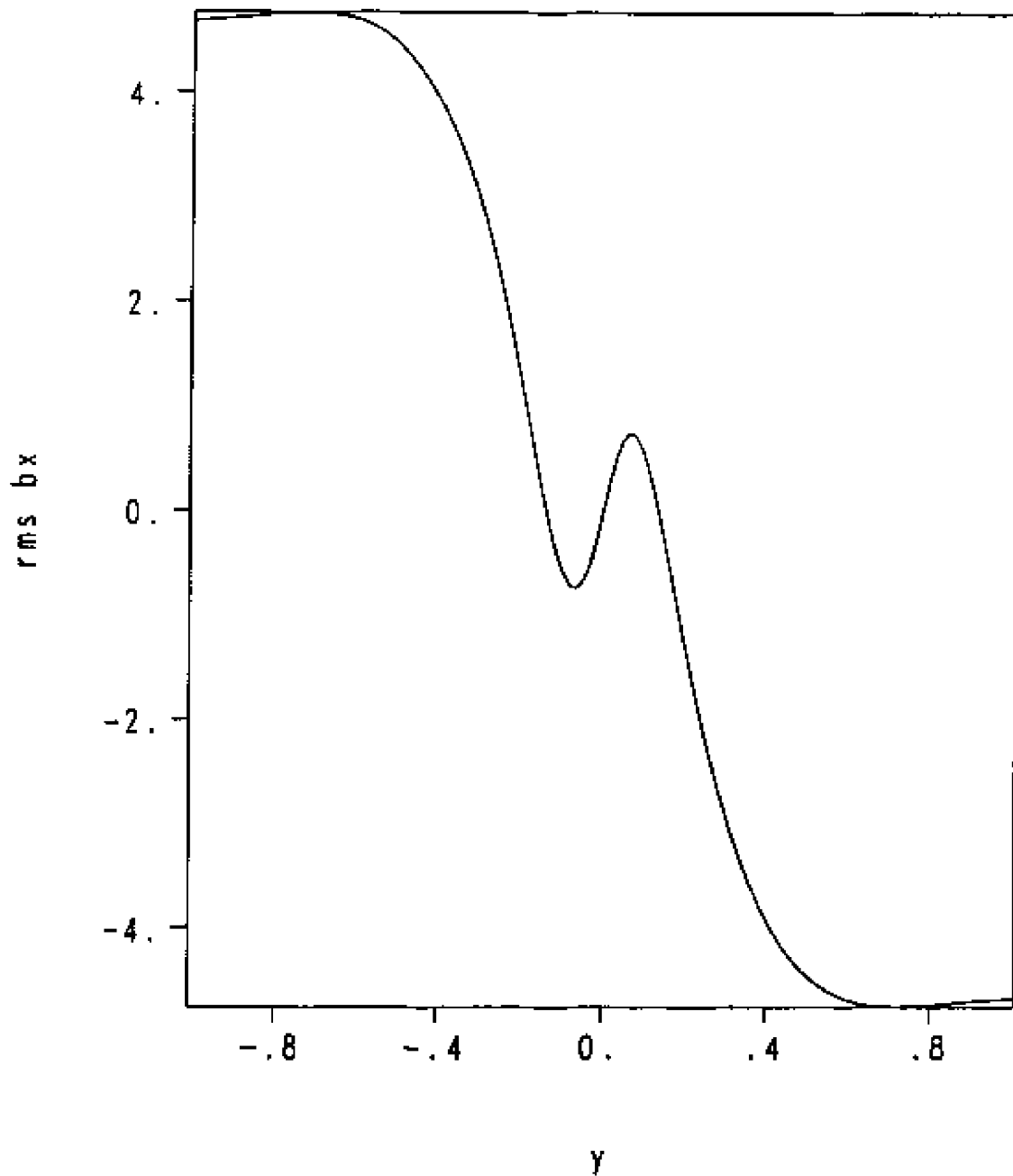


Figure III - 3. Root mean square x component of perturbed magnetic field.

$$B_0(y) = \arctan(\beta y), \quad \alpha = 1, \quad M = S = 50.$$

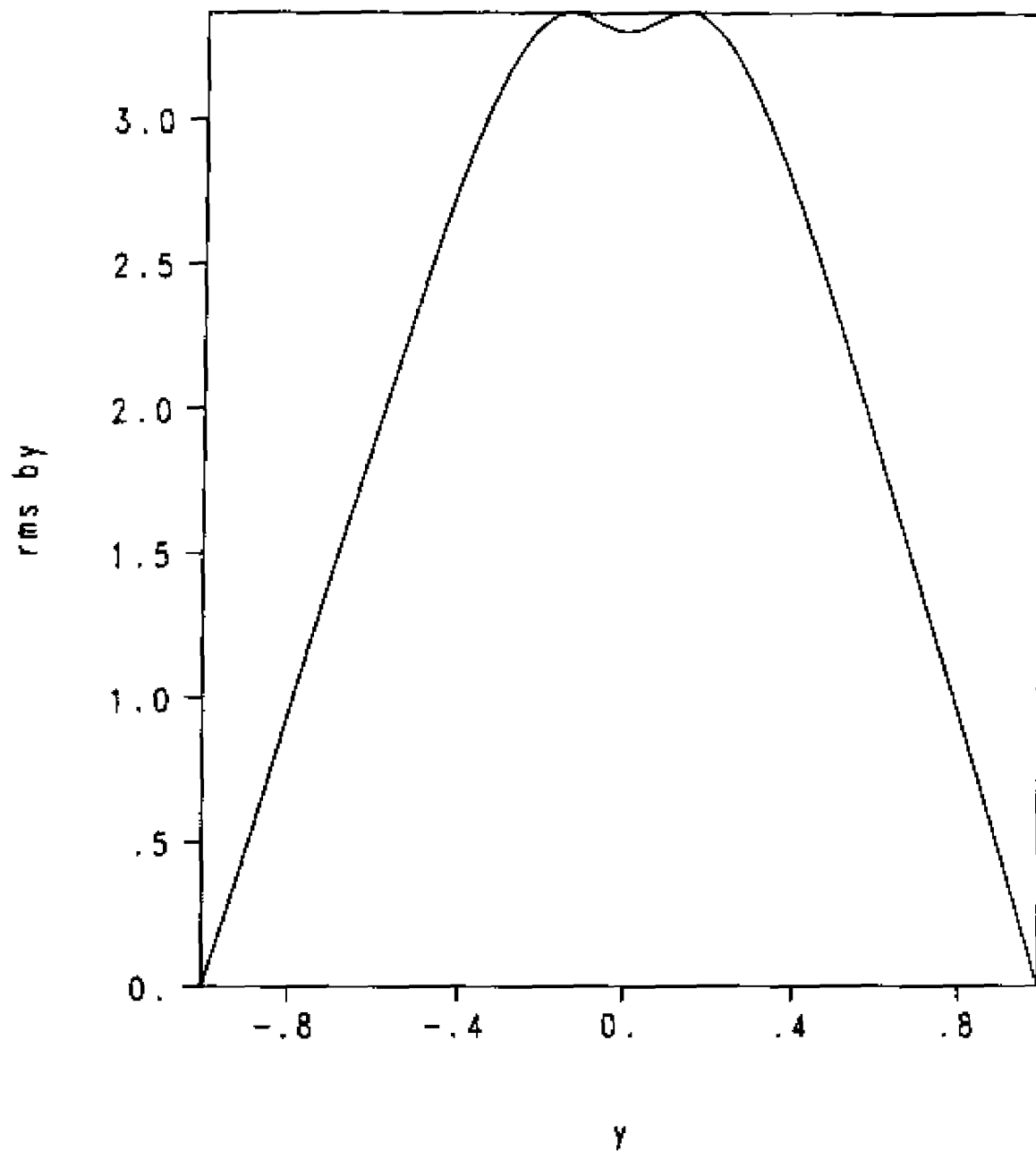


Figure III - 4. Root mean square y component of perturbed magnetic field:

$$B_0(y) = \arctan(\theta y), \text{ alpha} = 1, M = S = 50.$$



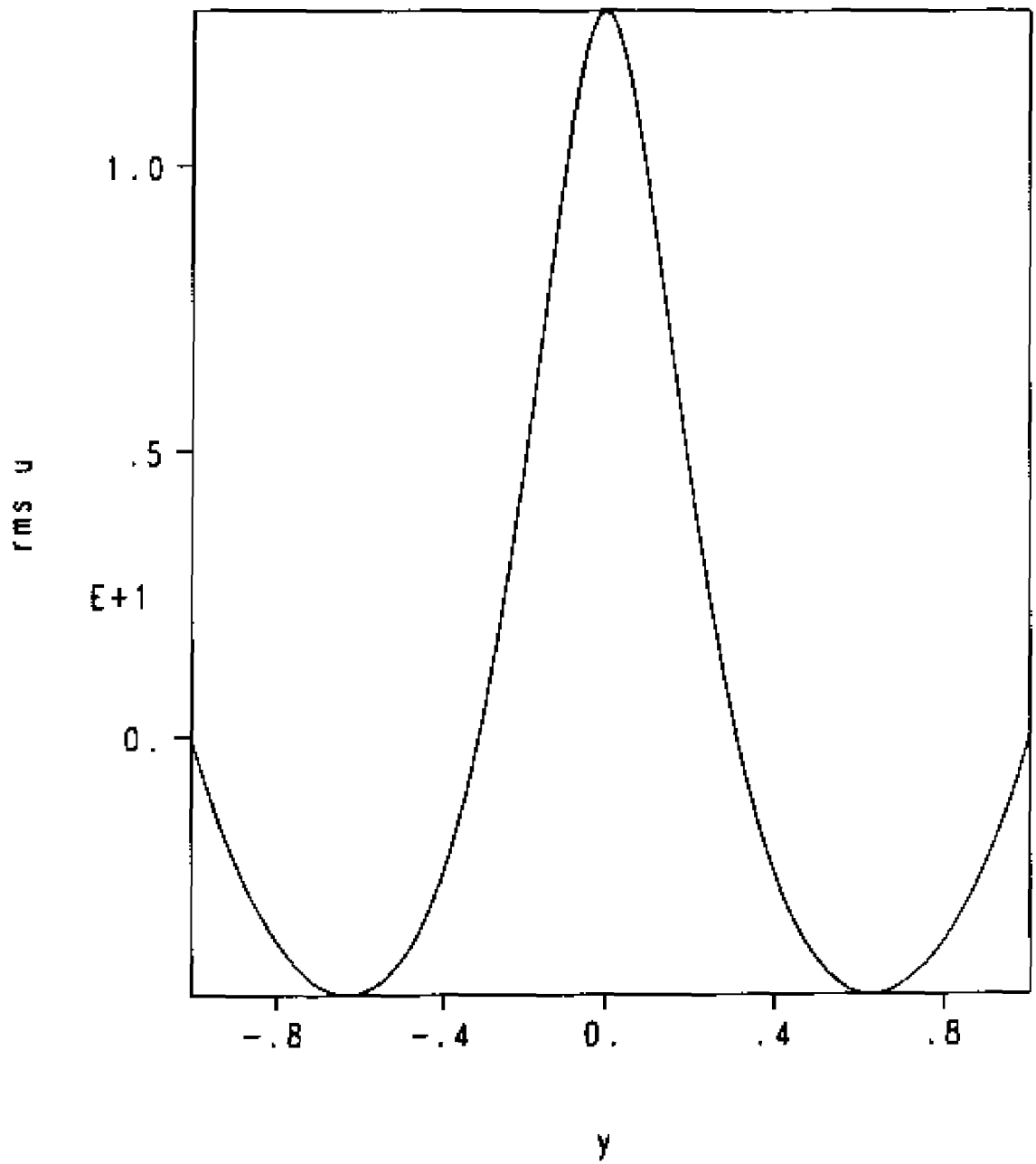


Figure III - 5. Root mean square x component of velocity field.  
 $B_0(y) = \arctan(\theta y)$ ,  $\alpha = 1$ ,  $M = S = 50$

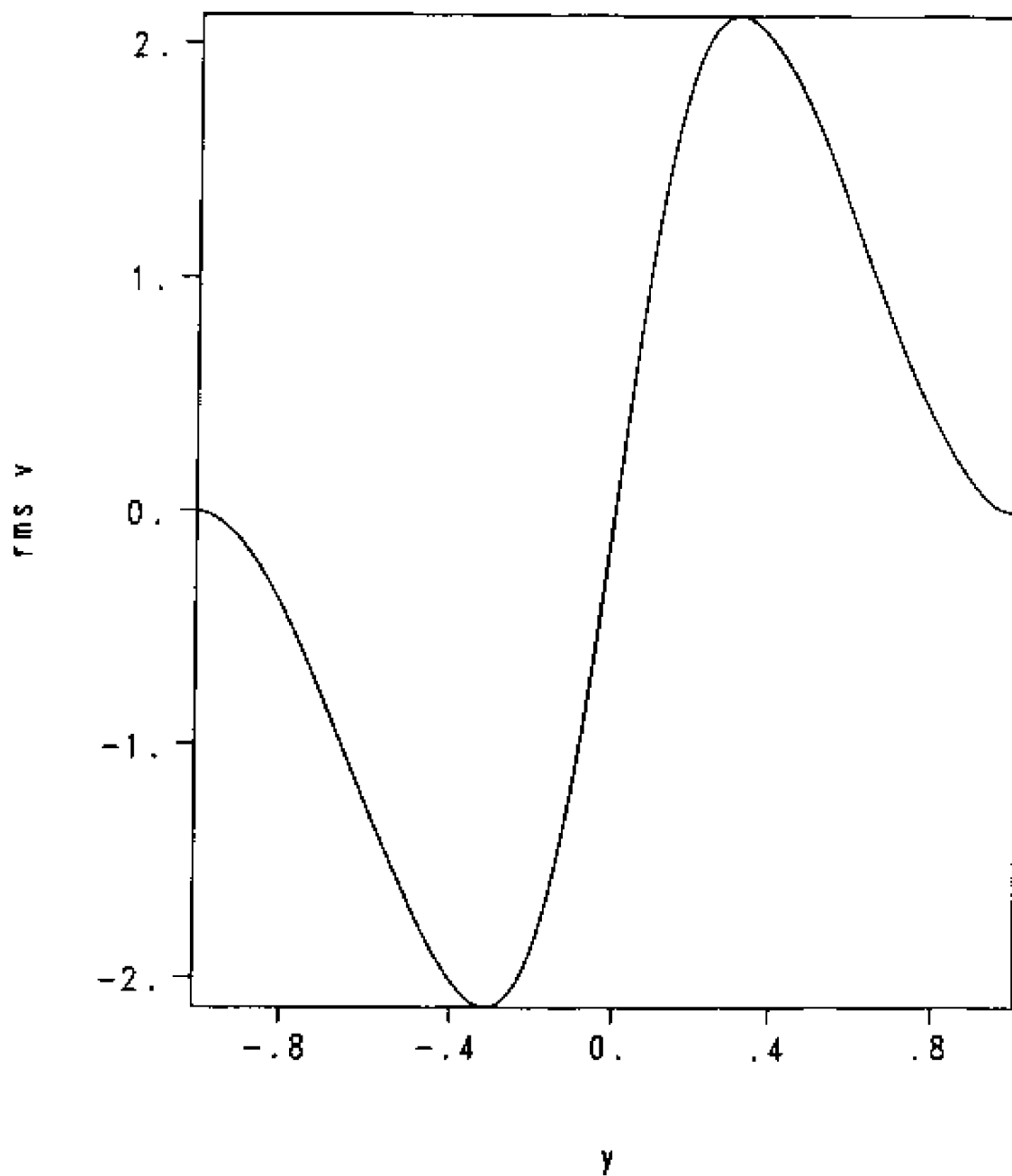


Figure III - 6. Root mean square  $v_y$  component of velocity field;

$$E_0(y) = \arctan(8y), \alpha = 1, M = 5 = 5\bar{8}$$

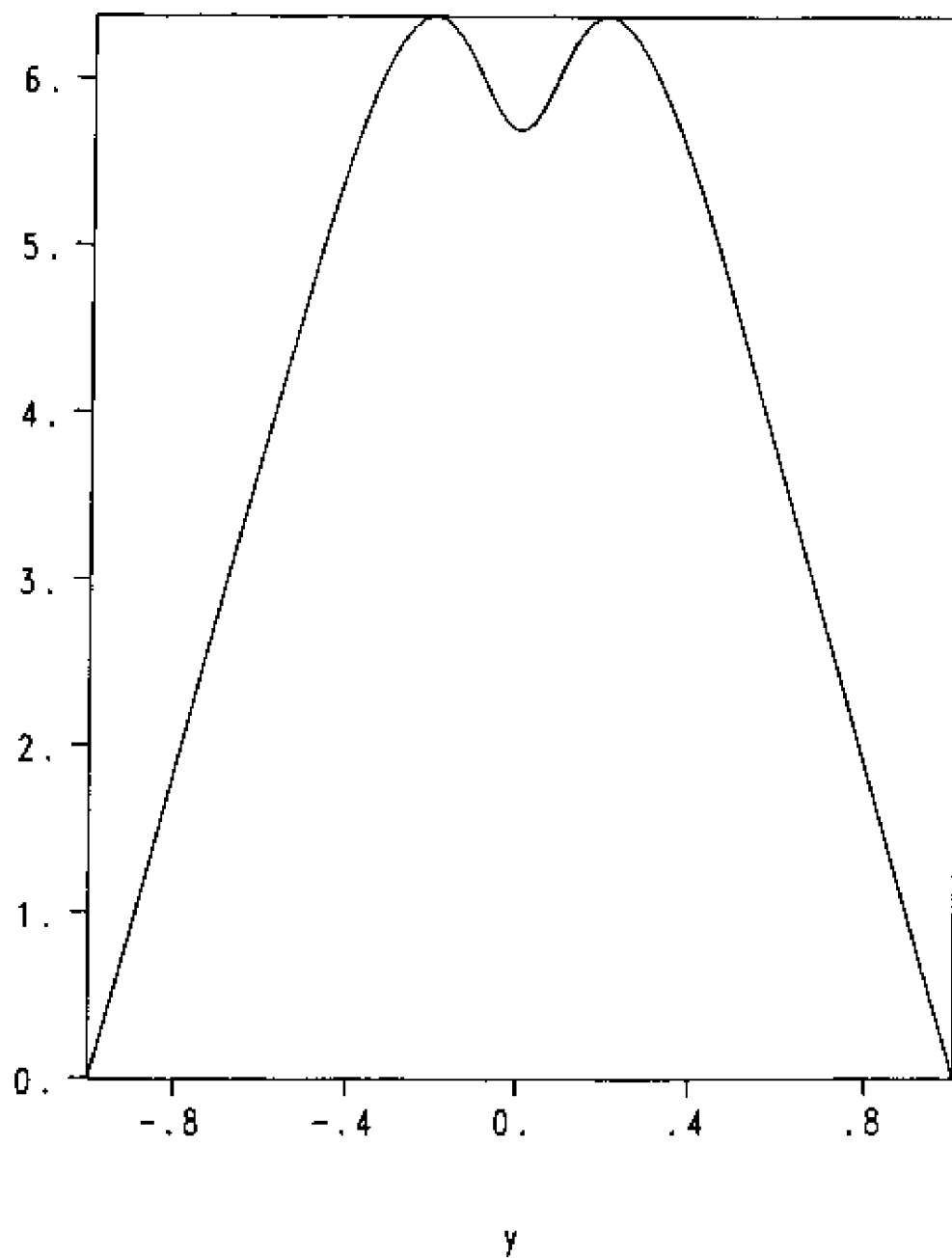


Figure III - 7. Magnetic eigenfunction;  $B_0(y) = \arctan(8y)$ ,  $\alpha = 1$ ,  
 $M = S = 100$ .

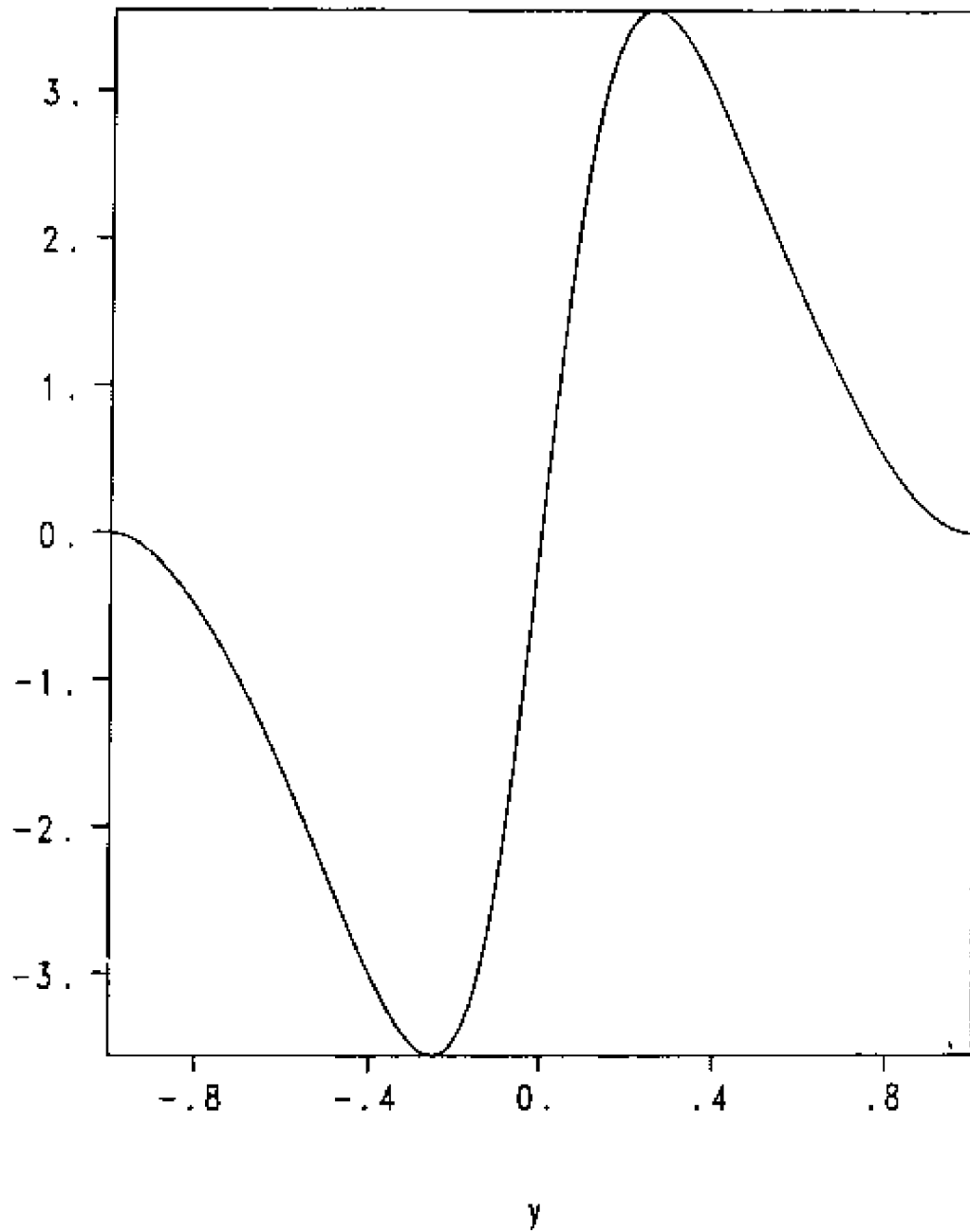


Figure III - 3. Velocity eigenfunction;  $3_0(y) = \arctan(8y)$ ,  $\alpha = 1$ ,  
 $M = S = 100$ .

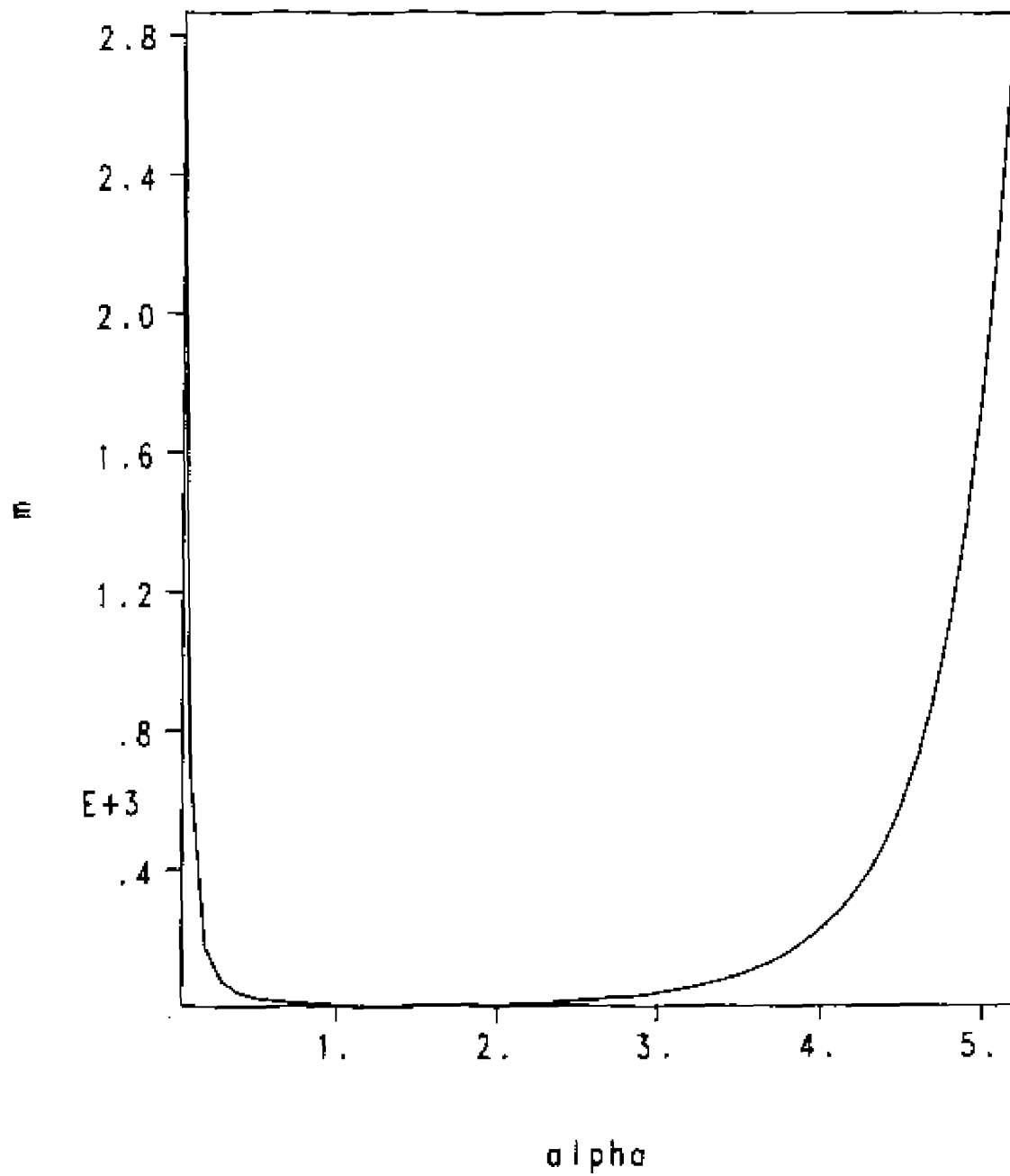


Figure III - 9. Neutral stability curve,  $B_p(\gamma) = \arctan : \theta \gamma$ ,  
 $S = 100$ .

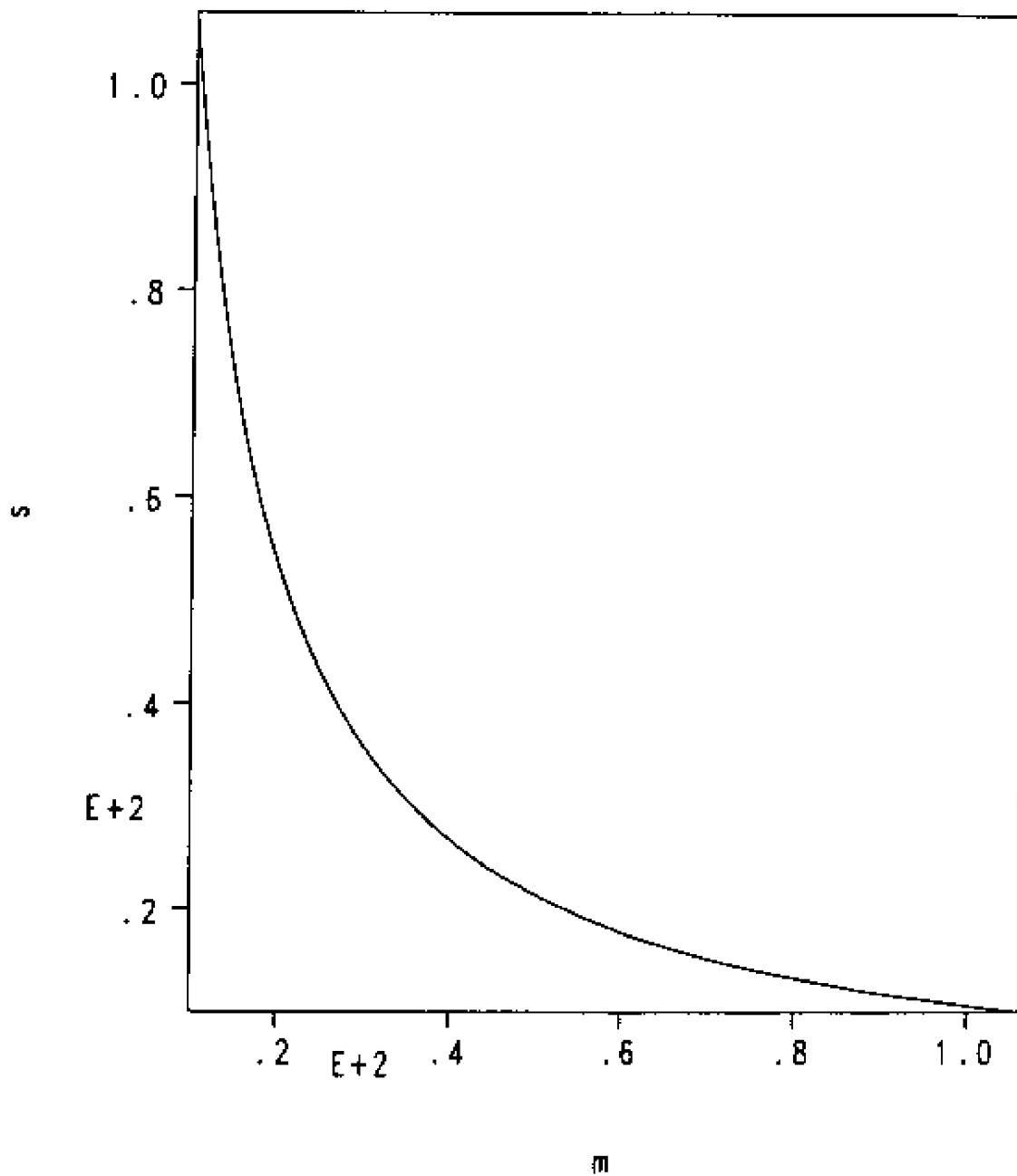


Figure III - 14. Locus of critical Lundquist numbers;  $\beta(y) = \arctan(8y)$ ,  
critical  $\alpha = 1.4$ .

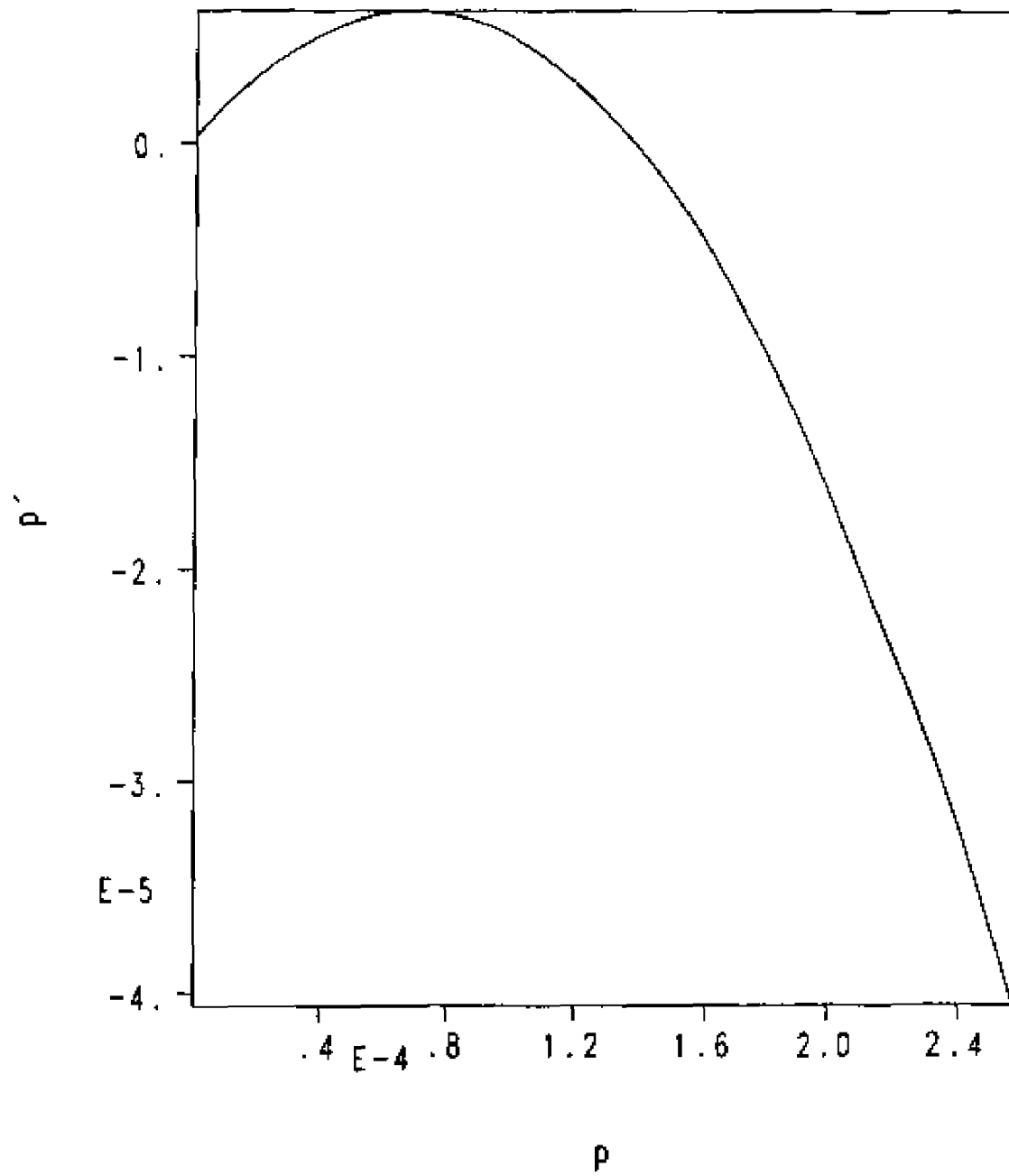


Figure IV - 1. Amplitude phase plane;  $B_p / y = \arctan (B y)$ ,  $\alpha = 1$ ,  
 $M = S = 50$ .

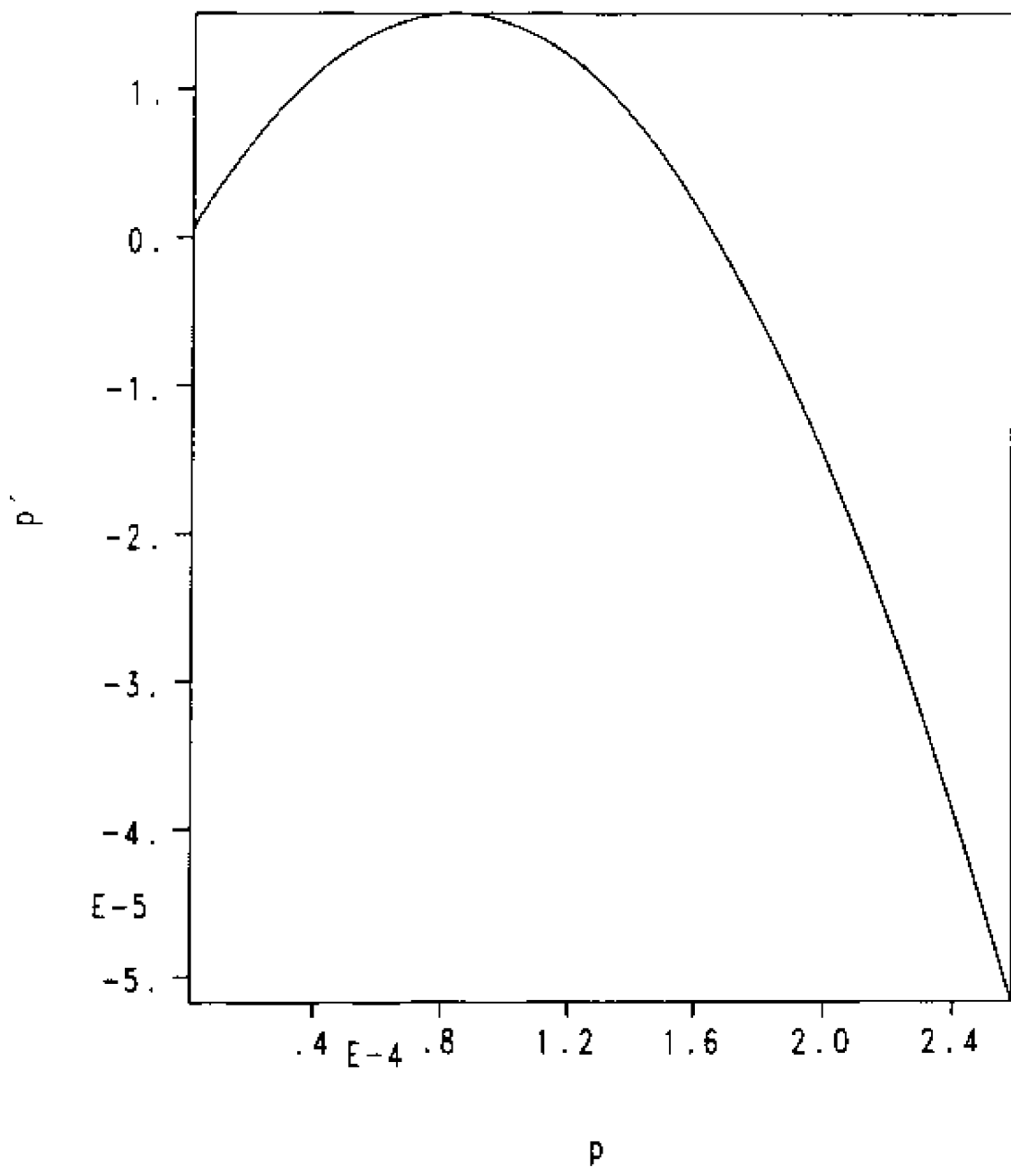


Figure IV - 2. Amplitude phase plane;  $B_{\bullet}(y) = \arctan(\theta y)$ ,  $\alpha = 1$ ,  
 $M = S = 100$ .



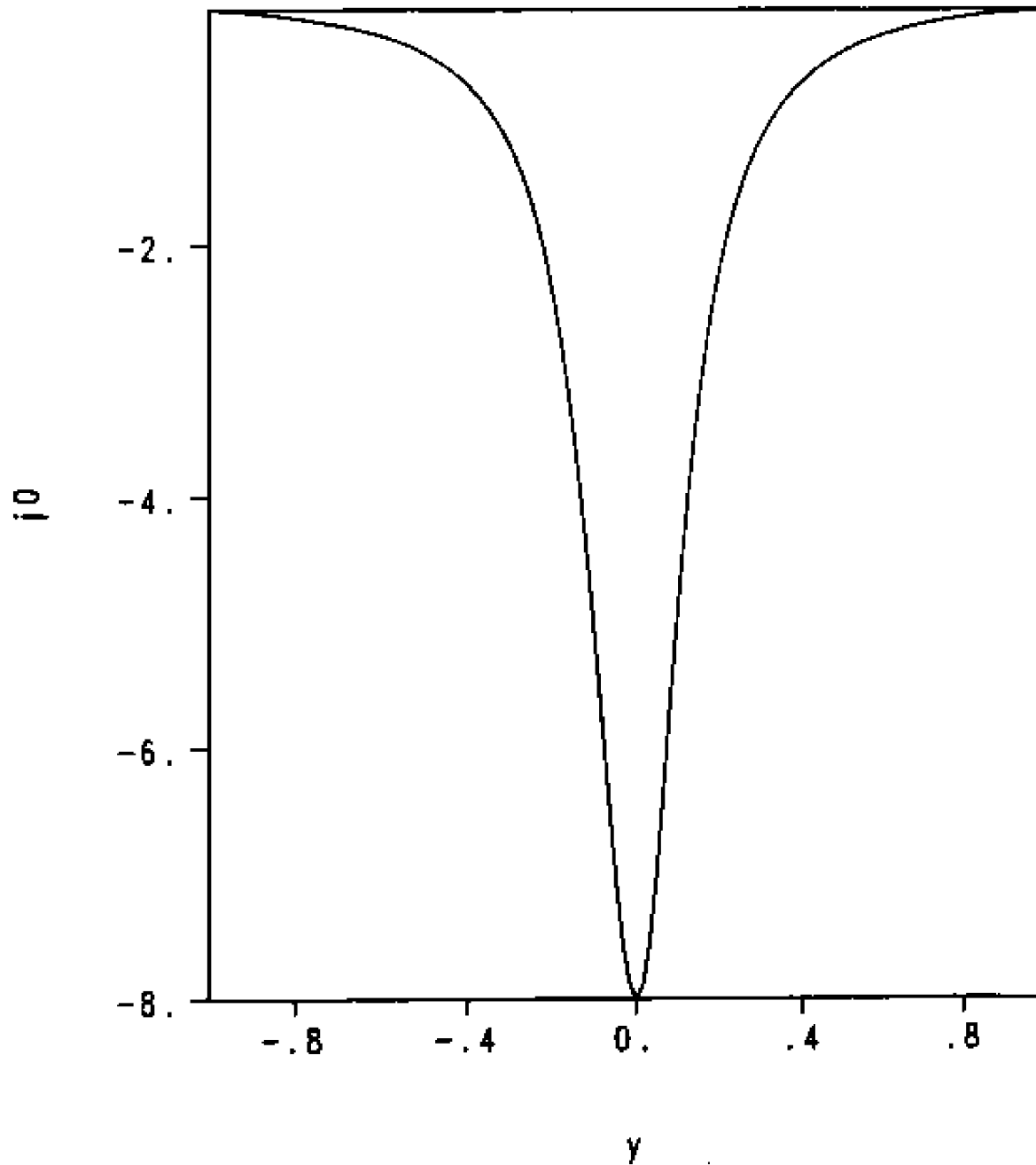


Figure IV - 3. Initial mean current profile;  $B_0(y) = \arctan(B y)$ ,  
 $\alpha = 1$ ,  $M = B = 50$ .

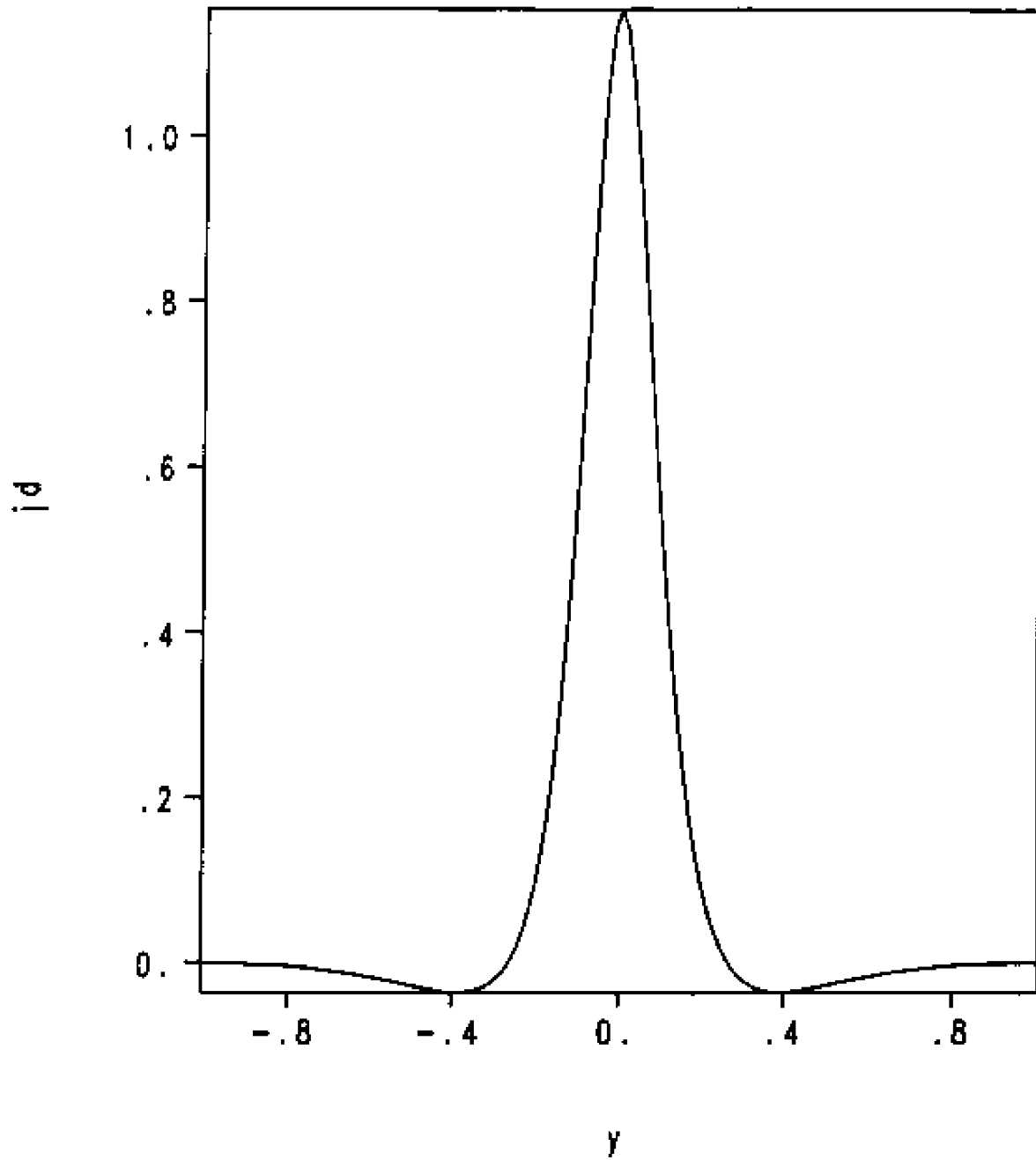


Figure IV - 4. Perturbed current density;  $B_0(y) = \arctan(8y)$ ,  $\alpha = 1$ ,  
 $H = 5 = 50$ .

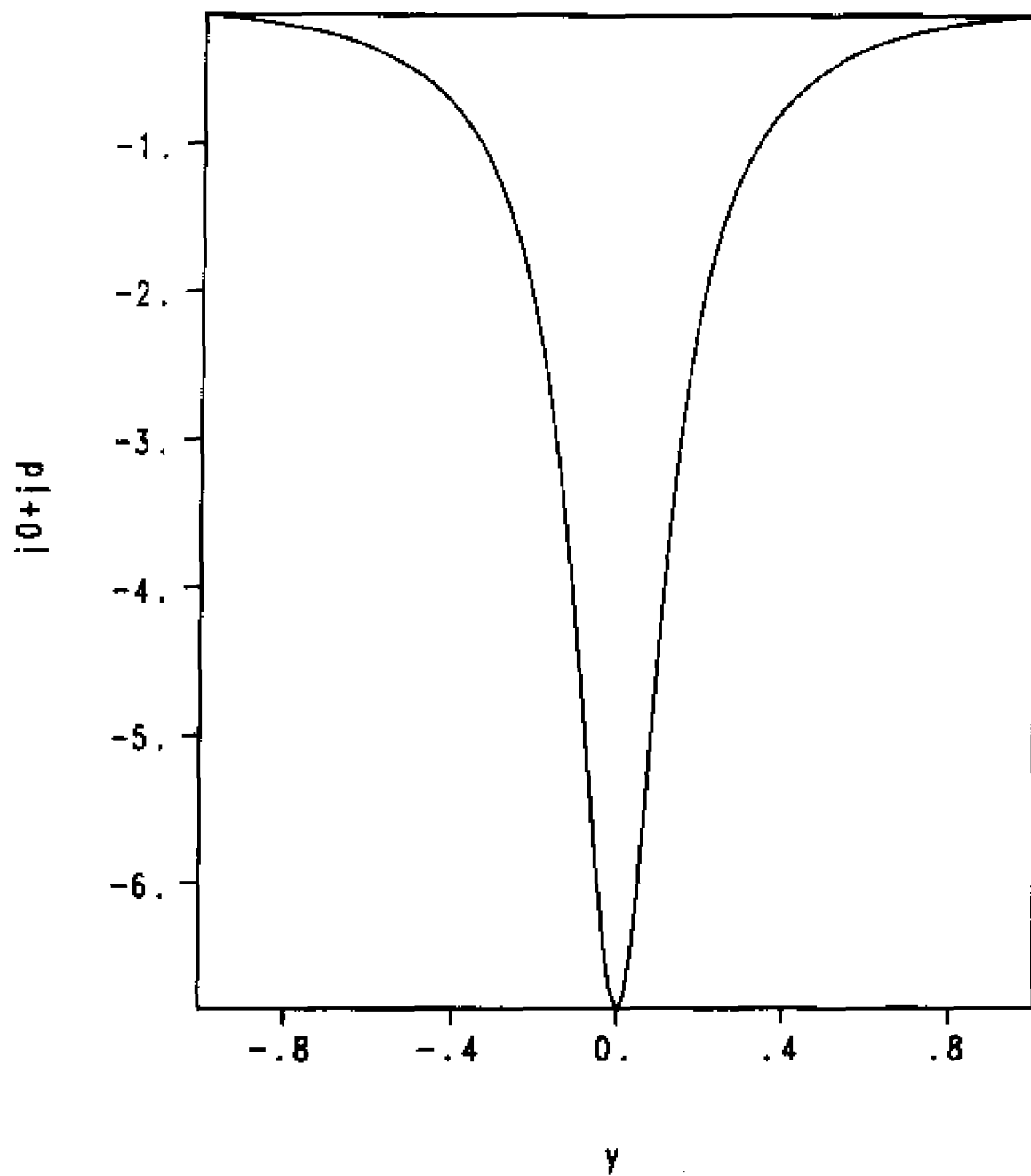


Figure IV - 5. Distorted mean current profile;  $B_0(y) = \arctan(8y)$ ,  
 $\alpha = 1$ ,  $M = S = 50$ .

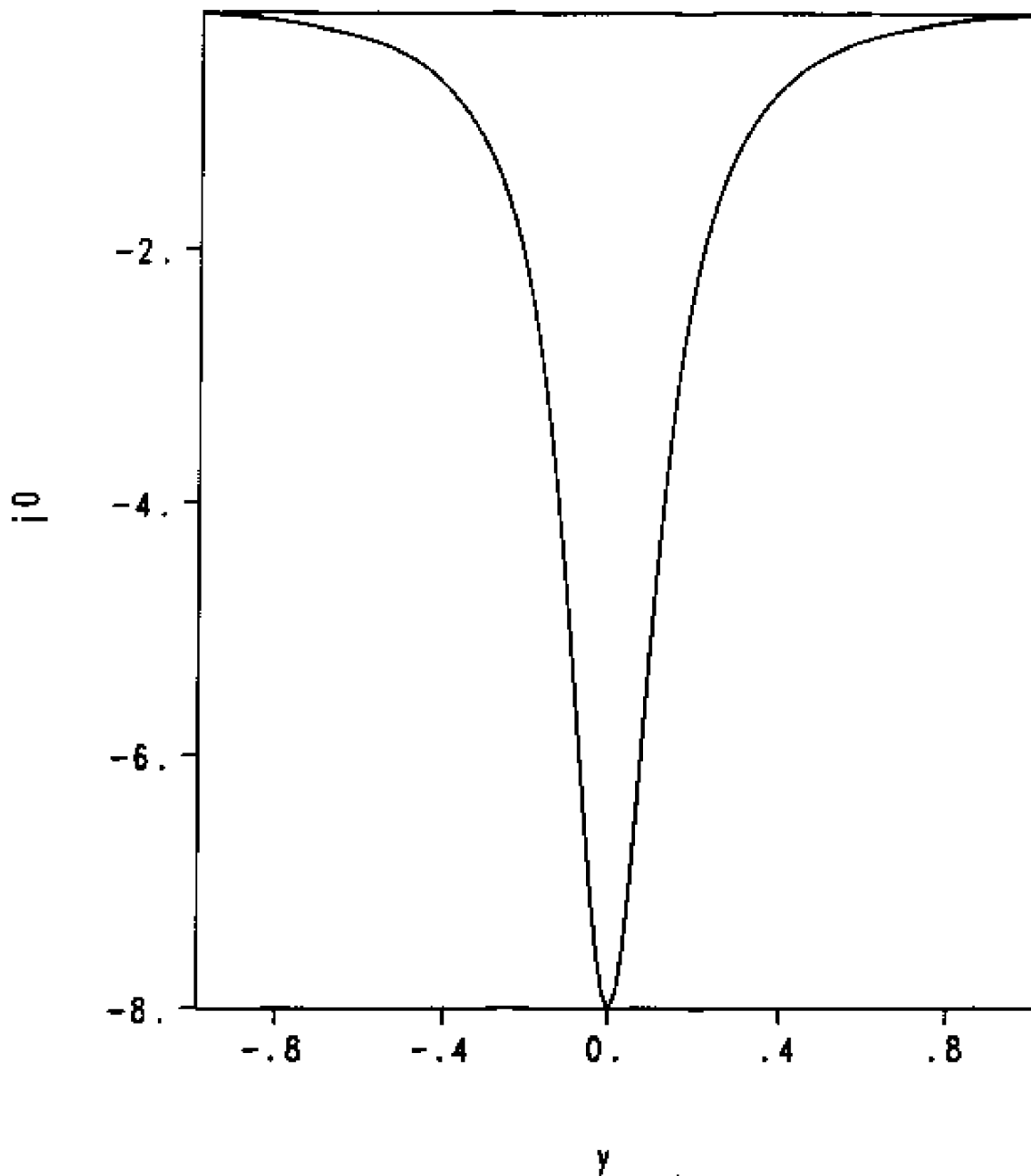


Figure IV - 6. Initial mean current profile;  $B_0(y) = \arctan(8y)$ ,  
 $\alpha = 1$ ,  $M = S = 100$ .

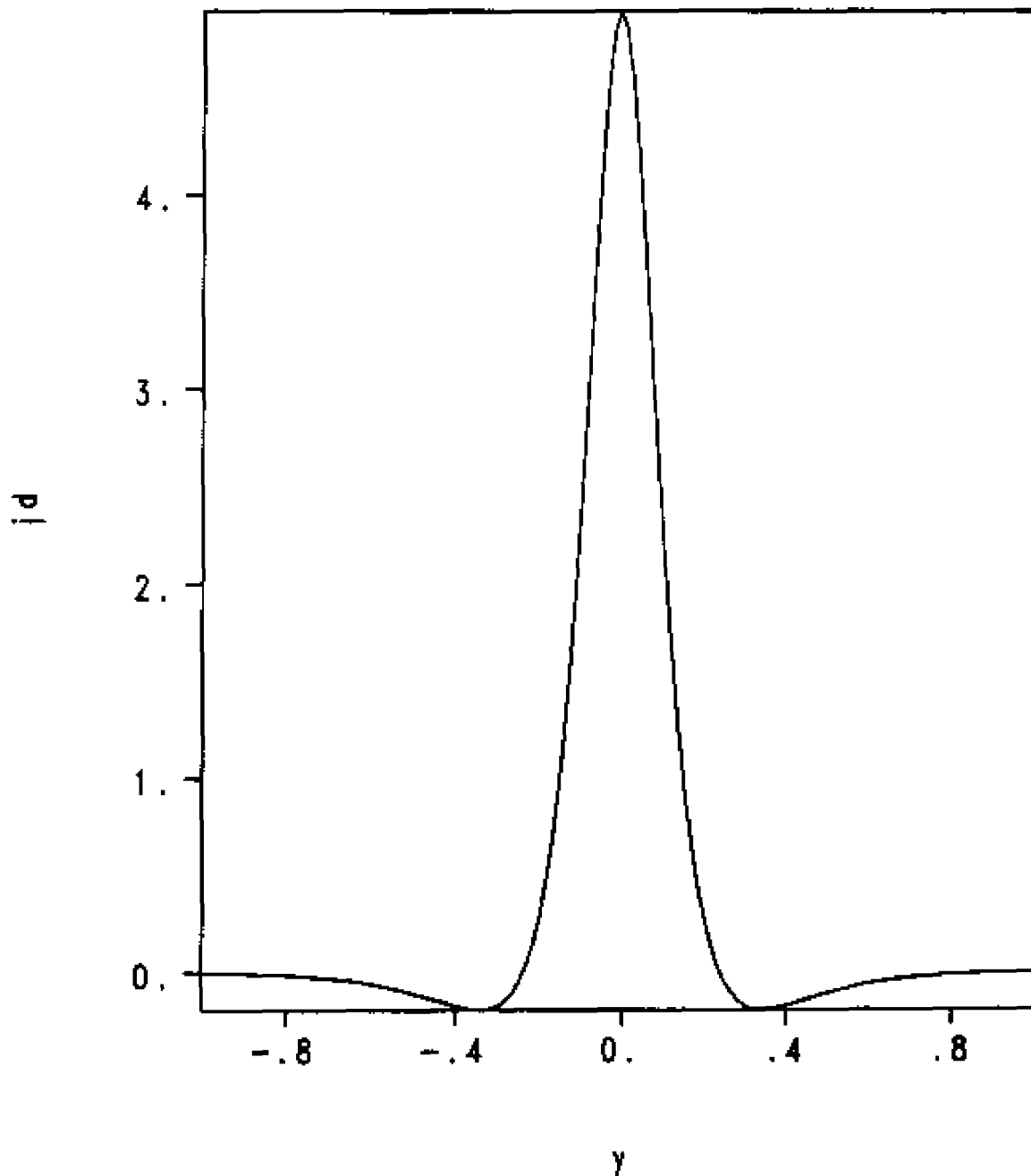


Figure IV - 7. Perturbed current density,  $B_0(y) = \arctan(\delta y)$ ,  $\alpha = 1$ ,  
 $M = \delta = 10^6$ .

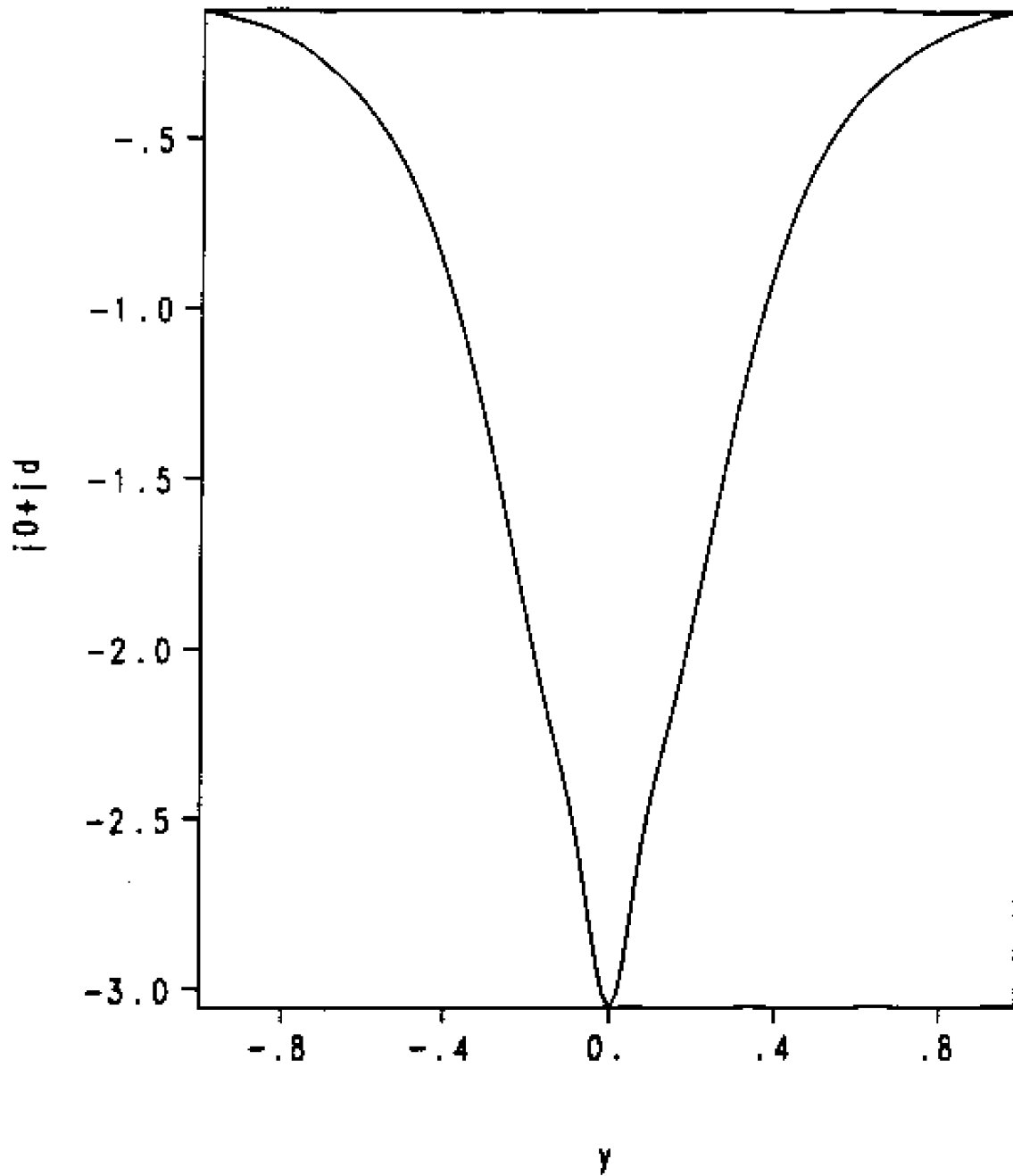


Figure IV - 8. Distorted mean current profile;  $B_0(y) = \arctan(\theta y)$ ,  
 $\alpha = 1$ ,  $M = S = 100$ .

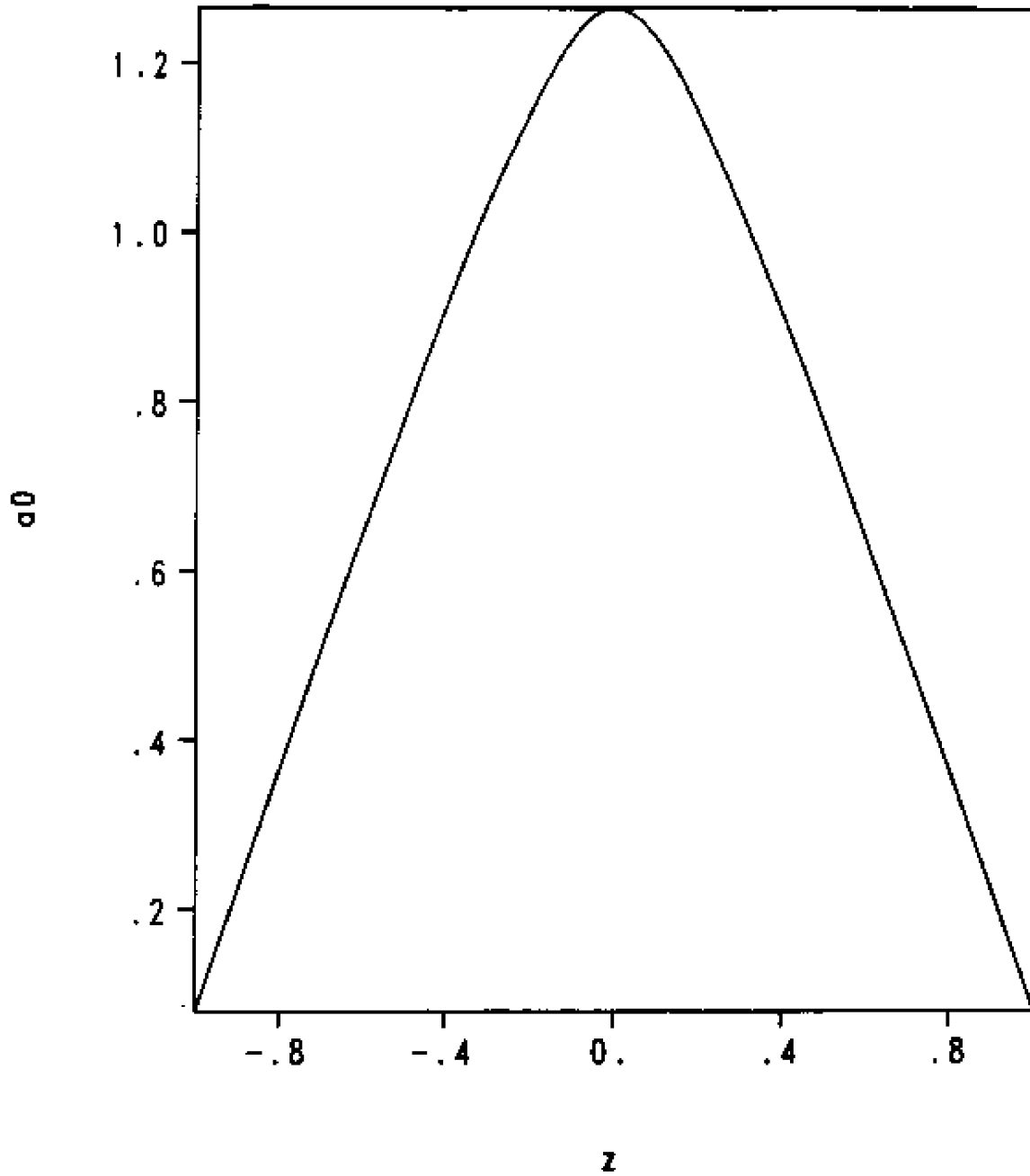


Figure VI - 1 Mean magnetic vector potential at  $t = \frac{1}{2}$ .

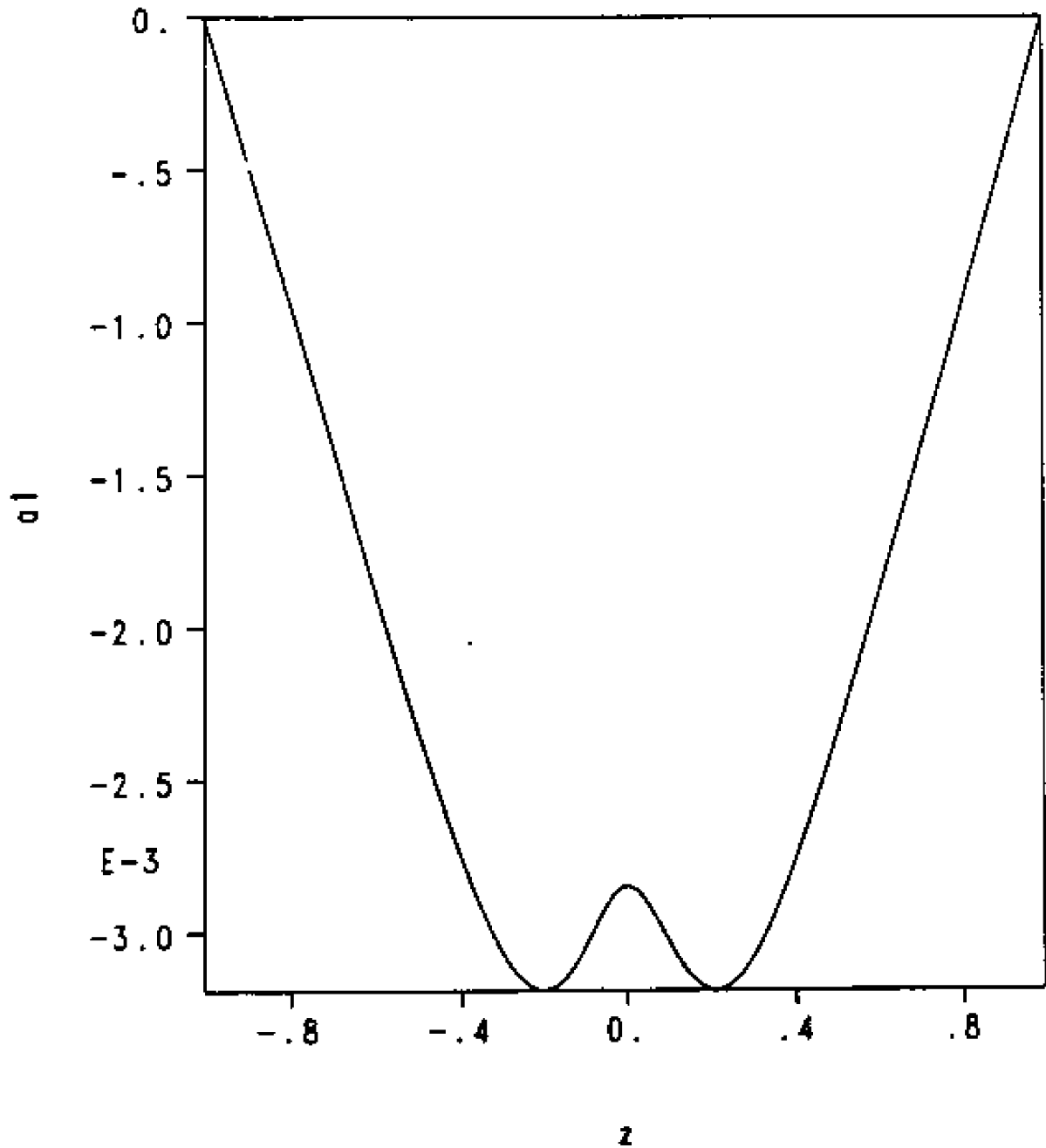


Figure VI - 2 Primary magnetic disturbance at  $t = 0$ .





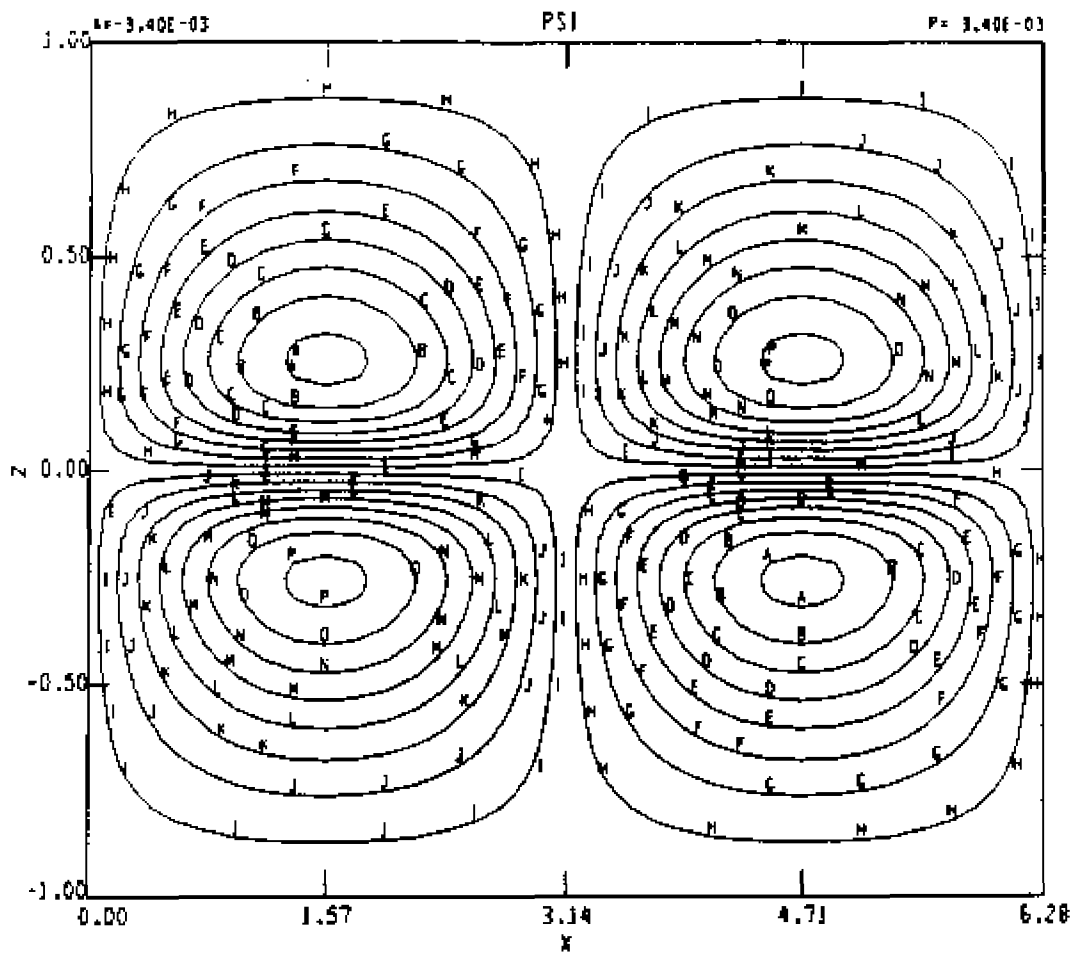


Figure VI - 4 Contour plot of velocity stream function at  $t = 0$ .

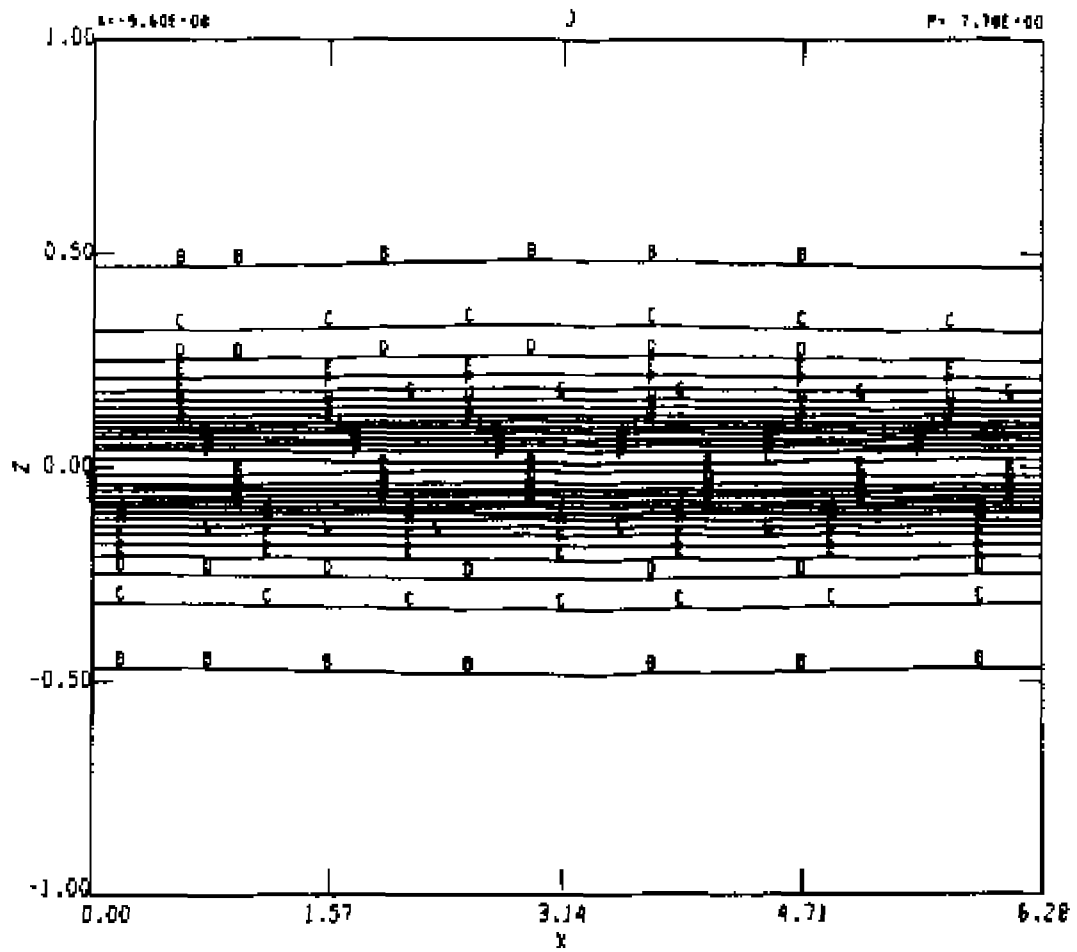


Figure VI - 5 Contour plot of electric current density at  $t = 0$ .

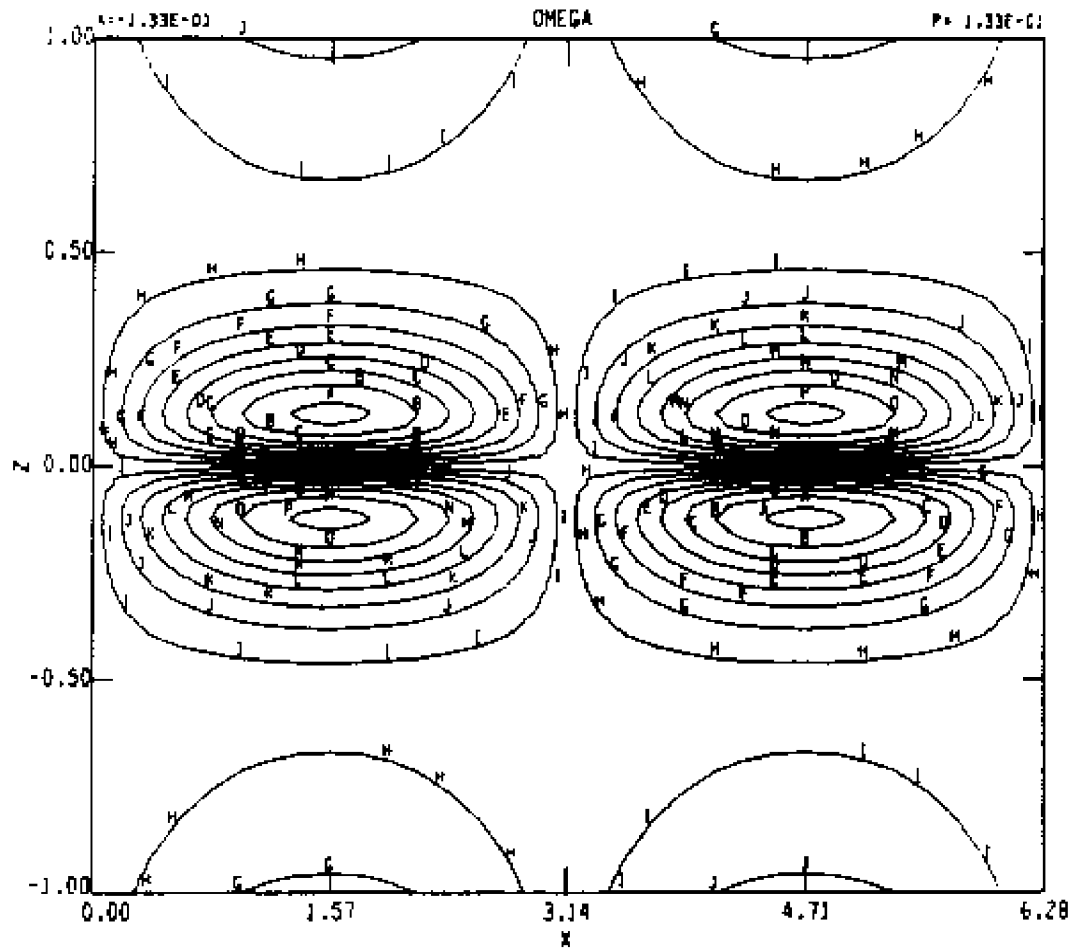


Figure VI - 6 Contour plot of vorticity at  $t = \pi$ .

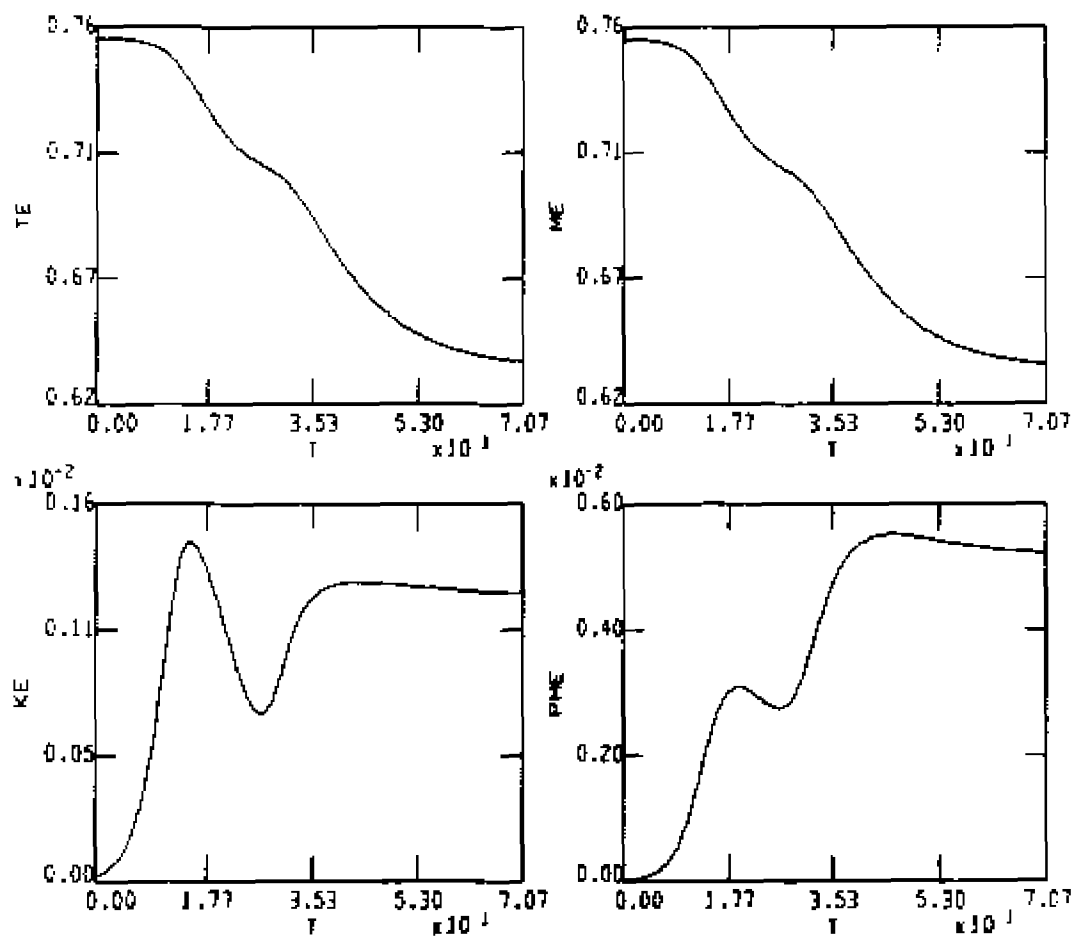


Figure VI - 7a Plots of global quantities versus time;

TE = total energy, ME = magnetic energy, KE = kinetic energy.

PME = perturbed magnetic energy.

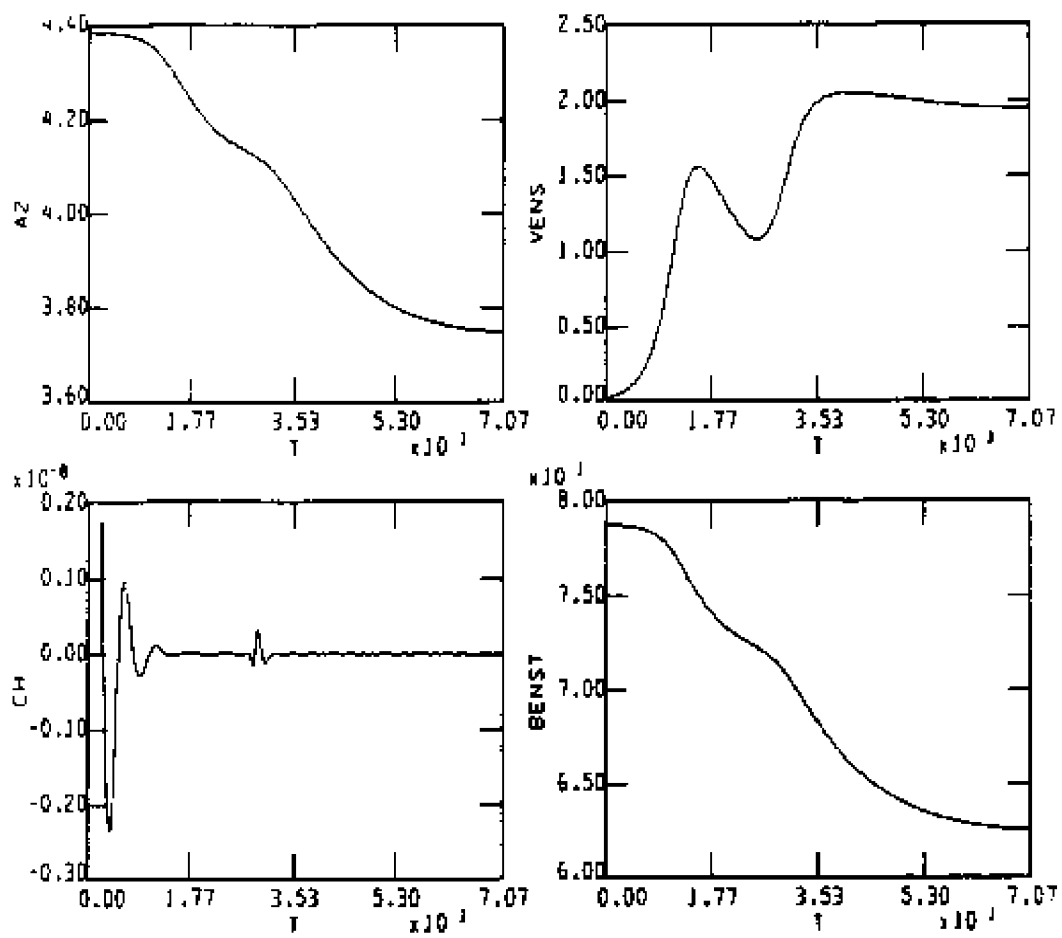


Figure VI - 7b Plots of global quantities versus time;  
 $A2$  = mean square vector potential,  $CH$  = cross helicity,  
 $VENST$  = enstrophy,  $BENST$  = magnetic enstrophy.

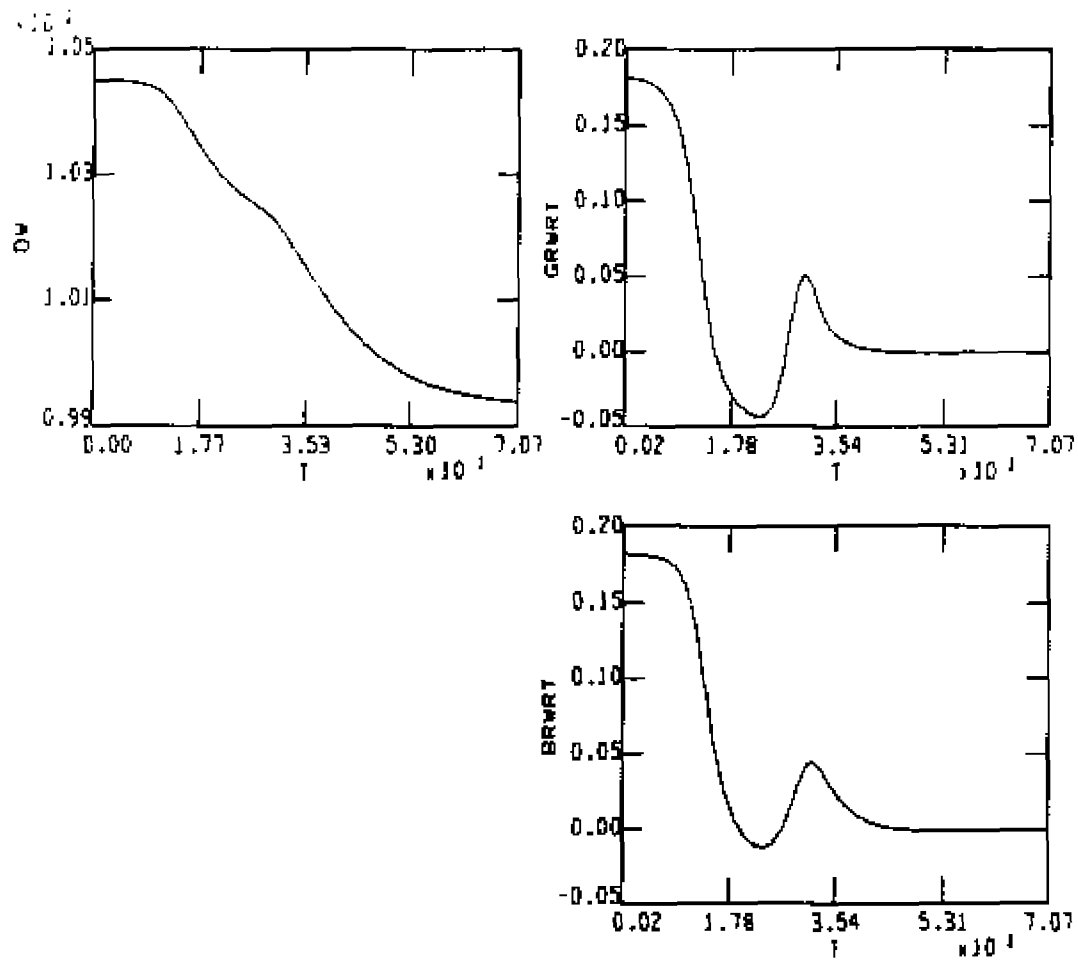


Figure V1 - 7c Plots of global quantities versus time;

$DW$  = dissipation wavenumber,  $GRWRT$  = kinetic energy growth rate,  $BRWRT$  = perturbed magnetic energy growth rate.

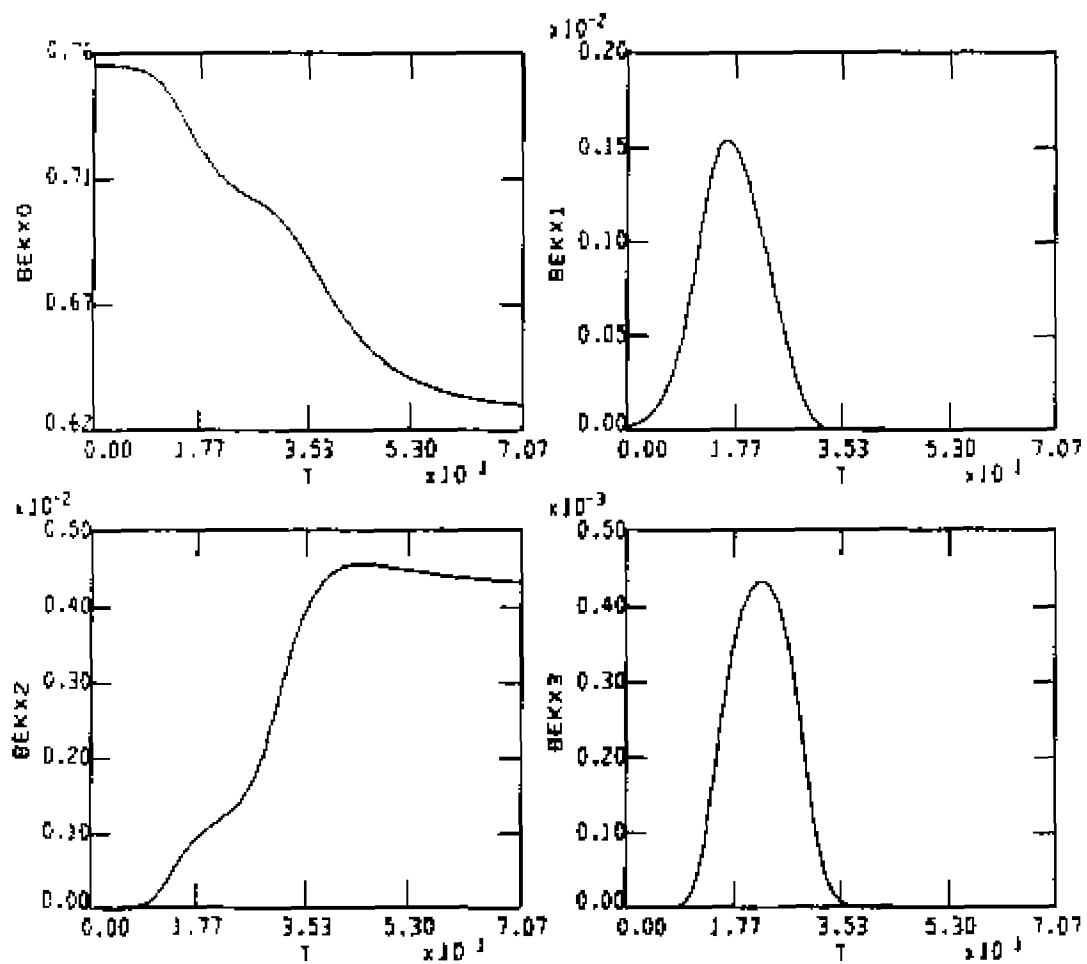


Figure VI - 7d Plots of one dimensional modal magnetic energies versus time:  
 BEKX0 = magnetic energy ( $k_x = 0$ ), BEKX1 = magnetic energy  
 ( $k_x = 1$ ), BEKX2 = magnetic energy ( $k_x = 2$ ),  
 BEKX3 = magnetic energy ( $k_x = 3$ ).



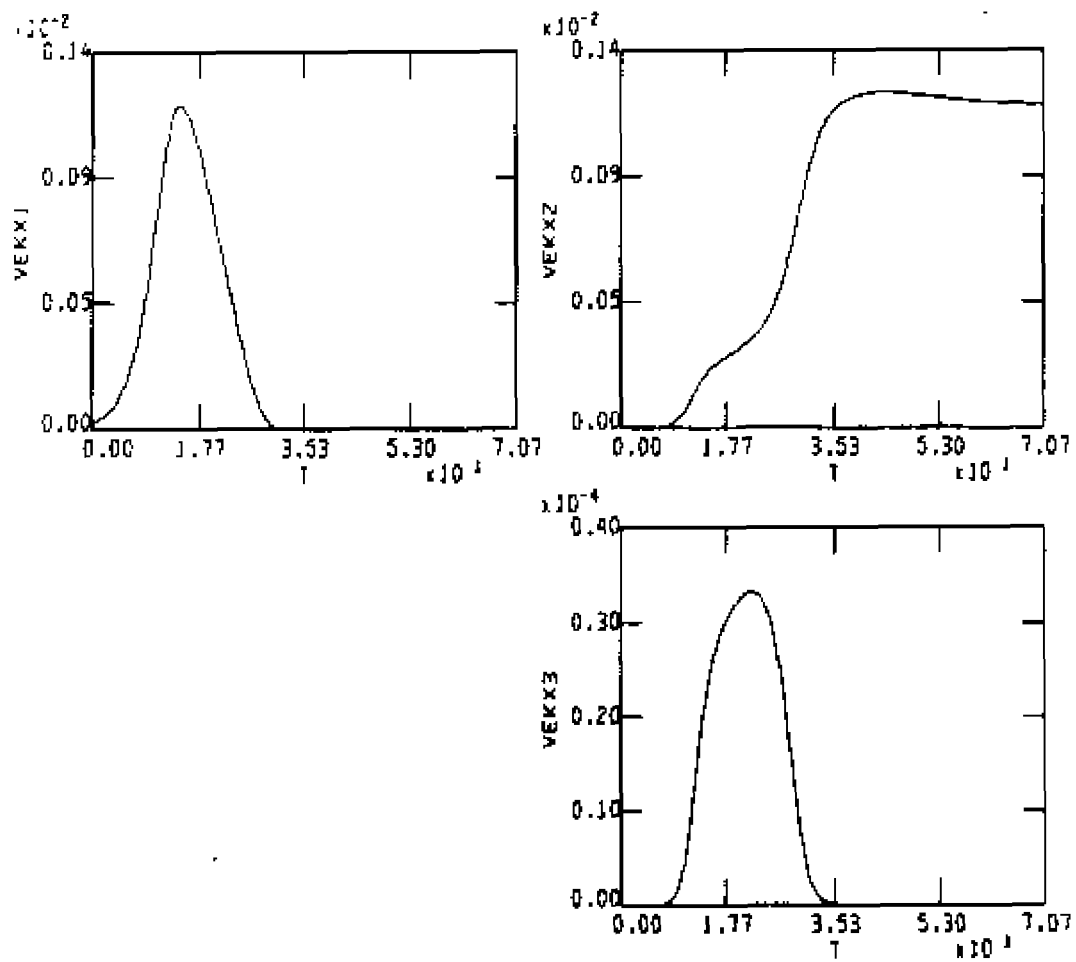


Figure VI - 7e Plots of one dimensional modal kinetic energies versus time;  
 VEXX1 = kinetic energy ( $k_x = 1$ ), VEXX2 = kinetic energy  
 ( $k_x = 2$ ), VEXX3 = kinetic energy ( $k_x = 3$ ).

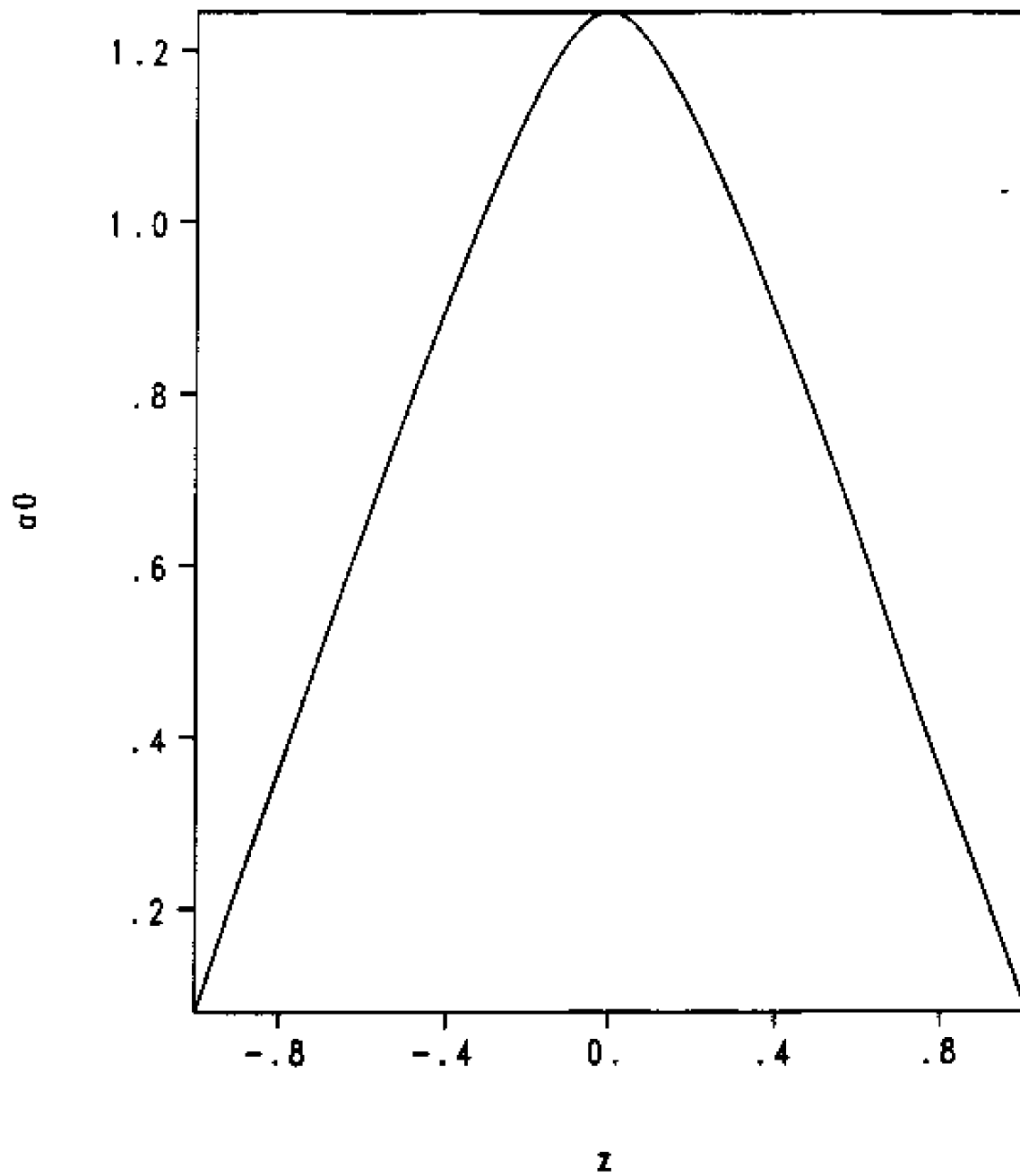


Figure VI - 8 Mean magnetic vector potential at  $t = 15.70796$ .

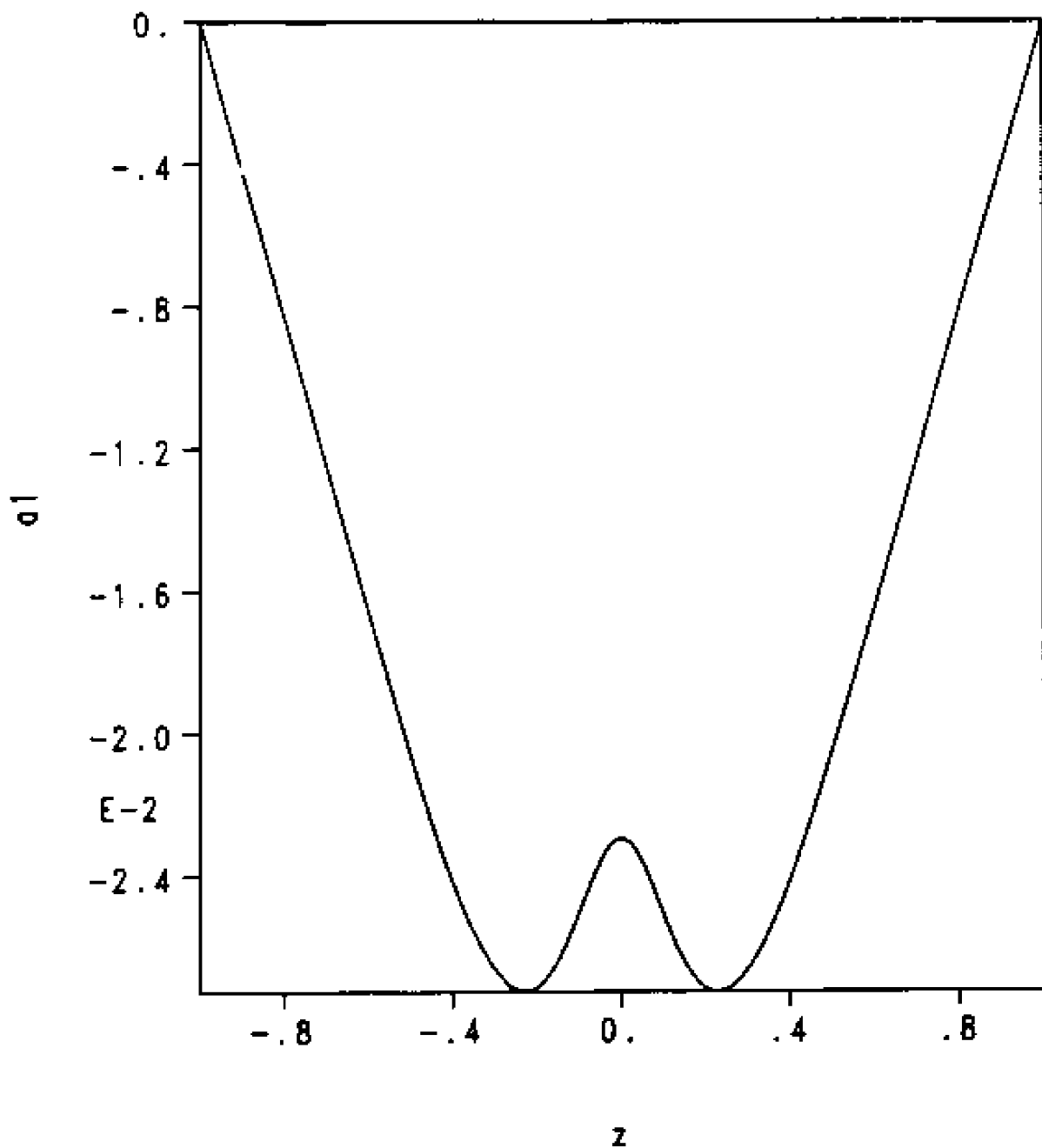


Figure VI - 9 Primary magnetic disturbance at  $t = 15.70796$ .

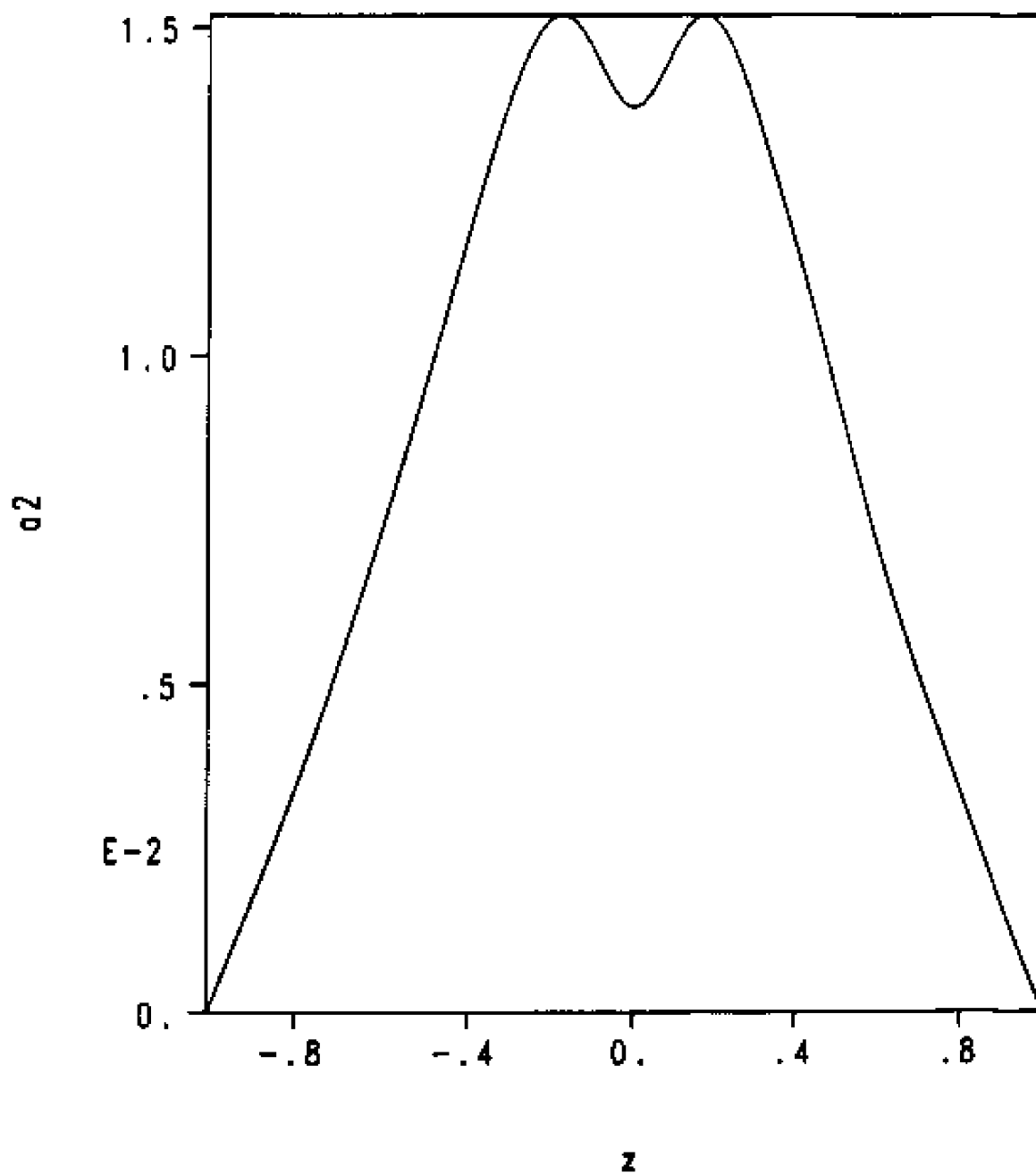


Figure VI - 10 . Secondary magnetic disturbance at  $t = 15.70796$ .

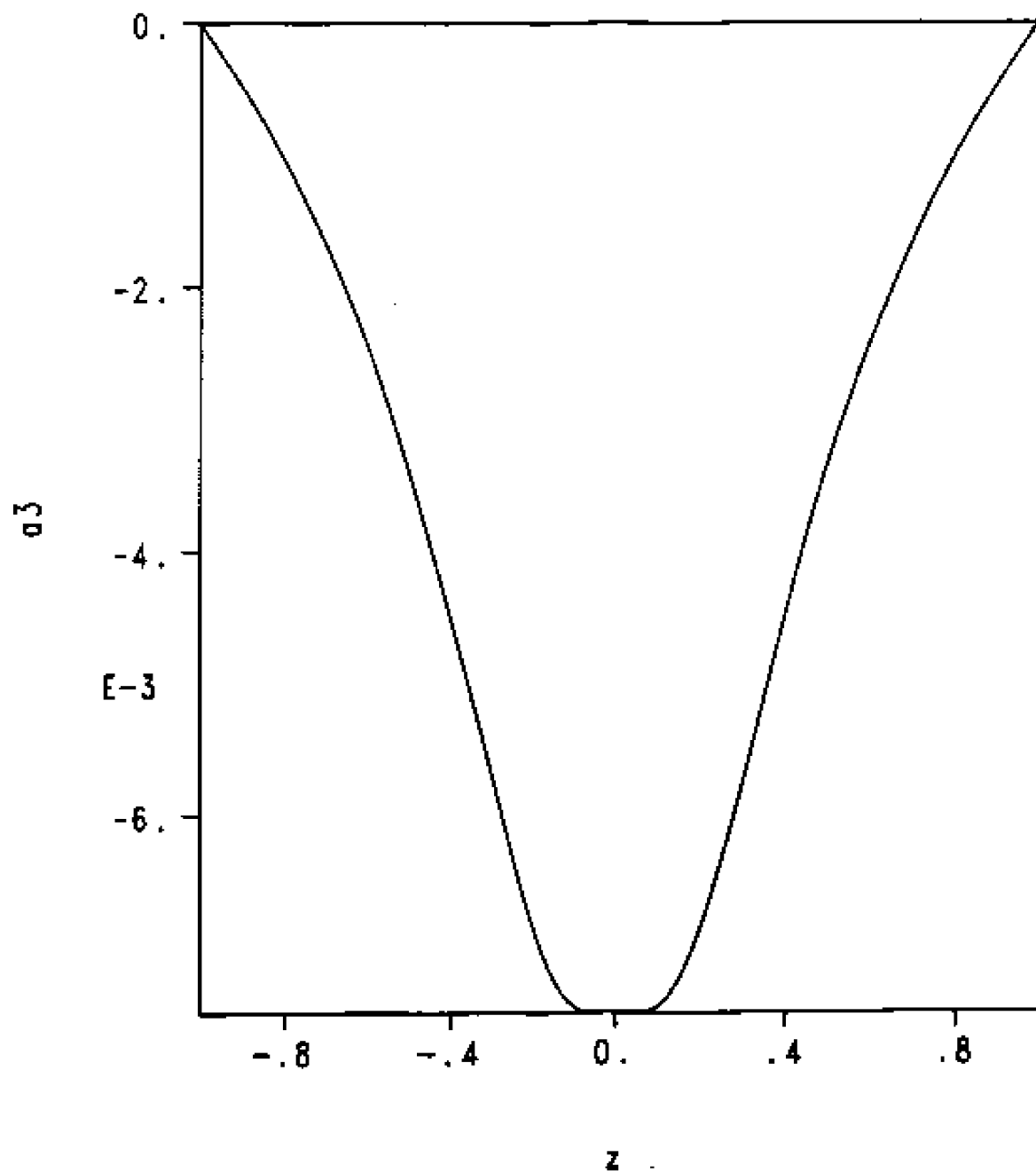


Figure VI - 11 Tertiary magnetic disturbance at  $t = 15.71796$ .

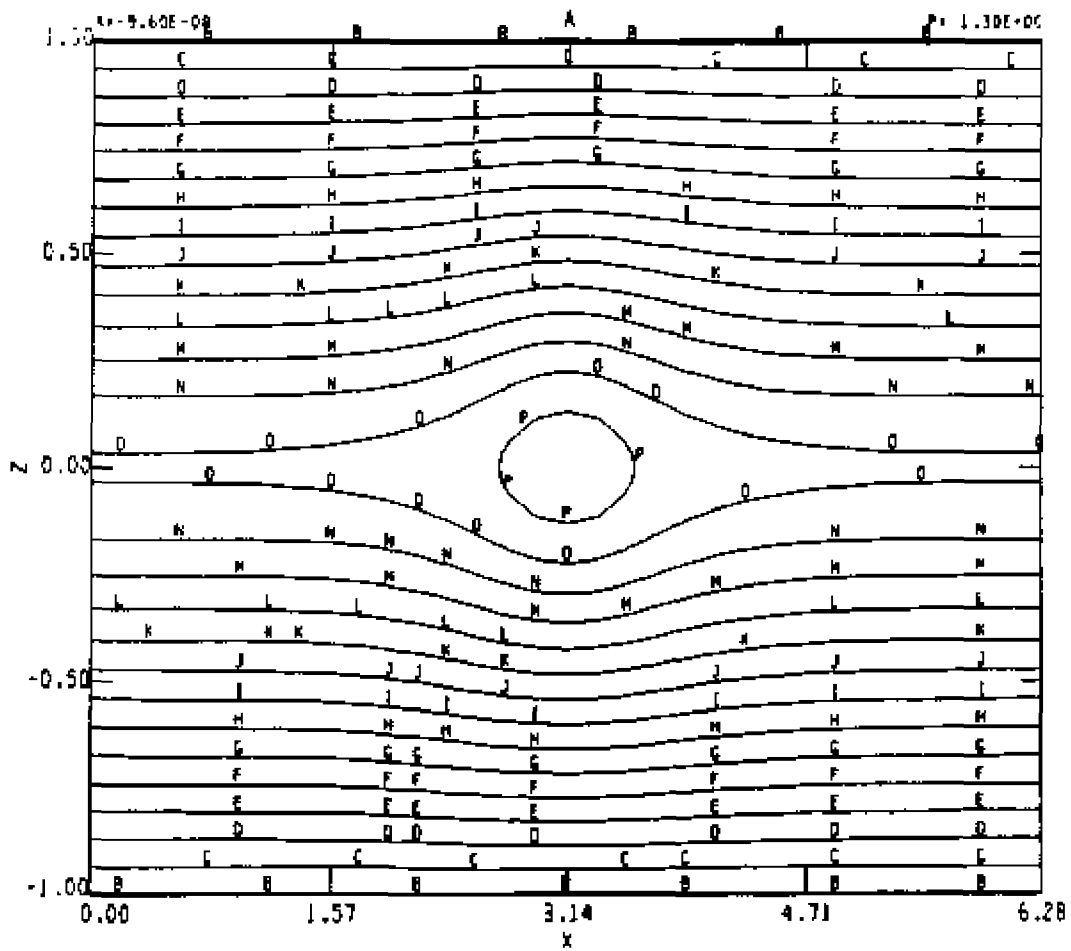


Figure VI - 12 Contour plot of magnetic vector potential at  $t = 15.70796$ .

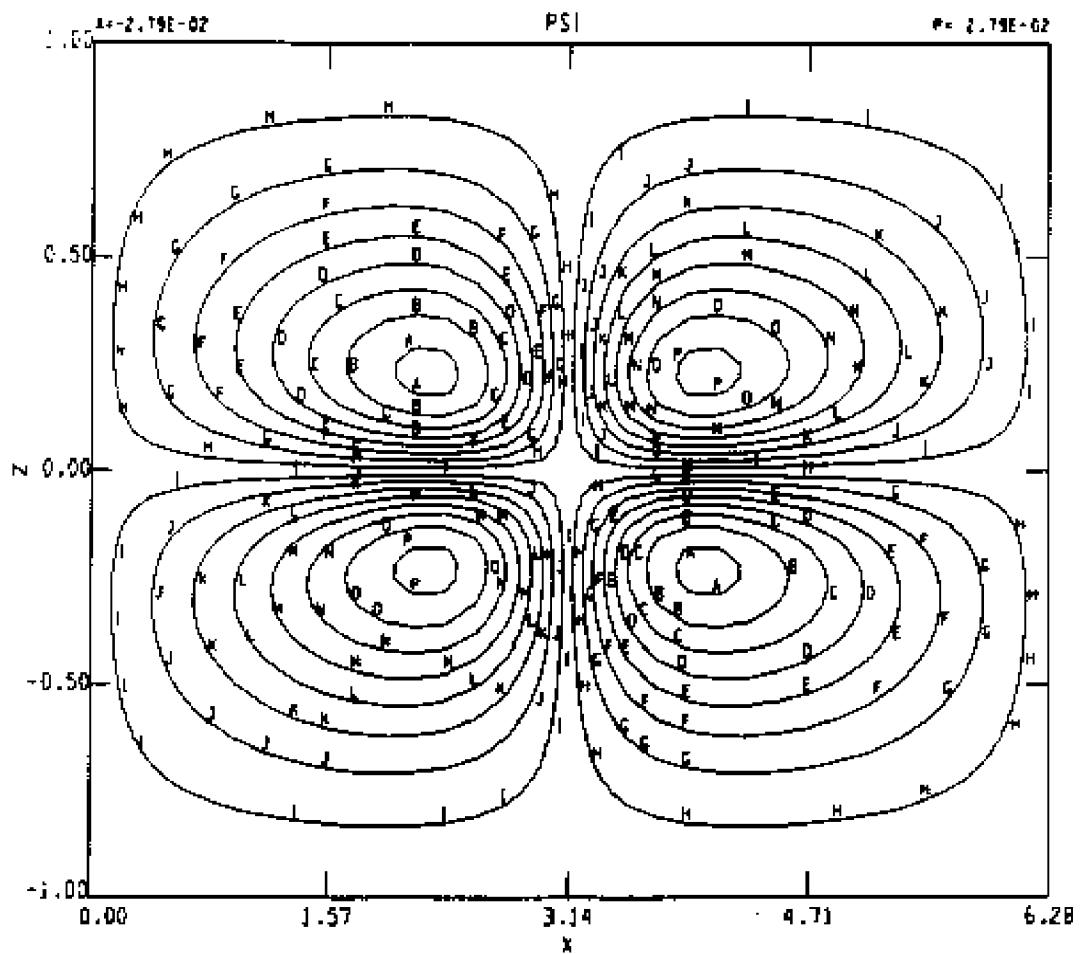


Figure V1 - 13 Contour plot of velocity stream function at  $t = 15.78796$ .

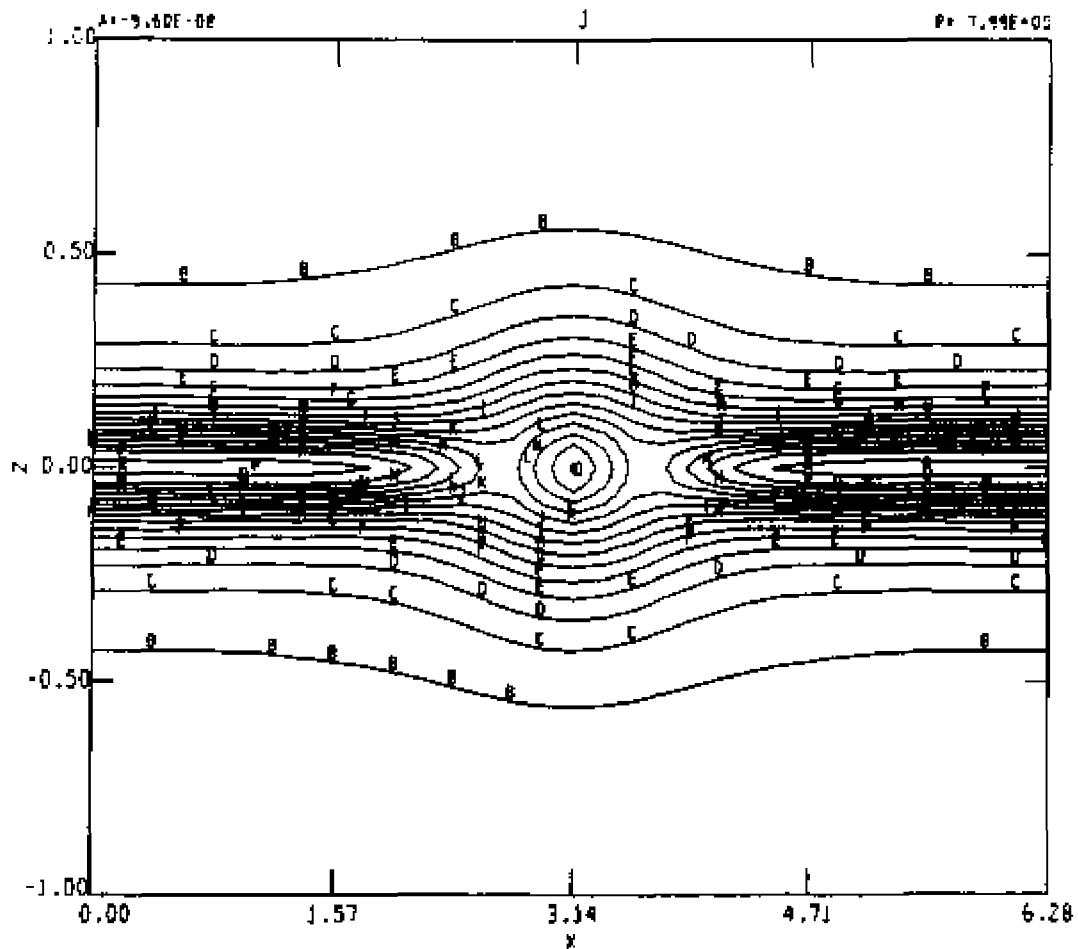


Figure VI - 14 Contour plot of electric current density at  $t = 15.70796$ .



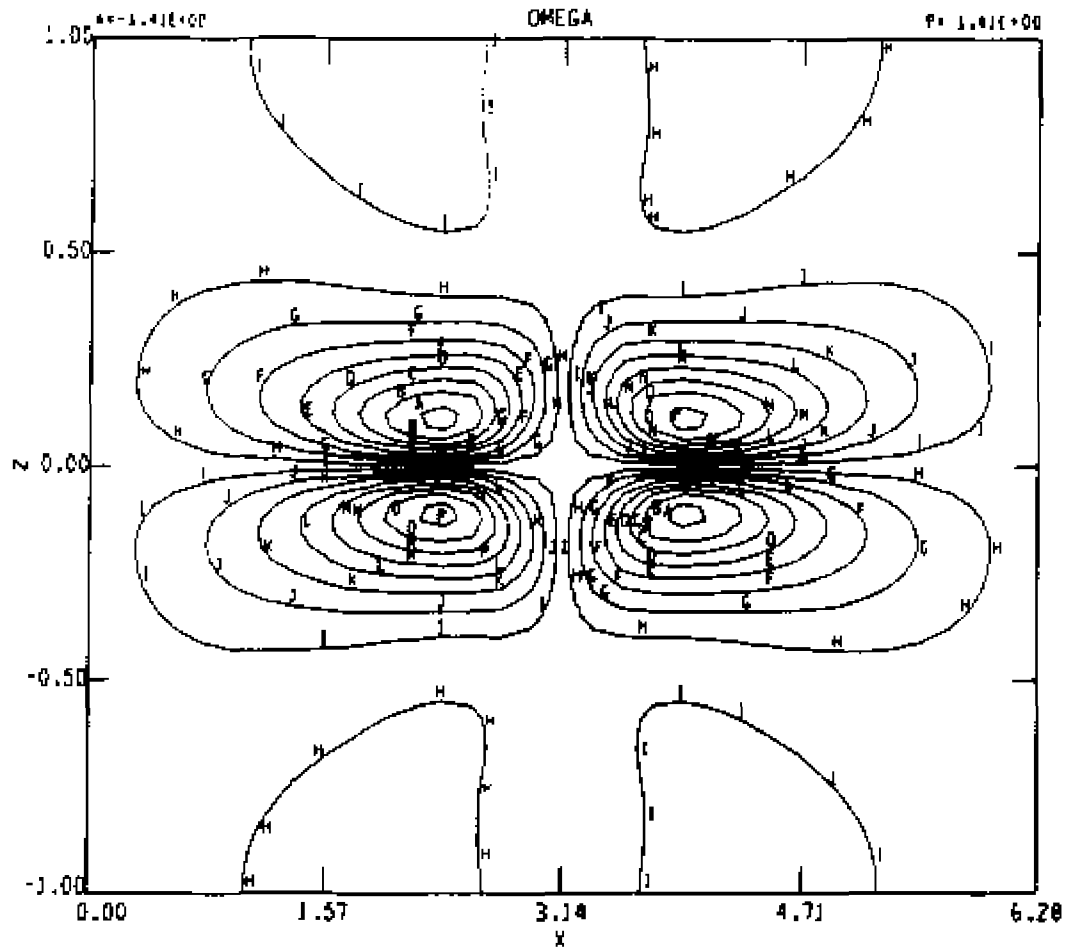


Figure VI - 15 Contour plot of vorticity at  $t = 15.70796$ .

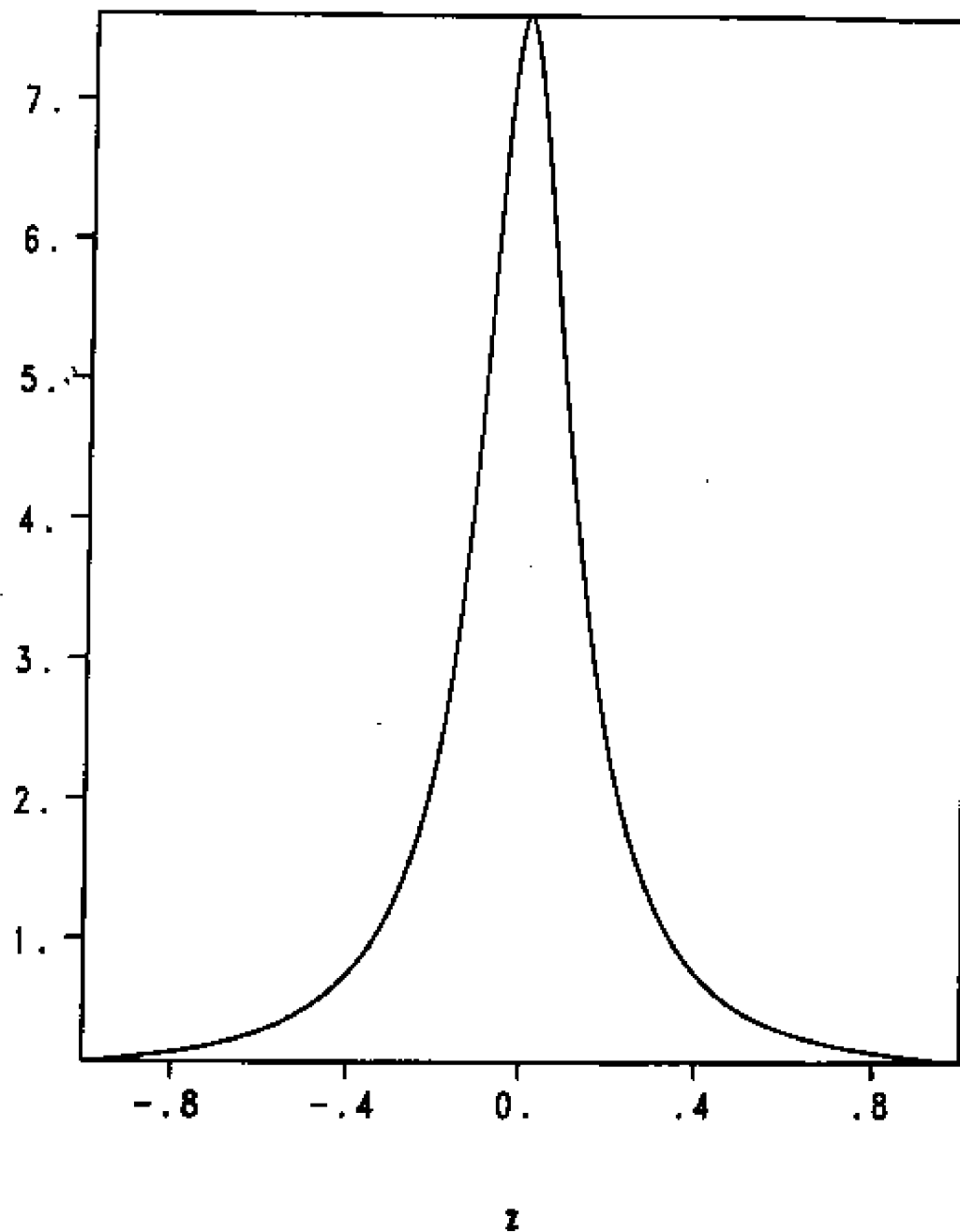


Figure VI - 16 Distorted mean current profile at  $t = 15.70796$ .

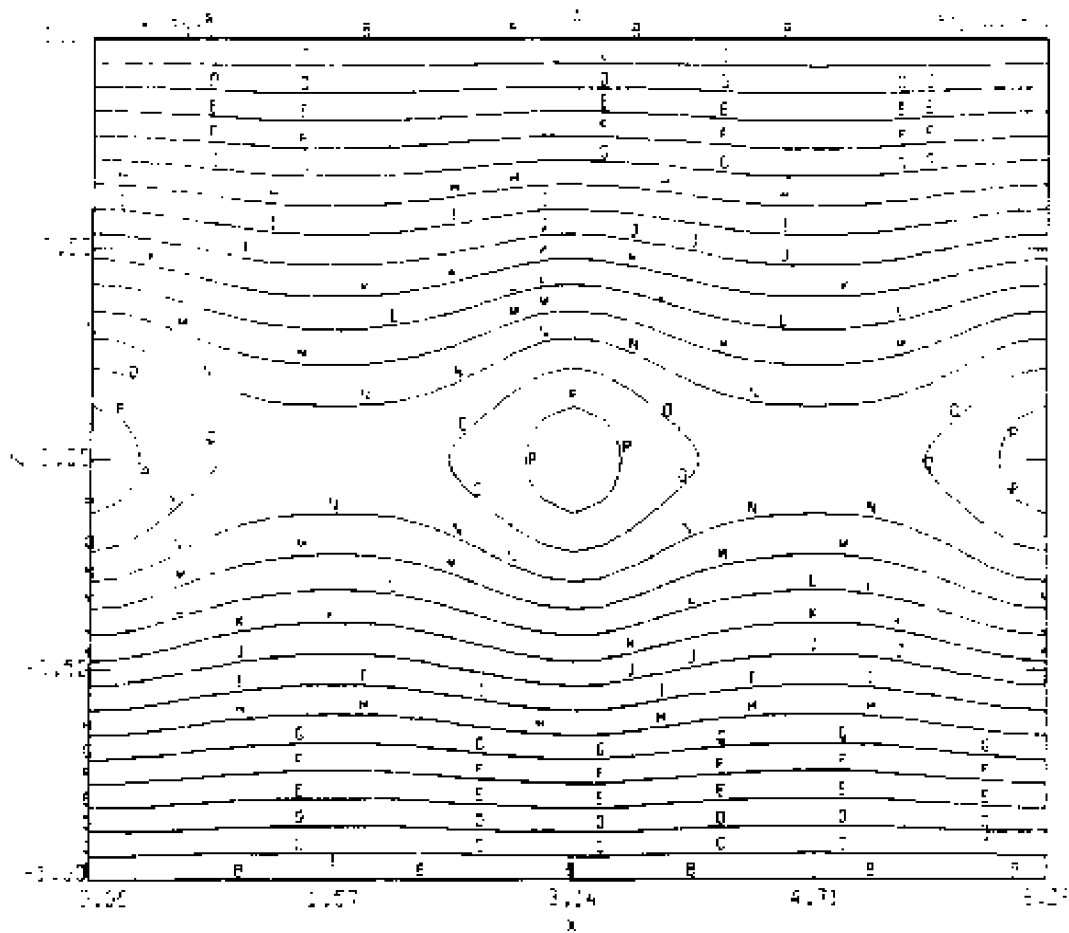


Figure VI - 17 Contour plot of magnetic vector potential at  $t = 54.989$ .

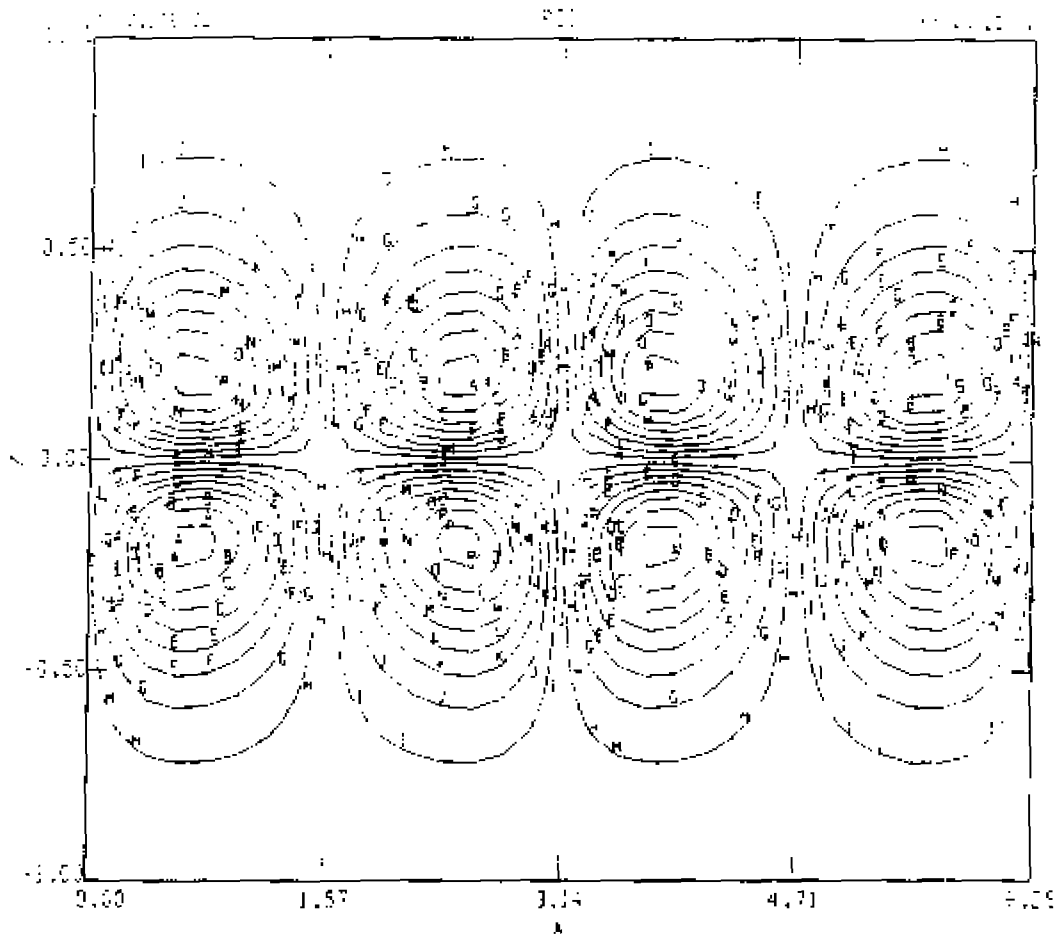


Figure VI - 19 Contour plot of velocity stream function at  $t = 54.980$ .

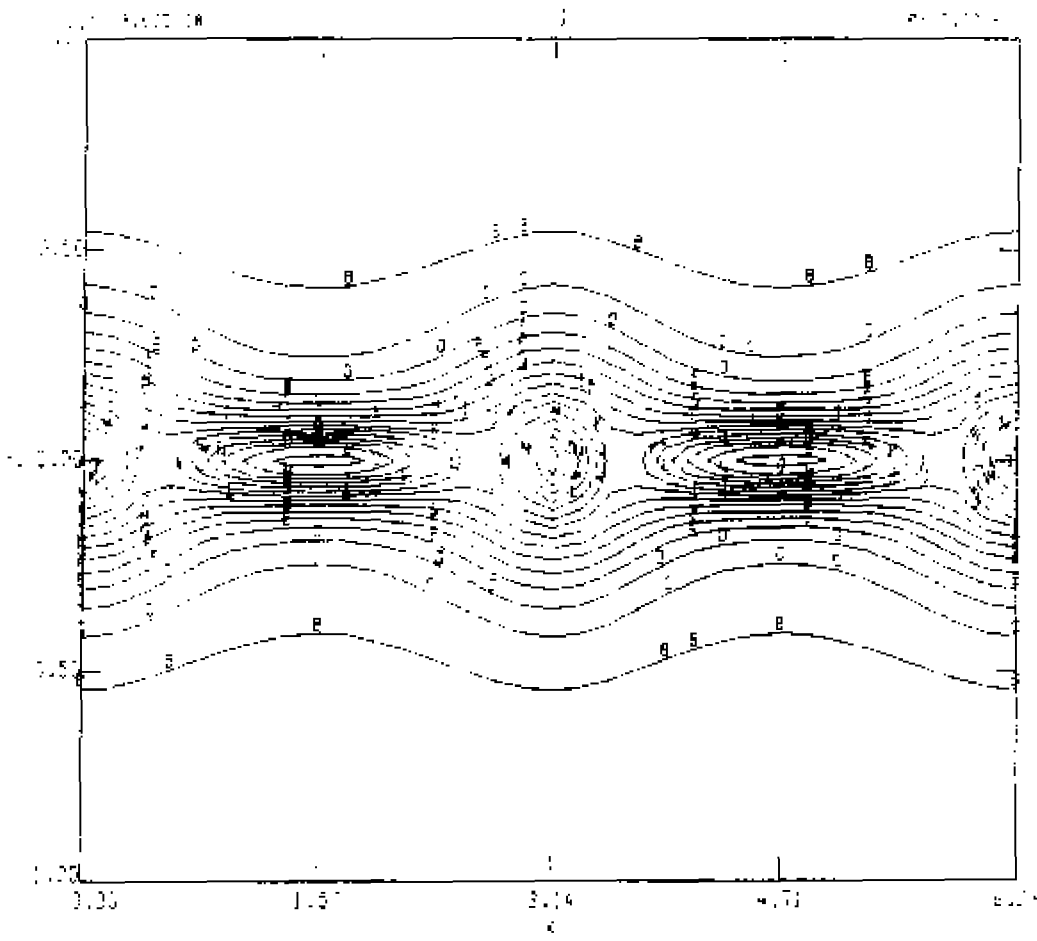


Figure VI - 19 Contour plot of electric current density at  $t = 54.960$ .



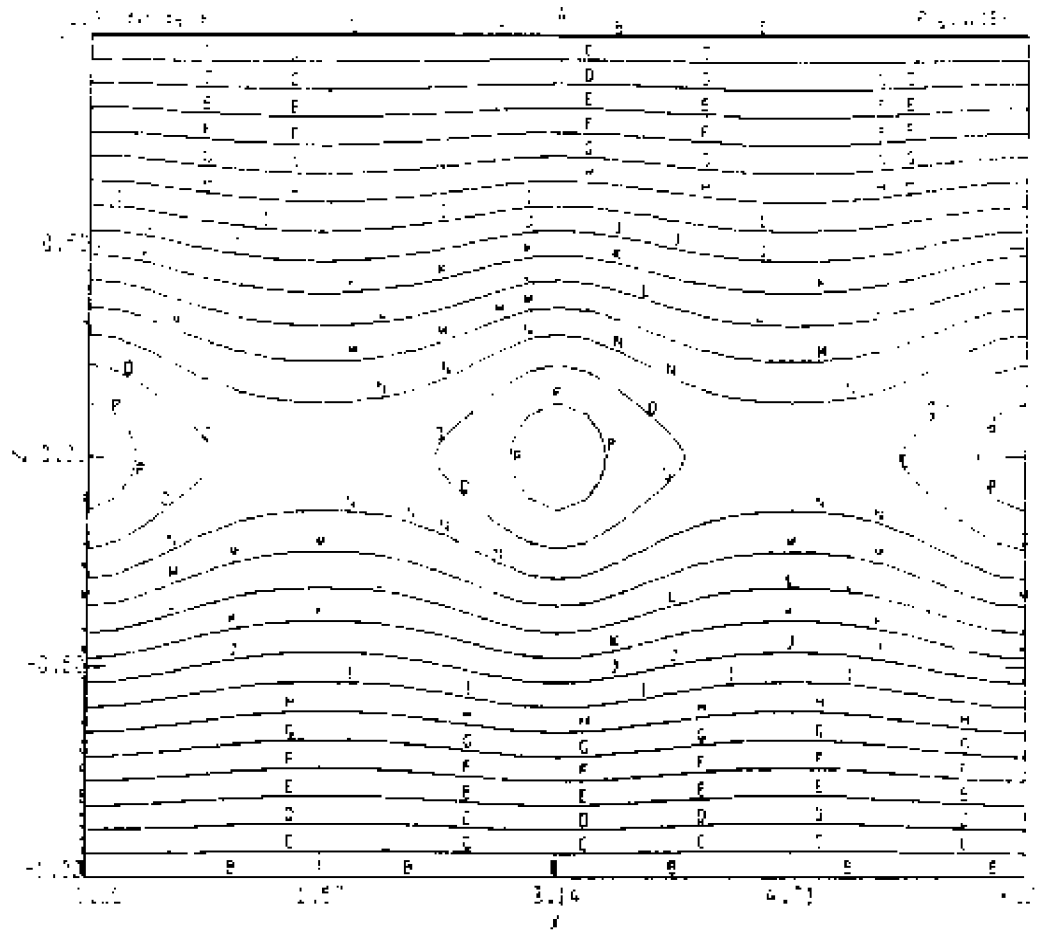


Figure VI - 21 Contour plot of magnetic vector potential at  $t = 79.680$

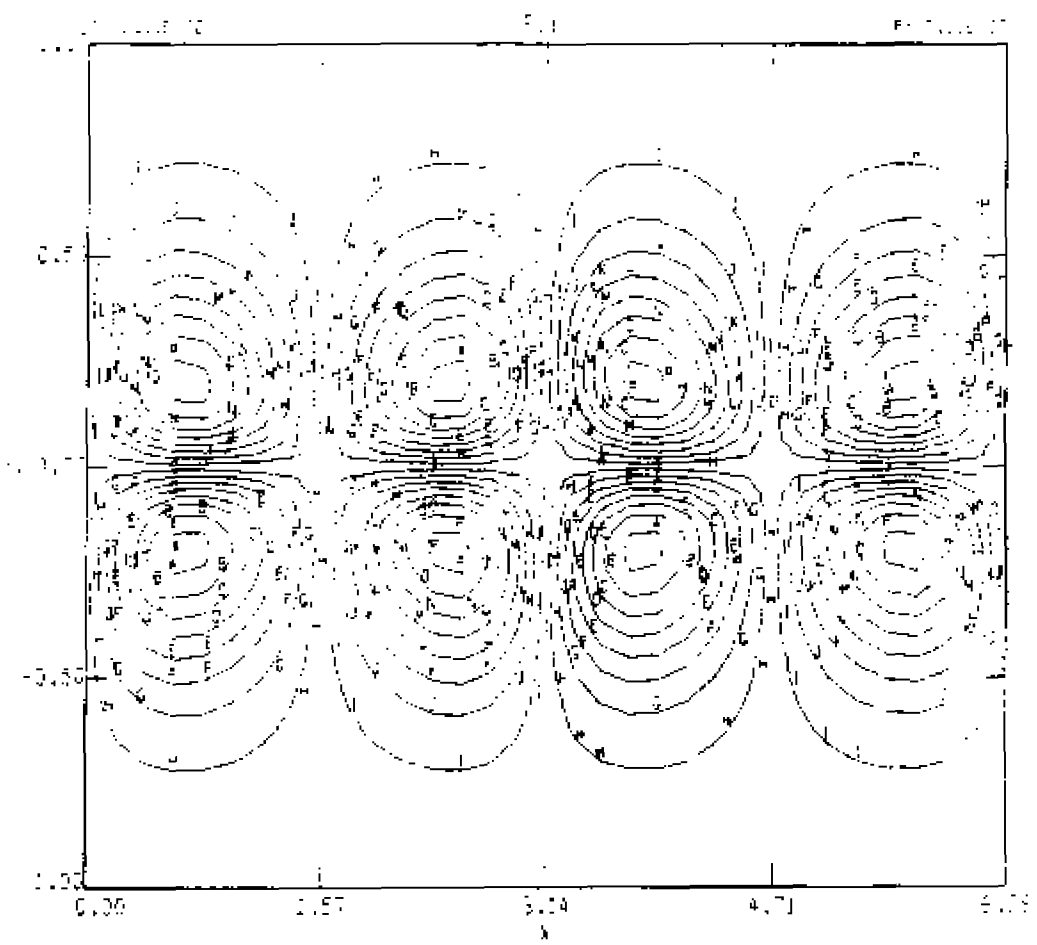


Figure VI - 22 Contour plot of velocity stream function at  $t = 70.688$ .



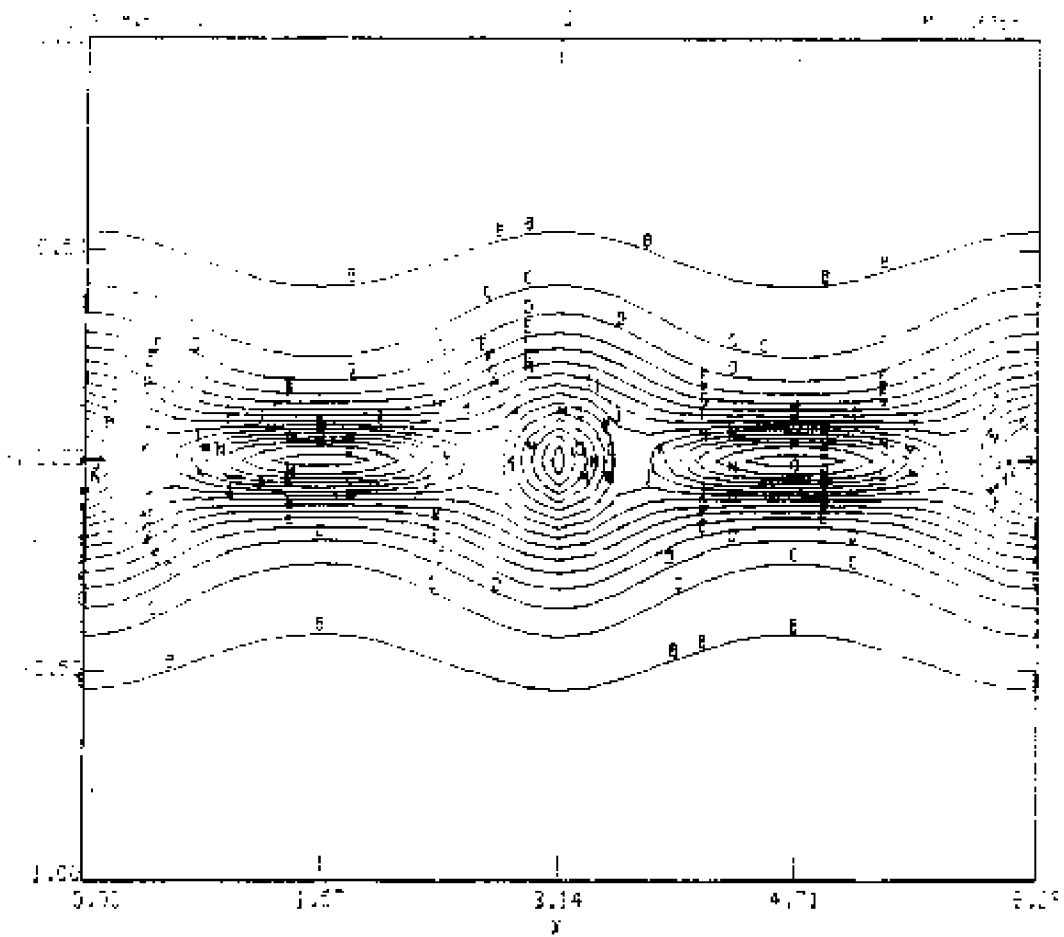


Figure VI - 23 Contour plot of electric current density at  $t = 7\# 682$

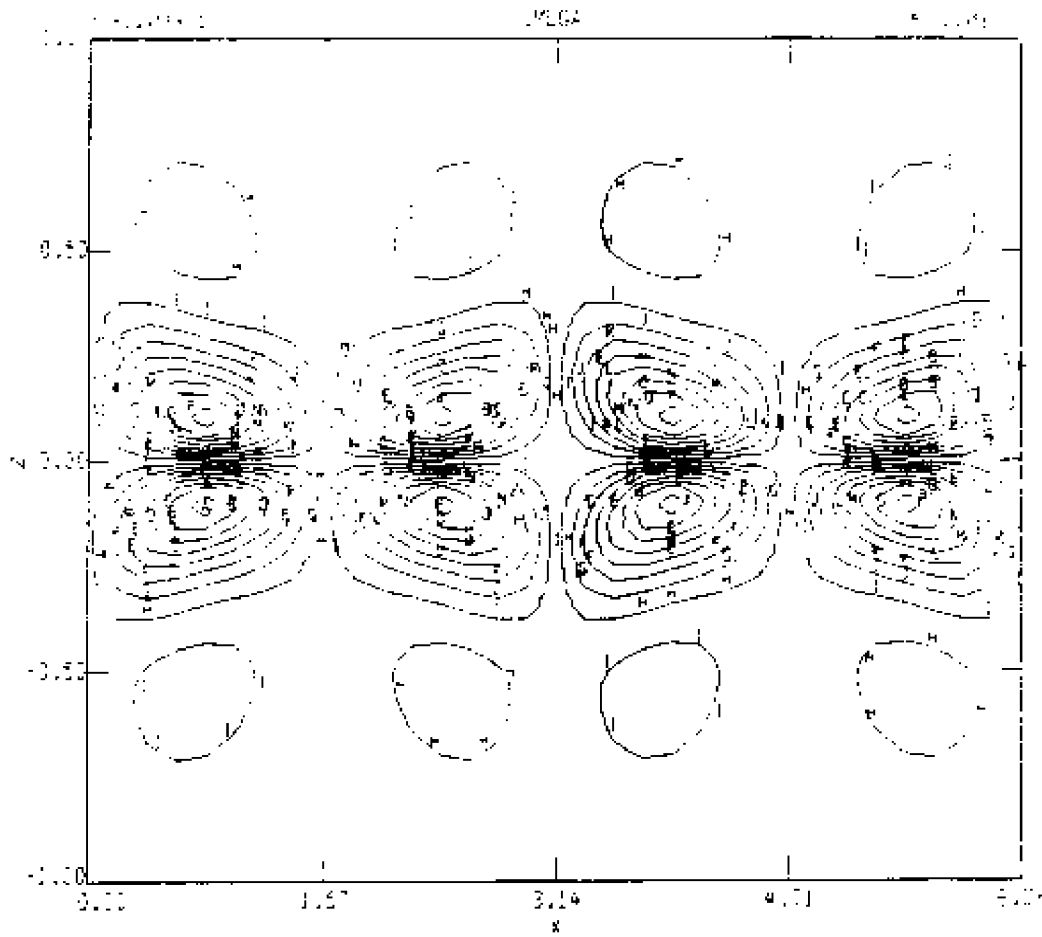


Figure VI - 24 Contour plot of vorticity at  $t = 78\ 688$

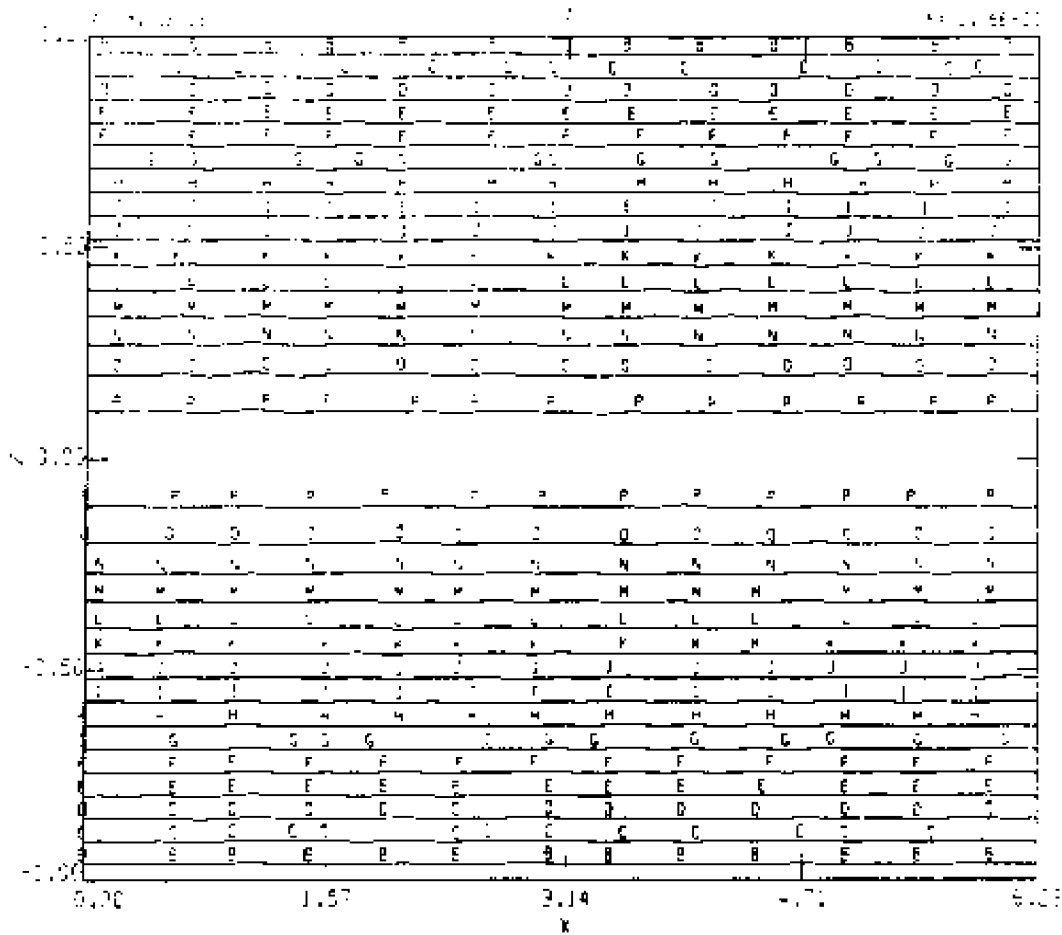


Figure VII - 1a Contour plot of magnetic vector potential at  $t = 0$ .

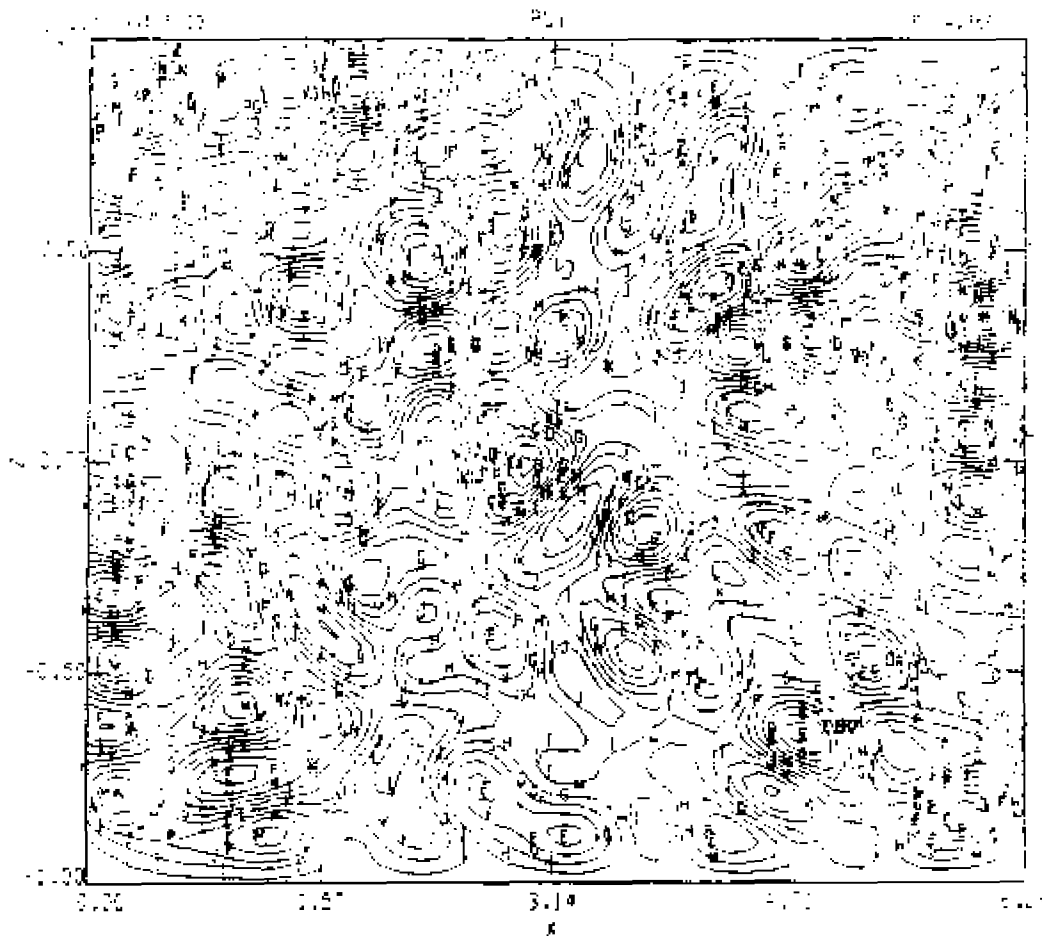


Figure VII - 1b Contour plot of velocity stream function at  $t = 0$ .

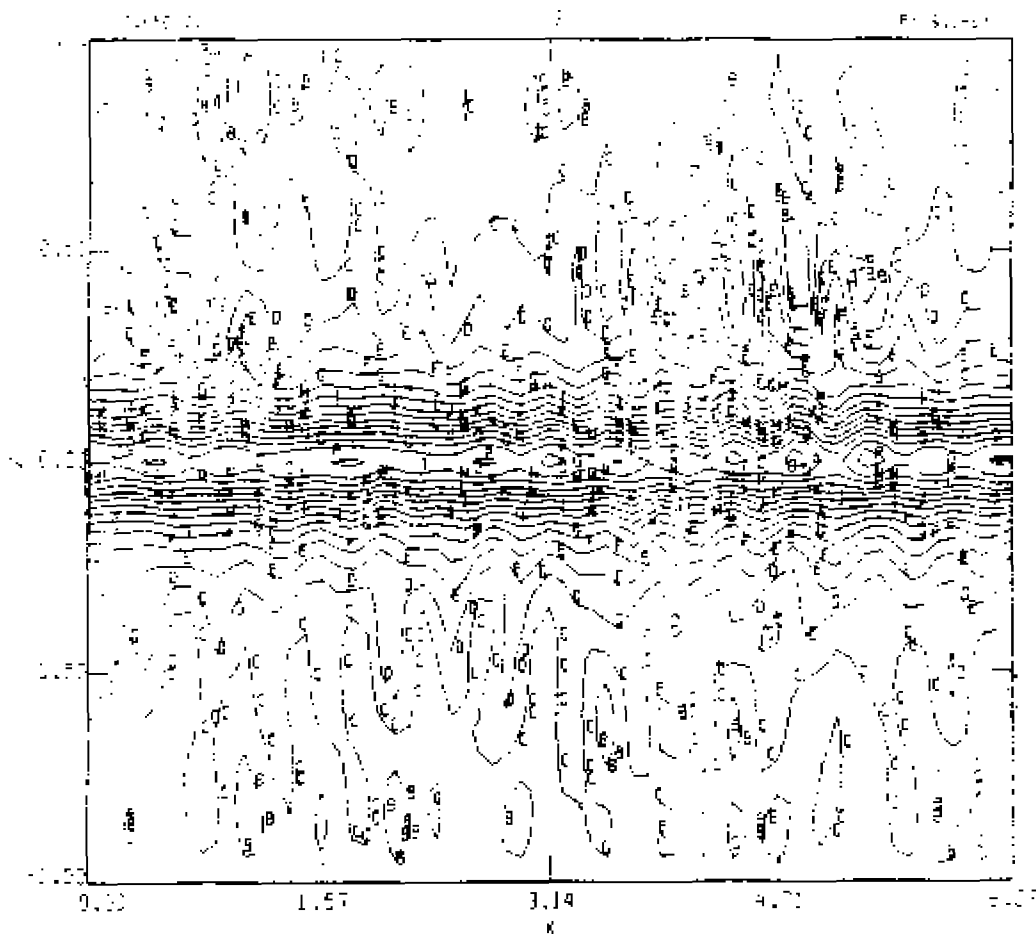


Figure VII - 1c Contour plot of electric current density at  $t = 0$ .

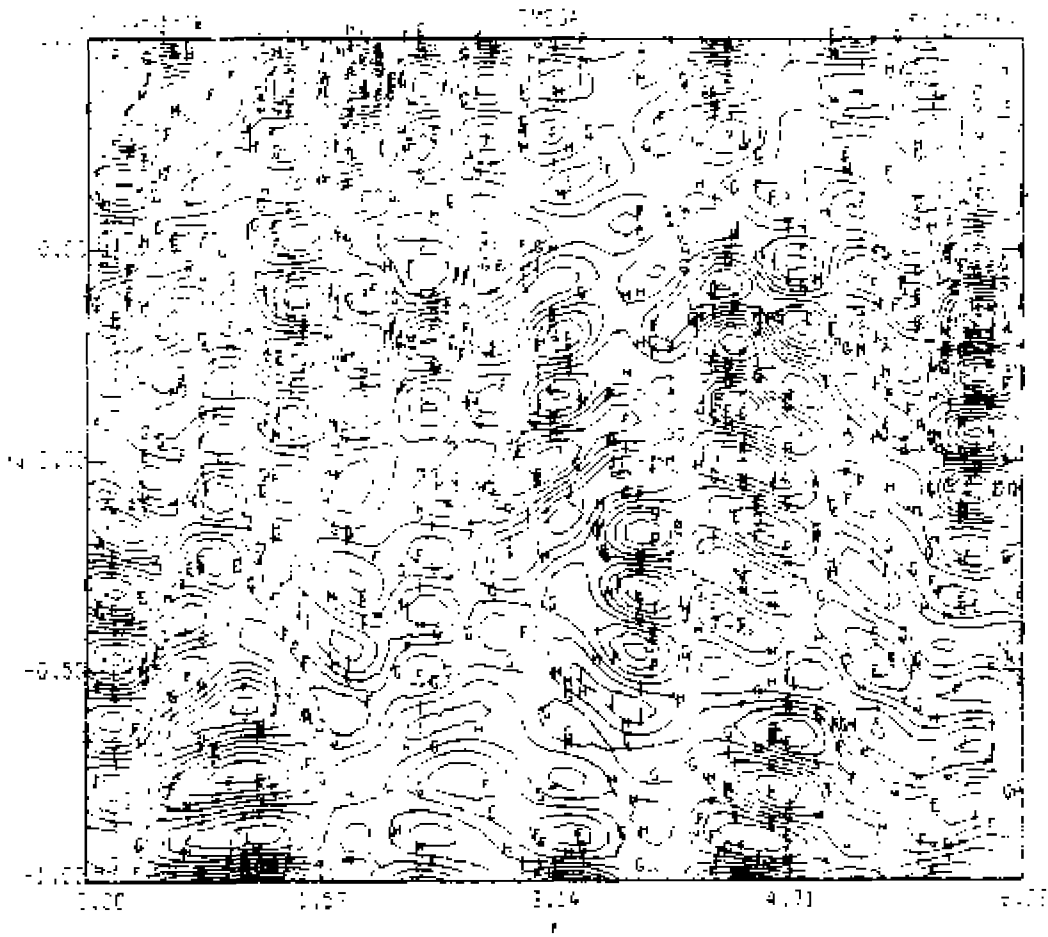


Figure VII - 1d Contour plot of vorticity at  $t = 0$

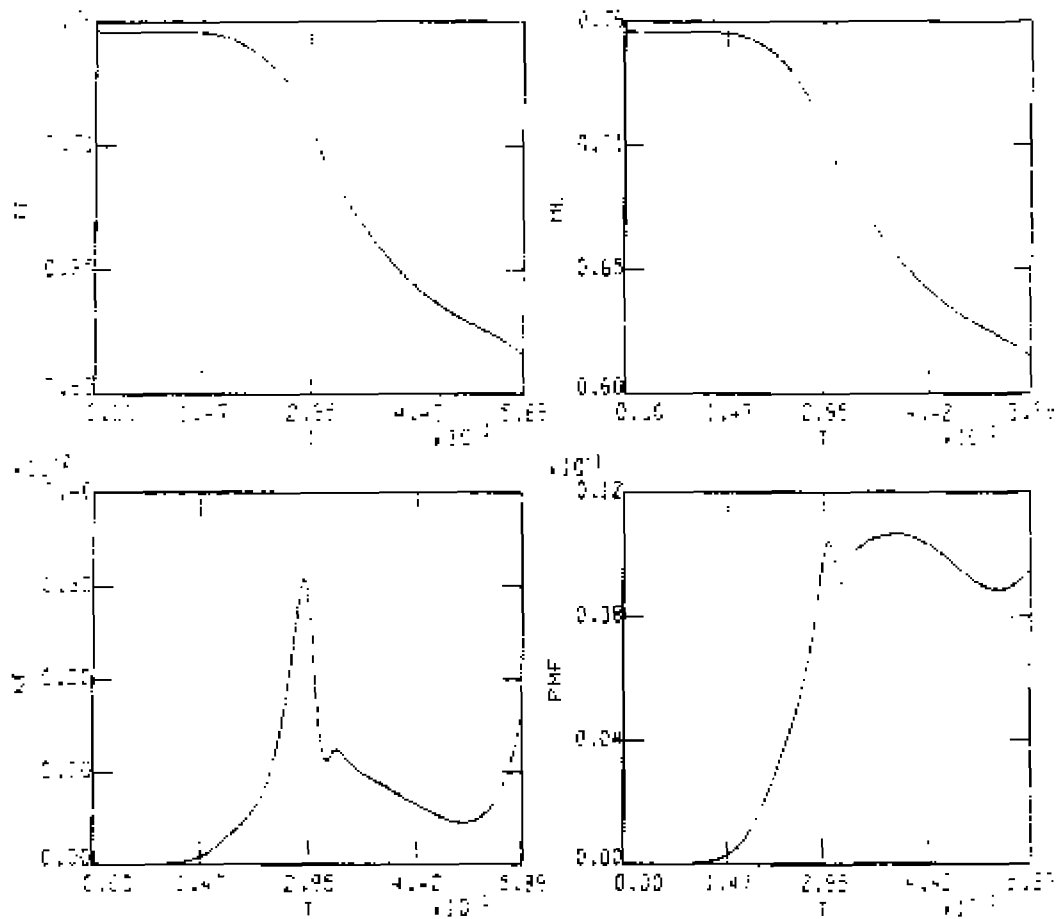


Figure VII - 3a Plots of global quantities versus time

TE = total energy, ME = magnetic energy, KE = kinetic energy,

PME = perturbed magnetic energy.

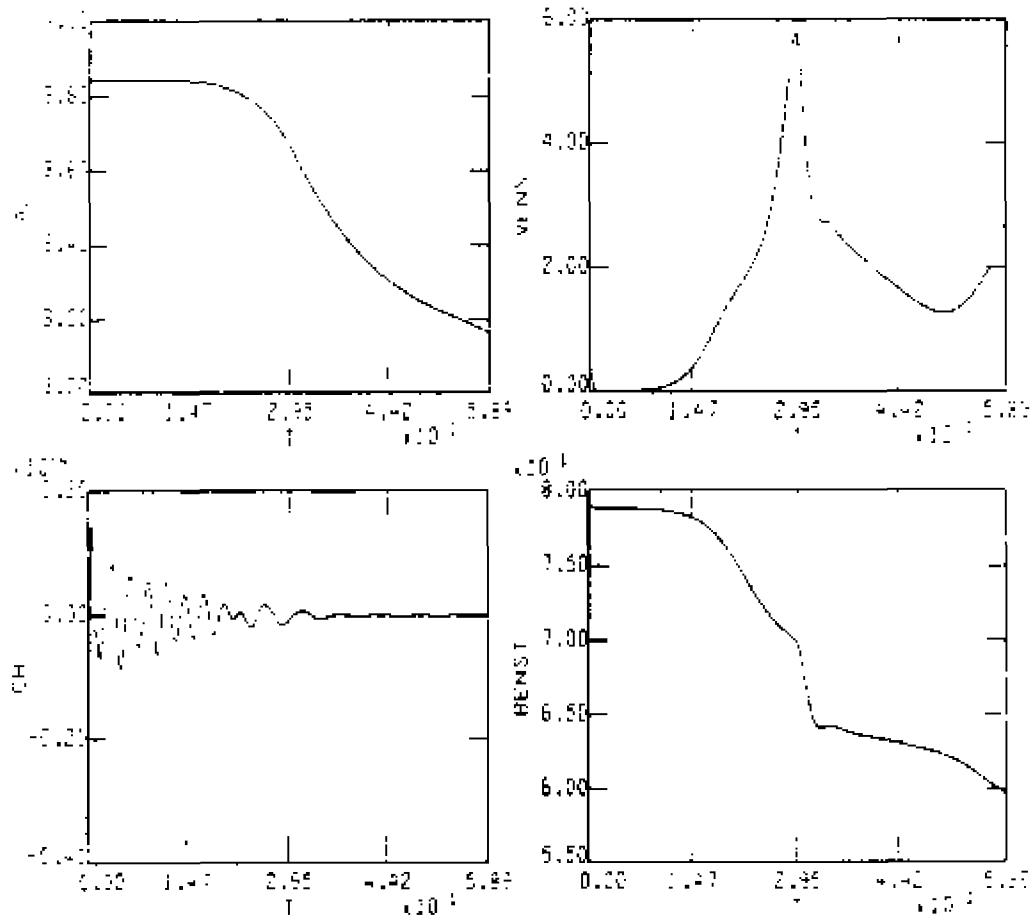


Figure VII - 2b Plots of global quantities versus time.

$A2$  = mean square vector potential,  $CH$  = cross helicity.

$VENST$  = enstrophy,  $BENST$  = magnetic enstrophy.



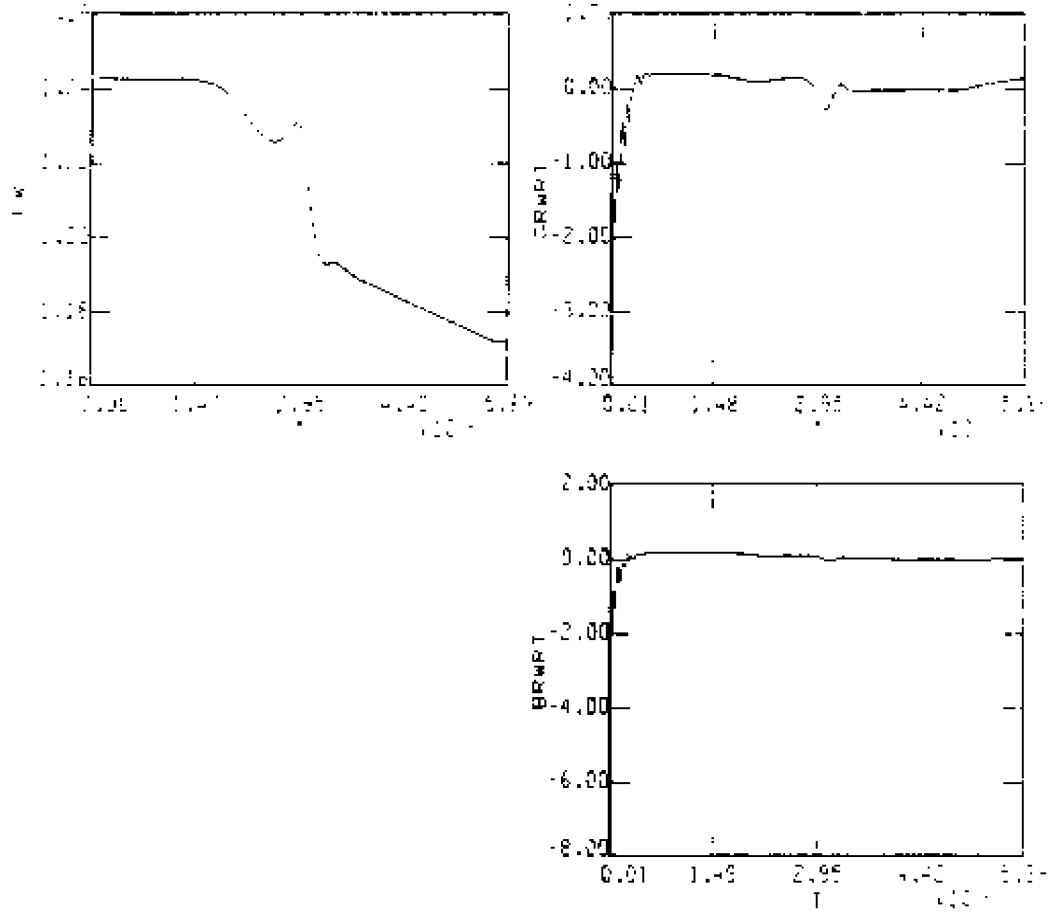


Figure VII - 2c Plots of global quantities versus time:

DW = dissipation wavenumber, GRWRT = kinetic energy growth

rate, BRWRT = perturbed magnetic energy growth rate.

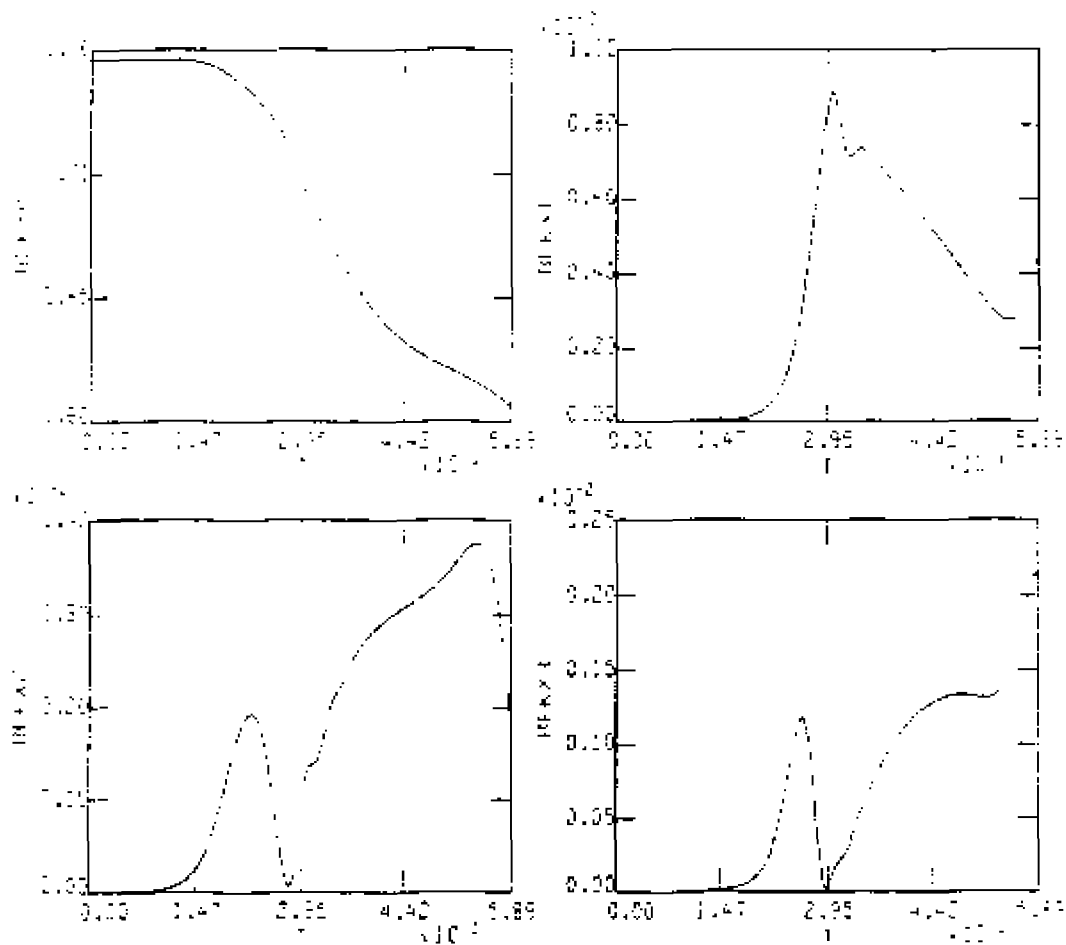


Figure VII - 2d Plots of one dimensional modal magnetic energies versus time:

$BERX0$  = magnetic energy (  $k_x = 0$  ),  $BERX1$  = magnetic energy

(  $k_x = 1$  ),  $BERX2$  = magnetic energy (  $k_x = 2$  ),

$BERX3$  = magnetic energy (  $k_x = 3$  ).

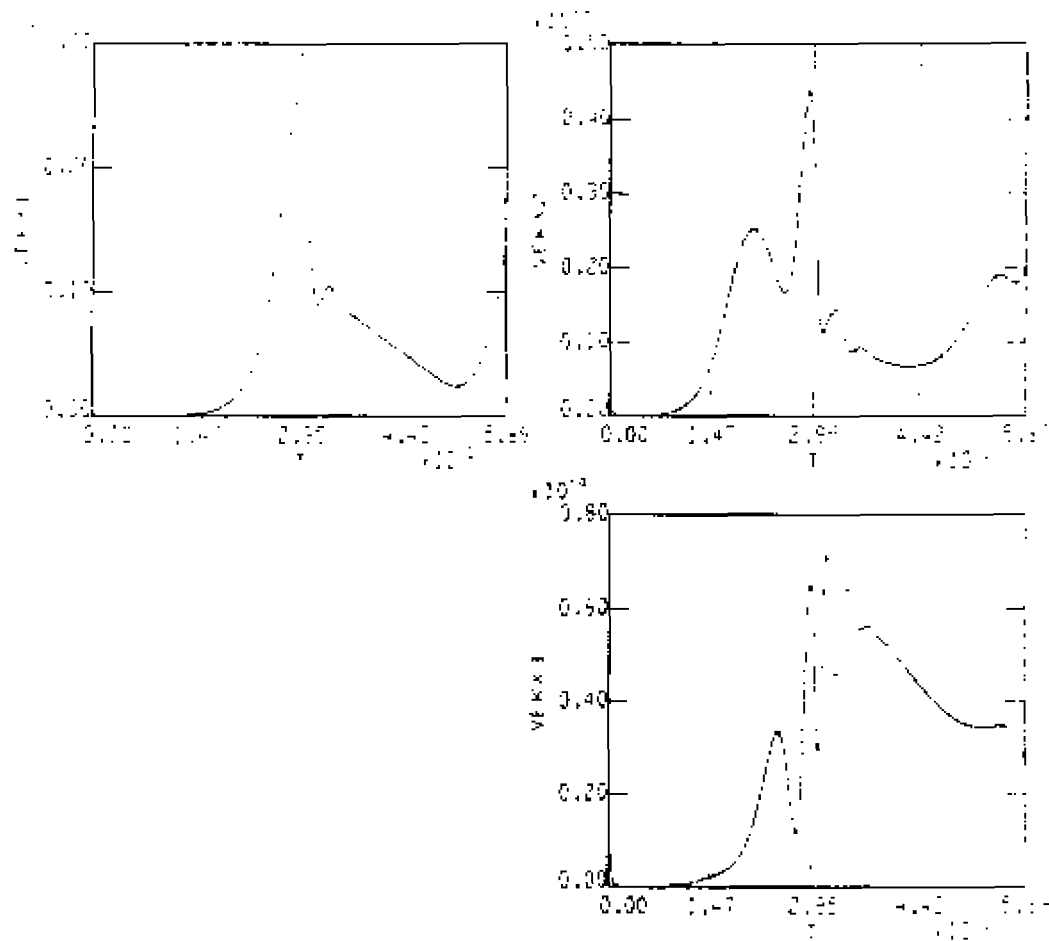


Figure VII - 2e Plots of one dimensional modal kinetic energies versus time:

$VEKX1$  = kinetic energy ( $k_x = 1$ ),  $VEKX2$  = kinetic energy

( $k_x = 2$ ),  $VEKX3$  = kinetic energy ( $k_x = 3$ ).

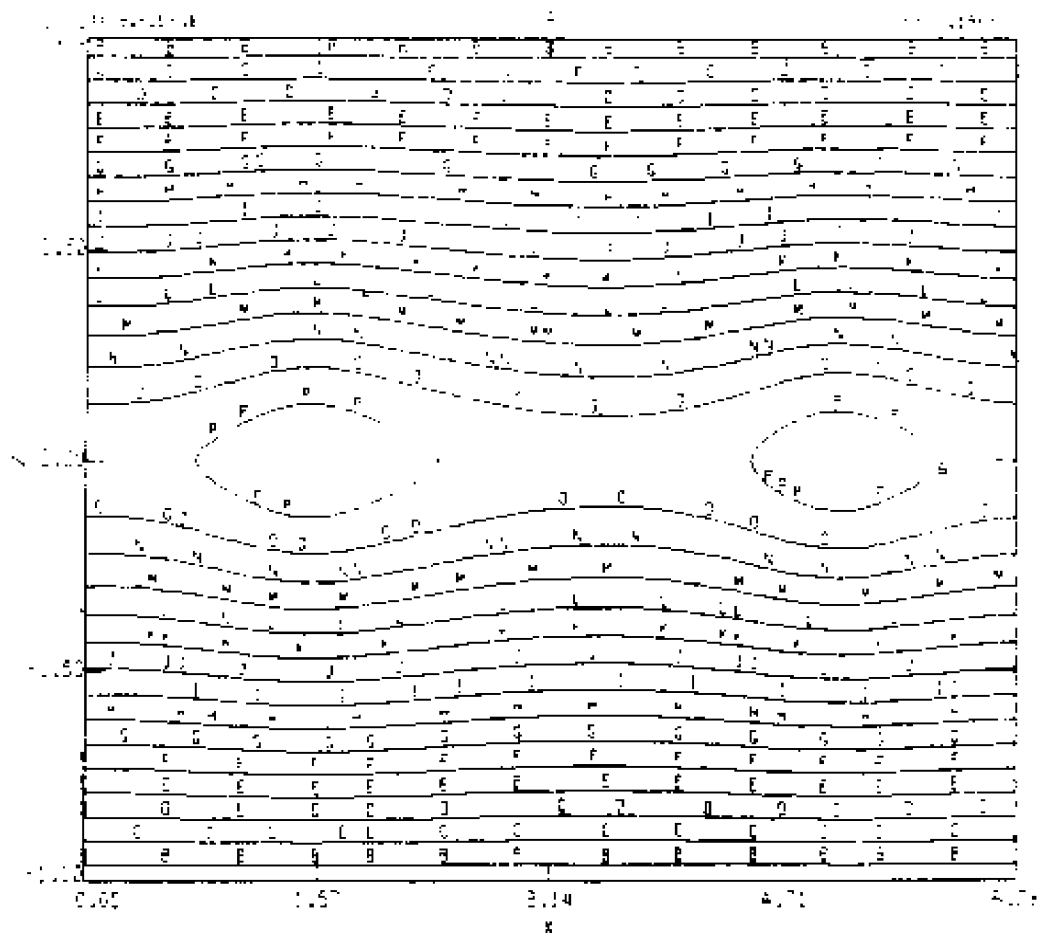


Figure VII - 3a Contour plot of magnetic vector potential at  $t = 19.63495$ .

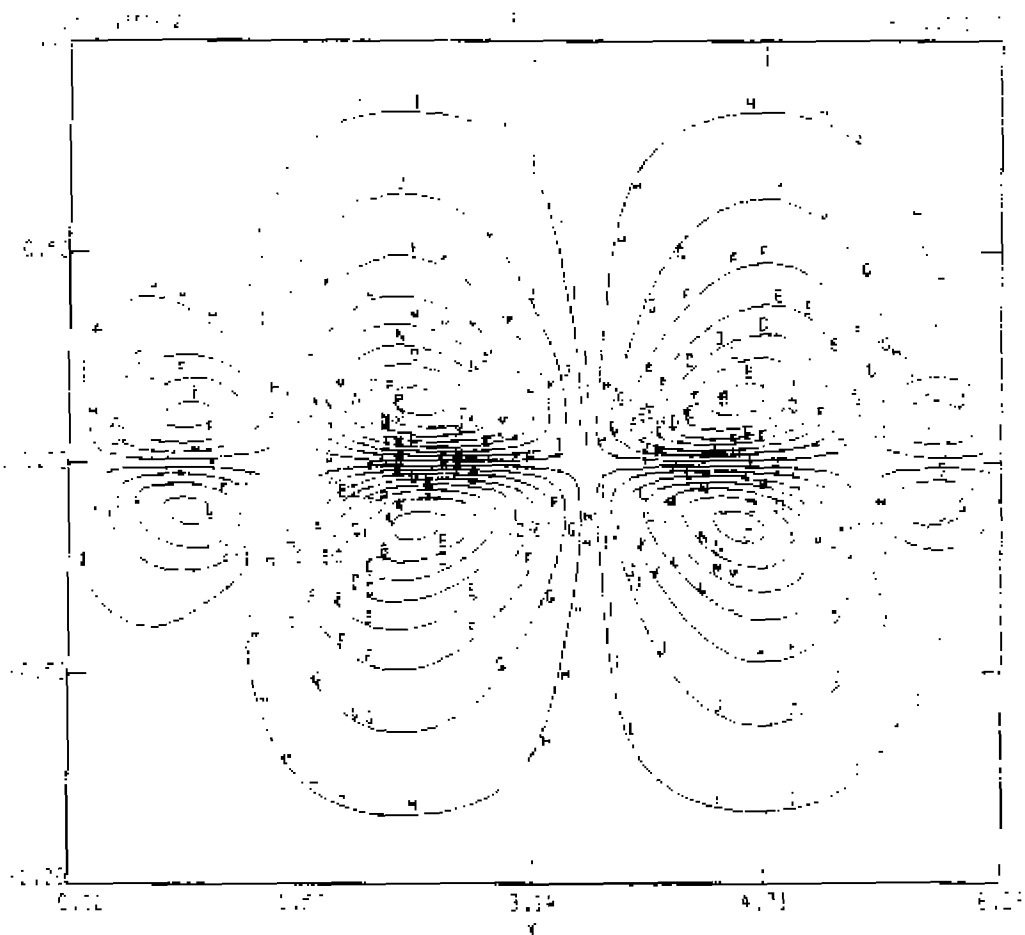


Figure VII - 3b Contour plot of velocity stream function at  $t = 19\ 63495$ .

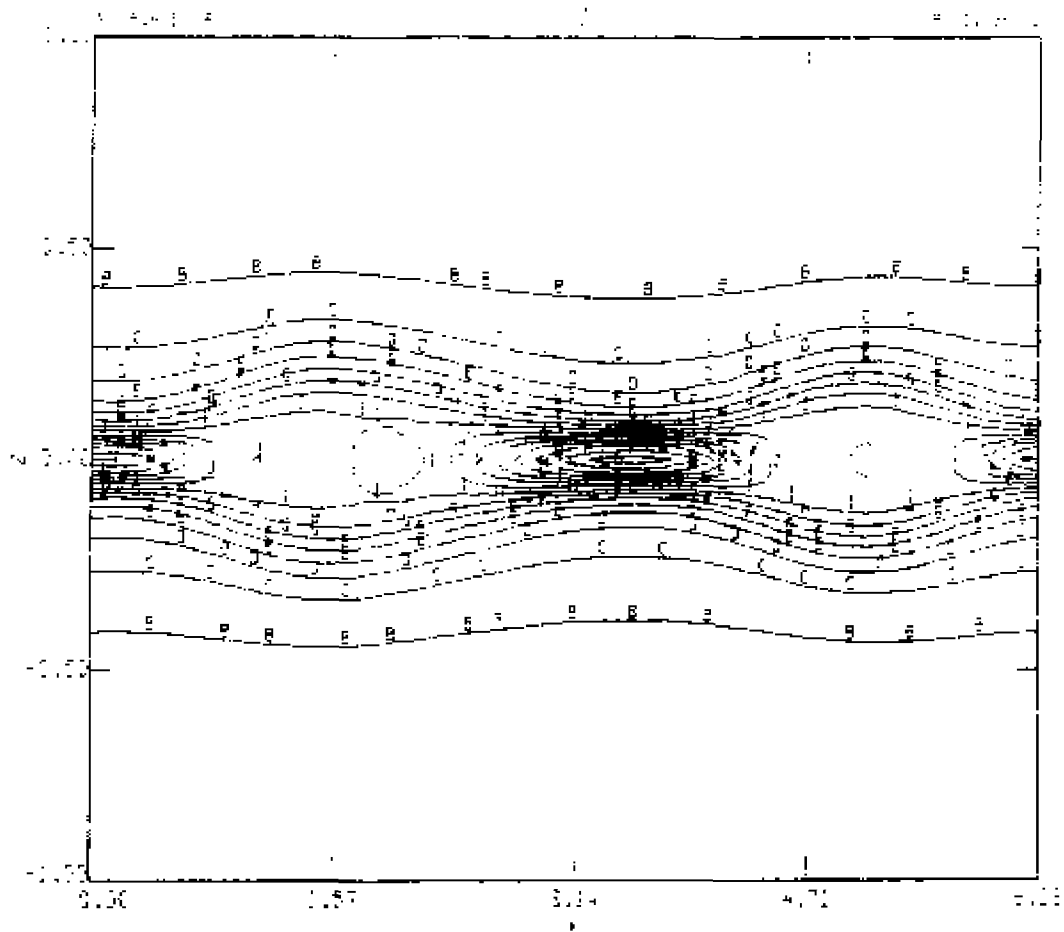


Figure VII - 3r Contour plot of electric current density at  $t = 19.63495$ .

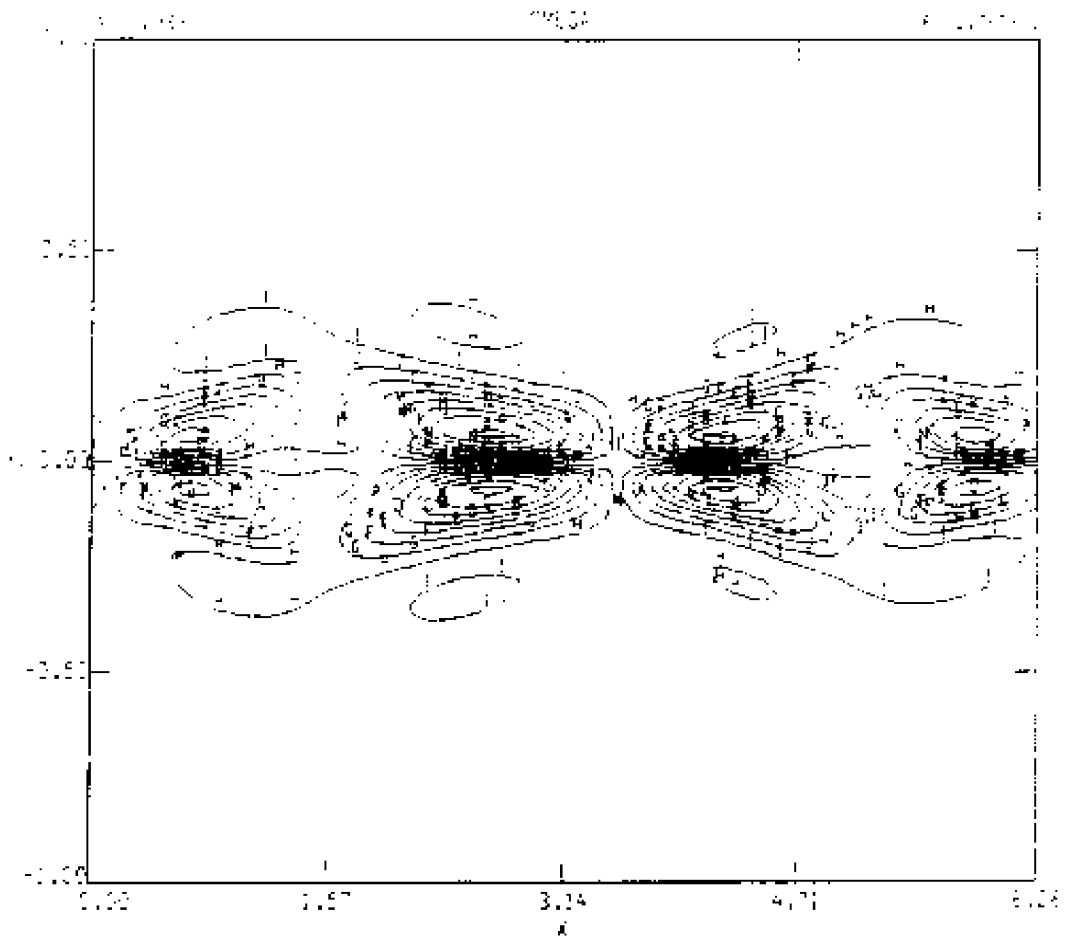


Figure VII - 3d Contour plot of vorticity at  $t = 19.63495$

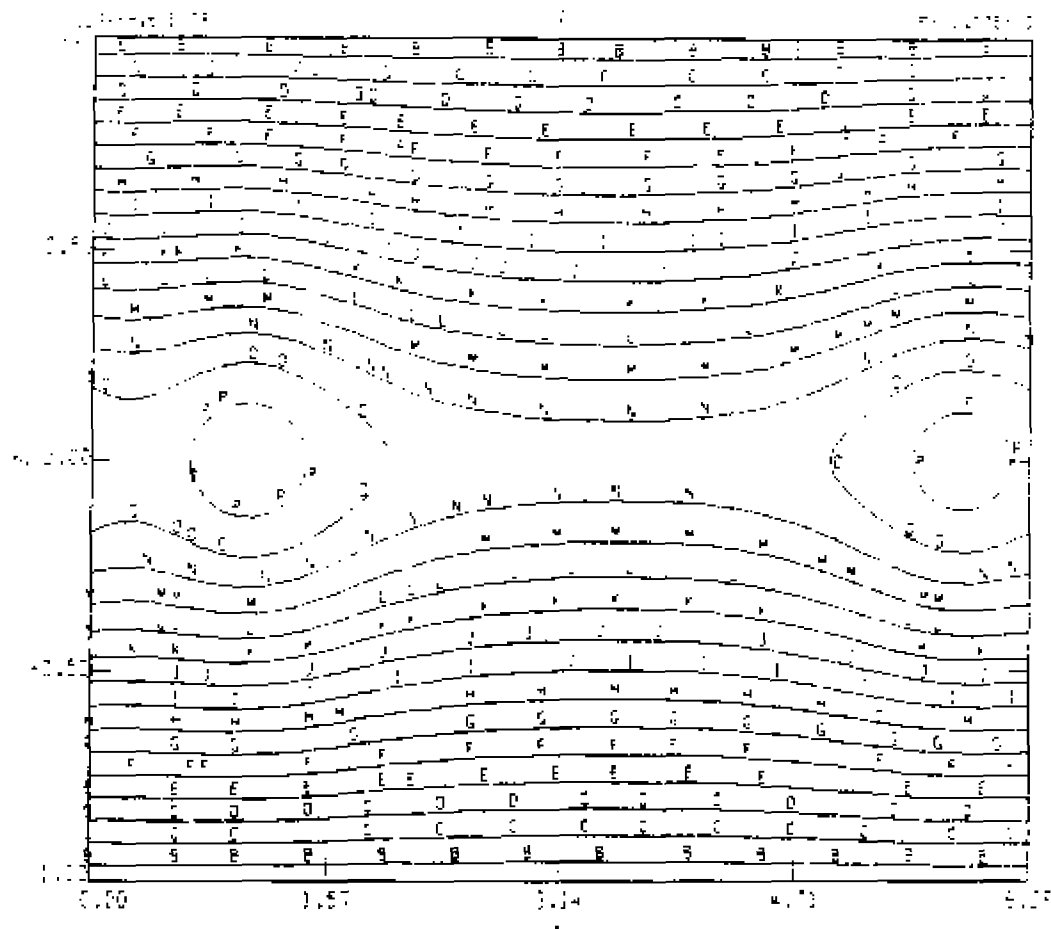


Figure VII - 4a Contour plot of magnetic vector potential at  $t = 27.46893$ .



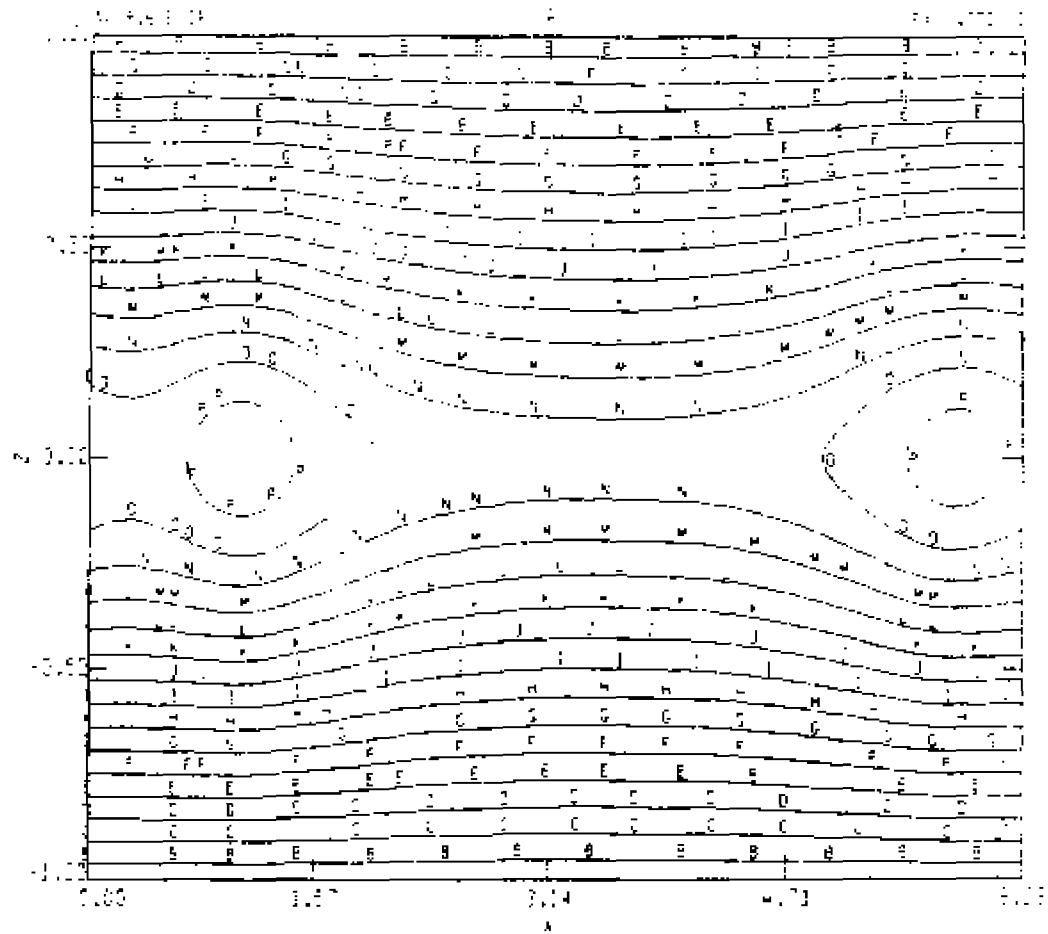


Figure VII: - 4a Contour plot of magnetic vector potential at  $t = 27.48893$ .

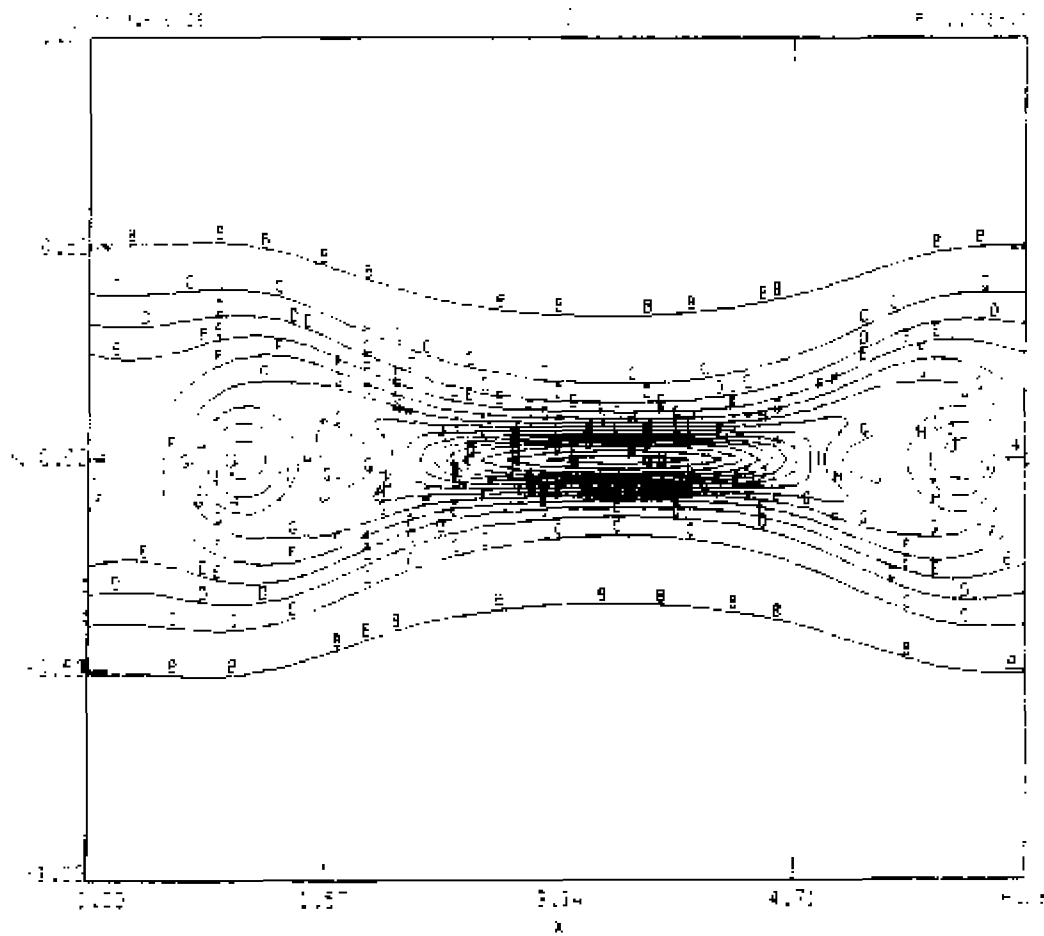


Figure VII - 4c Contour plot of electric current density at  $t = 27.48393$

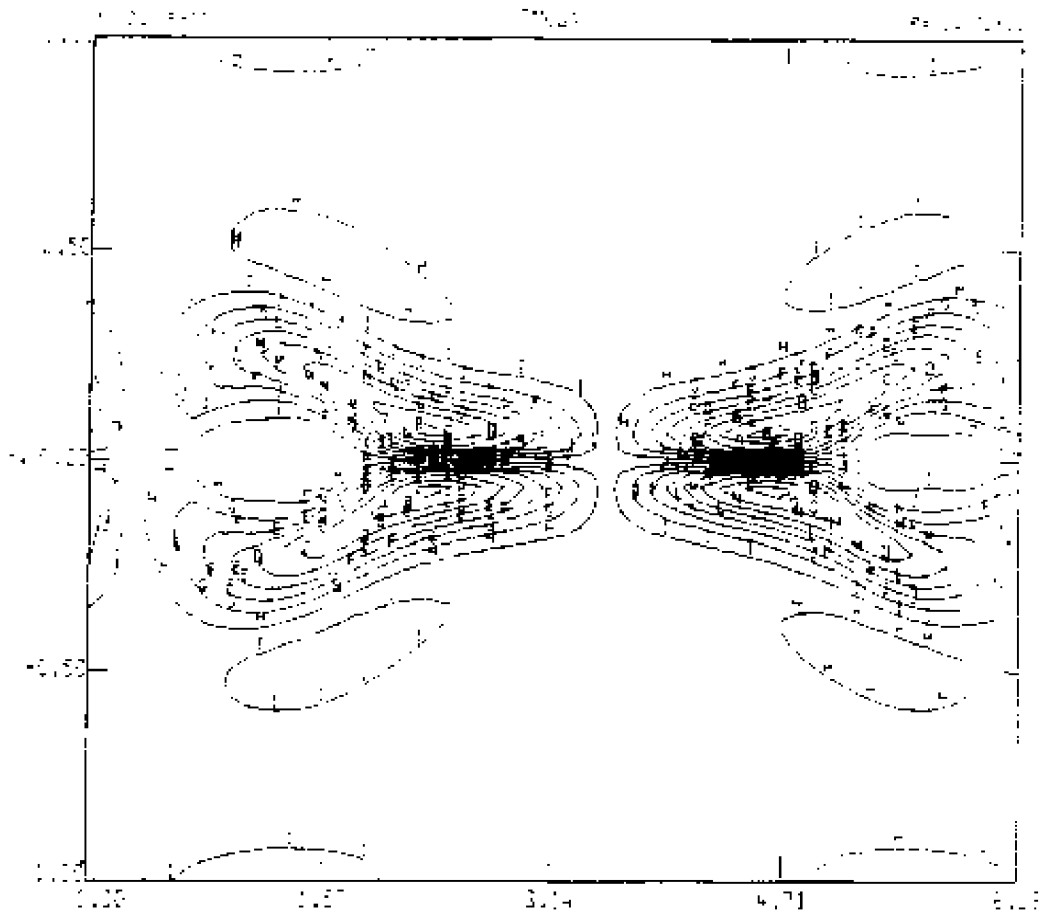


Figure VII - 4d Contour plot of vorticity at  $t = 27.48893$ .

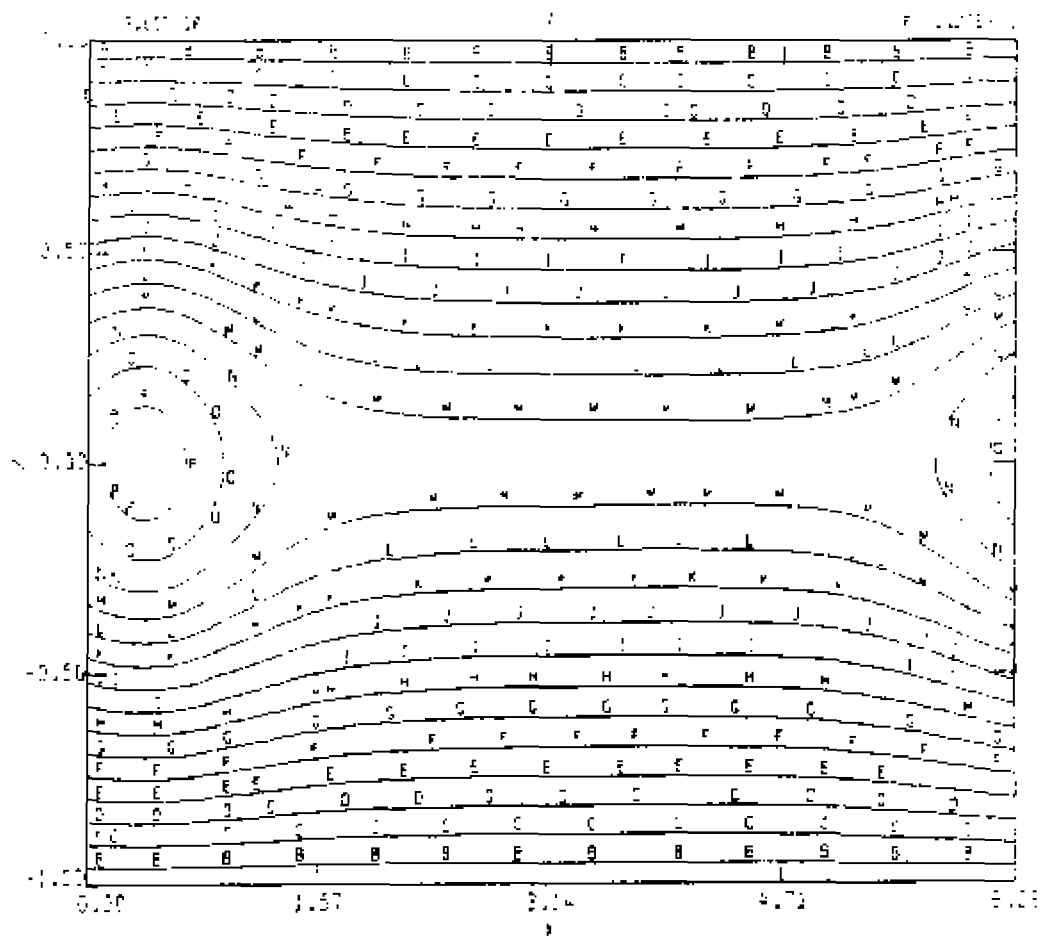


Figure VII - 5a Contour plot of magnetic vector potential at  $t = 39\ 26991$ .

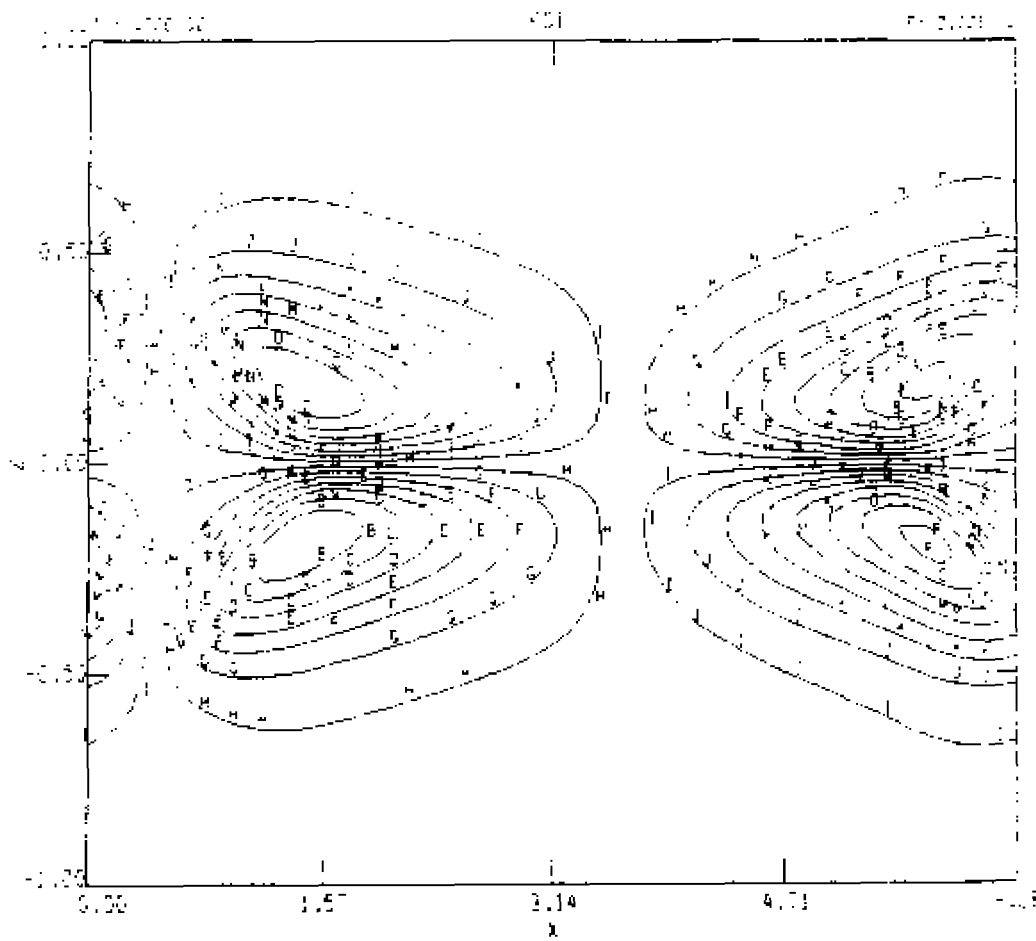


Figure VII - 5b Contour plot of velocity stream function at  $t = 39.26391$ .

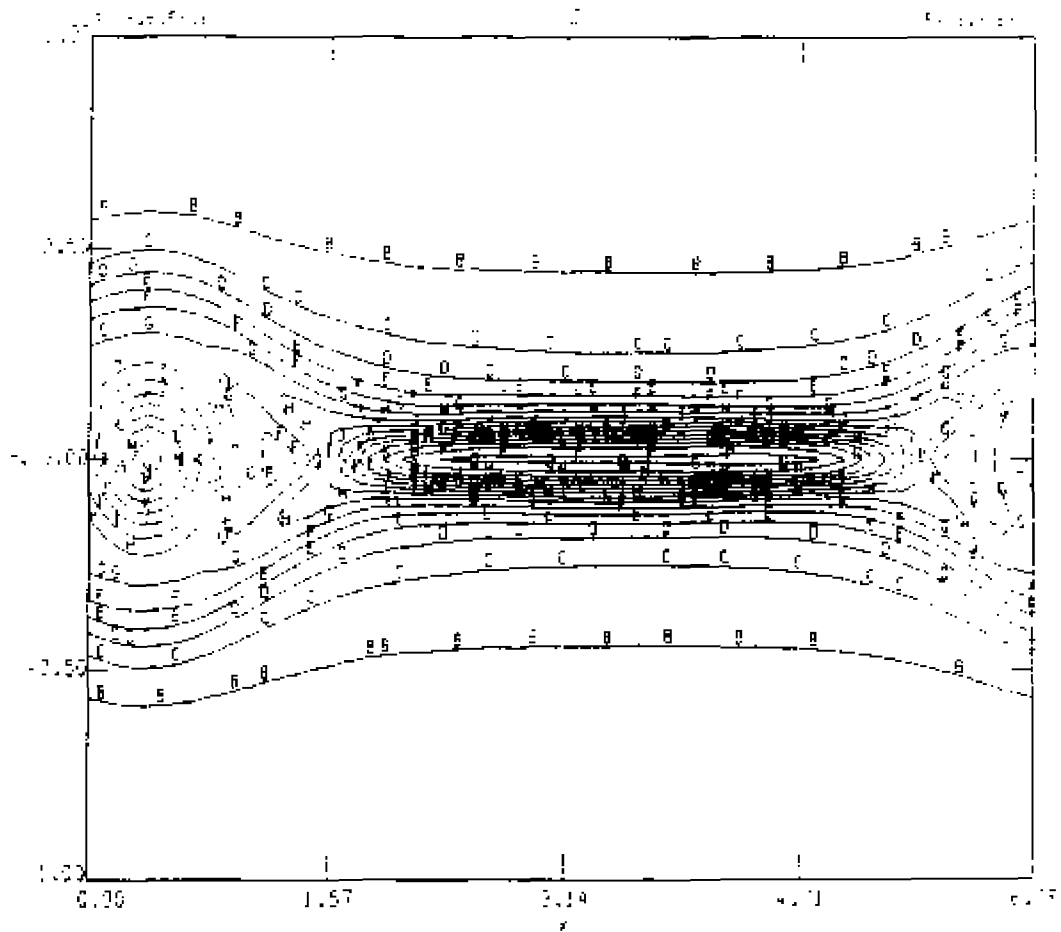


Figure V12 - Sc Contour plot of electric current density at  $t = 39.26991$

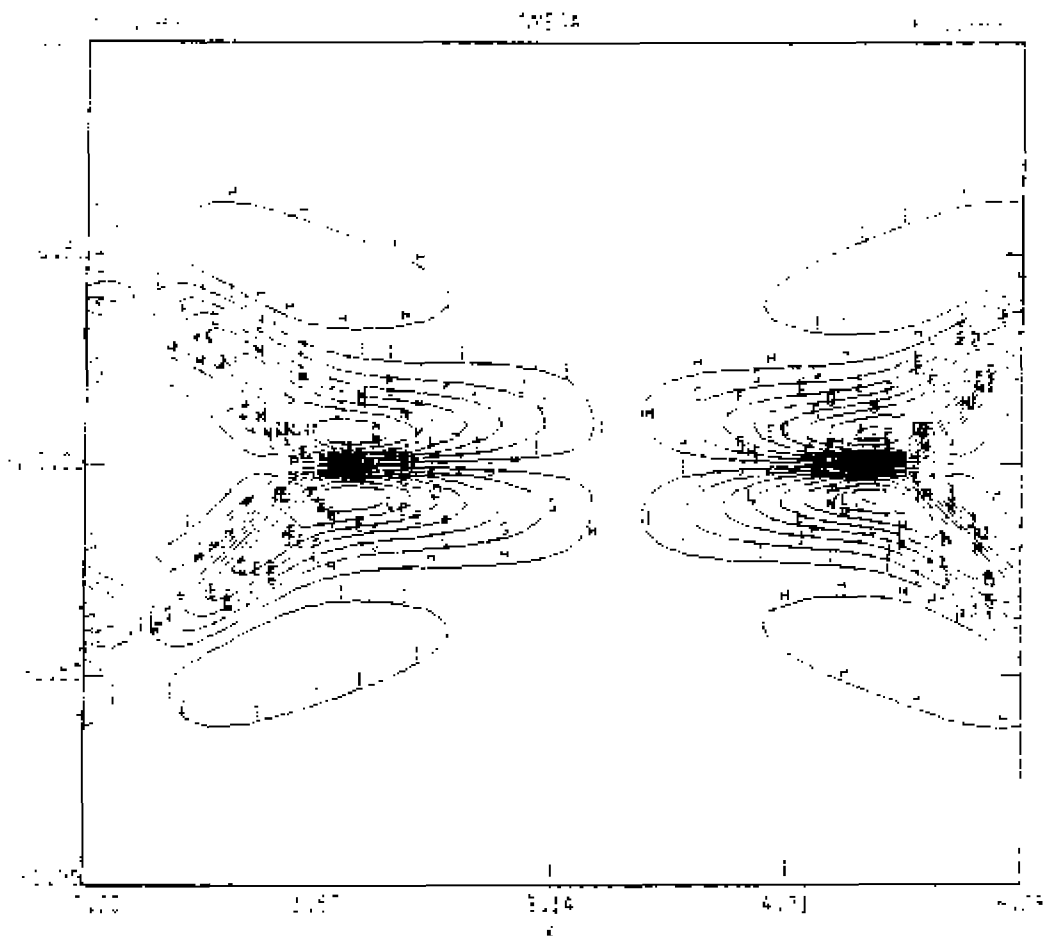


Figure VII - 5d Contour plot of vorticity at  $t = 39.26991$

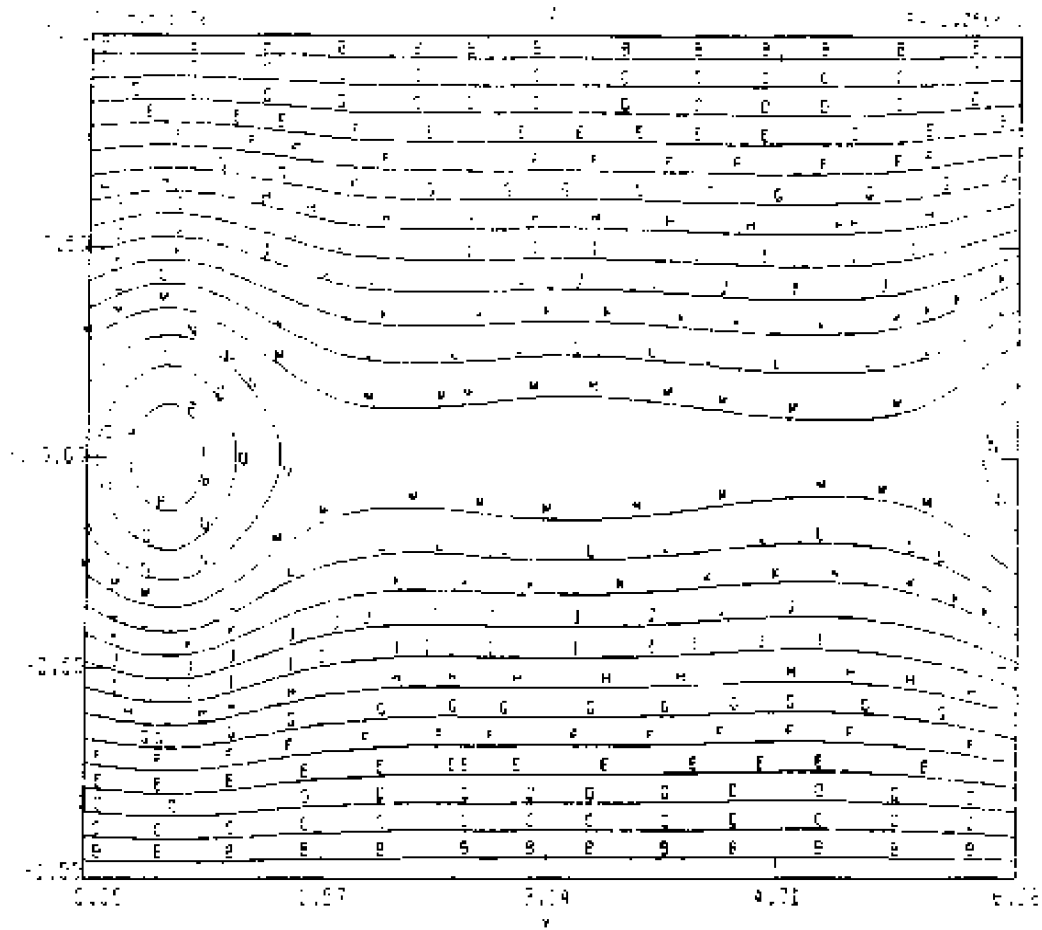


Figure VII - 6a Contour plot of magnetic vector potential at  $t = 51.05186$ .



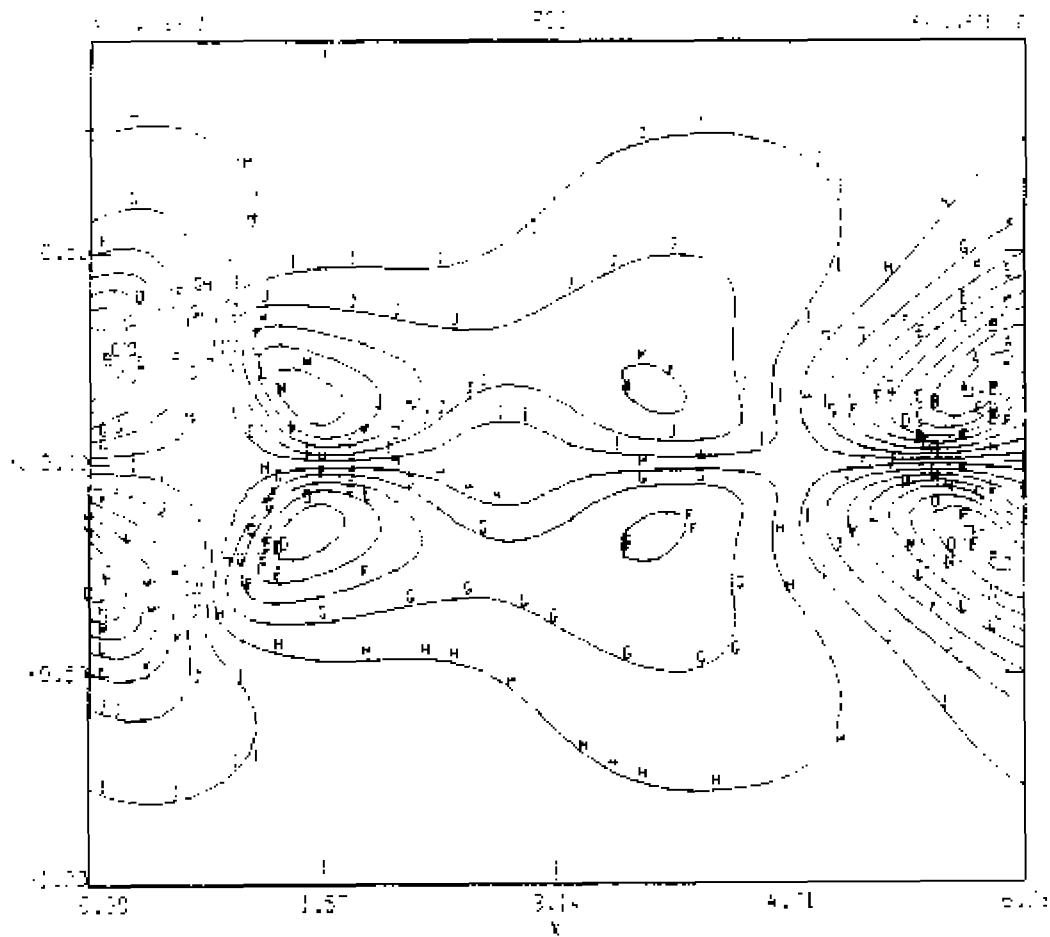


Figure VII - 6b Contour plot of velocity stream function at  $t = 51.05196$ .

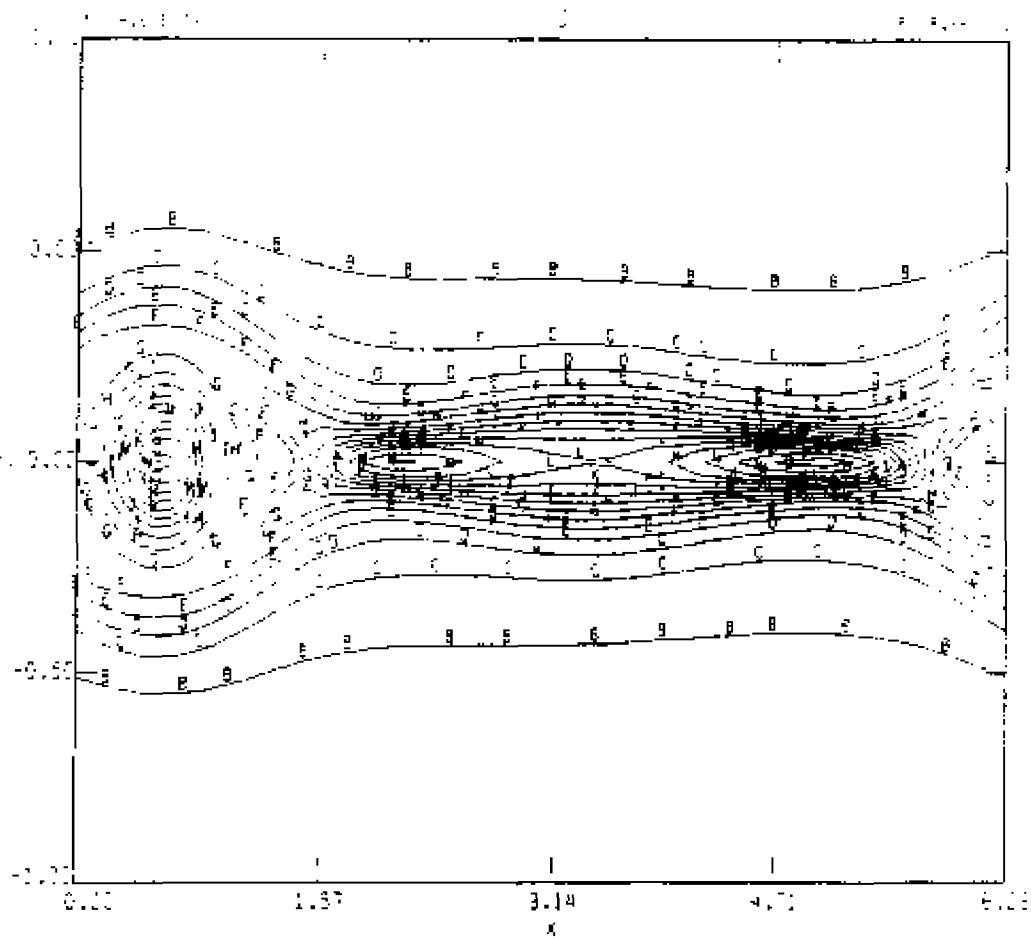


Figure VII - 6c Contour plot of electric current density at  $t = 51.05186$ .

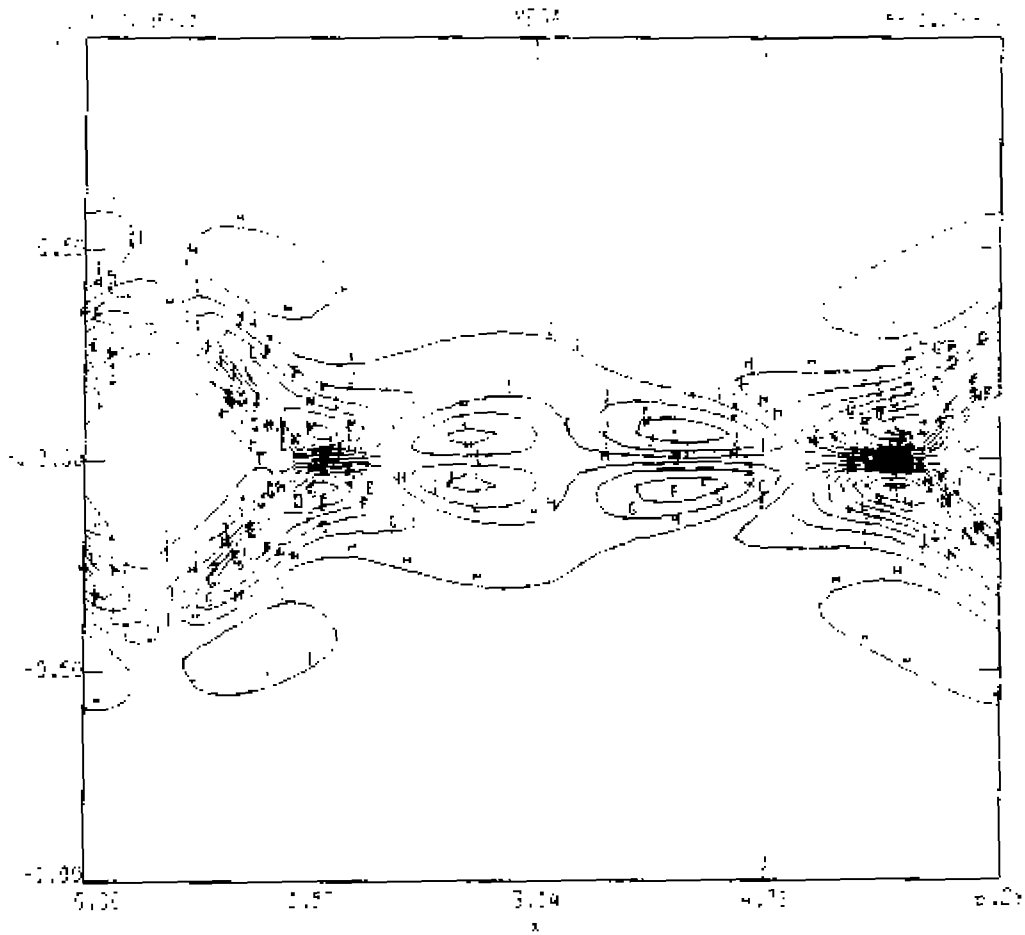


Figure VII - 6d Contour plot of vorticity at  $t = 51.05186$ .

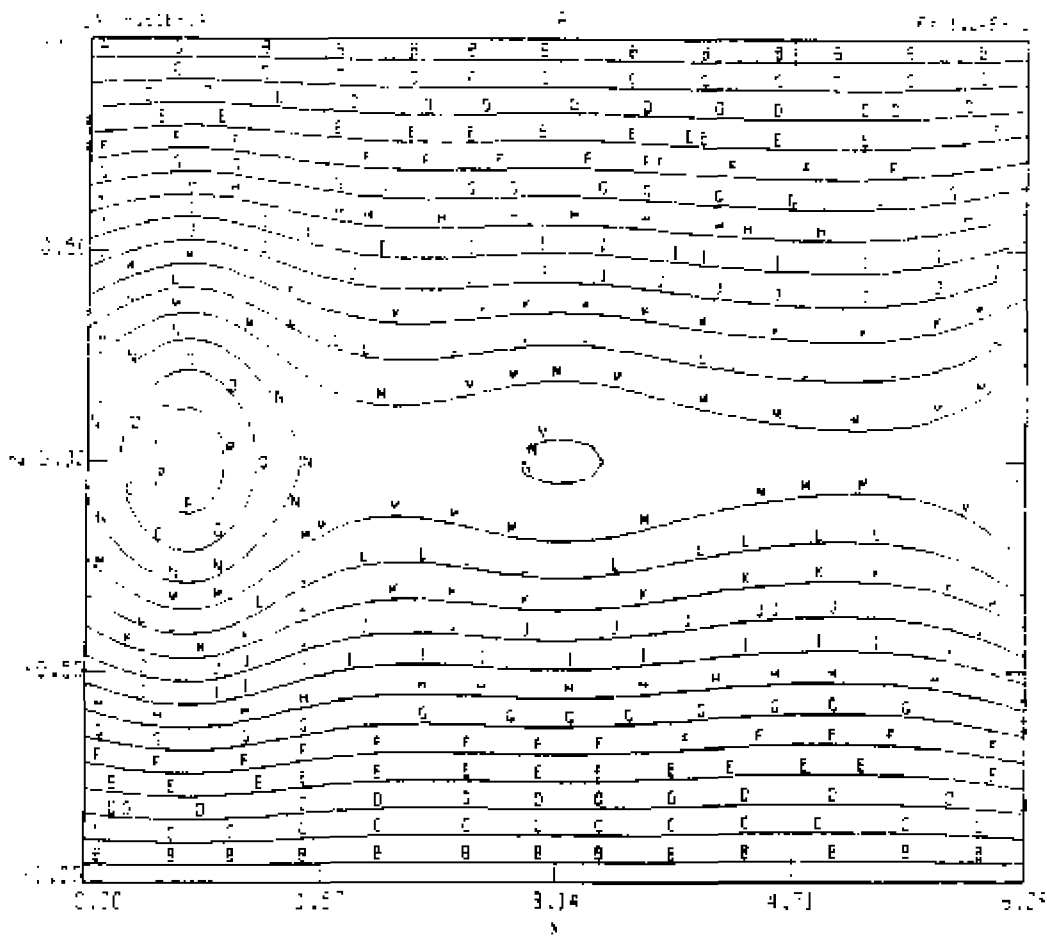


Figure VII - 7a Contour plot of magnetic vector potential at  $t = 54.97835$ .

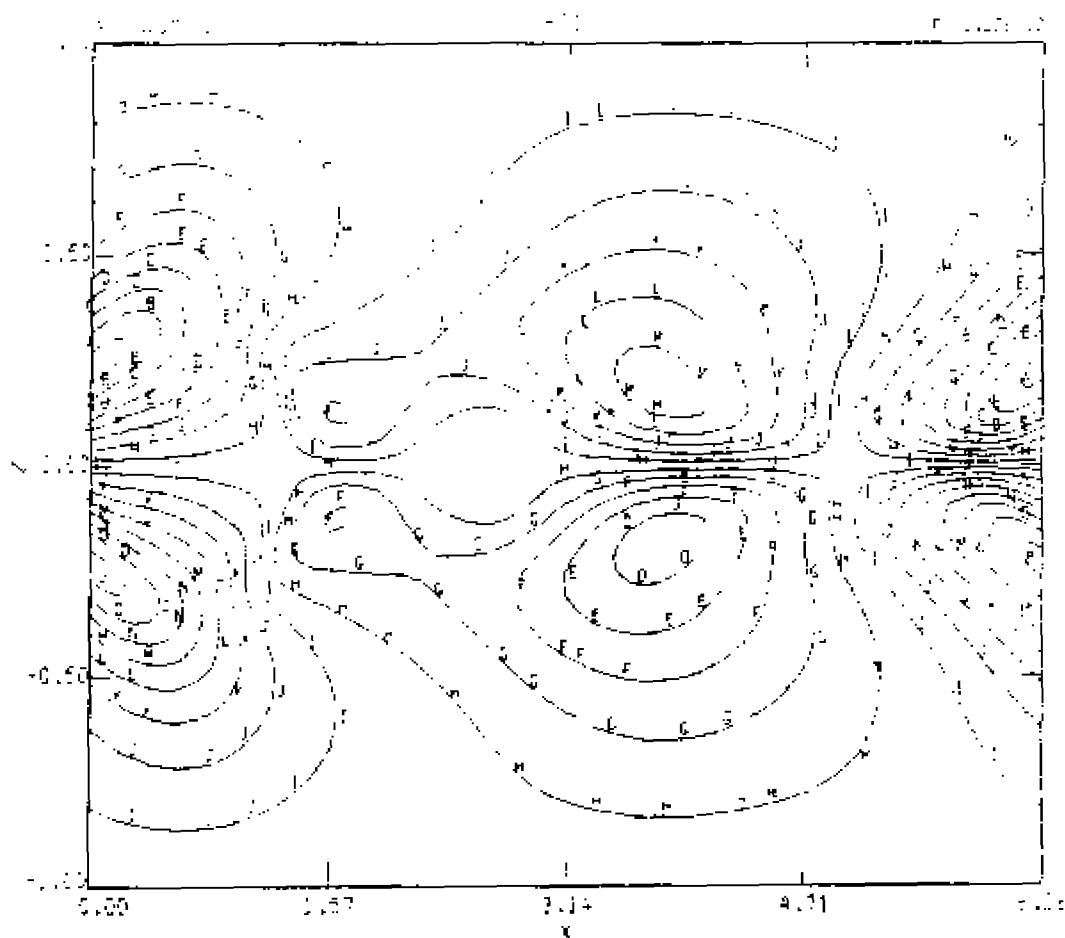


Figure VII - 7b Contour plot of velocity stream function at  $t = 54.97093$ .

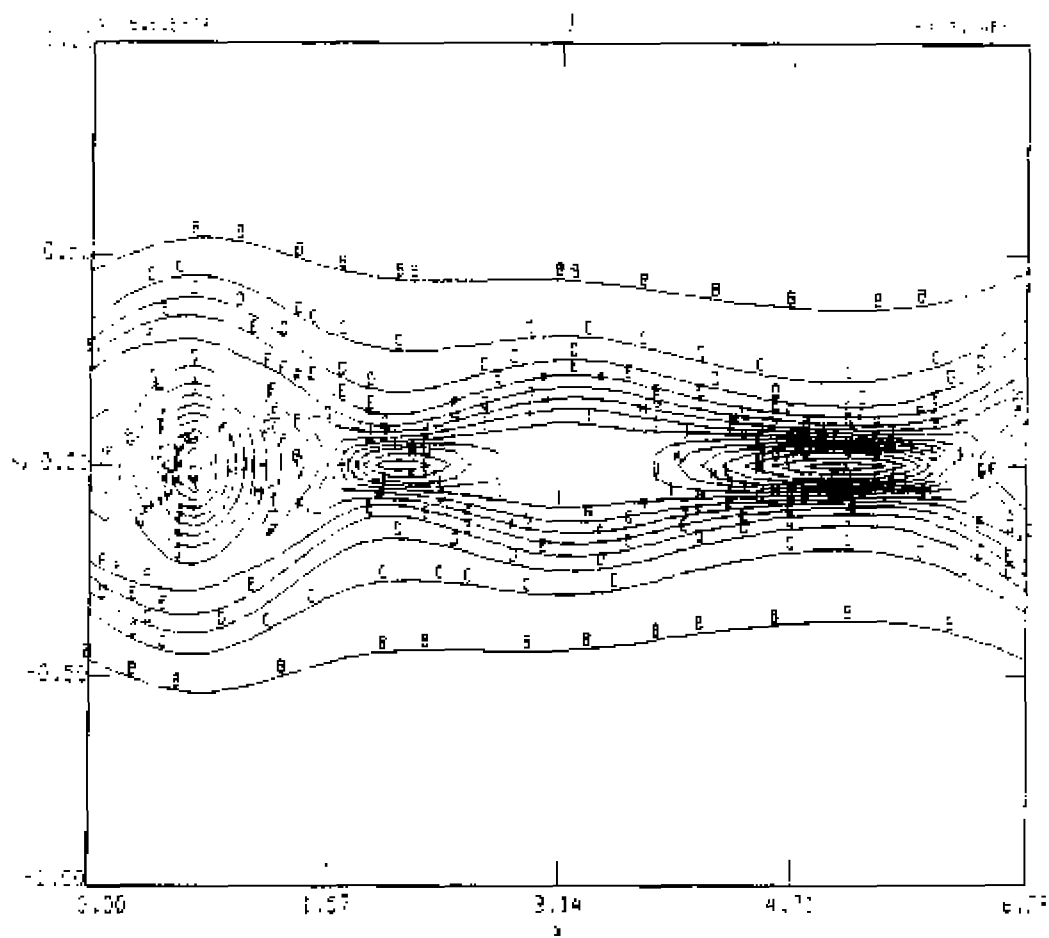


Figure VII - 7c Contour plot of electric current density at  $t = 54.97385$ .

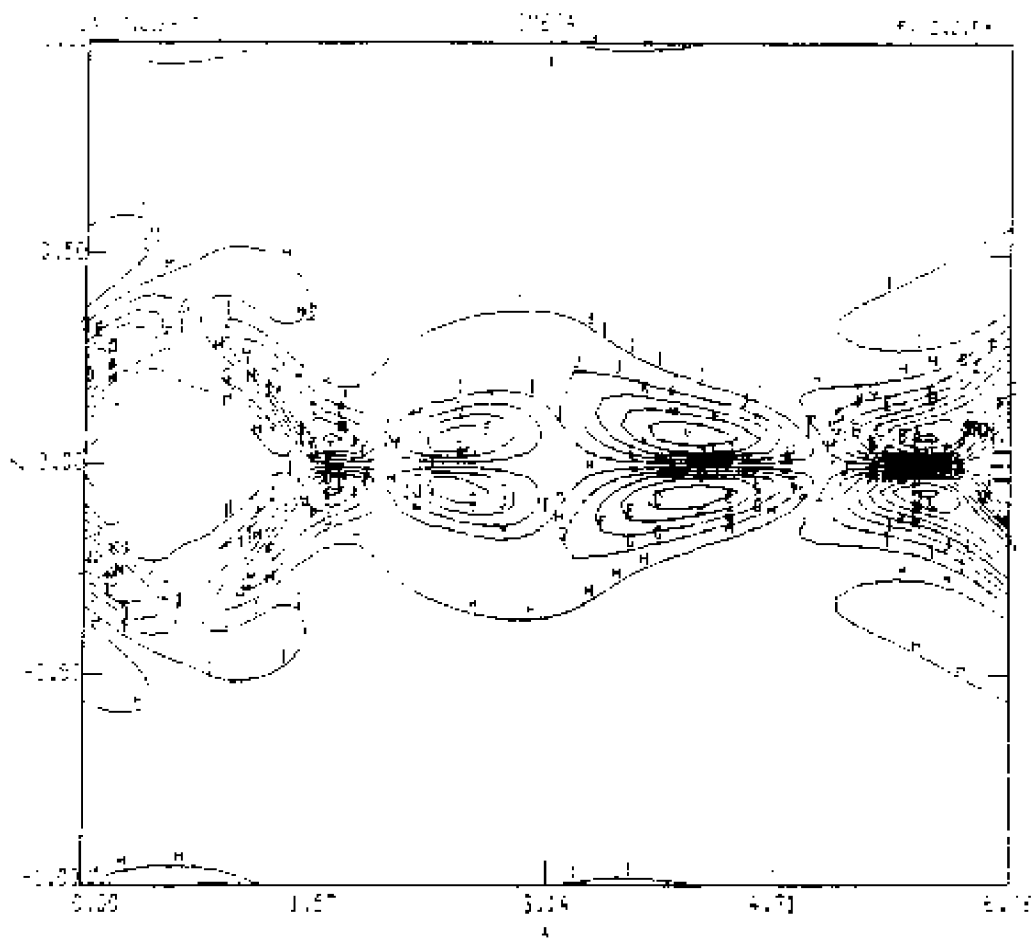


Figure VII - 7d Contour plot of vorticity at  $t = 54.97885$ .

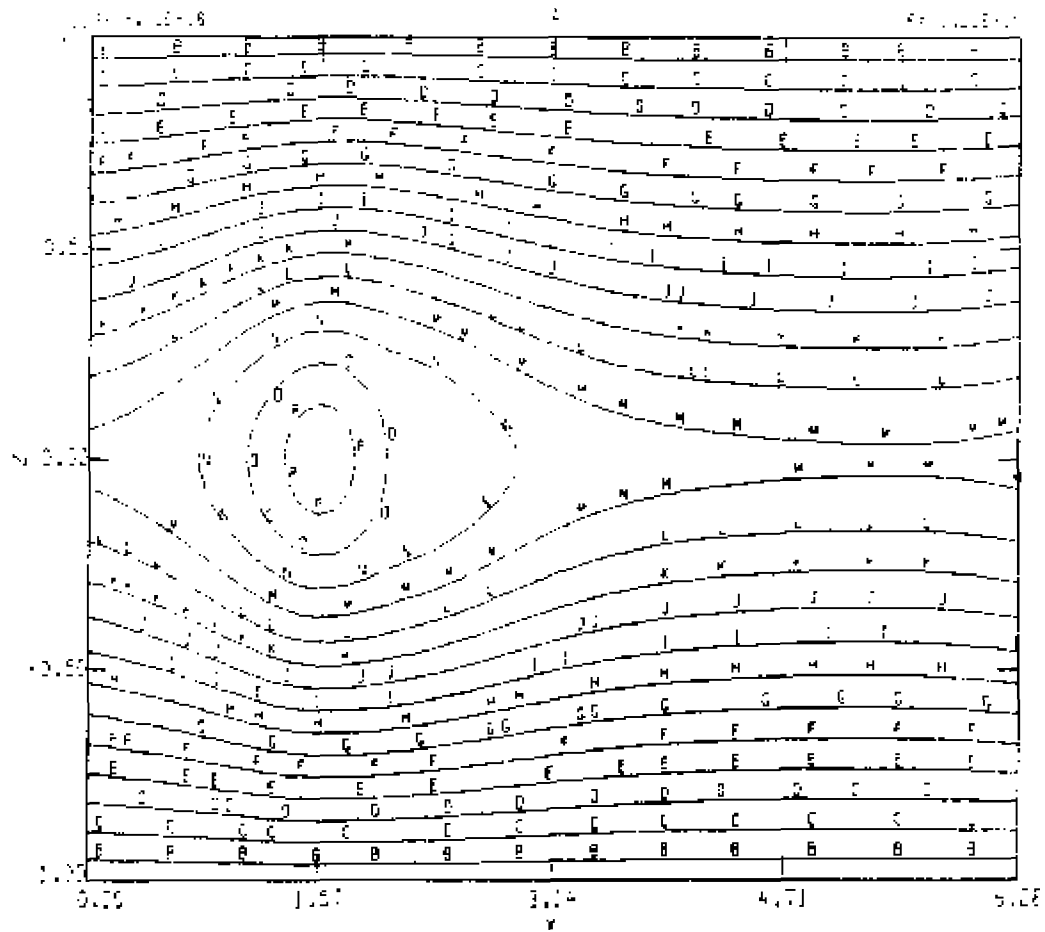


Figure VII - 9a Contour plot of magnetic vector potential at  $t = 58.9453$



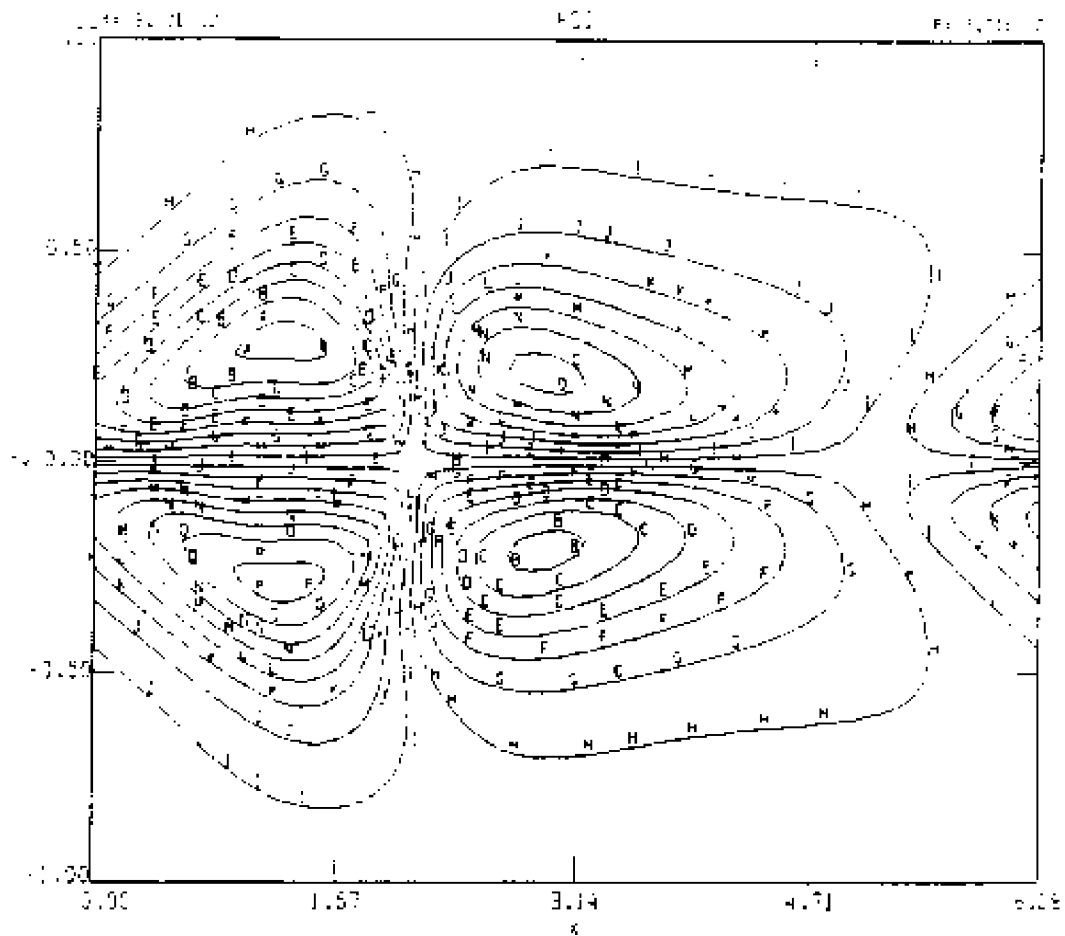


Figure VII - 8b Contour plot of velocity stream function at  $t = 58.9958$ .

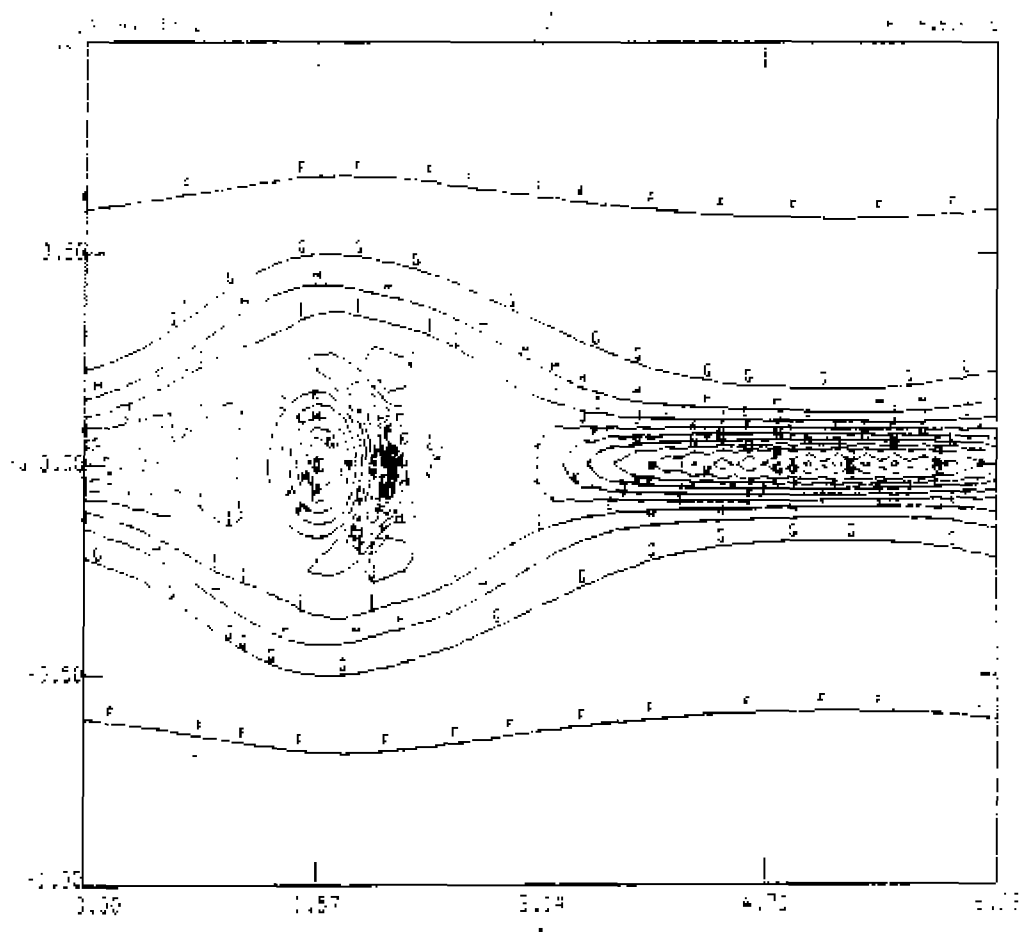


Figure VII - 8c Contour plot of electric current density at  $t = 58.9058$ .

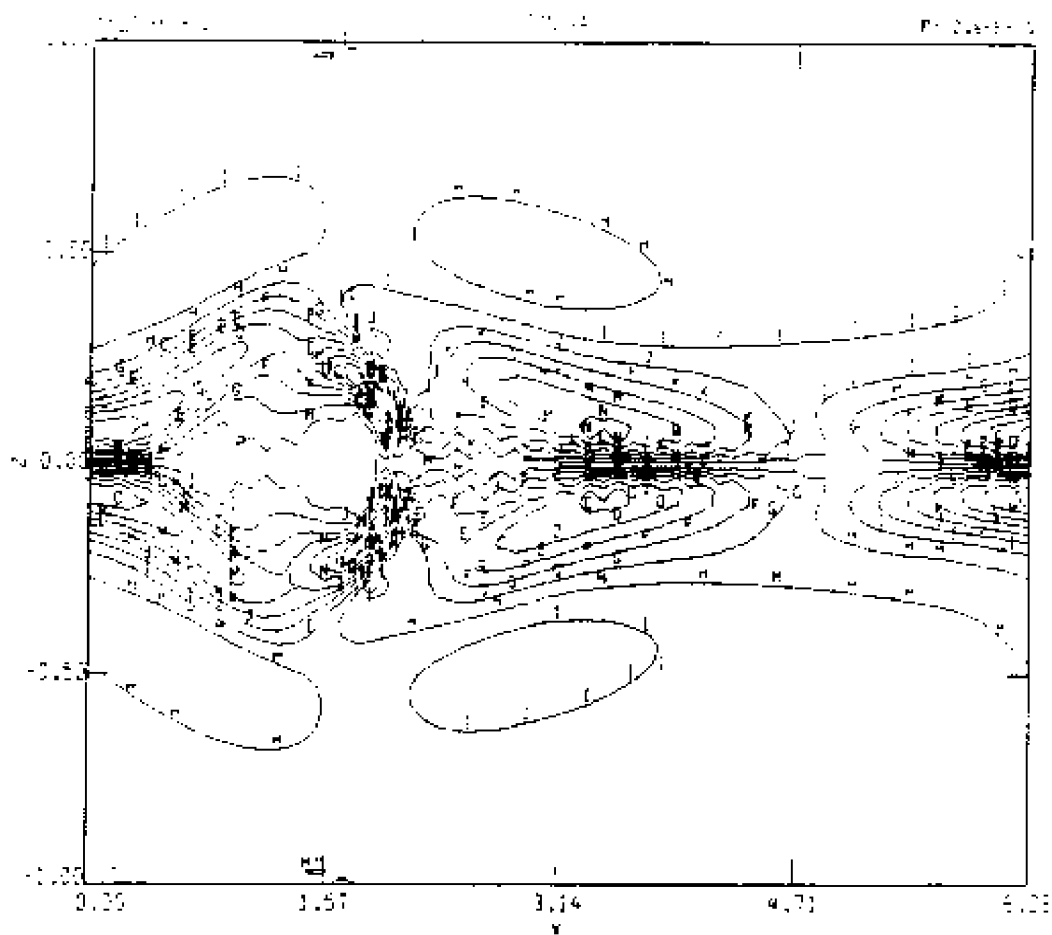


Figure VII - 8d Contour plot of vorticity at  $t = 50.9053$ .

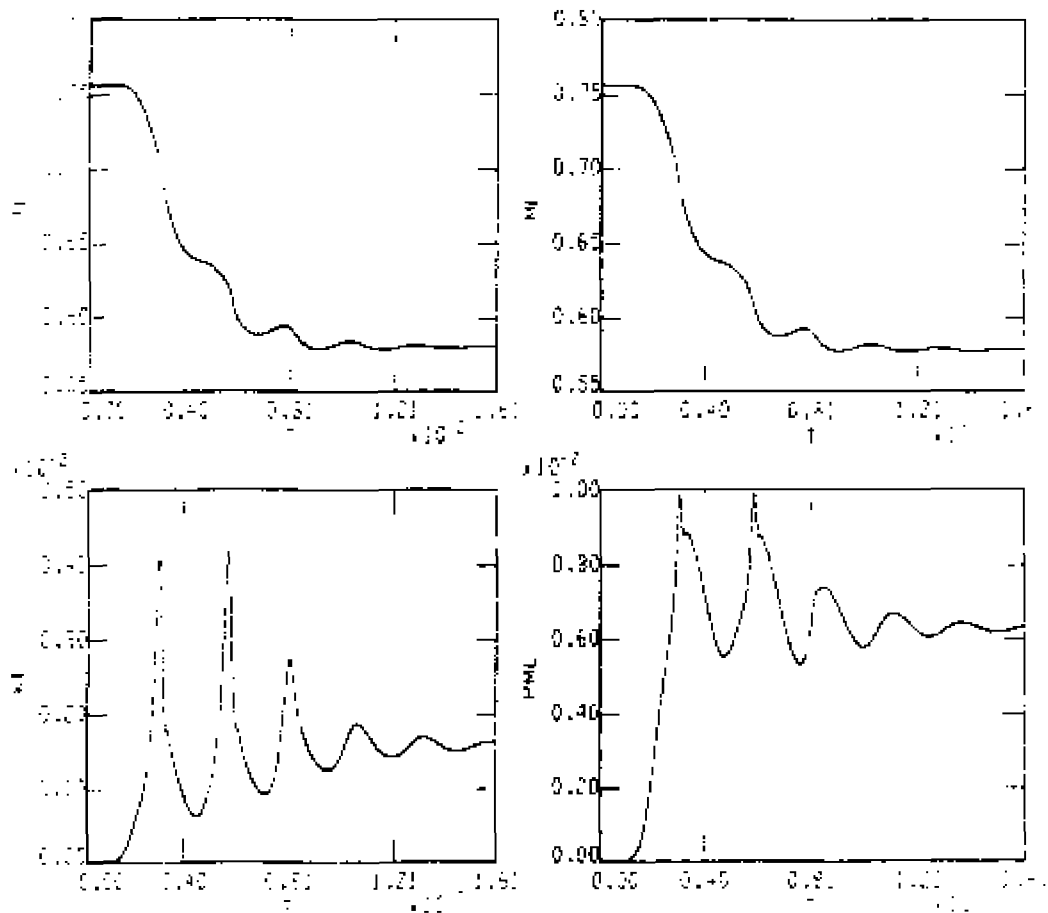


Figure VII - 9a Plots of global quantities versus time.

TE = total energy, ME = magnetic energy, KE = kinetic energy,

PME = perturbed magnetic energy.

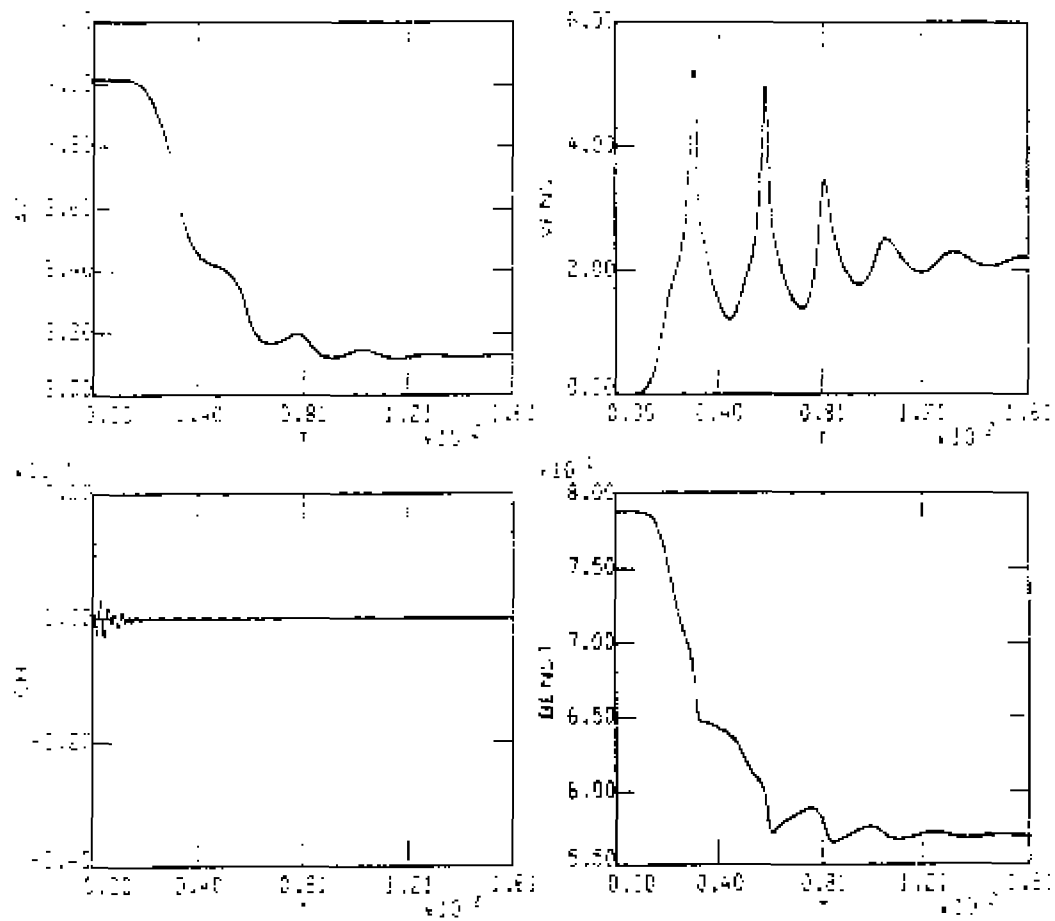


Figure VII - 9b Plots of global quantities versus time;

$A2$  = mean square vector potential,  $CH$  = cross helicity,

$VENST$  = enstrophy,  $BENST$  = magnetic enstrophy.

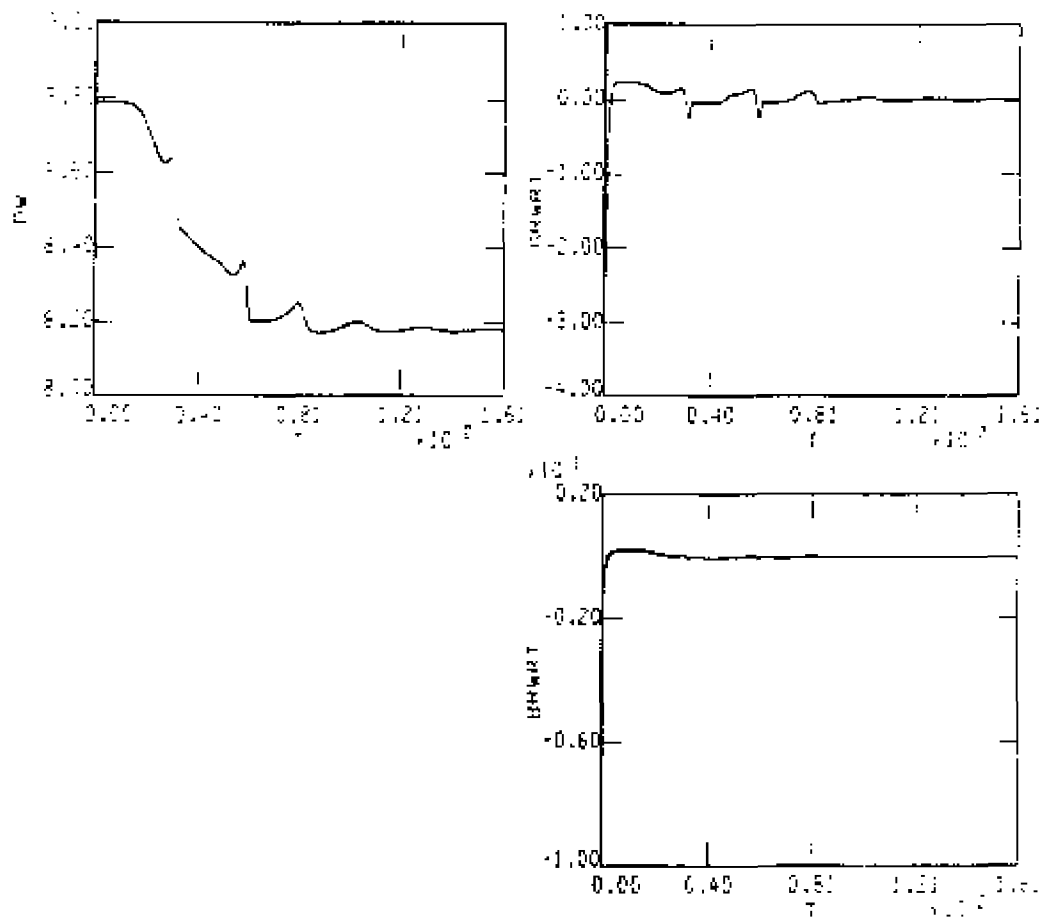


Figure VII - 9c Plots of global quantities versus time;

DW = dissipation wavenumber, GRWRT = kinetic energy growth rate, BRWRT = perturbed magnetic energy growth rate.

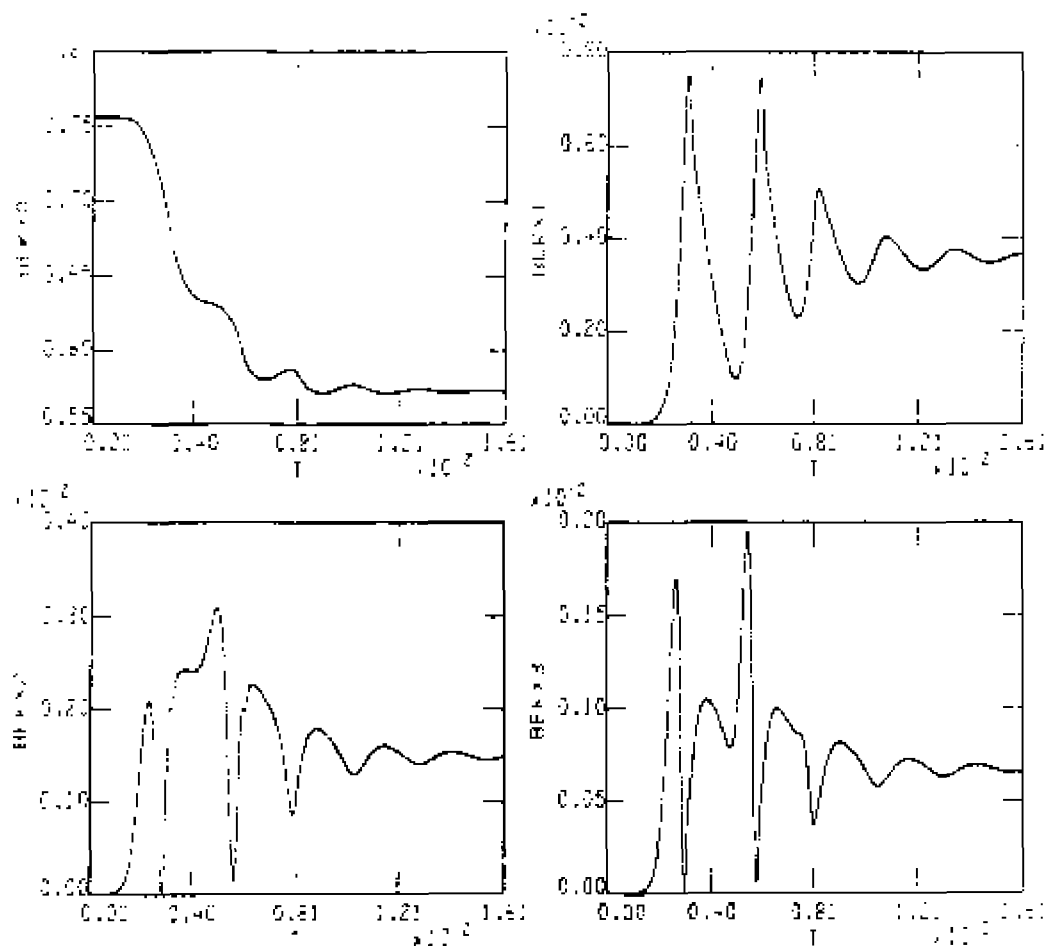


Figure VII - 9d Plots of one dimensional modal magnetic energies versus time:

BEKX0 = magnetic energy ( $k_x = 0$ ), BEKX1 = magnetic energy

( $k_x = 1$ ), BEKX2 = magnetic energy ( $k_x = 2$ ),

BEKX3 = magnetic energy ( $k_x = 3$ ).

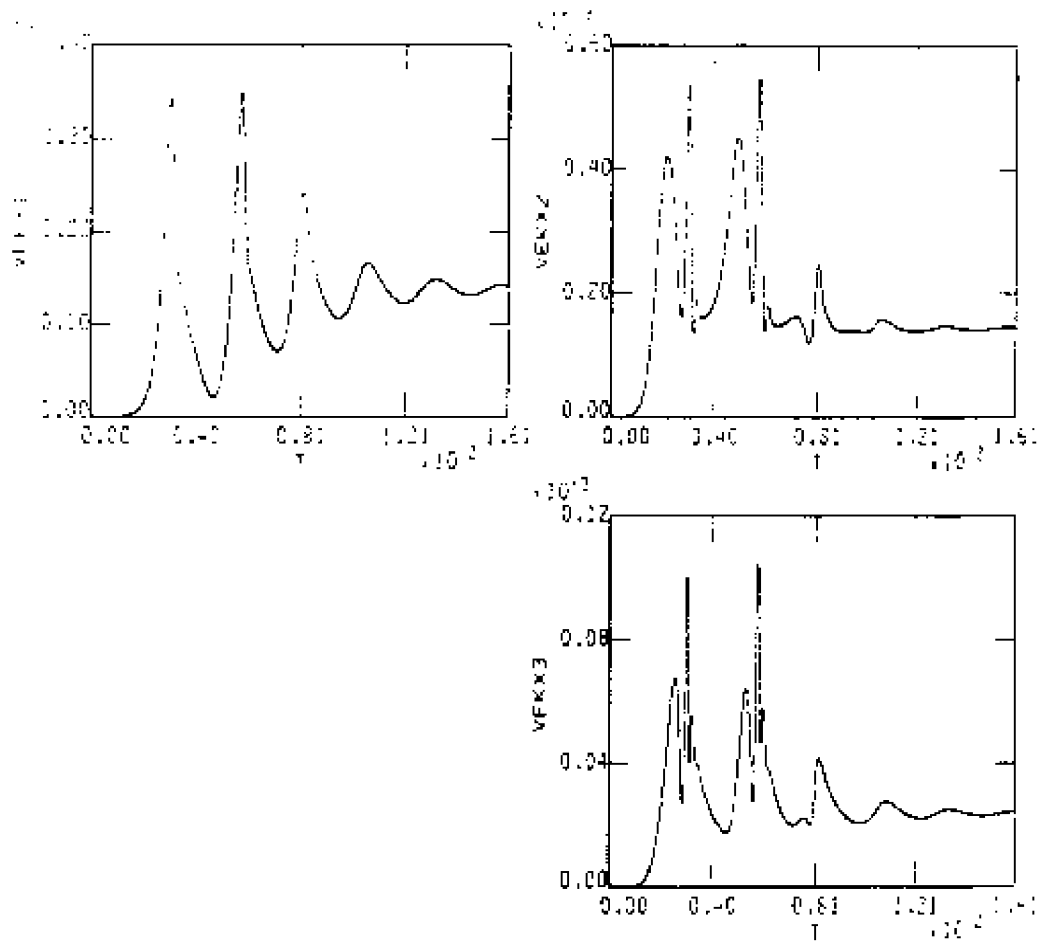


Figure VII - 9e Plots of one dimensional modal kinetic energies versus time;  
 $VEXX1$  = kinetic energy ( $k_x = 1$ ),  $VEXX2$  = kinetic energy  
( $k_x = 2$ ),  $VEXX3$  = kinetic energy ( $k_x = 3$ ).



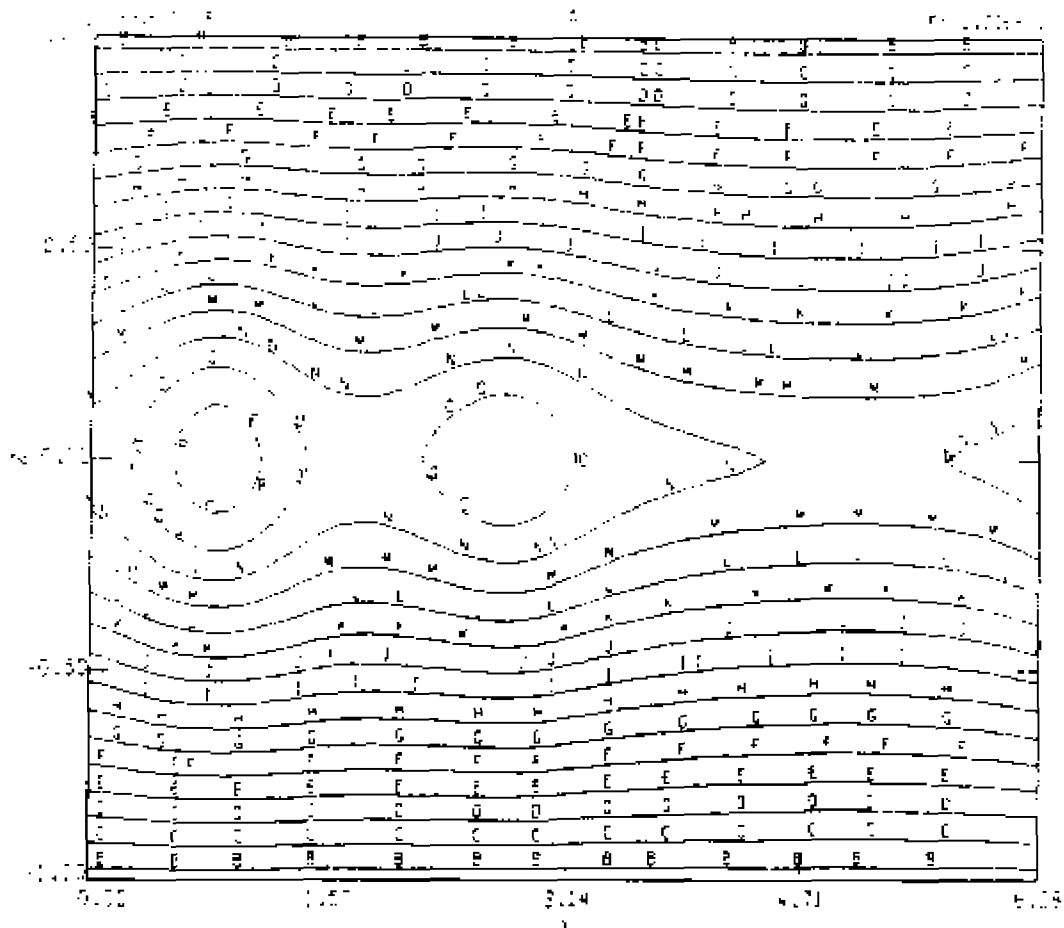


Figure VII - 14a Contour plot of magnetic vector potential at  $t = 54.97865$ .

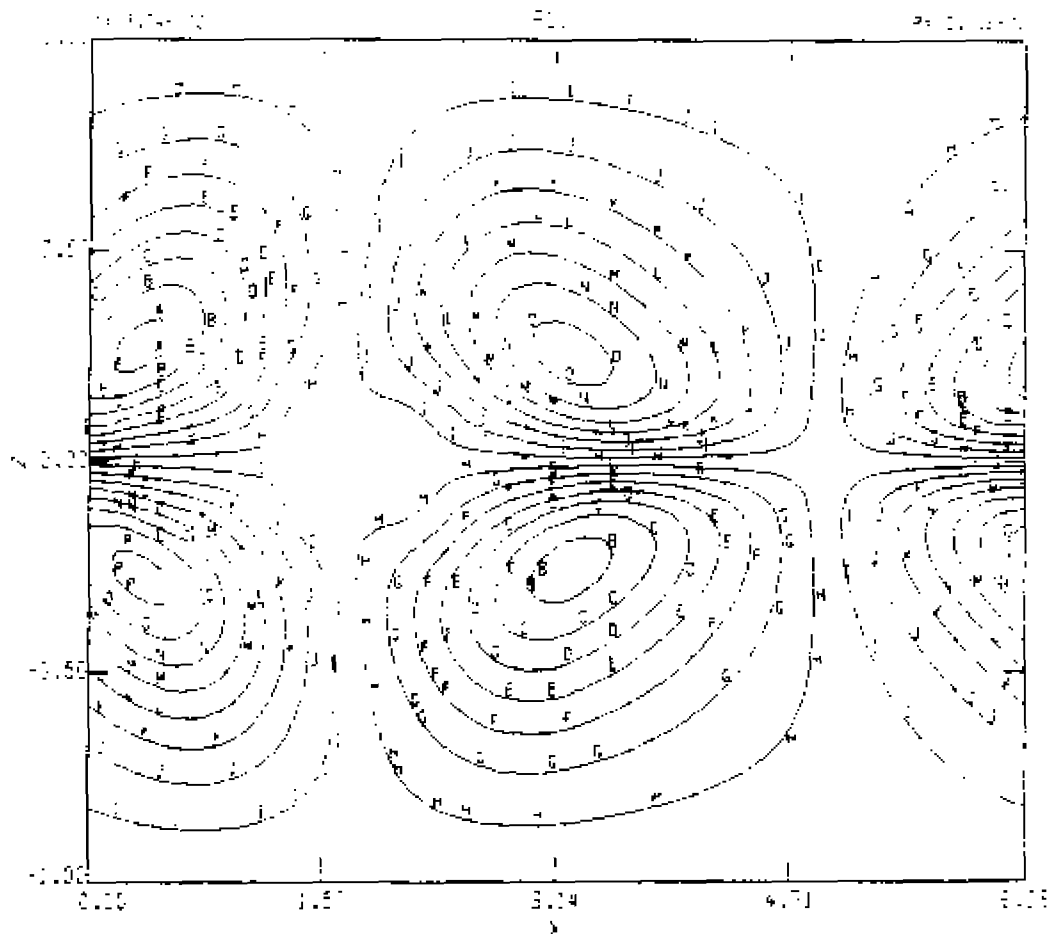


Figure VII - 10b Contour plot of velocity stream function at  $t = 54.97885$ .

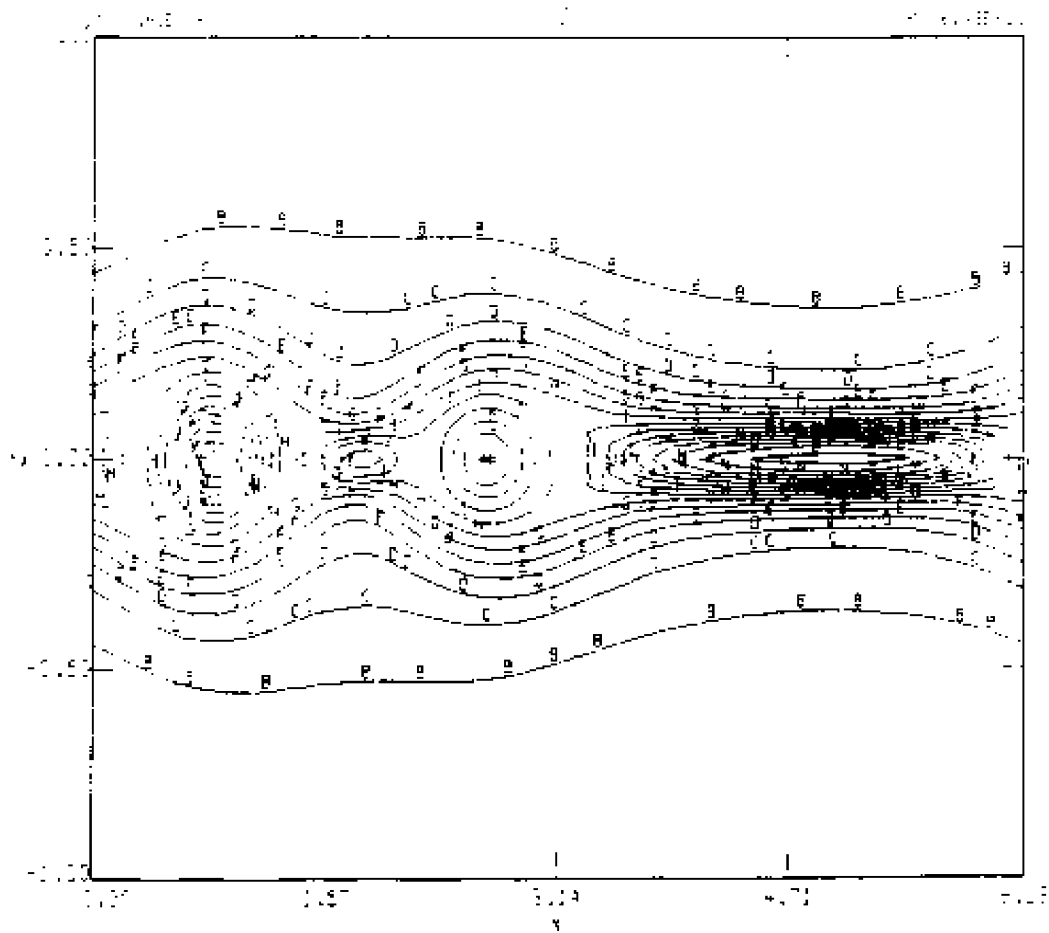


Figure VII - 10c Contour plot of electric current density at  $t = 54.97085$

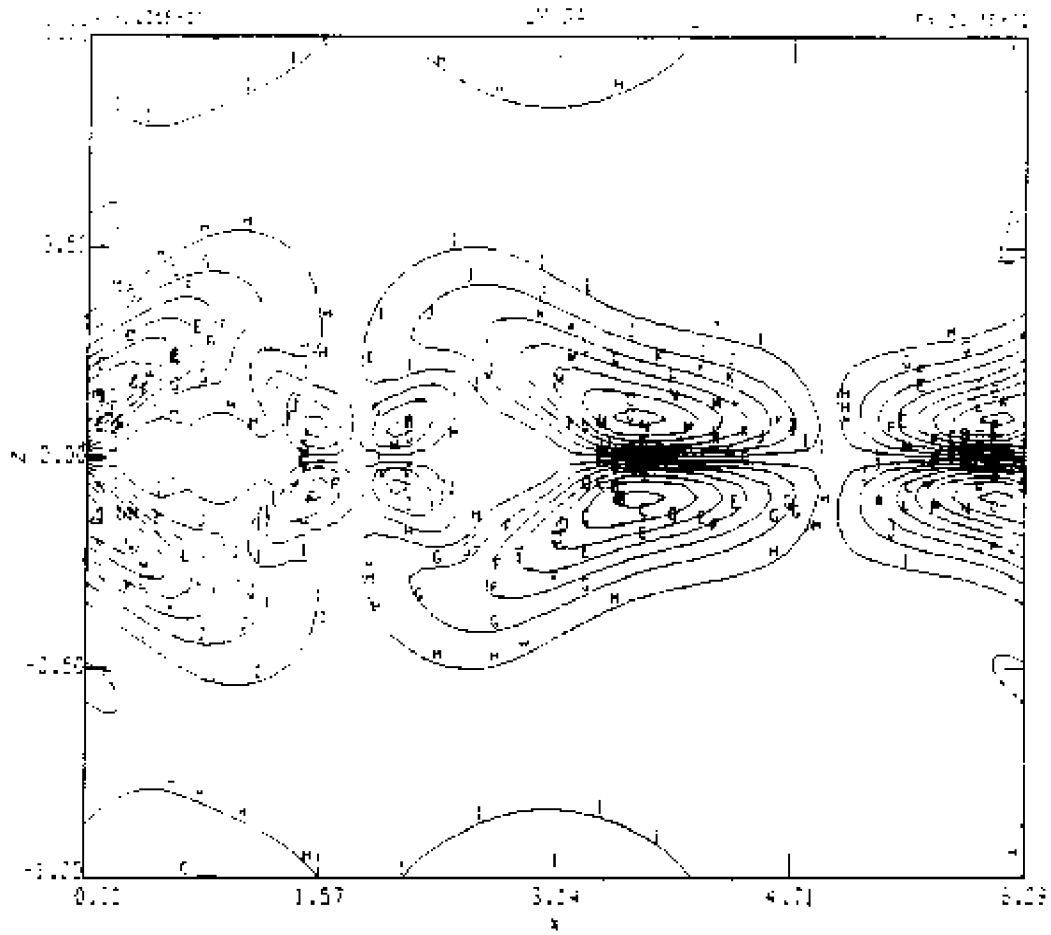


Figure VII - 10c Contour plot of vorticity at  $t = 54.97885$ .

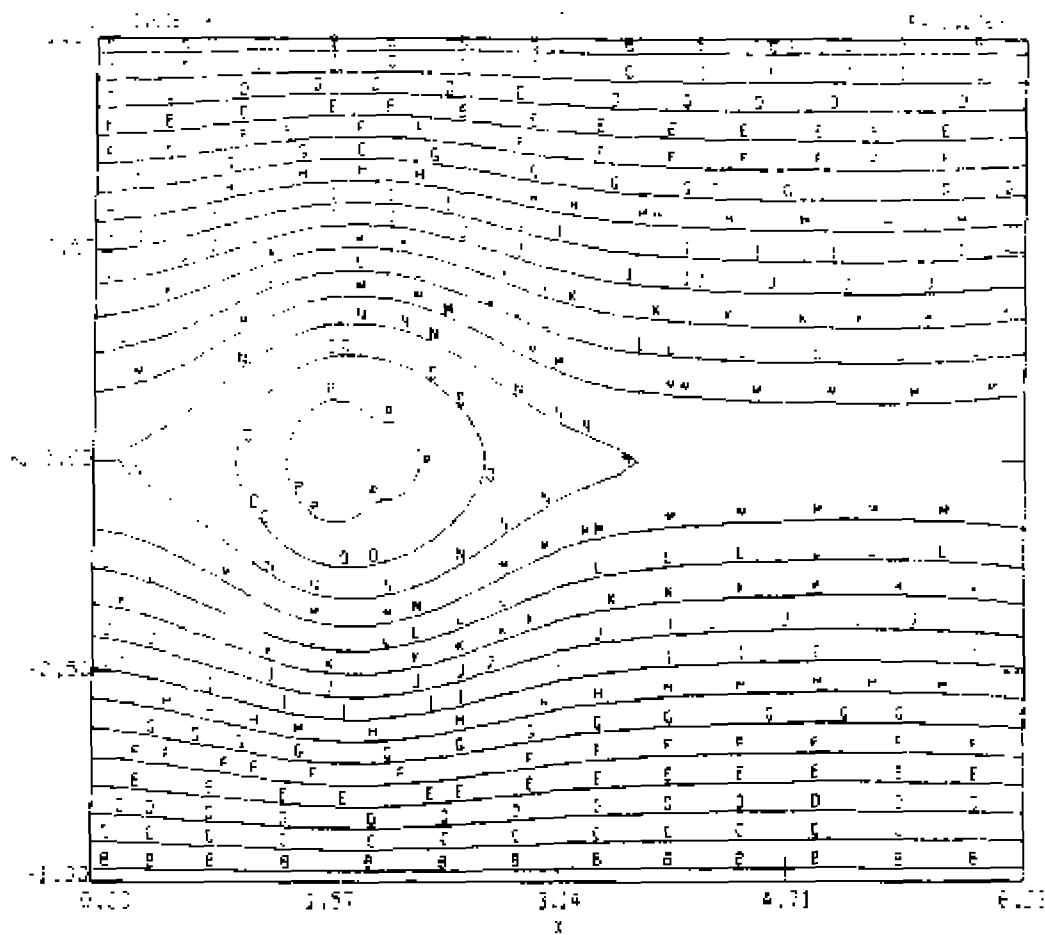


Figure VII - 11a Contour plot of magnetic vector potential at  $t = 58.9050$ .

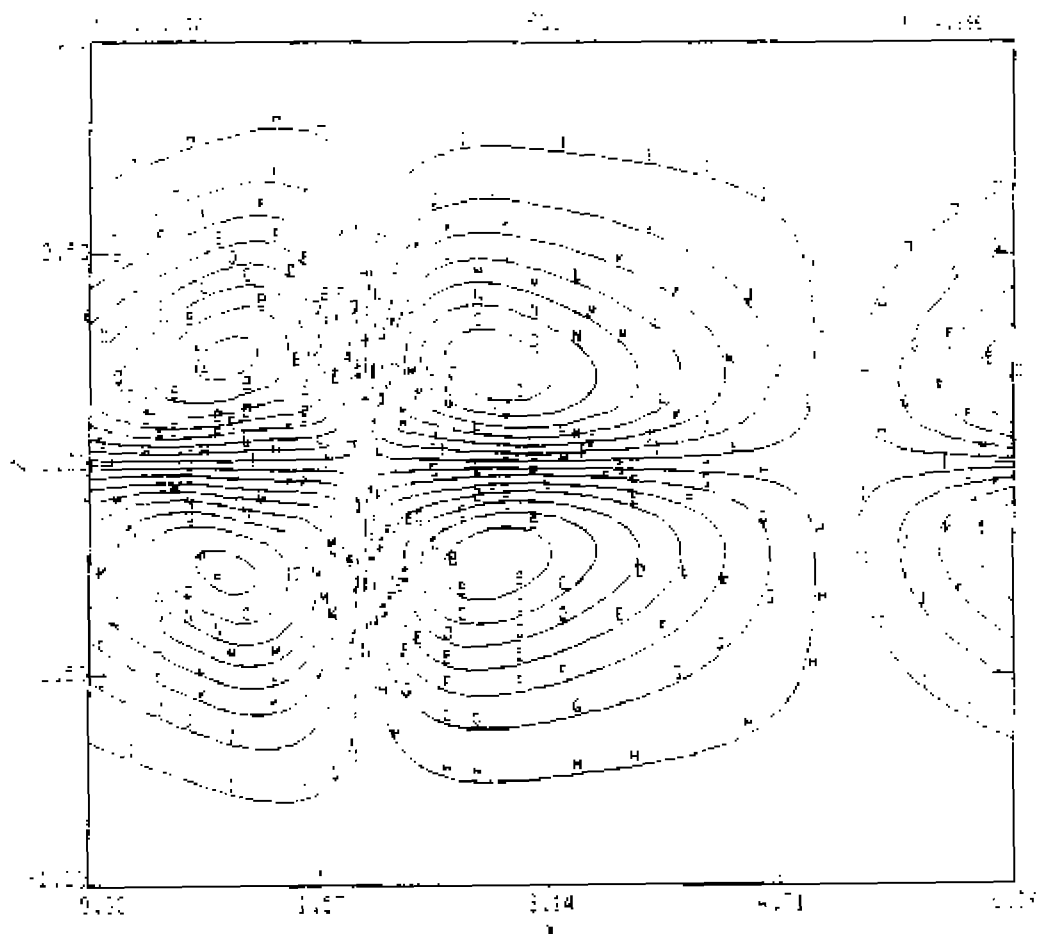


Figure VII - 11b Contour plot of velocity stream function at  $t = 58.9452$

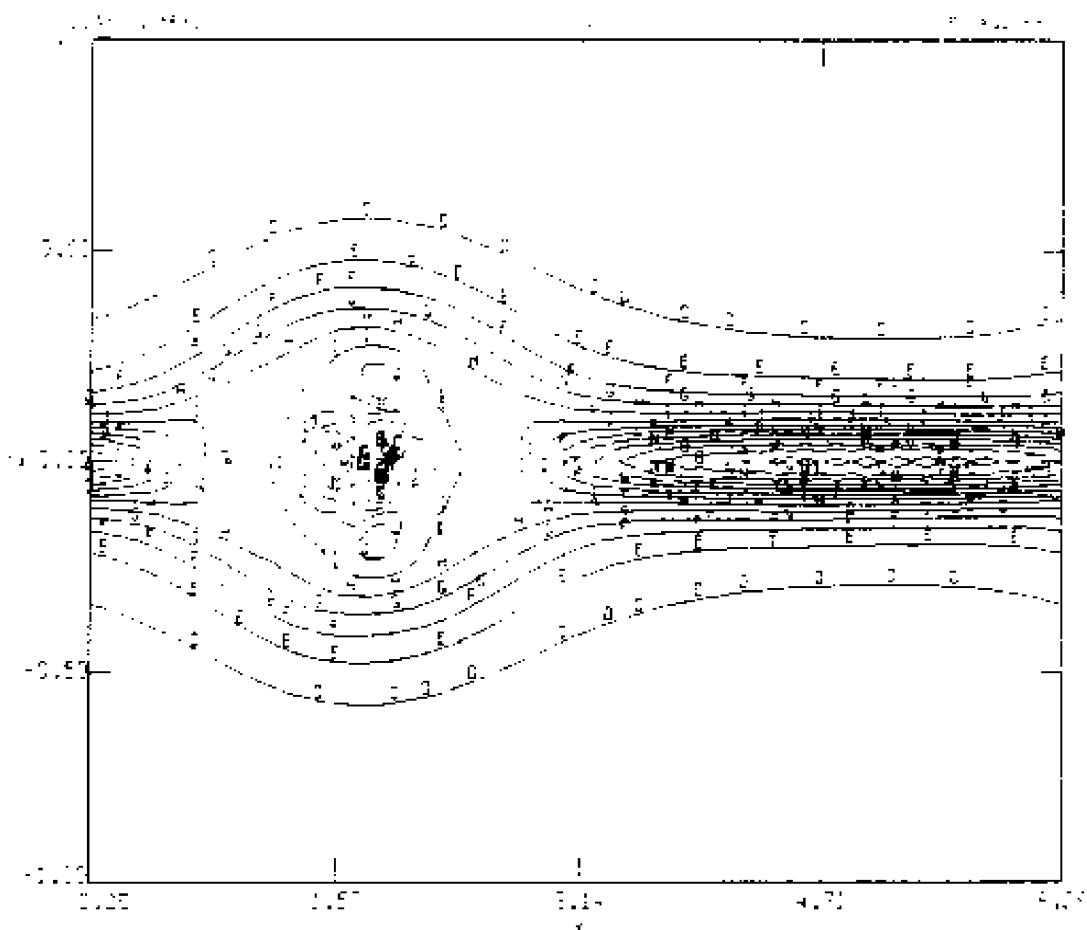


Figure VII - 11c Contour plot of electric current density at  $t = 58.9952$ .

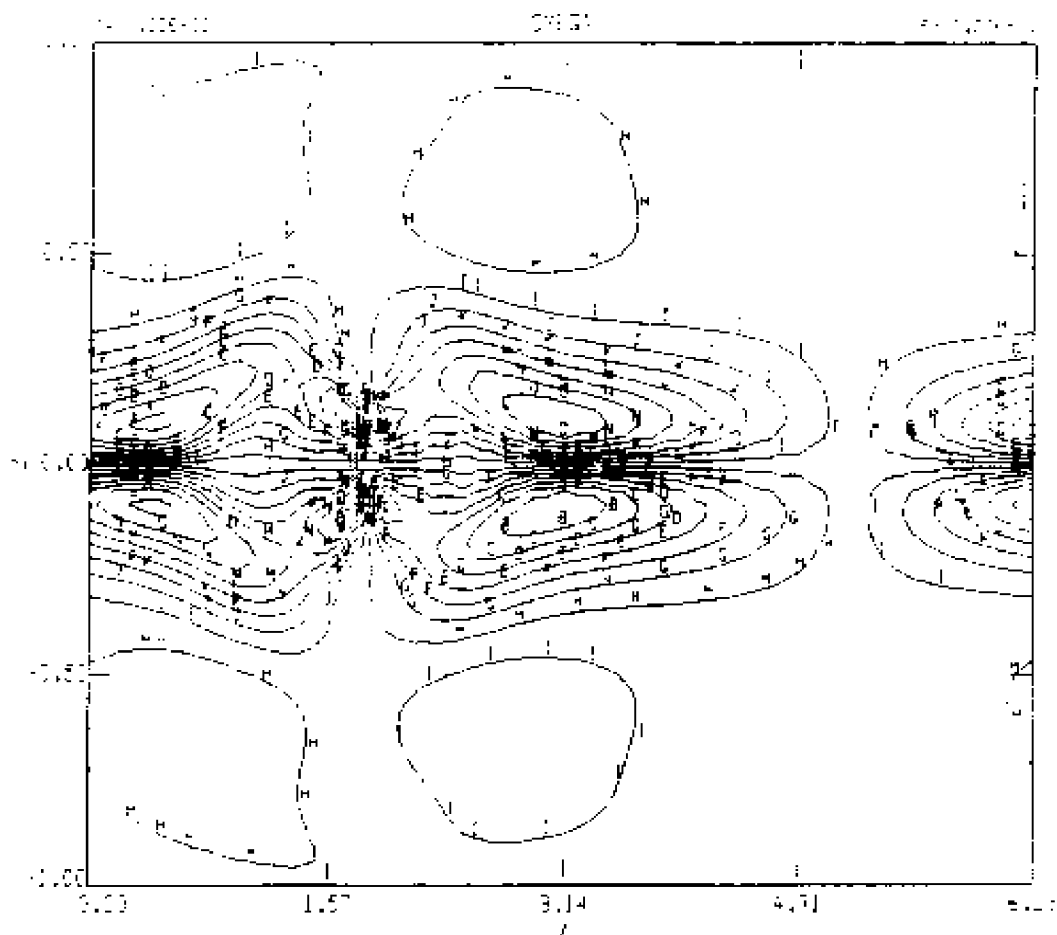


Figure VII - lid Contour plot of vorticity at  $t = 53.9058$ .



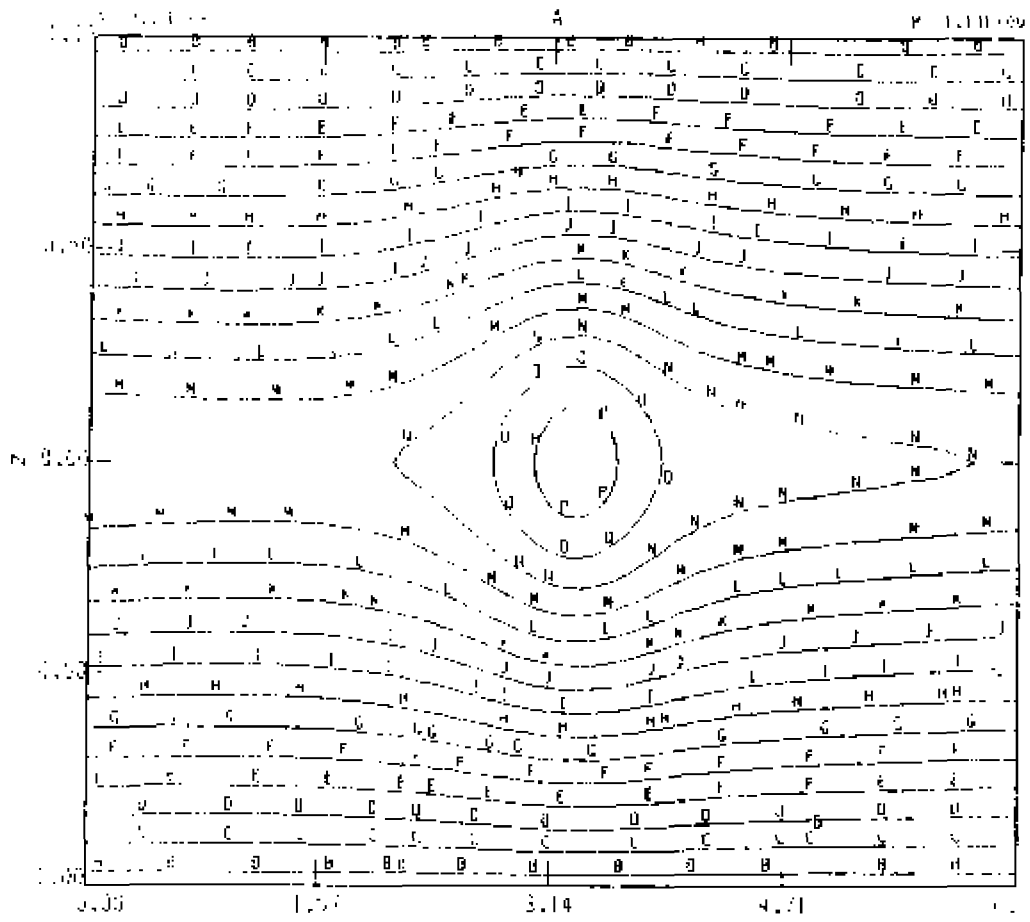


Figure VII - 12a Contour plot of magnetic vector potential at  $t = 161.498$ .

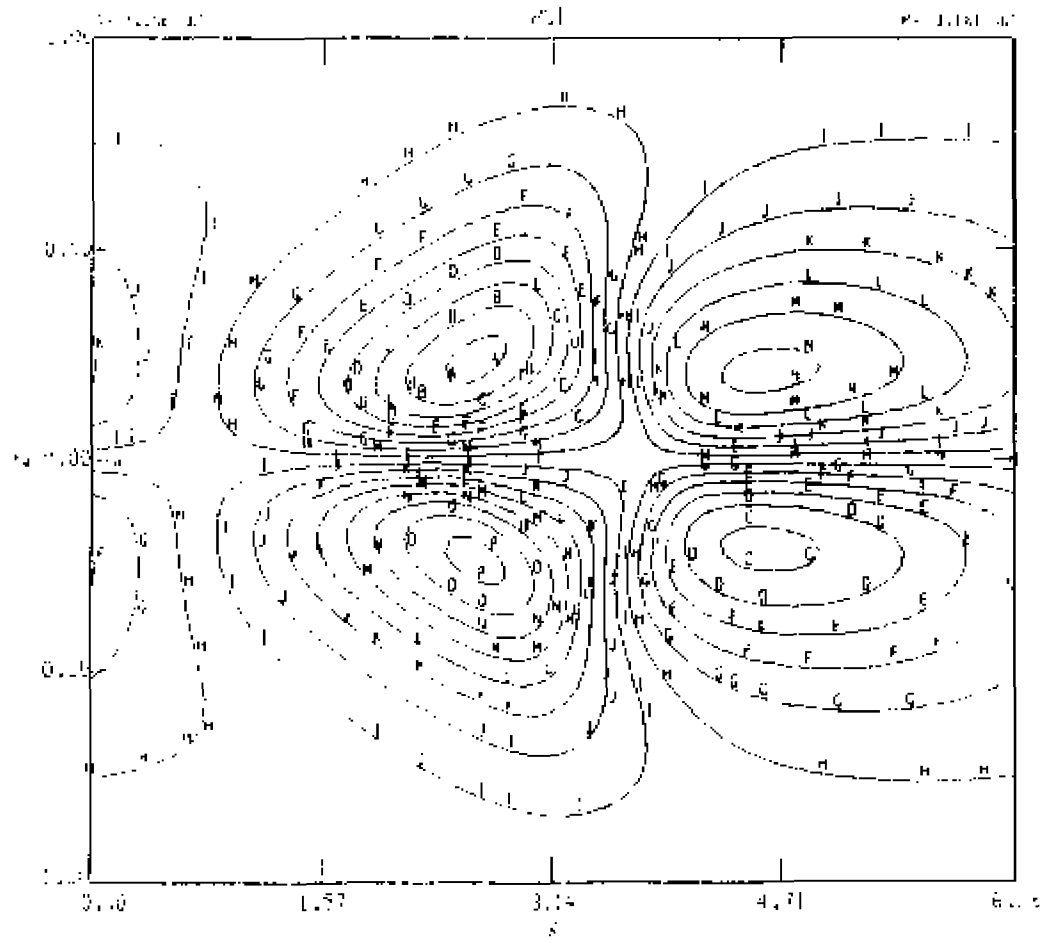


Figure VII - 12b Contour plot of velocity stream function at  $t = 161.408$ .

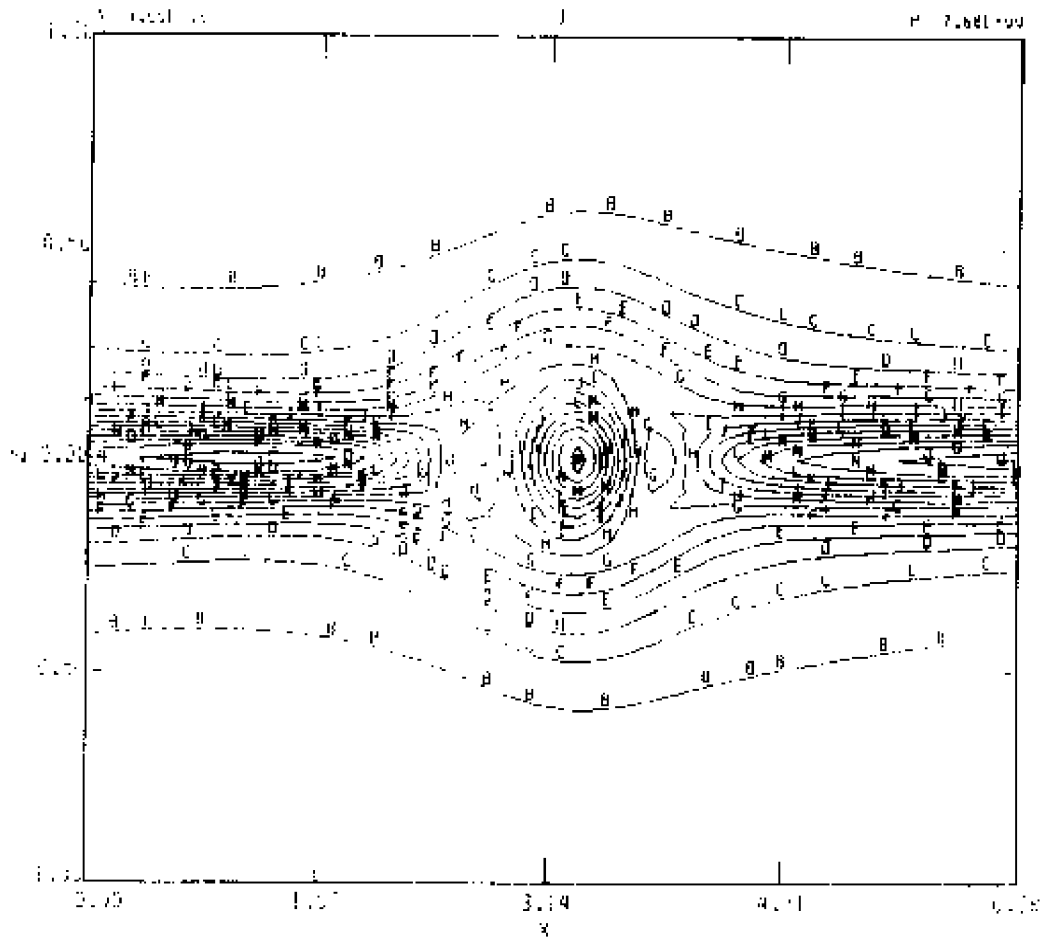


Figure VII - 13c Contour plot of electric current density at  $t = 161.806$ .



VITA

Russell B. Dahlburg

Born in Glen Ridge, New Jersey, December 6, 1954. He graduated from Conestoga Senior High School in Berwyn, Pennsylvania, June, 1972. He attended St. John's College in Annapolis, Maryland in 1974 and graduated in May, 1978, with a Bachelor of Arts degree, with concentration in liberal arts.

In June, 1979, the author entered the College of William and Mary as a graduate assistant in the Department of Physics.